

5-2015

## CANCER ASSOCIATED FIBROBLAST DERIVED ANGIOGENIC FACTOR MFAP5 IN OVARIAN CANCER PROGRESSION

SZE LEE CECILIA LEUNG

Follow this and additional works at: [https://digitalcommons.library.tmc.edu/utgsbs\\_dissertations](https://digitalcommons.library.tmc.edu/utgsbs_dissertations)

 Part of the [Cancer Biology Commons](#), and the [Oncology Commons](#)

### Recommended Citation

LEUNG, SZE LEE CECILIA, "CANCER ASSOCIATED FIBROBLAST DERIVED ANGIOGENIC FACTOR MFAP5 IN OVARIAN CANCER PROGRESSION" (2015). *The University of Texas MD Anderson Cancer Center UTHealth Graduate School of Biomedical Sciences Dissertations and Theses (Open Access)*. 555.  
[https://digitalcommons.library.tmc.edu/utgsbs\\_dissertations/555](https://digitalcommons.library.tmc.edu/utgsbs_dissertations/555)

This Dissertation (PhD) is brought to you for free and open access by the The University of Texas MD Anderson Cancer Center UTHealth Graduate School of Biomedical Sciences at DigitalCommons@TMC. It has been accepted for inclusion in The University of Texas MD Anderson Cancer Center UTHealth Graduate School of Biomedical Sciences Dissertations and Theses (Open Access) by an authorized administrator of DigitalCommons@TMC. For more information, please contact [digitalcommons@library.tmc.edu](mailto:digitalcommons@library.tmc.edu).

**CANCER ASSOCIATED FIBROBLAST DERIVED ANGIOGENIC FACTOR MFAP5 IN  
OVARIAN CANCER PROGRESSION**

**A  
DISSERTATION**

Presented to the Faculty of  
The University of Texas  
Health Science Center at Houston  
and  
The University of Texas  
MD Anderson Cancer Center  
Graduate School of Biomedical Sciences  
in Partial Fulfillment

of the Requirements

for the Degree of

**DOCTOR OF PHILOSOPHY**

by

Sze Lee Cecilia Leung, M.S.

Houston, Texas

May, 2015

## **Acknowledgements**

I would like to sincerely thank all the people involved and contributed in this project. My deepest appreciation goes to my thesis advisor, Dr. Samuel C. Mok, who has been a mentor, colleague and friend. His guidance has made this a thoughtful and rewarding journey.

I also owe my gratitude to my dissertation committee of Drs. Robert C. Bast, Russell R. Broaddus, Anil K. Sood and Kwong-Kwok Wong for their intellectual guidance and valuable advice. I would like to specially thank Dr. Wong, who has trusted me and gave me lots of encouragement and support over the years. I feel indebted to him for recruited me and gave me the opportunity to work at MD Anderson before enrolling at GSBS. Moreover, I would like to thank Dr. Sood, a wonderful collaborator who generously shared resources and provided insightful ideas and suggestions.

I am very fortunate to have Dr. Daniel K.P. Yip, an expert in calcium signaling and traction force microscopy, as a collaborator and friend. The training and support he provided has made the completion of this project possible. I am also grateful for the support and help given by the past and present members of Mok and Wong lab. Particularly, I would like to thank Dr. Tsz-Lun Yeung for his endless patience, helpful discussions and unconditional technical support.

Last but not least, I want to thank my loving and caring family and friends in Hong Kong. Their love and encouragements have always been my continuous motivation during my doctoral studies. Particularly, my aunt, Ms. Yin-Ping Wong, and my sister, Ms. Catherine Leung, are my soulmates and heartfelt companions. To my Lord, Jesus Christ, thank you for walked me through the darkest nights and guides me along the right paths.

# CANCER ASSOCIATED FIBROBLAST DERIVED ANGIOGENIC FACTOR MFAP5 IN OVARIAN CANCER PROGRESSION

Sze Lee Cecilia Leung, M.S.

Advisory Professor: Samuel C. Mok, Ph.D.

## Abstract

Advanced stage ovarian cancer is the most lethal gynecologic malignancy. No major improvement on patient survival has been achieved in the past decade. Therefore, identification of predictive or prognostic markers and further understanding of the molecular mechanisms in ovarian cancer progression are of paramount importance.

While cancer cells have always been the targets for the identification of prognostic and predictive markers, the potential for developing new diagnosis and treatments based on the tumor supporting stromal microenvironment is relatively unexplored. Using transcriptome profiling analysis on microdissected stromal and epithelial components of normal and malignant ovarian tissues, we identified a gene signature in the fibroblastic stromal component of the tumor tissue. Among the differentially expressed genes identified in microdissected cancer associated fibroblasts, microfibrillar associated protein 5 (MFAP5), which showed 10 folds increase in expression showed significant association with poorer overall survival in patients with high grade serous ovarian cancer. In addition, we identified a positive correlation between stromal MFAP5 expression and intratumor microvessel density, suggested a pro-angiogenic role of MFAP5. This study aims at delineating the functional roles and mechanisms by which stromal MFAP5 modulates ovarian tumor progression and angiogenesis and investigating the potential of targeting stromal MFAP5 as therapy for ovarian cancer.

Functional studies demonstrated that MFAP5 stimulated motility and invasion potential of ovarian cancer cells and microvascular endothelial cells through the binding of  $\alpha_v\beta_3$  integrin receptor. *In vivo*, targeting stromal MFAP5 using siRNA incorporated chitosan nanoparticles



significantly reduced tumor growth, metastasis and intratumoral microvessel density. Further, pathway analyses and western blot analyses demonstrated that CAF-derived MFAP5 modulates ovarian cancer cell motility and invasion potential through the calcium dependent FAK/CREB/TNNC1 signaling pathway and MFAP5 enhanced endothelial cell motility potential and permeability via focal adhesion and stress fiber formation by activating the calcium dependent FAK/ERK/LPP signaling pathway. Finally, monoclonal anti-MFAP5 antibodies were developed. These antibodies demonstrated inhibitory effects on tumor growth and improved paclitaxel bioavailability via the reduction of intratumoral microvessel leakiness.

To conclude, our results demonstrated the important roles of MFAP5 in promoting ovarian tumor progression and the potential of targeting stromal MFAP5 as a novel therapeutic approach for ovarian cancer.

## Table of Contents

<b>Approval sheet</b>	i
<b>Title Page</b>	ii
<b>Acknowledgements</b>	iii
<b>Abstract</b>	iv
<b>Table of Contents</b>	vi
<b>List of Figures</b>	xii
<b>List of Tables</b>	xxii
<b>Abbreviations</b>	xxiii
<b>Introduction</b>	1
1 Rationale and significance	2
2 Hypothesis	5
3 Specific aims	5
4 Epithelial ovarian cancer	6
A. Histopathology and molecular pathology	7
B. Treatments for ovarian cancer	9
5 Tumor microenvironment in cancer progression	10
6 Cancer associated fibroblasts in tumor progression	12

7	Tumor angiogenesis	17
8	Microfibrillar associated protein 5	22
9	Calcium signaling	22
10	Role of calcium signaling in tumor migration, invasion and metastasis	26
11	Troponin C type I (TNNC1)	29
12	LIM-containing lipoma preferred partner (LPP)	29
<b>Materials and Methods</b>		<b>31</b>
1	Tissue samples, microdissection, RNA extraction, Affymetrix GeneChip hybridization, and image acquisition	32
2	Cell lines and culture conditions	32
3	Quantitative real-time PCR analysis	33
4	Western blot analysis	33
5	Immunohistochemical analysis	34
6	CAF-derived MFAP5-stimulated motility of ovarian cancer cells	35
7	Recombinant MFAP5-increased ovarian cancer cell motility	35
8	Recombinant MFAP5-increased microvascular endothelial cell motility	36

9	MFAP5-stimulated ovarian cancer cell and microvascular endothelial cell invasion	37
10	Recombinant MFAP5-induced endothelial barrier disruption and increased permeability of endothelial cell monolayer	38
11	Tube formation assay	39
12	<i>In vivo</i> angiogenesis assay	39
13	Derivation of MFAP5-overexpressing NOFs	40
14	MFAP5-overexpressing fibroblast-stimulated ovarian cancer cell migration and invasion <i>in vivo</i>	40
15	Fibroblast-derived MFAP5 enhanced intratumoral microvessel formation and ovarian tumor growth	41
16	Stromal MFAP5 silencing reduced intratumoral microvessel formation and ovarian tumor progression	41
17	Murine stromal Mfap5 silencing reduced ovarian tumor growth and metastasis <i>in vivo</i>	42
18	Transcriptome profiling to identify signaling mechanism underlying MFAP5's effect on ovarian cancer and microvascular endothelial cells	42
19	MFAP5 stimulates calcium-dependent F-actin rearrangement	43
20	Protein fractionation and Western blot analysis of TNNC1 expression in TNNC1 siRNA-transfected cell lines	43
21	Traction force microscopy	44
22	[Ca <sup>2+</sup> ] <sub>i</sub> measurement	45

23	Immunofluorescence labeling of LPP and focal adhesion markers	45
24	Monoclonal anti-mfap5 antibody attenuated ovarian cancer cell and microvascular endothelial cell motility	46
25	Clone 130A anti-mfap5 antibody suppressed ovarian tumor growth <i>in vivo</i>	47
26	Anti-mfap5 antibody clone 130A increased paclitaxel bioavailability in ovarian tumor tissues	48
27	Toxicity test on anti-MFAP5 antibodies	48
28	Statistical analysis	49
29	Accession numbers	49
<b>Results</b>		<b>50</b>
1	The role of CAF derived MFAP5 on ovarian cancer cell growth, motility and invasion potential	51
	A. Ovarian cancer associated fibroblasts express high levels of MFAP5	52
	B. Overexpression of stromal MFAP5 predicts poor patient survival	53
	C. CAF-derived MFAP5 protein stimulates motility and invasiveness of ovarian cancer cells	57
	D. CAF-derived MFAP5 stimulated motility and invasion potential of ovarian cancer cells <i>in vivo</i>	62

E.	<i>In vivo</i> stromal Mfap5 silencing reduced ovarian tumor growth and metastasis	64
F.	Transcriptome profiling identified calcium-dependent signaling pathway activation and troponin C type 1 upregulation in MFAP5-treated ovarian cancer cells	67
G.	MFAP5's effect on motility is mediated via calcium mobilization and increased traction force in ovarian cancer cells	72
H.	TNNC1 upregulation by MFAP5 was mediated through the activation of calcium-dependent FAK/CREB/TNNC1 signaling pathway	77
I.	Correlation between tumor TNNC1 and stromal MFAP5 expression in human HGSOC samples revealed the clinical relevance of TNNC1	92
2	The pro-angiogenic roles of stromal MFAP5 in ovarian cancer progression	96
A.	Pro-angiogenic MFAP5 stimulates endothelial cell motility potential and permeability	96
B.	Stromal MFAP5 enhanced matured intratumoral microvessel formation	103
C.	Silencing of MFAP5 reduces intratumoral microvessel density and inhibits ovarian tumor progression	108
D.	MFAP5 induces endothelial cell stress fiber formation in a calcium-dependent manner	112
E.	MFAP5 induces LPP upregulation and increases focal adhesion assembly	120

F.	Calcium-dependent FAK/ERK/LPP signaling pathway modulates MFAP5-induced endothelial cell motility and permeability	130
3	Development of MFAP5-targeted therapeutic agents for ovarian cancer treatment	145
A.	Characterization of anti-MFAP5 antibodies by western blot analysis and epitope mapping	145
B.	Functional assays demonstrated inhibitory effect of anti-MFAP5 antibodies on cell motility	149
C.	<i>In vivo</i> animal study showed tumor suppressing effects of clone 130A anti-mfap5 antibody	151
D.	Evaluation of the effect of clone 130A anti-mfap5 antibody on intratumoral microvessel leakiness and drug delivery efficiency	154
E.	Toxicity test showed no observable adverse effects due to administration of anti-MFAP5 antibodies	155
	<b>Discussions</b>	159
	<b>Bibliography</b>	172
	<b>Vita</b>	196

## List of Figures

Figure 1:	The major histologic subtypes of ovarian carcinoma	7
Figure 2:	Epithelial subtypes of ovarian cancer and associated mutations	8
Figure 3:	The primary tumor microenvironment	11
Figure 4:	The expression of $\alpha$ -SMA and FAP in ovarian tissues	14
Figure 5:	Tentative models for evolution of the stromal fibroblasts in human carcinomas	16
Figure 6:	The balance hypothesis for the angiogenic switch	19
Figure 7:	The classical angiogenic switch	20
Figure 8:	Proposed role of vessel normalization in the response of tumors to antiangiogenic therapy	21
Figure 9:	Elements of the $\text{Ca}^{2+}$ signaling toolkit	25
Figure 10:	Molecular organization of focal adhesion complexes and their regulation by $\text{Ca}^{2+}$	27
Figure 11:	Major $\text{Ca}^{2+}$ entry and $\text{Ca}^{2+}$ release systems involved in migration, invasion and metastasis	28
Figure 12:	Microdissection of (A) normal ovarian tissue and (B) high-grade serous ovarian tumor samples	53
Figure 13:	Differentially expressed genes in ovarian cancer-associated fibroblasts	54
Figure 14:	Validation of MFAP5 overexpression in ovarian cancer-associated fibroblasts at mRNA level	55



Figure 15:	Immunolocalization of MFAP5 in advanced stage high-grade serous ovarian tumor tissues	56
Figure 16:	Validation of MFAP5 overexpression in ovarian cancer-associated fibroblasts at protein level	56
Figure 17:	Evaluation of clinical significance of MFAP5 overexpression	57
Figure 18:	Immunocytochemical analysis on the differential expression of $\alpha_v\beta_3$ integrin receptor in a panel of HGSOc cell lines	58
Figure 19:	Relative motility of ovarian cancer cells when co-cultured with CAF793092 primary ovarian CAFs in the presence of different antibodies	59
Figure 20:	Exogenous MFAP5 enhanced OVCA432 cell motility	60
Figure 21:	Exogenous MFAP5 enhanced ovarian cancer cell motility in Boyden chambers	61
Figure 22:	Exogenous MFAP5 enhanced ovarian cancer cell invasiveness	62
Figure 23:	Validation of MFAP5-overexpressing fibroblast line generated	63
Figure 24:	Growth rate of MFAP5-overexpressing fibroblasts compared to parental fibroblast line	63
Figure 25:	Stromal MFAP5 stimulated motility and invasion of ovarian cancer cells <i>in vivo</i>	65
Figure 26:	<i>In vivo</i> stromal Mfap5 silencing reduced ovarian tumor growth and metastasis	66

Figure 27:	Motility-promoting genes upregulated by MFAP5 in ovarian cancer cells	68
Figure 28:	Pathway analysis of genes upregulated by MFAP5	69
Figure 29:	Validation of TNNC1 upregulation in recMFAP5-treated cancer cells by quantitative RT-PCR	70
Figure 30:	Evaluation of the role of TNNC1 in MFAP5 induced ovarian cancer cell motility	71
Figure 31:	Fluorescent labeling of F-actin in MFAP5 treated ovarian cancer cells	71
Figure 32:	MFAP5 induced increase in density and rearrangement of F-Actin cytoskeleton were abrogated by siRNA silencing of TNNC1 in A224 and ALST cells	72
Figure 33:	Evaluation of the role of calcium signaling in MFAP5 induced ovarian cancer cell motility	74
Figure 34:	The mean normalized time course of Ca <sup>2+</sup> mobilization in A224 and ALST cells induced by MFAP5	74
Figure 35:	Calcium influx in ovarian cancer cells induced by MFAP5 treatment in the presence of different channel blockers	75
Figure 36:	Traction force induction by MFAP5 in ovarian cancer cells	76
Figure 37:	The effect of TNNC1 silencing on traction force generation in ovarian cancer cells	77
Figure 38:	Western blot analyses on proteins isolated from MFAP5-treated A224 and ALST ovarian cancer cells	78
Figure 39:	Molecular mechanism by which MFAP5 induces ovarian cancer cell motility and invasion potential	79

Figure 40:	Western blots showing blockade of $\alpha_v\beta_3$ integrin attenuated MFAP5 stimulated FAK and PLC- $\gamma$ 1 phosphorylation	80
Figure 41:	Western blots showing FAK inhibitor abrogated MFAP5 stimulated PLC- $\gamma$ 1 phosphorylation	81
Figure 42:	Western blots showing FAK inhibitor abrogated MFAP5 stimulated PKC $\theta$ phosphorylation	82
Figure 43:	Effects of PKC $\theta$ and PLC inhibitors on calcium influx induced by recombinant MFAP5	83
Figure 44:	Western blots showing the effects of PKC $\theta$ and PLC inhibitors on PLC- $\gamma$ 1 and PKC $\theta$ phosphorylation respectively	84
Figure 45:	Western blots showing the effects of calcium chelation on FAK phosphorylation	85
Figure 46:	Western blots showing the effects of calcium chelation on ERK and CREB phosphorylations	86
Figure 47:	Western blots showing the effects of PKC $\theta$ and PLC inhibitors on ERK phosphorylation	87
Figure 48:	Western blots showing the effects of ERK1/2 inhibitor on CREB phosphorylation	88
Figure 49:	Promoter analysis revealed multiple potential AP-1 binding sites in the TNNC1 promoter	89
Figure 50:	Western blots showing the effects of CBP/CREB interaction inhibitor on c-Jun and p-c-Jun expressions	90

Figure 51:	Western blots showing the effect of c-Jun inhibitor on MFAP5 induced TNNC1 overexpression	90
Figure 52:	TNNC1 expression in ovarian cancer cells after pretreatment with calcium chelator and different inhibitors	91
Figure 53:	Validation of pERK and TNNC1 overexpressions in MFAP5 overexpressing fibroblasts embedded Matrigel plugs	92
Figure 54:	Correlation between stromal MFAP5 and TNNC1 expressions in ovarian tumor samples	93
Figure 55:	Spearman's rank correlation analysis between stromal MFAP5 and tumor TNNC1 expressions	94
Figure 56:	Kaplan-Meier analysis of the clinical significance of tumor TNNC1 expression with 107 FFPE tumor samples obtained from HGSOC patients.	95
Figure 57:	Spearman's rank correlation analysis between stromal MFAP5 and CD31 positive vessel density in HGSOC patient samples.	96
Figure 58:	Attenuation of MFAP5-induced microvascular endothelial cell motility by the presence of anti- $\alpha_v\beta_3$ antibodies	97
Figure 59:	Exogenous MFAP5 promoted microvascular endothelial cell invasiveness.	98
Figure 60:	<i>In vitro</i> tube formation assay on MFAP5 treated microvascular endothelial cells	99
Figure 61:	Quantitative analysis for <i>in vitro</i> tube formation assay	100
Figure 62:	Permeability assay using the xCELLigence system	102

Figure 63:	Permeability assay using Boyden chambers	103
Figure 64:	The effects of stromal MFAP5 on ovarian cancer cells growth <i>in vivo</i>	104
Figure 65:	The effect of stromal MFAP5 on pericyte coverage on intratumoral microvessels	105
Figure 66:	Effects of MFAP5 on tube formation of endothelial cells was demonstrated by <i>in vivo</i> angiogenesis assay	106
Figure 67:	Quantitative analysis for <i>in vivo</i> angiogenesis assay	107
Figure 68:	Luminescence imaging of tumor volume in mice treated with control siRNA or mfap5-targeting siRNAs encapsulated chitosan nanoparticles	109
Figure 69:	Tumor weight of mice injected with control siRNA or mfap5-targeting siRNAs encapsulated chitosan nanoparticles	110
Figure 70:	Validation of stromal mfap5 silencing by mfap5-targeting siRNAs encapsulated nanoparticles and evaluation of mfap5 knockdown on intratumoral microvessel density	111
Figure 71:	The effect of stromal mfap5 silencing on intratumoral microvessel density in an intraovarian cancer cell injection animal model	112
Figure 72:	Traction force induction by MFAP5 in microvascular endothelial cells	114
Figure 73:	Fluorescent labeling of F-actin in MFAP5 treated microvascular endothelial cells	115
Figure 74:	Exogenous MFAP5 stimulated focal adhesion formation in microvascular endothelial cells	116
Figure 75:	Evaluation of the role of calcium signaling in MFAP5 induced microvascular endothelial cell motility	117

Figure 76:	Evaluation of the role of calcium signaling in MFAP5 induced stress fiber formation in microvascular endothelial cells	118
Figure 77:	Calcium influx induced by recombinant MFAP5 protein in the absence or presence of channel blockers in microvascular endothelial cells	119
Figure 78:	Heat map showing differential expressed genes in endothelial cells retrieved from <i>in vivo</i> angiogenesis assay	121
Figure 79:	Validation of LPP upregulation induced by MFAP5	122
Figure 80:	Immunolocalization of LPP in recMFAP5 treated microvascular endothelial cells	122
Figure 81:	Co-localization of LPP with focal adhesion proteins in microvascular endothelial cells	123
Figure 82:	The effect of LPP silencing on MFAP5 stimulated microvascular endothelial cell motility	124
Figure 83:	The effect of LPP silencing on tube formation in recMFAP5-treated hMEC-1 cells	126
Figure 84:	The effect of LPP silencing on tube formation in recMFAP5-treated TIME cells	127
Figure 85:	The effect of LPP silencing on stress fiber formation in recMFAP5-treated hMEC-1 cells	128
Figure 86:	The effect of LPP silencing on stress fiber formation in recMFAP5-treated TIME cells	128
Figure 87:	The effect of LPP silencing on focal adhesion formation in recMFAP5-treated hMEC-1 cells	129

Figure 88:	The effect of LPP silencing on focal adhesion formation in recMFAP5-treated TIME cells	129
Figure 89:	The effect of LPP silencing on MFAP5 induced monolayer permeability in microvascular endothelial cells	130
Figure 90:	Transcription factor binding site analysis on LPP promoter sequence	132
Figure 91:	Western blot analyses on proteins isolated from MFAP5-treated hMEC-1 and TIME cells	133
Figure 92:	Western blots showing the effects of calcium chelation on FAK phosphorylation in microvascular endothelial cells	134
Figure 93:	Diagram showing the proposed signaling pathways by which MFAP5 regulates LPP expression and LPP increases cell permeability and motility in endothelial cells	135
Figure 94:	Western blots showing blockade of $\alpha_v\beta_3$ integrin attenuated MFAP5 stimulated FAK phosphorylation in microvascular endothelial cells	136
Figure 95:	Western blots showing blockade of $\alpha_v\beta_3$ integrin attenuated MFAP5 stimulated PLC- $\gamma$ 1 phosphorylation in microvascular endothelial cells	136
Figure 96:	Western blots showing FAK inhibitor abrogated MFAP5 stimulated PKC $\theta$ phosphorylation in microvascular endothelial cells	137
Figure 97:	Western blots showing FAK inhibitor abrogated MFAP5 stimulated PLC- $\gamma$ 1 phosphorylation in microvascular endothelial cells	138
Figure 98:	Western blots showing PLC inhibitor abrogated MFAP5 stimulated PKC $\theta$ phosphorylation in microvascular endothelial cells	138

Figure 99:	Western blots showing PKC inhibitor abrogated MFAP5 stimulated PLC- $\gamma$ 1 phosphorylation in microvascular endothelial cells	139
Figure 100:	Western blots showing the effects of calcium chelation on ERK phosphorylation in microvascular endothelial cells	140
Figure 101:	Western blots showing the effects of calcium chelation on CREB phosphorylation in microvascular endothelial cells	140
Figure 102:	Western blots showing PKC inhibitor abrogated MFAP5 stimulated ERK1/2 phosphorylation in microvascular endothelial cells	141
Figure 103:	Western blots showing ERK inhibitor abrogated MFAP5 stimulated MLC2 phosphorylation in microvascular endothelial cells.	141
Figure 104:	Western blots showing ERK inhibitor abrogated MFAP5 stimulated CREB phosphorylation in microvascular endothelial cells	142
Figure 105:	Western blots showing CBP/CREB interaction inhibitor abrogated MFAP5 stimulated c-Jun and p-c-Jun expression in microvascular endothelial cells	143
Figure 106:	Western blots showing the effect of c-Jun inhibitor on MFAP5 induced LPP overexpression in microvascular endothelial cells	143
Figure 107:	Western blots showing the effect of LPP silencing on MFAP5 induced FAK phosphorylation in microvascular endothelial cells	144
Figure 108:	Western blot screening to identify specific anti-MFAP5 antibodies	146
Figure 109:	Epitope mapping for antibodies specific for human MFAP5	147
Figure 110:	Specificity of clone 64A, 117B and 130A to human and/or mouse MFAP5	148
Figure 111:	Epitope mapping for clone 130A anti-MFAP5 antibody	148



Figure 112:	Protein sequences of mouse and human MFAP5 showing the epitopes recognized by the three clones (64A, 117B and 130A) of anti-MFAP5 antibodies.	149
Figure 113:	<i>In vitro</i> functional assay showed inhibitory effect of clones 64A and 117B on MFAP5 enhanced cell motility	150
Figure 114:	<i>In vitro</i> functional assay showed inhibitory effect of clones 130A on mouse mfap5 enhanced mouse endothelial cell motility	151
Figure 115:	Anti-MFAP5 antibody clone 130A suppressed ovarian tumor growth <i>in vivo</i>	153
Figure 116:	Anti-MFAP5 antibody clone 130A reduced tumor angiogenesis and intratumoral microvessel leakiness <i>in vivo</i>	154
Figure 117:	Clone 130A anti-mfap5 antibody facilitated systematic administered paclitaxel delivery to ovarian tumors	155
Figure 118:	Toxicity test on anti-MFAP5 antibodies by complete blood count	156
Figure 119:	Toxicity test on anti-MFAP5 antibodies by chemistry tests	157
Figure 120:	Histological examination to evaluate tissue damages due to anti-MFAP5 antibodies treatment	158
Figure 121:	The overall mechanism by which stromal MFAP5 stimulates ovarian cancer progression, metastasis and tumor angiogenesis	171

## List of Table

Table 1:	Secretory proteins upregulated in CAFs compared with HOSE, NOFs and ovarian cancer epithelia.	55
----------	---	----

## Abbreviations

ADP	Adenosine diphosphate
ALP	Alkaline phosphatase
ALT	Alanine aminotransferase
AP-1	Activator protein 1
ARC	Arachidonate-regulated calcium
ARID1A	AT rich interactive domain 1A (SWI-like)
AST	Aspartate aminotransferase
Bad	BCL2-associated agonist of cell death
Bak	BCL-2 homologous antagonist/killer
BAPTA	1,2-bis(o-aminophenoxy)ethane-N,N,N',N'-tetraacetic acid
Bax	BCL-2-associated X protein
Bcl-2	B-cell lymphoma 2
Bcl-XL	B-cell lymphoma-extra large
bFGF	Basic fibroblast growth factor
BRCA1	Breast cancer 1, early onset
BRCA2	Breast cancer 2, early onset
BUN	Blood urea nitrogen
c-Fos	FBJ murine osteosarcoma viral oncogene homolog
c-Jun	Jun proto-oncogene
Ca <sup>2+</sup>	Calcium ion
cADPR	Cyclic ADP ribose
CAF	Cancer-associated fibroblast

CAM	Calmodulin
CAMK	Ca <sup>2+</sup> /calmodulin-dependent protein kinase
cAMP	Cyclic adenosine monophosphate
CAS	CRK-associated substrate
CBP	CREB-binding protein
CD31	Cluster of differentiation 31
CD34	Cluster of differentiation 34
CH-NP	Chitosan nanoparticles
CI	Cell index
CICR	Calcium-induced calcium release
CRE	cAMP-response element
CREB	cAMP response element-binding protein
CTSB	Cathepsin B
DAG	Diacylglycerol
DAPI	4',6-diamidino-2-phenylindole
DMSO	Dimethyl sulfoxide
DOCK 180	Dedicator of cytokinesis of 180kDa
ECM	Extracellular matrix
ELISA	Enzyme linked immunosorbent assay
ELMO	Engulfment and cell motility protein
EPAC	Exchange proteins directly activated by cAMP
ER	Endoplasmic reticulum
ERK	Extracellular signal-regulated kinases

FAK	Focal adhesion kinase
FAP-1 $\alpha$	Fibroblast activation protein-1 $\alpha$
FFPE	Formalin fixed paraffin embedded
FGF	Fibroblast growth factor
FITC	Fluorescein isothiocyanate
FSP1	Fibroblast-specific protein-1
GEO	Gene Expression Omnibus
GPCRs	G protein-coupled receptors
HAMA	Human anti-mouse antibody
H&E	Hematoxylin and eosin
HBSS	Hank's balanced salt solution
HER2	Erb-b2 receptor tyrosine kinase 2
HGSOC	High grade serous ovarian cancer
hMEC-1	Human microvascular endothelial cells
HOSE	Human ovarian surface epithelial cells
HV	Heavy chain
I.P.	Intraperitoneal
I.V.	Intravenous
ICAM-1	Intercellular adhesion molecule-1
IgG	Immunoglobulin G
IL-1 $\beta$	interleukin 1, beta
IP <sub>3</sub>	1,4,5-inositol triphosphate
IP <sub>3</sub> Rs	Inositol-1,4,5-triphosphate receptors

JNK	JUN N-terminal kinase
kDa	Kilodalton
kg	Kilogram
KRAS	Kirsten rat sarcoma viral oncogene homolog
LPP	LIM-containing lipoma preferred partner
LV	Light chain
MAGP2	Microfibril-associated glycoprotein 2
MDSC	Myeloid-derived suppressor cell
MFAP5	Microfibrillar associated protein 5
mg	Milligram
mL	Millilitre
MLC	Myosin light chain
MLC2	Myosin light chain 2
MLCK	Myosine light chain kinase
MMP2	Matrix metalloproteinase 2
MMP9	Matrix metalloproteinase 9
mRNA	Messenger ribonucleic acid
MSC	Mesenchymal stem cell
MTD	Maximum tolerated dose
Na <sup>+</sup>	Sodium ion
NAADP	Nicotinic acid dinucleotide phosphate
NAD	Nicotinamide-adenine dinucleotide
NADP	Nicotinamide adenine dinucleotide phosphate

NES	Nuclear export sequence
ng	Nanogram
NG2	Neuron-glia antigen 2
nM	Nanomolar
nm	Nanometre
NOF	Normal ovarian fibroblast
ORAI1	Calcium release-activated calcium channel protein 1
p-c-Jun	Phosphorylated Jun proto-oncogene
p-CREB	Phosphorylated cAMP response element-binding protein
p-ERK	Phosphorylated extracellular signal-regulated kinase
p-FAK	Phosphorylated focal adhesion kinase
p-MLC2	Phosphorylated myosin light chain 2
p-PKC $\theta$	Phosphorylated protein kinase C-theta
p-PLC- $\gamma$ 1	Phosphorylated phospholipase C- $\gamma$ 1
PARP	Poly (ADP-ribose) polymerase
PBS	Phosphate-buffered saline
PCR	Polymerase chain reaction
PFS	Progression free survival
PI3KCA	Phosphatidylinositol-4,5-bisphosphate 3-kinase, catalytic subunit alpha
PIP <sub>2</sub>	Phosphatidylinositol 4, 5 bisphosphate
PKC	Protein kinase C
PKC $\theta$	Protein kinase C-theta
PLC- $\beta$	Phospholipase C- $\beta$

PLC- $\gamma$ 1	Phospholipase C- $\gamma$ 1
PMCA	Plasma membrane Ca <sup>2+</sup> -ATPase
PTP	Permeability transition pore
PYK	Proline-rich kinase 2
RAC1	Ras-related C3 botulinum toxin substrate 1
recMFAP5	Recombinant MFAP5
RNA	Ribonucleic acid
ROCs	Receptor-operated channels
RT-PCR	Real-time polymerase chain reaction
RTCA	Real-time cell analyzer
RTK	Receptor tyrosine kinase
RYRs	Ryanodine receptors
S100A4	S100 calcium-binding protein A4
scFv	Single chain variable fragment
SD	Standard deviation
SDF-1 $\alpha$	Stromal-derived factor 1 $\alpha$
SEM	Standard error of the mean
SERCA	Sarco-endoplasmic reticulum ATPase
SH2	Src Homology 2
siRNA	Small interfering RNA
SOCE	Store-operated calcium entry
SOCs	Store-operated channels
Src	Src proto-oncogene



STIM1	Stromal interaction molecule 1
TEM	TIE2-expressing monocyte
Thy-1	Thy-1 cell surface antigen
TIME	Telomerase-immortalized microvascular endothelial cells
TME	Tumor microenvironment
TNNC1	Troponin C type 1
TRP	Transient receptor potential
TRPM7	Transient receptor potential cation channel subfamily M membrane 7
TSP-1	Thrombospondin 1
Tyr	Tyrosine
VASP	Vasodilator-stimulated phosphoprotein
VEGF	Vascular endothelial growth factor
VEGFR2	Vascular endothelial growth factor receptor 2
VGCCs	Voltage-gated calcium channels
VOCs	Voltage-operated channels
XC	Xestospongine C
$\alpha$ -SMA	$\alpha$ smooth muscle actin
$\mu$ g	Microgram
$\mu$ L	Microlitre
$\mu$ m	Micrometer
$\mu$ M	Micromolar

## Introduction

## 1. Rationale and significance

In the United States, researchers have estimated the diagnosis of 21,290 new cases of and 14,180 deaths owing to ovarian cancer in 2015,<sup>1</sup> making it the most lethal gynecologic malignancy. Being the most common histological subtype of ovarian cancers, high-grade serous ovarian cancer (HGSOC) is often regarded as the silent killer as HGSOC is usually diagnosed at late stage with significantly decreased 5-year survival rate. Ovarian cancer is notable for initial chemotherapy sensitivity using combination platinum and taxane-based therapy following debulking surgery. However, the vast majority of ovarian cancer patients will have their disease recur within 12 - 24 months after initial diagnosis. Recurring tumors are frequently resistant to chemotherapy. Without an effective treatment option, patients will die of progressive chemotherapy-resistant tumor.

To improve treatment effectiveness and survival of ovarian cancer patients, we are desperately in need of new therapeutic targets, which can be used to develop new treatment regimen. While most current treatment options and therapeutic agents are targeting the biology of ovarian cancer cells, the importance of tumor supportive microenvironment must not be overlooked. The tumor microenvironment, composed primarily of fibroblasts, endothelial cells, lymphocytic infiltrates and extracellular matrix proteins, can directly affect cancer cell growth, migration, and differentiation,<sup>2</sup> thereby presenting an unique aspect of diagnosing and treating cancer. Fibroblasts are primarily responsible for producing the structural components of the stromal microenvironment, which is mostly composed of collagen type I, II and IV as well as fibronectin.<sup>2</sup> Fibroblasts also produce secreted factors such as cytokines and growth factors, which maintain normal tissue homeostasis by signaling to other cell components in the stroma, such as immune, fat, vascular, smooth muscle and epithelial cells. Fibroblasts in the tumor stromal microenvironment exhibit altered secretion of extracellular proteins as well as paracrine growth factors, which modify the niche of tumor microenvironment and promote cancer cell proliferation, migration, and invasion potentials. Previous transcriptome profiling studies

identified prognostic gene signatures for advanced HGSOC.<sup>3-5</sup> However, large-scale transcriptome profiles generated using the stromal component of ovarian tumors are lacking, and the prognostic significance of stromal gene expression remains largely unknown.

To address the gap of knowledge, we performed transcriptome profiling on microdissected ovarian cancer associated fibroblasts (CAFs) (N=33) from patients with HGSOC. When their expression profiles were compared against those of microdissected normal ovarian fibroblasts (N=8), normal ovarian surface epithelial cells (N=6) and ovarian cancer cells (N=33), we identified a list of differentially expressed genes in CAFs. Among them, MFAP5 is significantly upregulated for 10 folds and follow up survival study suggested it as a poor prognostic marker for HGSOC. In addition, we identified a positive correlation between stromal MFAP5 expression levels and CD31 positive microvessel density in ovarian tumor samples, suggested a pro-angiogenic role of stromal MFAP5.

Tumor-induced angiogenesis is a process by which growing solid tumors produce diffusible angiogenic factors that induce host capillary endothelial cells to proliferate, migrate and form new vessels.<sup>6-9</sup> In addition, microvessel density has been shown to be a prognostic marker for different types of tumors.<sup>10-13</sup> Molecules or markers related to angiogenesis including VEGF and FGF have been extensively studied.<sup>14</sup> Multiple therapeutic agents targeting these proteins, such as the anti-VEGF monoclonal antibody, bevacizumab, and various FGF inhibitors have been developed.<sup>14</sup> However, drug toxicity and their modest therapeutic efficacy remain outstanding concerns.<sup>14,15</sup> Toxicity of these antiangiogenic agents is likely due to the fact that a majority of these pro-angiogenic molecules being targeted are expressed at high levels by normal tissues and organs.<sup>16</sup> Therefore, finding new molecular targets that can improve therapeutic benefit from anti-angiogenic strategies are of paramount importance. In addition, identifying new targets from the tumor stroma may compensate the deficiency of current agents that are designed to target tumor-derived factors only.

Based on our preliminary findings, this proposed study aims at delineating the functional roles of CAFs-derived MFAP5 from two different angles: First, the effects of MFAP5 on ovarian cancer progression through modulation of the aggressive phenotypes of ovarian cancer cells, and second, the effects of MFAP5 on promoting tumor growth by mediating angiogenesis. Uncovering the roles of MFAP5 in ovarian tumor progression and dissecting the molecular signaling mechanisms behind will provide us with the strong foundation for the final aim of the proposed study: To evaluate the potential of MFAP5 targeted therapy in ovarian cancer treatment.

In short term, this study will provide insights into the importance of microenvironment in cancer progression. Including MFAP5 as a prognostic marker for advanced stage HGSOc could benefit disease diagnosis and prediction of clinical outcomes. In long term, MFAP5's tumor promoting and pro-angiogenic roles suggested its potential as a novel therapeutic target. Besides targeting MFAP5 alone, since therapeutic approaches that target both cancer cells and the surrounding tumor-supporting microenvironment could potentially be more effective, MFAP5 targeted therapy can be used in synergy with standard cytotoxic chemotherapy agents to enhance treatment effectiveness, as well as in combination with current anti-angiogenic therapy which targets tumor-derived angiogenic factors to improve therapeutic benefit from anti-angiogenic strategies. Furthermore, the stratification of patients according to stromal MFAP5 expression will provide the basis for new trial designs for new therapeutic agents targeting MFAP5 in patients with HGSOc. This effort will form the basis of "personalized" medicine for ovarian cancer patients. Last but not least, predictive markers will enable physicians to identify patients who will not respond to newly developed therapy. This would allow the avoidance of unnecessary toxicity and the opportunity to be treated with experimental therapy.

Taken together, our understanding of the oncogenic role of stromal MFAP5 in ovarian cancer will certainly provide a novel insight into stromal markers, which will definitely reflect on the strategies for innovative treatment of ovarian cancer.

## 2. Hypothesis

Using transcriptome profiling analysis on microdissected stromal and epithelial components of normal and malignant ovarian tissues, we identified a gene signature in the fibroblastic stromal component of the tumor tissue. Among the differentially expressed genes identified in microdissected cancer associated fibroblasts (CAFs), microfibrillar associated protein 5 (MFAP5), which showed 10 folds increase in expression and significantly associated with poorer overall survival in patients with HGSOC was selected for further studies. Our immunostaining data showed that a high level of stromal MFAP5 expression is significantly correlated to the density of intra-tumor CD31 positive microvessels, suggested that MFAP5 may play a role in tumor angiogenesis. Based on the immunostaining and survival analysis results, **we hypothesize that CAFs-derived MFAP5 promotes ovarian cancer progression by enhancing the aggressiveness of cancer cells and increasing tumor angiogenesis. Hence, targeting MFAP5 in the tumor microenvironment may be a new modality in ovarian cancer treatment.**

## 3. Specific aims

**I) To evaluate the role of CAF derived MFAP5 on ovarian cancer cell growth, motility and invasion potential and delineate the underlying signaling mechanism.** The effects of MFAP5 on ovarian cancer cell proliferation, motility and invasion potential were evaluated by treating cancer cells with recombinant MFAP5 protein and silencing stromal

mfap5 in animal models. The underlying molecular mechanism of MFAP5-modulated tumor progression was delineated by transcriptome profiling and pathway analysis.

**II) To evaluate the angiogenic role of CAF derived MFAP5 in ovarian cancer microenvironment using microvascular endothelial cells and mouse models.** We treated endothelial cells with exogenous MFAP5 and study its effect on cell proliferation, migration and invasion potentials *in vitro*. We also performed *in vivo* angiogenesis assay by injecting MFAP5 supplemented Matrigel into mice to study the angiogenic effect of MFAP5 *in vivo*.

**III) To develop MFAP5 targeted therapeutic agents for ovarian cancer treatment.** Monoclonal anti-MFAP5 antibodies were developed and the efficacy of abrogating the pro-angiogenic and tumor-promoting effects of MFAP5 *in vitro* and *in vivo* for ovarian cancer treatment was evaluated.

#### **4. Epithelial ovarian cancer**

Epithelial ovarian cancer is the fourth commonest cause of female cancer death.<sup>17</sup> In the United States, researchers have estimated the diagnosis of 21,290 new cases of and 14,180 deaths owing to ovarian cancer in 2015,<sup>1</sup> making it the most lethal gynecologic malignancy. The disease typically presents in postmenopausal women, with a few months of abdominal discomfort, bloating, gas, nausea and urinary urgency, which are usually mistaken for gastrointestinal problems at the early stage.<sup>18,19</sup> The high mortality rate is due to the late presentation of the disease, usually when it is widely metastatic within the abdomen and caused abdominal pain or distension (International Federation of Gynecology and Obstetrics [FIGO] stage III).<sup>20,21</sup> Although the 5 years survival rate for stage I ovarian cancer is >90%, most patients (~75%) present with advanced stage (III/IV) tumors have a 5 years survival rate of a dismal 30%.<sup>22</sup>

## A. Histopathology and molecular pathology

It has been claimed that ovarian cancer is a general term for a variety of molecularly and histologically distinct diseases that simply share an anatomical location.<sup>23</sup> Ovarian cancers consist of 4 major histological subtypes (Fig. 1), which have been shown to associate with different mutations (Fig. 2).<sup>17</sup>

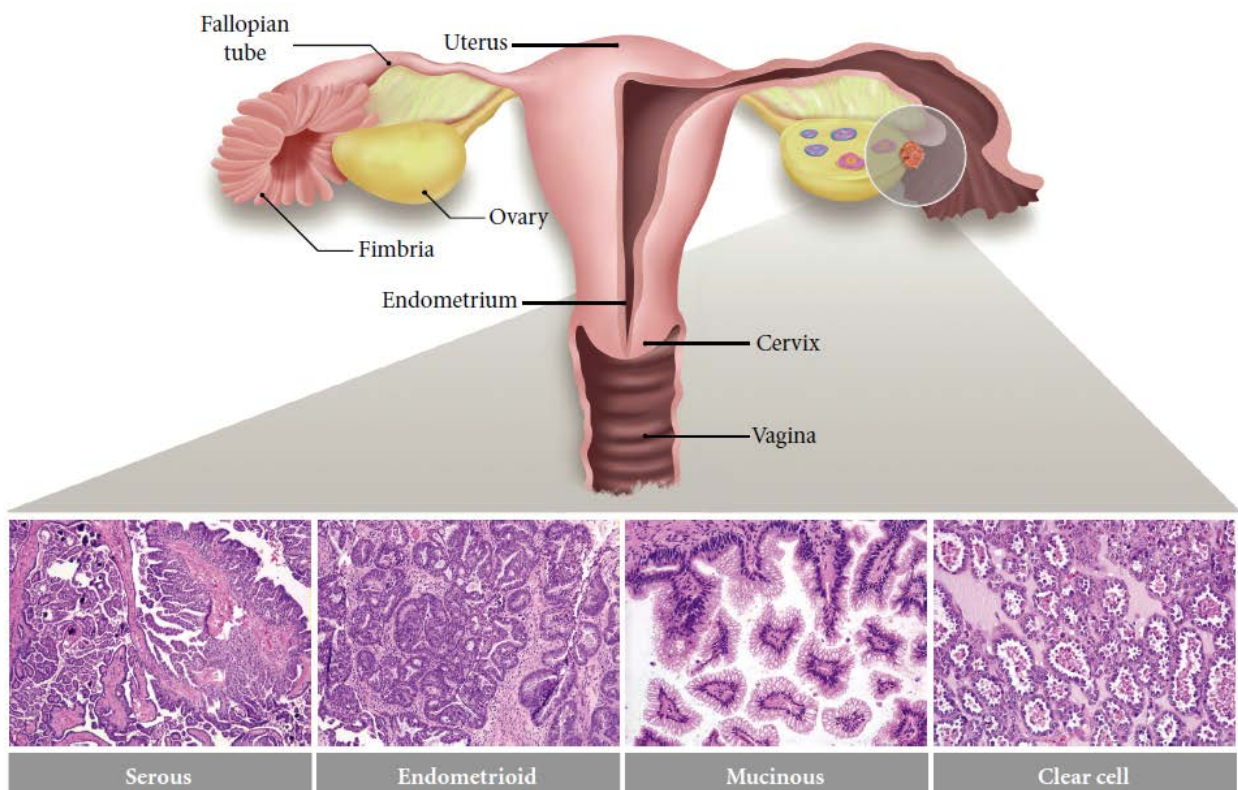


**Fig. 1: The major histologic subtypes of ovarian carcinoma.** Serous carcinomas resemble fallopian tube epithelium, endometrioid carcinomas resemble endometrial glands, and mucinous carcinomas resemble endocervical epithelium. Photographs show representative tumor sections stained with hematoxylin and eosin. The shaded circle represents the general anatomical location from which ovarian carcinomas are thought to arise. The pink and blue entities within the cross-sectioned ovary represent maturing ovarian follicles. (Alison M. Karst and Ronny Drapkin, "Ovarian Cancer Pathogenesis: A Model in Evolution," *Journal of Oncology*, vol. 2010, Article ID 932371, 13 pages, 2010. doi:10.1155/2010/932371)



Epithelial ovarian cancer				
High-grade serous	Low-grade serous	Endometrioid	Clear cell	Mucinous
TP53 BRCA1/2 NF1 CDK12 Homologous Recombination Repair genes  Pathway alterations PI3/Ras/Notch/ FoxM1	BRAF KRAS NRAS ERBB2	ARID1A PI3KCA PTEN PPP2R1A  MMR deficiency	ARID1A PI3KCA PTEN CTNNB1 PP2R1A	KRAS ERBB2 ampl

**Fig. 2: Epithelial subtypes of ovarian cancer and associated mutations.** (Reprinted from The Lancet 384 (9951), Jayson, G.C., Kohn, E.C., Kitchener, H.C. & Ledermann, J.A., Ovarian cancer, 1376-88 (2014), with permission from Elsevier)

**High-grade serous ovarian cancers** are derived from the surface of the ovary and/ or the distal fallopian tube.<sup>23</sup> It is characterized by nearly universal p53 gene abnormalities,<sup>24,25</sup> DNA copy number abnormalities, but few distinct and recurrent mutations.<sup>5</sup> Most hereditary high-grade serous ovarian cancer associated to deleterious mutations in *BRCA1* and *BRCA2*. Approximately 70% of ovarian cancer patients will be diagnosed with high-grade serous ovarian cancer, and these women have a substantially worse outcome than the outcome of those with early stage disease. It is also characterized by the initial chemosensitivity with subsequent acquisition of increasing resistance at each recurrence.<sup>17</sup>

**Low-grade serous and endometrioid ovarian cancer** shows more indolent behavior and they have low response rates to cytotoxic drugs and hormonal agents. *KRAS* mutation is prevalent in low grade serous ovarian cancer and *PI3KCA* mutation is common in endometrioid subtype of ovarian cancer.

**Clear cell ovarian cancers** are derived from endometriosis and frequently bear the *ARID1A* gene mutations.<sup>26</sup> They are characterized by the uniform high-grade nuclear features with clear

cytoplasm and poor response to chemotherapy.

Lastly, **mucinous ovarian cancers** are most commonly diagnosed at an early stage. Invasive mucinous ovarian cancers are mostly metastases from the gastrointestinal tract, including the colon, appendix or stomach, to the ovary. Nearly all cases of this rare type of cancer have *KRAS* mutation and a high frequency of *HER2* amplification.<sup>17,23</sup>

## **B. Treatments for ovarian cancer**

Depending on the stage of cancer, standard of care for epithelial ovarian cancer is surgery and platinum-based cytotoxic chemotherapy. Surgical options include: total hysterectomy, bilateral salpingo-oophorectomy, tumor debulking and omentectomy.<sup>27</sup> When optimal surgical debulking is not feasible, the use of neoadjuvant chemotherapy is widely accepted and supported by large randomized trials.<sup>28,29</sup> In the past 20 years, the global standard for first-line chemotherapy remains to be carboplatin and paclitaxel.<sup>17,30-32</sup> The median progression free survival (PFS) of advanced ovarian cancer is about 18 months and patients with the worst prognosis are those develop platinum-resistant disease.<sup>17</sup>

In seek of new treatment regimens, two new treatment strategies were proposed in recent years. **First**, poly (ADP-ribose) polymerase (PARP) inhibitors for ovarian cancers harbor *BRCA1* or *BRCA2* mutations. The mechanism of this chemosensitivity hinged on the crucial role that BRCA proteins play in the repair of double-strand DNA breaks by the error-free homologous recombination. When the gene of either BRCA protein is mutated, there is an increased reliance on the PARP single-strand repair pathway. Therefore, for cancer cells harboring *BRCA1* or *BRCA2* mutations, use of PARP inhibitors might cause significant lethality. Impressive tumor response and clinical benefit have been observed with olaparib, a PARP inhibitor, in phase 1 trials and in randomized trials comparing the efficacy and safety with liposomal doxorubicin in BRCA mutation carrying patients.<sup>33,34</sup> The **second** treatment approach is anti-angiogenic therapy. Rich vascular supply is vital for continuing tumor growth and the well-known prototype of angiogenesis inducer is vascular endothelial growth

factor (VEGF). Preclinical studies have used a number of approaches including (1) specific VEGF blockade with agents that interfere with VEGF binding to its receptors, such as anti-VEGF antibodies and the “VEGF-Trap” aflibercept; (2) inhibition of VEGFR2 function by VEGFR2 antibody or receptor tyrosine kinase inhibitors (TKIs) which inhibit the kinase domain of VEGFRs.<sup>35</sup> Most clinical trials have included the monoclonal anti-VEGFA antibody, bevacizumab. Particularly, GOG218 and ICON7 have showed efficacy in using bevacizumab in addition to carboplatin and paclitaxel chemotherapy followed by maintenance treatment in patients with FIGO stage III/IV disease with residual tumor after primary surgery.<sup>36,37</sup>

## **5. Tumor microenvironment in cancer progression**

The tumor microenvironment (TME), which consists of cells, soluble factors, signaling molecules, extracellular matrix and mechanical cues that can promote neoplastic transformation and support tumor growth, has received growing attention from cancer research scientists over the last decade (Fig. 3).<sup>2,38</sup> As our understanding on the contributions of the tumor microenvironment to tumorigenesis increases, new hallmarks of cancer that are crucial to cancer phenotypes and new frontier of therapeutic application targeting the tumor stroma have emerged.<sup>39</sup>

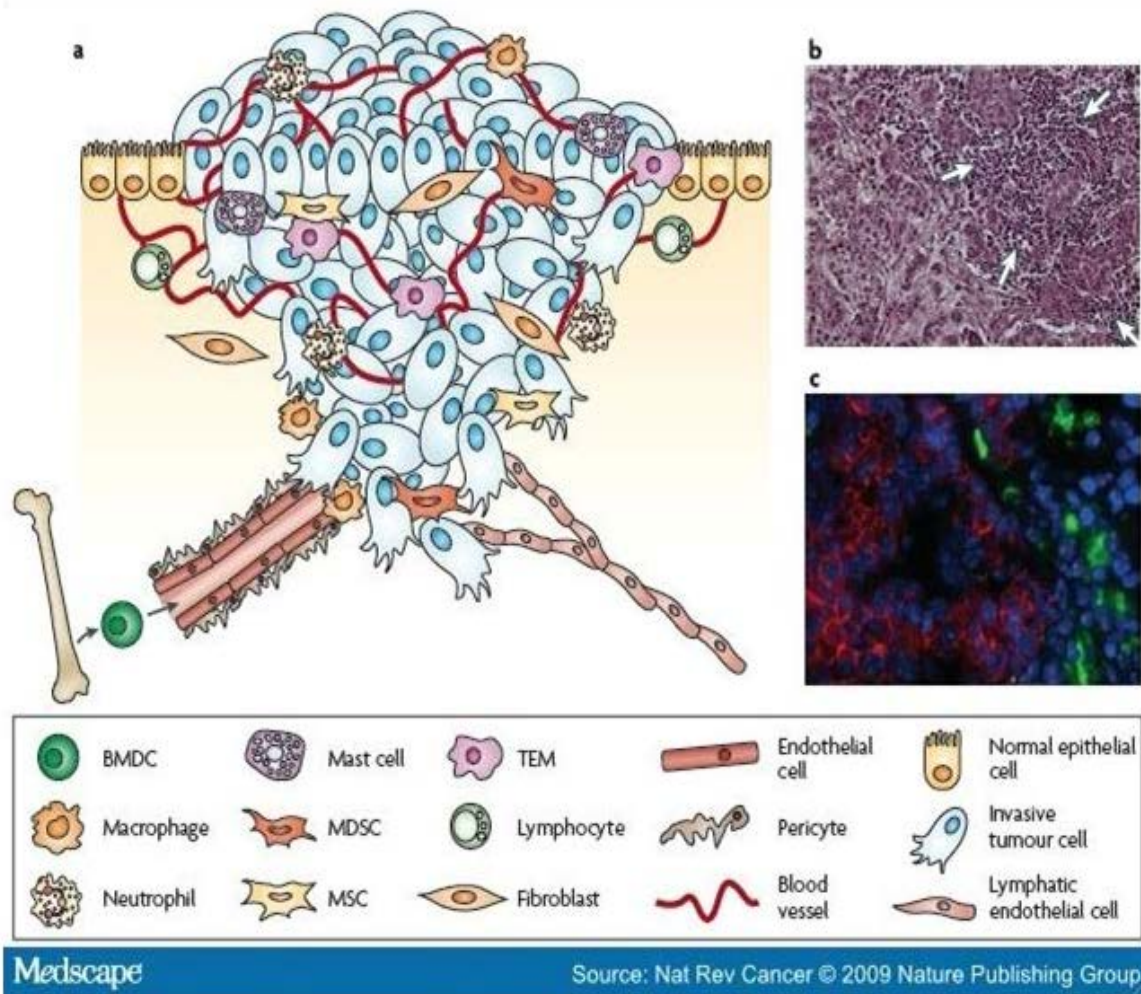


**Fig. 3: The primary tumor microenvironment.** **a)** Cancer cells in primary tumors are surrounded by a complex microenvironment comprising numerous cells including endothelial cells of the blood and lymphatic circulation, stromal fibroblasts and a variety of bone marrow-derived cells (BMDCs) including macrophages, myeloid-derived suppressor cells (MDSCs), TIE2-expressing monocytes (TEMs) and mesenchymal stem cells (MSCs). **b)** Invasive human breast cancer stained with haematoxylin and eosin in which a prominent infiltration of leukocytes (indicated by white arrows) is evident at the invasive margin. **c)** Macrophages at the invasive edge of pancreatic islet cancers express cathepsin B (green), which is associated with loss of epithelial cadherin (red) on the neighboring cancer cells. Cell nuclei are visualized by DAPI (blue). (Reprinted by permission from Macmillan Publishers Ltd: *Nature reviews, Cancer* **9**, 239-252, Joyce, J.A. & Pollard, J.W., Microenvironmental regulation of metastasis, 2009)

One important concept about TME is that it is a dynamic milieu, which is in constant evolution due to continuous tissue remodeling, metabolic alterations and changes in the recruitment of stromal cells. By changing the composition of the TME, tumors develop resistance towards antitumor therapies and therefore combined therapy targeting both cancer cells and the TME are being proposed.<sup>40-43</sup>

## 6. Cancer associated fibroblasts in tumor progression

Although the TME composed of complex variety of mesenchymal cells, notably fibroblasts, myofibroblasts, endothelial cells, pericytes and a variety of immune cells, fibroblasts and myofibroblasts often represent the majority of the stromal cells in various types of human carcinomas.<sup>44</sup> The relative proportion of stroma in advanced ovarian cancer ranges from 7% to 83% of tissue composition, with a median of 50% contribution.<sup>45</sup>

Normal fibroblasts are elongated cells residing in connective tissues and are responsible for the synthesis and turnover of the extracellular matrix (ECM). They control and support normal tissue homeostasis and involve in a plethora of biological processes such as wound healing and senescence.<sup>46</sup> Unlike normal fibroblasts, myofibroblasts residing at the tumor margins or infiltrated into the tumor mass, also termed cancer-associated fibroblasts (CAFs), possess greatly increased contractile ability, promote angiogenesis, and stimulate epithelial cell growth through the production of extracellular matrix and the secretion of growth factors and cytokines.<sup>47,48</sup> Common upregulated CAF markers include  $\alpha$  smooth muscle actin ( $\alpha$ -SMA),<sup>49</sup> stromal-derived factor 1 $\alpha$  (SDF-1 $\alpha$ ),<sup>50</sup> fibroblast activation protein-1 $\alpha$  (FAP-1 $\alpha$ ),<sup>44</sup> vimentin,<sup>51</sup> and fibroblast-specific protein-1 (FSP1).<sup>52</sup> Immunohistochemistry analysis of 91 ovarian tissue samples, including 61 epithelial ovarian cancer, 10 borderline tumors, 11 benign tumors and 9 normal ovarian tissues performed by Zhang et. al. showed almost all fibroblasts embedded in epithelial ovarian cancer stroma were  $\alpha$ -SMA positive and tumor cells were  $\alpha$ -SMA negative. In

normal ovary tissue,  $\alpha$ -SMA expression was detected only in vascular pericytes and weak expression of stroma  $\alpha$ -SMA was detected in 30% benign and borderline ovarian tumors (Fig. 4A-H).<sup>53</sup> There was no FAP expression in normal ovarian tissues, benign tumors and borderline tumors, while 91.8% of epithelial ovarian cancer specimens expressed FAP in the stroma. FAP expression was rarely detected in tumor cells (Fig. 4I-L).<sup>53</sup>



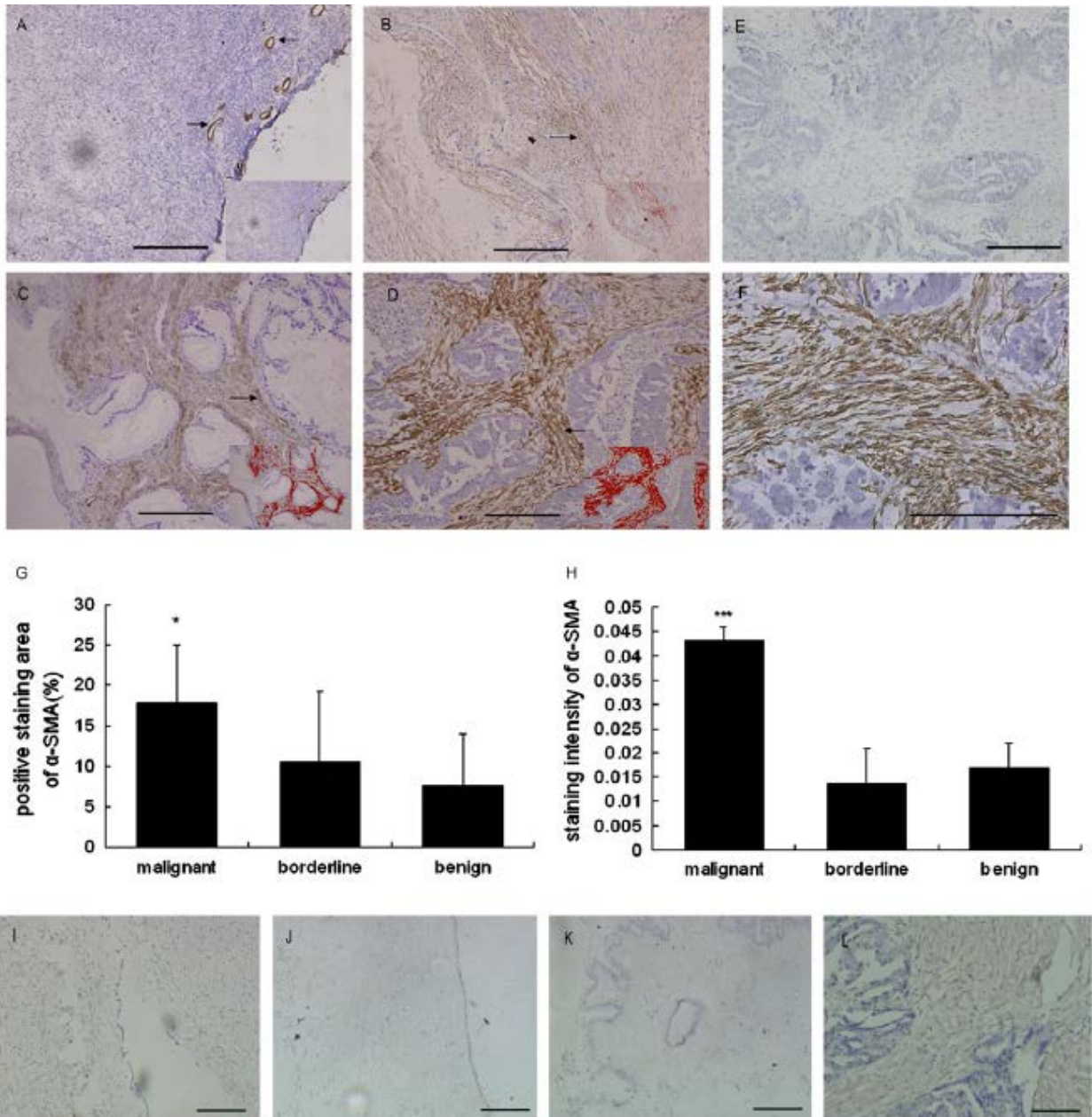


**Fig. 4: The expression of  $\alpha$ -SMA and FAP in ovarian tissues.** In normal ovary tissue (A),  $\alpha$ -SMA expression detected only in blood vessel walls (arrow); in benign ovarian tumor (B) and borderline ovarian tumor (C) there was only a very small proportion of stroma cells exhibited weak  $\alpha$ -SMA immunostaining (arrow); In malignant ovarian tumors (D) a large proportion of stroma cells were  $\alpha$ -SMA positive (arrow). A negative control without primary antibody is shown in (E). Magnification 200X. A zoomed-in section of D is shown (F). Magnification 400X. Quantitative analysis of the  $\alpha$ -SMA expression in ovarian tissues showed the positive staining area (G) and intensity (H) of  $\alpha$ -SMA in malignant ovarian tumors stroma was more prominent than in borderline tumors, benign tumors and normal ovarian tissues. FAP only existed in epithelial ovarian cancer stroma (I), but not in benign tumor (J), borderline tumor (K), or normal tissues (L). Bar = 100 $\mu$ m in length. \*\* $P < 0.001$  (ANOVA). (Reprinted from *Cancer letters* **303**, Zhang, Y., Tang, H., Cai, J., Zhang, T., Guo, J., Feng, D., Wang, Z., Ovarian cancer-associated fibroblasts contribute to epithelial ovarian carcinoma metastasis by promoting angiogenesis, lymphangiogenesis and tumor cell invasion, 47-55, (2011), with permission from Elsevier)

“Cell plasticity” describes the ability of cells in acquiring genetic mutations, epigenetic alterations and changes due to persistent environmental effects to alter their differentiation status.<sup>46</sup> Intuitively, CAFs are regarded as normal fibroblasts that have been transformed as a result of continuous exposure to cancer cells. Indeed, CAFs often share several similarities with normal fibroblasts morphologically and phenotypically with respect to expressions of intercellular adhesion molecule-1 (ICAM-1), laminin and Thy-1, a surface glycoprotein that involved in cell adhesion, migration and myofibroblastic differentiation.<sup>54-56</sup> Regarding the transformation from normal fibroblasts to CAFs, three models of stromal fibroblast evolution were proposed: 1) Though relatively uncommon, genetic alterations (e.g. loss of heterozygosity and somatic mutations) could be acquired by normal residential fibroblasts;<sup>57</sup> 2) transdifferentiation of normal fibroblasts into CAFs without acquiring genetic alterations; and 3) differentiation from bone marrow derived progenitor cells recruited to the tumor site (Fig. 5). Through the exchange of intercellular secreted factors (e.g. chemokines like IL-1 $\beta$  and SDF-1) with other cell types in the TME, CAFs promote tumor growth, angiogenesis, inflammation and metastasis.<sup>46,50</sup> Therefore, CAF-specific proteins may serve as both prognostic markers and therapeutic targets. It was believed that targeting CAFs for cancer treatment has two advantages: 1) the ongoing functions of CAFs is critical to the growth of nearby neoplastic cells and 2) the stromal cells are relatively genetically stable compared to carcinoma cells which could accumulate adaptive mutations during the course of therapy in order to acquire drug resistance.<sup>58-60</sup>



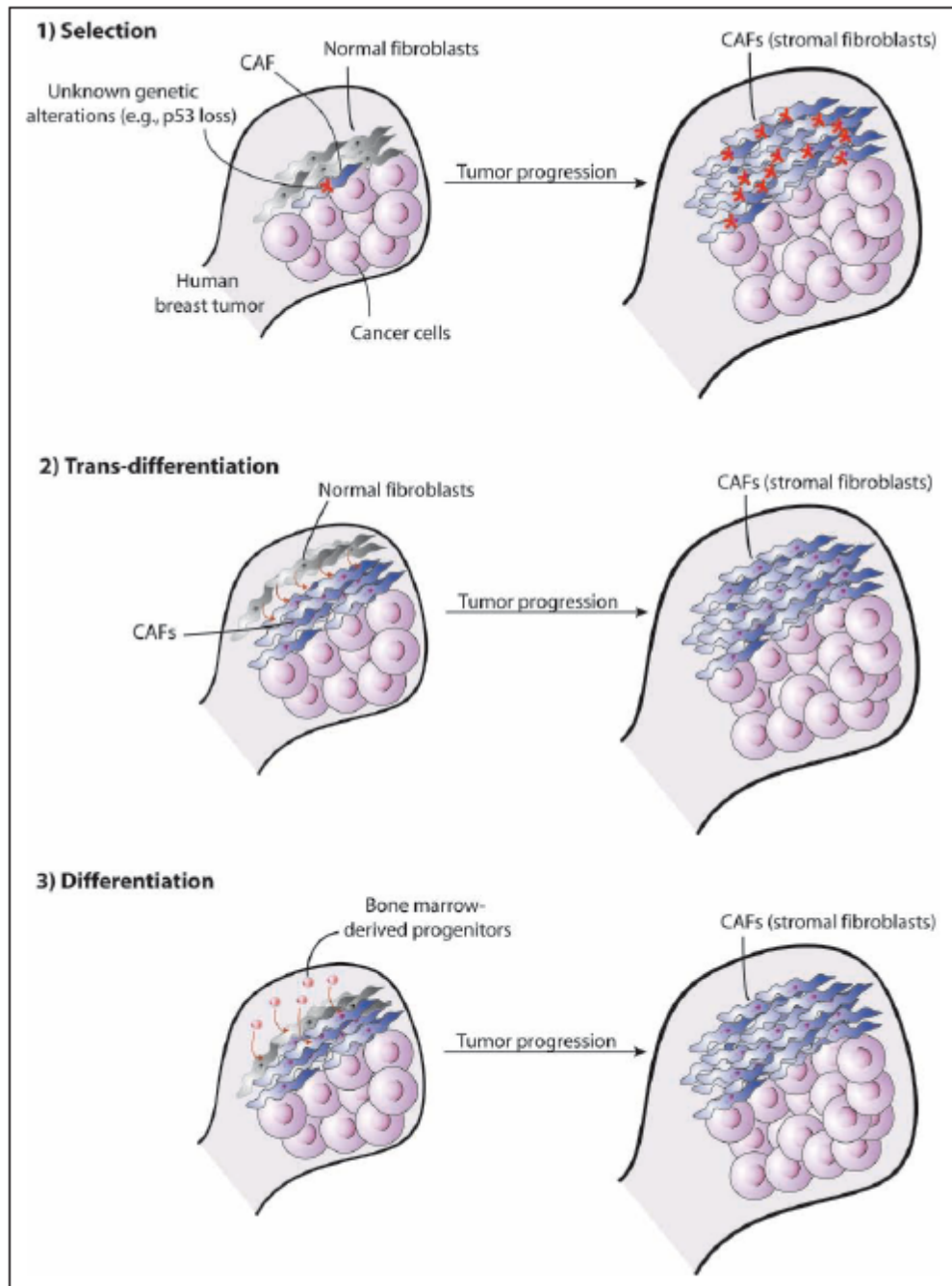


**Fig. 5: Tentative models for evolution of the stromal fibroblasts in human carcinomas.** (1) Clonal selection from a small population of fibroblasts or progenitors that have undergone genetic alterations. (2) Trans-differentiation from, for example, pre-existing normal fibroblasts. (3) Differentiation from bone marrow-derived progenitors. (Orimo, A. & Weinberg, R.A. Stromal fibroblasts in cancer: a novel tumor-promoting cell type. *Cell cycle* 5, 1597-1601 (2006), reprinted by permission of Taylor & Francis LLC (<http://www.tandfonline.com>))

## 7. Tumor angiogenesis

Like normal tissues, tumor tissues require nutrients and oxygen as well as an effective way to eliminate metabolic wastes and carbon dioxide.<sup>61</sup> Formation of tumor-associated neovasculature by angiogenesis covers these needs.<sup>39,62</sup> Pathological angiogenesis, which ensure exponential growth of tumors, is driven by the imbalance between pro- and anti-angiogenic signaling, and the activation of the “angiogenic switch” (Fig. 6).<sup>62,63</sup> The angiogenic switch begins with pericyte detachment and vessel dilation before the basement membrane and extracellular matrix is degraded. This allows endothelial cells to migrate toward the chemotactic angiogenic stimuli generated by tumor cells. Subsequently, endothelial cells proliferate for the onset of angiogenic sprouting, new vessel formation and maturation (Fig. 7).<sup>63</sup> However, it has been widely reported that the tumor vasculature are both structurally and functionally abnormal compared to normal blood vessels.<sup>64,65</sup> Structurally, tumor vessels are often dilated with oversized diameter and the chaotic layout creates irregular blood flow. Also, absent or immature vessels make some tumor regions impenetrable. Functionally, oversized pores on vessel wall leak fluid from the vasculature into interstitial areas and the high interstitial fluid pressure built up blocks transport of drugs and oxygen out of vessels to tumor tissue. In addition, the fluidic buildup leads to swelling of tumor tissue, causing painful symptoms and more importantly, the fluidic pressure drives tumor-generated proteins and cells toward healthy tissues and into lymphatic system, which will increase the risk of metastasis.<sup>64</sup> To the tumor microenvironment, dysfunctional vessels produce conditions of low oxygen (hypoxia) and high acidity. Hence, radiation and certain chemotherapies that require oxygen to kill tumor cells are ineffective.<sup>66</sup> Moreover, immune cells that might attack cancer cells cannot function in an acidic environment and without oxygen<sup>67</sup> and changes in gene activity caused by hypoxia might also promote tumor cell migration toward healthy tissues.<sup>35,64</sup>

Although it is widely accepted that antiangiogenic therapies should destroy the tumor vasculature, thereby depriving the tumor of oxygen and nutrients. The “vascular normalization”

hypothesis proposed that rather than eliminating vessels, the judicious use of anti-angiogenic therapy to correct the imbalance between pro- and anti-angiogenic molecules in tumor tissues, which features the attenuation of hyperpermeability, increased vascular pericyte coverage, a more normal basement membrane, and a resultant reduction in tumor hypoxia and interstitial fluid pressure,<sup>65</sup> might normalize the tumor microenvironment and ultimately control tumor progression and improve the efficacy of conventional therapies (Fig. 8).<sup>65,68</sup> This might serve to explain the clinical trial data demonstrating synergism between anti-VEGF therapy and chemotherapy in the treatment of solid tumors.<sup>69-71</sup>

## THE BALANCE HYPOTHESIS FOR THE ANGIOGENIC SWITCH

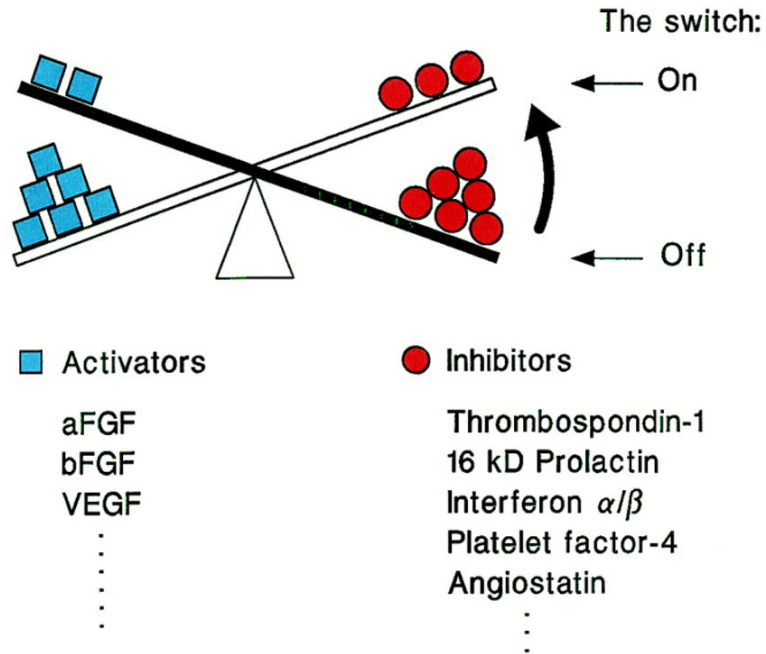


**Fig. 6: The balance hypothesis for the angiogenic switch.** The normally quiescent vasculature can be activated to sprout new capillaries (angiogenesis), a morphogenic process controlled by an angiogenic switch mechanism. The prevailing evidence suggests that changes in the relative balance of inducers and inhibitors of angiogenesis can activate the switch. In some tissues, the absence of angiogenesis inducers may keep the switch off, while in others the angiogenesis inducers are present but held in check by higher levels of angiogenesis inhibitors. Thus, both reducing the inhibitor concentration, e.g., for TSP-1, by loss of a tumor suppressor gene; or increasing the activator levels, e.g., for induction of VEGF, by hypoxia, can each change the balance and activate the switch, leading to the growth of new blood vessels. (Reprinted from *Cell* **86**, Hanahan, D. & Folkman, J., Patterns and emerging mechanisms of the angiogenic switch during tumorigenesis, 353-364, (1996), with permission from Elsevier)

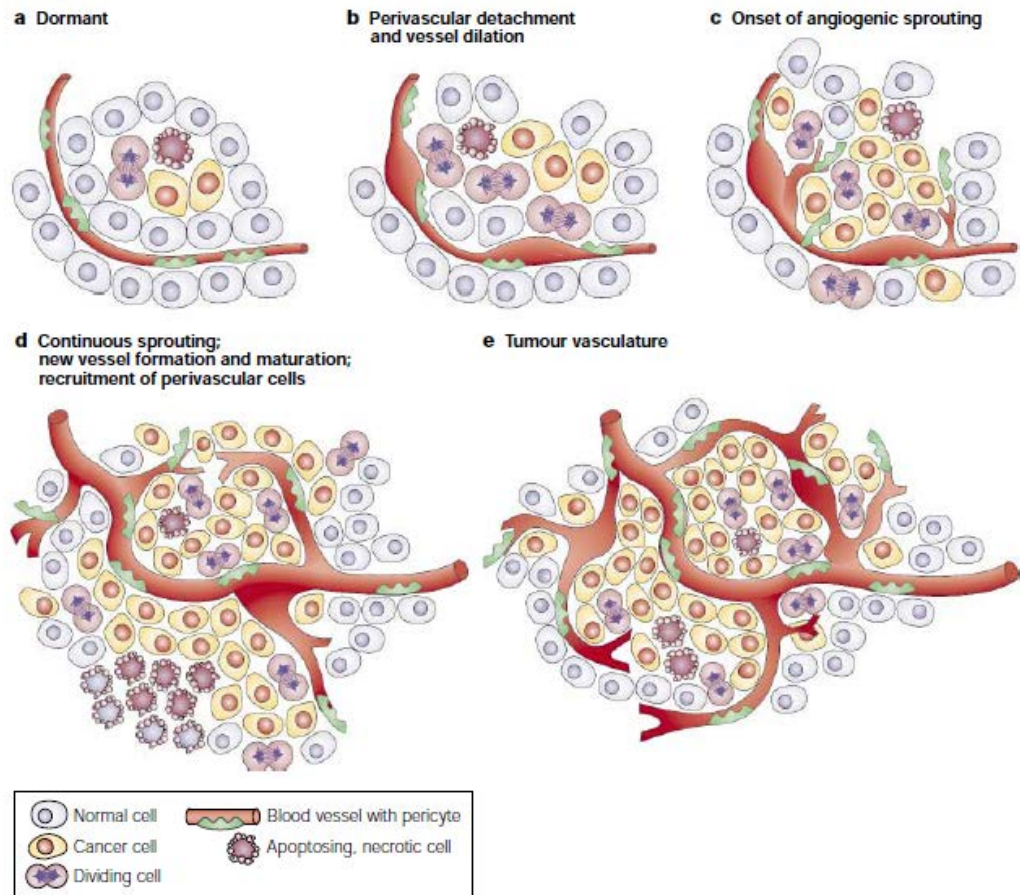


**Fig. 7: The classical angiogenic switch.** The angiogenic switch is a discrete step in tumor development that can occur at different stages in the tumor-progression pathway, depending on the nature of the tumor and its microenvironment. Most tumors start growing as avascular nodules (dormant) (a) until they reach a steady-state level of proliferating and apoptosing cells. The Initiation of angiogenesis, or the “angiogenic switch”, has to occur to ensure exponential tumor growth. The switch begins with perivascular detachment and vessel dilation (b), followed by angiogenic sprouting (c), new vessel formation and maturation, and the recruitment of perivascular cells (d), Blood-vessel formation will continue as long as the tumor grows, and the blood vessels specifically feed hypoxic and necrotic areas of the tumor to provide it with essential nutrients and oxygen (e). (Reprinted by permission from Macmillan Publishers Ltd: *Nature reviews, Cancer* 3, 401-410, Bergers, G. & Benjamin, L.E., Tumorigenesis and the angiogenic switch, 2003)



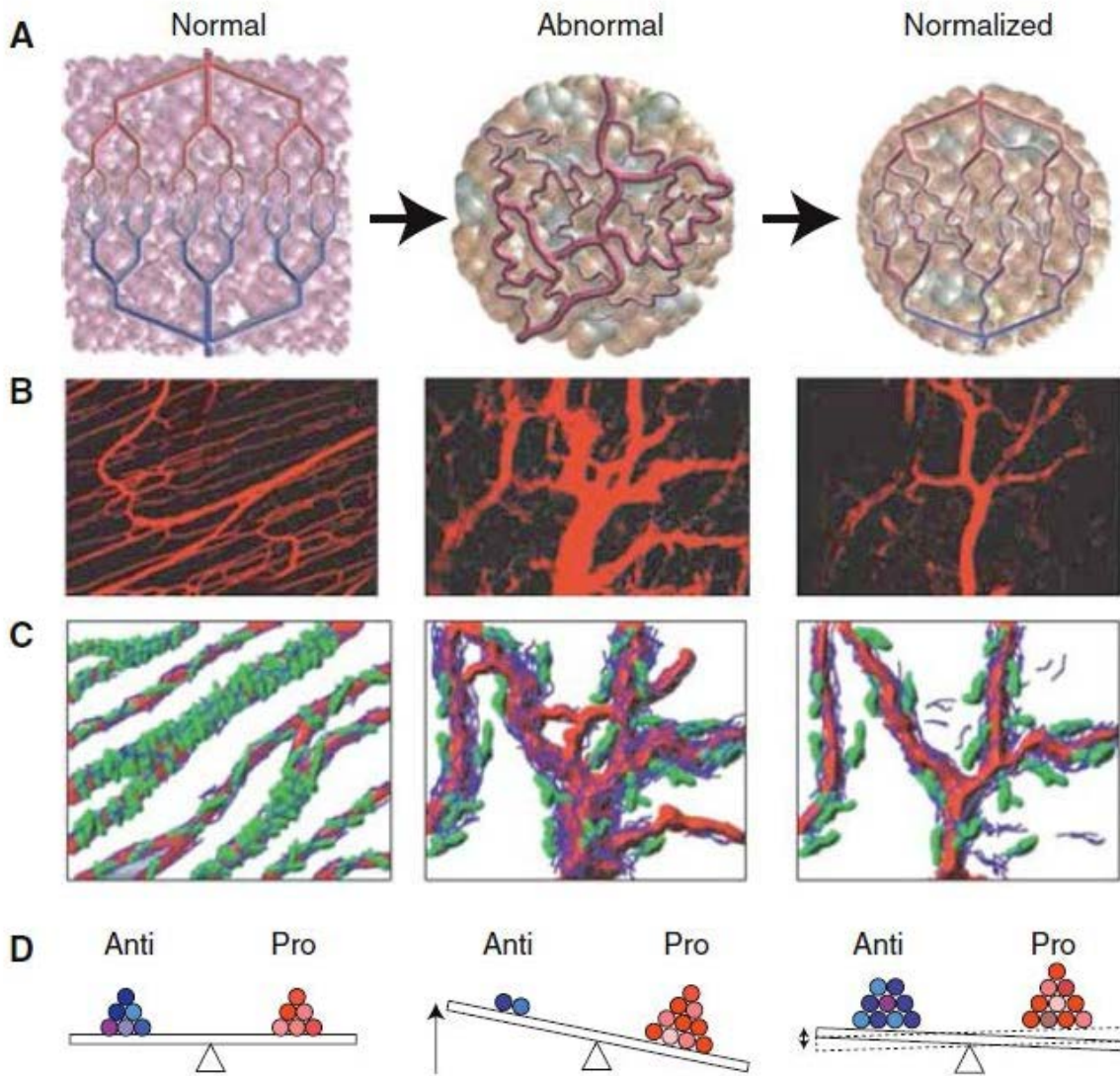


**Fig. 8: Proposed role of vessel normalization in the response of tumors to antiangiogenic therapy.** (A) Tumor vasculature is structurally and functionally abnormal. It is proposed that antiangiogenic therapies initially improve both the structure and the function of tumor vessels. However, sustained or aggressive antiangiogenic regimens may eventually prune away these vessels, resulting in a vasculature that is both resistant to further treatment and inadequate for the delivery of drugs or oxygen. (B) Dynamics of vascular normalization induced by VEGFR2 blockade. On the left is a two-photon image showing normal blood vessels in skeletal muscle; subsequent images show human colon carcinoma vasculature in mice at day 0 and day 3 after administration of VEGFR2-specific antibody. (C) Diagram depicting the concomitant changes in pericyte (green) and basement membrane (blue) coverage during vascular normalization. (D) These phenotypic changes in the vasculature may reflect changes in the balance of pro- and antiangiogenic factors in the tissue. (From Jain, R.K. Normalization of tumor vasculature: an emerging concept in antiangiogenic therapy. *Science* **307**, 58-62 (2005). Reprinted with permission from AAAS)

## 8. Microfibrillar associated protein 5

Microfibrillar associated protein 5, MFAP5, also known as microfibril-associated glycoprotein 2 (MAGP2). It is a 25-kDa extracellular glycoprotein. MFAP5 was demonstrated to be associated with fibrillin-containing microfibrils in fetal nuchal ligament, dermis, adventitia of aorta, glomerular mesangium and perimysium, and bound to fetal aortic smooth muscle cells and chondrocytes.<sup>72</sup> The C-terminal of MFAP5 containing 7 conserved cysteine residues, and was found to interact with fibrillin-1 and -2, as well as fibulin-1, another component of elastic fibers, suggesting that MFAP5 is an important component in the assembly of microfibrils.<sup>73</sup> The N-terminal of MFAP5 contains an RGD motif that has been shown to mediate adhesion and spreading of fetal bovine aortic smooth muscle cells, ear cartilage chondrocytes, arterial endothelial cells, human skin fibroblasts and osteoblasts through the  $\alpha_V\beta_3$  integrin.<sup>74</sup> The role of MFAP5 in cancer progression was first reported by our group that it is a prognostic factor in advanced stage ovarian cancer with the ability to prolong tumor cell survival and stimulate angiogenesis.<sup>75</sup>

## 9. Calcium signaling

Calcium is a ubiquitous intracellular signal that impacts nearly all aspect of cellular life, from changes in protein conformations to signal transduction and its specific roles in excitability, exocytosis, motility, apoptosis and transcription.<sup>76</sup> Its diversity of actions lies in the versatility of the  $Ca^{2+}$  signaling mechanism in terms of speed, amplitude and spatiotemporal patterning. Generally, cells at rest have a cytoplasmic  $Ca^{2+}$  concentration of 100nM and maintain a 20,000-fold gradient between the intracellular (~100nM)  $Ca^{2+}$  and extracellular (~2mM)  $Ca^{2+}$  concentrations. Cells are activated and calcium-mediated signal transduction takes place when intracellular  $Ca^{2+}$  level raises to roughly 1000nM. Further increase in intracellular  $Ca^{2+}$  concentrations that exceeds the normal range of spatial and temporal boundaries may result in

cell death through both necrosis and apoptosis.<sup>77</sup>

To generate  $\text{Ca}^{2+}$  mobilizing signals, cells have to control the entry of external  $\text{Ca}^{2+}$  or the release of  $\text{Ca}^{2+}$  from internal store, mainly from the endoplasmic reticulum (ER) (Fig. 9). For entry from extracellular space, voltage-operated channels (VOCs), which are activated by depolarizing membrane potentials and are mostly expressed in excitable cells, are the most well-known players. In addition, there are calcium channels that open in response to receptor activation called the receptor-operated channels (ROCs) and recent evidence showed that store-operated channels (SOCs) can be activated in response to store emptying by a conformational-coupling mechanism. Such mechanism involves direct coupling of inositol-1,4,5-triphosphate receptors ( $\text{IP}_3\text{Rs}$ ) in the ER to SOCs.<sup>78-80</sup> For  $\text{Ca}^{2+}$  signals that are derived from the intracellular stores, G protein-coupled receptors (GPCRs; primarily Gq/11 subtypes) activated phospholipase C- $\beta$  (PLC- $\beta$ ) and tyrosine kinase receptor (TKR) activated PLC- $\gamma$  are responsible for the cleaving of phosphatidylinositol 4, 5 bisphosphate ( $\text{PIP}_2$ ) into 1,4,5-inositol triphosphate ( $\text{IP}_3$ ) and diacylglycerol (DAG). Binding of  $\text{IP}_3$  to the  $\text{IP}_3\text{Rs}$  increase cytosolic  $\text{Ca}^{2+}$  concentration by allowing the diffusion of  $\text{Ca}^{2+}$  from the ER to the cytoplasm. On the other hand, DAG regulates protein kinase C (PKC), as well as some  $\text{Ca}^{2+}$  permeable transient receptor potential (TRP) channels directly.<sup>81</sup> The sister intracellular channel of  $\text{IP}_3\text{R}$ , the ryanodine receptors (RYRs), also gate ER membrane  $\text{Ca}^{2+}$  release via the binding of cytosolic  $\text{Ca}^{2+}$  to RYRs. This mechanism of  $\text{Ca}^{2+}$  mobilization is called calcium-induced calcium release (CICR).<sup>82</sup>

After excitation,  $\text{Ca}^{2+}$  is rapidly removed from the cytoplasm by various pumps and exchangers.<sup>83,84</sup> Plasma membrane  $\text{Ca}^{2+}$ -ATPase (PMCA) pumps and  $\text{Na}^+/\text{Ca}^{2+}$  exchangers extrude  $\text{Ca}^{2+}$  from the cytoplasm and the sarco-endoplasmic reticulum ATPase (SERCA) pumps return  $\text{Ca}^{2+}$  to its internal stores. On the other hand, mitochondrion has a huge capacity to accumulate  $\text{Ca}^{2+}$  and it sequesters  $\text{Ca}^{2+}$  rapidly during the development of  $\text{Ca}^{2+}$  signals. This uptake of  $\text{Ca}^{2+}$  not only favors the shaping of both the amplitude and spatio-temporal patterns of  $\text{Ca}^{2+}$  signals, it also contributes to the OFF mechanism in  $\text{Ca}^{2+}$  signaling.<sup>85-88</sup> However, when



mitochondrion is overloaded with  $Ca^{2+}$ , the high conductance of the permeability transition pore (PTP) might collapse the transmembrane potential of the mitochondrion, which leads to the release of cytochrome c and the initiation of apoptosis.<sup>89</sup> This mitochondria-mediated  $Ca^{2+}$  function in apoptosis might be interfered by the  $Ca^{2+}$  dynamics between ER and mitochondria via death antagonists (Bcl-2 and Bcl-X<sub>L</sub>) or death agonists (Bax, Bak and Bad).<sup>77,89</sup>

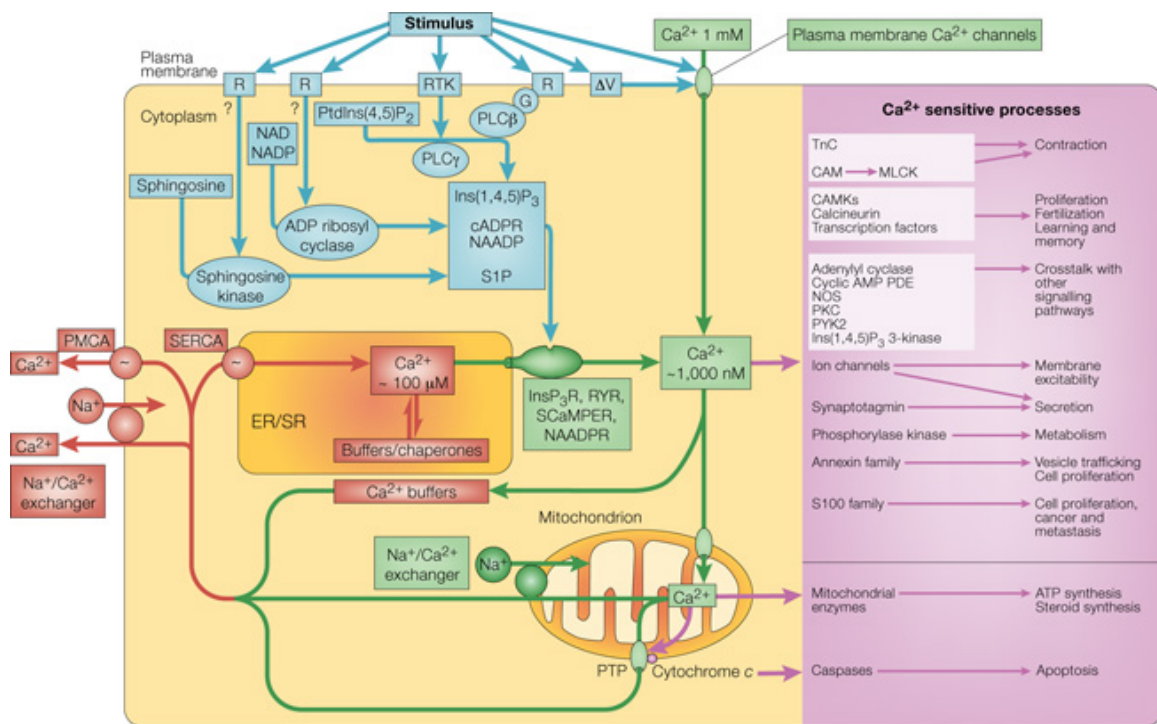


**Fig. 9: Elements of the  $\text{Ca}^{2+}$  signaling toolkit.** Cells have an extensive signaling toolkit that can be mixed and matched to create  $\text{Ca}^{2+}$  signaling of widely different properties.  $\text{Ca}^{2+}$ -mobilizing signals (blue) are generated by stimuli acting through a variety of cell-surface receptors, including G-protein (G)-linked receptors and receptor tyrosine kinase (RTK). The signals generated include: inositol-1,4,5-triphosphate ( $\text{IP}_3$ ), generated by the hydrolysis of phosphatidylinositol-4,5-bisphosphate ( $\text{PIP}_2$ ) by a family of phospholipase C enzymes ( $\text{PLC-}\beta$ ,  $\text{PLC-}\gamma$ ); cyclic ADP ribose (cADPR) and nicotinic acid dinucleotide phosphate (NAADP), both generated from nicotinamide-adenine dinucleotide (NAD) and its phosphorylated derivative NADP by ADP ribosyl cyclase; and sphingosine 1-phosphate (S1P), generated from sphingosine by a sphingosine kinase. ON mechanisms (green) include plasma membrane  $\text{Ca}^{2+}$  channels, which respond to transmitters or to membrane depolarization ( $\Delta V$ ), and intracellular  $\text{Ca}^{2+}$  channels—the  $\text{IP}_3$  receptor ( $\text{IP}_3\text{R}$ ), ryanodine receptor (RYP), NAADP receptor and sphingolipid  $\text{Ca}^{2+}$  release-mediating protein of the ER (SCaMPER). The  $\text{Ca}^{2+}$  released into the cytoplasm by these ON mechanisms activates different  $\text{Ca}^{2+}$  sensors (purple), which augment a wide range of  $\text{Ca}^{2+}$ -sensitive processes (purple), depending on cell type and context. OFF mechanisms (red) pump  $\text{Ca}^{2+}$  out of the cytoplasm: the  $\text{Na}^+/\text{Ca}^{2+}$  exchanger and the plasma membrane  $\text{Ca}^{2+}$  ATPase (PMCA) pumps  $\text{Ca}^{2+}$  out of the cell and the sarco-endoplasmic reticulum  $\text{Ca}^{2+}$  ATPase (SERCA) pumps it back into the ER/SR. (TnC, troponin C; CAM, calmodulin; MLCK, myosine light chain kinase; CAMK,  $\text{Ca}^{2+}$ /calmodulin-dependent protein kinase; cyclic AMP PDE, cyclic AMP phosphodiesterase; NOS, nitric oxide synthase; PKC, protein kinase C; PYK, proline-rich kinase 2; PTP, permeability transition pore.) (Reprinted by permission from Macmillan Publishers Ltd: *Nature reviews, Molecular cell biology* 1, 11-21, Berridge, M.J., Lipp, P. & Bootman, M.D., The versatility and universality of calcium signalling, 2000)

## 10. Roles of calcium signaling in tumor migration, invasion and metastasis

The ability to migrate is a prerequisite for cancer cells to escape the primary tumor and disseminate to metastatic sites, which makes a tumor difficult to be eradicated and causes mortality.<sup>39</sup> Polarized, migrating cells exhibit a stable and transient gradient of  $[Ca^{2+}]$ , increasing from the front of the cell to the rear for the rear-end retraction.<sup>90,91</sup> Such retraction is supported by myosin II contraction, which is regulated by  $Ca^{2+}$ -dependent MLC kinase (MLCK) mediated myosin light-chain (MLC) phosphorylation and the disassembly of adhesions at the rear of the cell. The coordinated and dynamic formation and disassembly of cell adhesions, known as focal adhesion turnover, with the ECM is necessary for cell migration. The components of focal adhesion complex are regulated by  $Ca^{2+}$  (Fig. 10). Furthermore, migration, invasion and metastasis of cancer cells involve multiple  $Ca^{2+}$  entry and release systems (Fig. 11).<sup>82</sup>

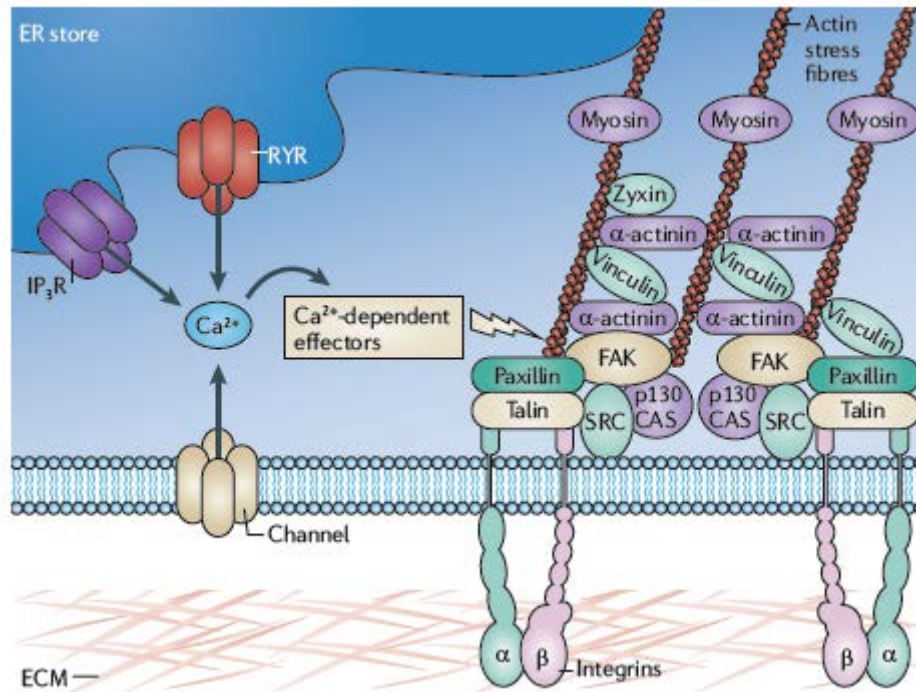


**Fig. 10: Molecular organization of focal adhesion complexes and their regulation by  $\text{Ca}^{2+}$ .** Integrins are  $\alpha$ - and  $\beta$ -transmembrane heterodimeric proteins that function as adhesion receptors and that span the cell plasma membrane to link the extracellular matrix (ECM) with the cytoskeleton through numerous intracellular molecules. The integrin-binding proteins paxillin and talin recruit focal adhesion kinase (FAK) and vinculin. Cytoskeleton protein  $\alpha$ -actinin is phosphorylated by FAK, binds to vinculin, crosslinks actomyosin stress fibers and tethers them to focal contacts. Zyxin is an  $\alpha$ -actinin and stress fiber-binding protein that is present in mature contacts. The membrane-associated protein tyrosine kinase SRC and the adaptor protein p130CAS associate with focal contacts following integrin clustering. Proteins that are transiently present at focal contacts, such as ERK2 and calpain, are not shown. Spatially confined sustained or transient increases of  $\text{Ca}^{2+}$  concentration can occur in the form of waves, sparks or flickers. Such increases can occur as a result of  $\text{Ca}^{2+}$  entry through plasma membrane  $\text{Ca}^{2+}$ -permeable channels and  $\text{Ca}^{2+}$  liberation from an endoplasmic reticulum (ER) calcium store through ryanodine (RyR) and/or inositol triphosphate ( $\text{IP}_3\text{R}$ ) receptor channels. These changes influence  $\text{Ca}^{2+}$ -dependent effectors (kinases, proteases and phosphatases), which in turn regulate focal adhesion components, this facilitating the formation or disassembly (that is, turnover) of focal adhesions. (Reprinted by permission from Macmillan Publishers Ltd: *Nature reviews, Cancer* 11, 609-618, Prevarskaya, N., Skryma, R. & Shuba, Y. Calcium in tumour metastasis: new roles for known actors, 2011)

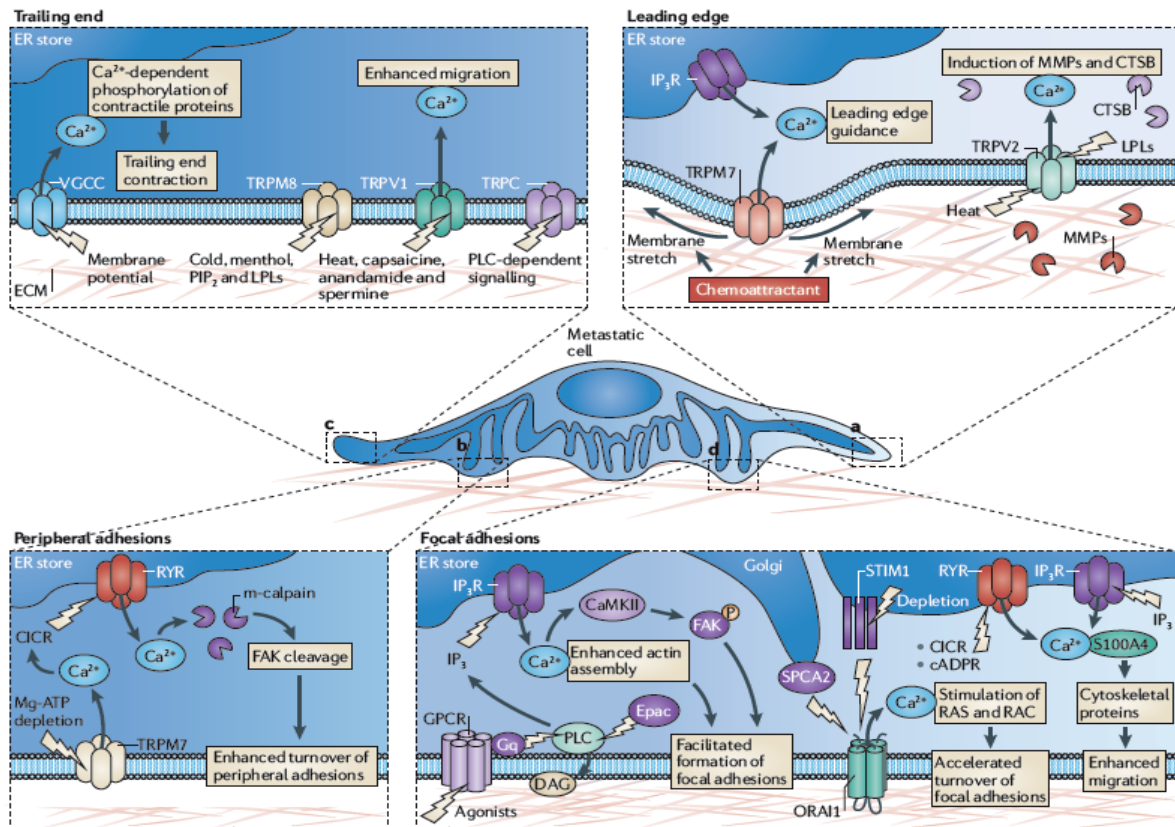


**Fig. 11: Major Ca<sup>2+</sup> entry and Ca<sup>2+</sup> release systems involved in migration, invasion and metastasis.** Different panels represent a magnified view of the events taking place within the areas of the migrating metastatic cell (shown in the middle of the figure). Lightning bolts indicate activating stimuli. At the leading edge (a) membrane stretch-activated, transient receptor potential cation channel subfamily M membrane 7 (TRPM7)-mediated Ca<sup>2+</sup> influx coupled to inositol triphosphate receptor (IP<sub>3</sub>R)-mediated Ca<sup>2+</sup> release participates in the guidance of the leading edge towards a chemoattractant. Ca<sup>2+</sup> influx through TRPV2 promotes migration by induction of key invasion markers, matrix metalloproteinase (MMP2), MMP9 and cathepsin B (CTSB). Activation of TRPM7 and associated Ca<sup>2+</sup> influx at peripheral adhesions (b) promotes m-calpain-mediated disassembly or turnover of peripheral adhesion complexes, thus contributing to enhanced motility. At the trailing end (c) Ca<sup>2+</sup> influx through L-type voltage-gated calcium channels (VGCCs) regulates contraction through Ca<sup>2+</sup>-dependent phosphorylation of contractile proteins, whereas certain types of Ca<sub>v</sub>3 VGCCs and TRP members, TRPC1, TRPM8 and TRPV1, are implicated in the enhanced migration of cancer cells through unknown effectors. Formation of focal adhesions (d) is facilitated by IP<sub>3</sub>R-mediated Ca<sup>2+</sup> release that is stimulated through surface G protein-coupled receptors (GPCRs) or exchange proteins directly activated by cAMP (EPAC) leading to Ca<sup>2+</sup>/calmodulin-dependent protein kinase II (CaMKII)-dependent focal adhesion kinase (FAK) phosphorylation or enhanced actin assembly, respectively, by stromal interaction molecule 1 (STIM1)-calcium release-activated calcium channel protein 1 (ORAI1)-based store-operated Ca<sup>2+</sup> entry, resulting in RAS and RAC activation and by secretory pathway Ca<sup>2+</sup>-ATPase (SPCA2)-ORAI1 complex-mediated constitutive Ca<sup>2+</sup> influx. IP<sub>3</sub>R- and ryanodine receptor (RYR)-mediated Ca<sup>2+</sup> mobilization from the endoplasmic reticulum (ER) stores also promotes cell migration in an S100A4-dependent manner. cADPR, cyclic ADP-ribose; CICR, Ca<sup>2+</sup>-induced Ca<sup>2+</sup> release; DAG, diacylglycerol; ECM, extracellular matrix; LPLs, lysophospholipids; PLC, phospholipase C. (Reprinted by permission from Macmillan Publishers Ltd: *Nature reviews, Cancer* 11, 609-618, Prevarskaya, N., Skryma, R. & Shuba, Y. Calcium in tumour metastasis: new roles for known actors, 2011)



## 11. Troponin C type I (TNNC1)

Troponin is a complex made up of 3 individual subunits: troponin C, troponin T and troponin I. Troponin C is a calcium-binding component of the troponin complex that triggers skeletal and cardiac muscle contraction in response to increasing calcium levels.<sup>92,93</sup> Under resting intracellular  $Ca^{2+}$  level, troponin and tropomyosin work together to block the myosin binding sites on actin. When calcium ions bind to troponin C, which leads to a conformational change in troponin I, the troponin-tropomyosin complex moves and release the blockage on the active sites. As soon as the myosin heads bind to the active sites, contraction begins.<sup>94</sup> Interestingly, troponin C also expresses in non-muscle cells<sup>93,95</sup> and various potential functions for cellular locomotion, cytoplasmic streaming, and cytokinesis have been reported.<sup>93</sup>

## 12. LIM-containing lipoma preferred partner (LPP)

The LPP gene, located at chromosome region 3q27-q28, is the preferred translocation partner of the HMGIC gene in a subclass of human benign mesenchymal tumors known as lipomas.<sup>96,97</sup> The N-terminal of the LPP contains two proline-rich stretches (DFLPPPPPLD and NFPPPPPLD) similar to the "FPPPP" motifs that are found in focal adhesion-associated proteins such as zyxin and vinculin, which are believed to be involved in actin cytoskeleton organization.<sup>98-101</sup> These proline-rich motifs are the interacting sequence with actin regulatory proteins of the VASP (Vasodilator-stimulated phosphoprotein) family. The C-terminal of LPP contains three cysteine and histidine rich LIM domains, which form zinc fingers that are capable of mediating protein-protein interactions.<sup>96,102-104</sup> LPP localizes at focal adhesions as well as at cell-to-cell contacts. It binds VASP and such binding is required for  $\alpha$ -actinin anchoring into detergent-insoluble cytoskeletal elements, suggesting that LPP may coordinate the actin regulatory activities of VASP and  $\alpha$ -actinin at cell-cell contacts.<sup>96,105</sup> In addition, LPP transiently localized in the nucleus and displayed transcriptional activation capacity, as measured by

GAL4-based assays. In fact, a nuclear export sequence (NES) was identified in the N-terminal region of LPP and deletion of the NES caused an accumulation of LPP in the nucleus.<sup>96,102</sup> Taken together, LPP is a multifunctional protein that serves a role in both actin cytoskeleton organization and gene regulation.

## Materials and Methods



## **1. Tissue samples, microdissection, RNA extraction, Affymetrix GeneChip hybridization, and image acquisition**

Ovarian tissue samples were obtained from the ovarian cancer repository of the Department of Gynecologic Oncology and Reproductive Medicine at The University of Texas MD Anderson Cancer Center under protocols approved by the MD Anderson Institutional Review Board. All tumor samples were obtained from the primary ovarian sites of pre-treatment cases. Microdissection was performed to isolate the stromal and epithelial components of normal and malignant ovarian tissue for RNA extraction. Tissue sections were first fixed in 70% ethanol and then stained with 1% methyl green to visualize the histologic features. During microdissection, the areas of interest in the tissue sections were carefully outlined. Areas with immune cell and blood vessel infiltration were excluded to minimize contamination. Purified RNA samples from microdissected tissue samples were amplified, labeled, and hybridized onto GeneChip Human Genome U133 Plus 2.0 microarrays (Affymetrix Inc., Santa Clara, CA) according to the manufacturer's protocol. After hybridization, arrays were washed and stained using a Fluidics Station 450 and then scanned using a GeneChip Scanner 3000 7G (Affymetrix Inc., Santa Clara, CA).

## **2. Cell lines and culture conditions**

Human ovarian adenocarcinoma cell lines A224, ALST, OVCA432, and SKOV3ipluc were maintained in RPMI 1640 medium supplemented with 10% fetal bovine serum, 2 mM glutamine, and penicillin/streptomycin (Life Technologies Corp., Grand Island, NY). The immortalized human normal ovarian fibroblast (NOF) cell line NOF151-hTERT and primary CAF cells were cultured in 1:1 MCDB105/199 medium supplemented with 10% fetal bovine serum, 10 ng/ml epidermal growth factor, and penicillin/streptomycin. Human microvascular endothelial cells, hMEC-1, were cultured in MCDB131 medium supplemented with 10% fetal

bovine serum, 10 mM L-glutamine, 10 ng/ml epidermal growth factor, 1 µg/mL hydrocortisone and penicillin/streptomycin. Telomerase-immortalized microvascular endothelial cells, TIME, were cultured in EGM-2 medium (Lonza Group Ltd., Basel, Switzerland).

### 3. Quantitative real-time PCR analysis

The relative expression of each target gene was calculated using the  $2^{-\Delta\Delta C_T}$  method to average the  $C_T$  value of the housekeeping gene for a single reference gene value. Pre-designed human MFAP5 (Hs00185803\_m1), TNNC1 (Hs00896999\_g1), LPP (Hs00944352\_m1), cyclophilin A (Hs99999904\_m1), and murine Mfap5 (Mm00489404\_m1) TaqMan gene expression assays (Life Technologies Corp., Grand Island, NY) were used in quantitative real-time PCR analyses.

### 4. Western blot analysis

Protein lysates from CAFs, NOFs, ovarian cancer cells and microvascular endothelial cells were separated on 10% sodium dodecyl sulfate NuPAGE gels under denaturing conditions and transferred onto nitrocellulose membranes using an iBlot Western blotting system (Life Technologies Corp., Grand Island, NY) before being incubated with primary antibodies. Anti-human MFAP5 (#HPA010553) was purchased from Sigma-Aldrich (St. Louis, MO). An anti-p-FAK antibody (Y861; #44-626G) was purchased from Life Technologies Corp. (Grand Island, NY). All other antibodies, including anti-FAK (#3285), anti-PLC- $\gamma$ 1 (#2822), anti-p-PLC- $\gamma$ 1 (T783; #2821), anti-PKC $\theta$  (#2059), anti-p-PKC $\theta$  (T538; #9377), anti-ERK1/2 (#9102), anti-p-ERK1/2 (T202/204; #9101), anti-CREB (#9197), anti-p-CREB (S133; #9198), anti-c-Jun (#9165), anti-p-cJun (S63, S73, and S243; #2361, #9164, and #2994), anti-MLC2 (#8505), anti-p-MLC2 (T18/S19; #3674), and LPP (#3389) were purchased from Cell Signaling Technology

Inc. (Beverly, MA). After being washed with Tris-buffered saline with Tween, the membranes were incubated with a goat anti-rabbit IR dye-conjugated secondary antibody (LI-COR Biosciences, Lincoln, NE). Protein bands were detected using an Odyssey infrared imaging system (LI-COR Biosciences, Lincoln, NE). Relative normalized protein expression levels with respect to the corresponding control were calculated based on the band intensity values measured using the ImageJ software program (National Institutes of Health, Bethesda, MD).

The inhibitors used in pathway analyses included a PLC inhibitor (U73122; #sc-3574), PKC $\theta$  pseudosubstrate inhibitor (#sc-3097), and ERK inhibitor II (FR180204; #sc-203945), which were purchased from Santa Cruz Biotechnology (Santa Cruz, CA). FAK inhibitors (SU6656; #S9692 and PF-573228; #PZ0117) and a c-Jun inhibitor (#SP600125) were purchased from Sigma-Aldrich Co. (St. Louis, MO), and a CBP/CREB interaction inhibitor (#217505) was purchased from EMD Millipore Corp. (Billerica, MA).

## 5. Immunohistochemical analysis

Immunolocalization of MFAP5 and TNNC1 was performed using 130 and 107 FFPE HGSOE tissue sections, respectively. Tissue sections were stained with commercially available anti-MFAP5 (1:500; #HPA010553) and anti-TNNC1 (1:100; #WH0007134M1) antibodies (Sigma-Aldrich Co., St. Louis, MO). Target protein expression was visualized using a Betazoid 3,3'-diaminobenzidine or a Warp Red chromogen kit (Biocare Medical, Concord, CA).

To quantify target protein expression in the FFPE sections, slides were scored according to the staining intensity and percentage of MFAP5- and TNNC1- positive cells. To quantify stromal MFAP5 expression, the expression scores were calculated by multiplying the staining intensity (range, 0-3) by the percentage of stroma with MFAP5-positive staining. Similarly, TNNC1 tumor expression scores were based on tumor TNNC1 staining intensity and percentage tumor cells stained TNNC1-positive.

## 6. CAF-derived MFAP5-stimulated motility of ovarian cancer cells

CAF793092 cells were seeded onto a 24-well plate at a density of  $5 \times 10^4$  cells/ well. The culture medium was then removed from the plate, and cells were washed with phosphate-buffered saline (PBS) the next day. Serum-free M105/199 media supplemented with 1 ng/ml epidermal growth factor and 10  $\mu\text{g/ml}$  of one of the following antibodies: 1) control IgG (EMD Millipore Corp., Billerica, MA), 2) anti-MFAP5 antibody (#HPA010553; Sigma-Aldrich, St. Louis, MO), 3) anti- $\alpha_v\beta_3$  antibody (#MAB1976Z; EMD Millipore Corp., Billerica, MA) and 4) anti- $\alpha_5$  antibody (#555615; BD Biosciences, San Jose, CA) was added to the wells. 72 hours later,  $5 \times 10^4$  A224 or ALST cells were seeded onto each of the 8  $\mu\text{m}$  porous cell culture inserts (BD Biosciences, San Jose, MA) in the serum-free medium and co-cultured with CAFs pre-incubated with antibodies. After 15 hours of co-culture, cancer cells were stained with calcein AM (Life Technologies Corp., Grand Island, NY). While non-migrated cancer cells in the cell culture inserts were removed, the number of cancer cells migrated through the 8  $\mu\text{m}$  pores were quantified by obtaining images of the stained cells from nine random fields of view per membrane using fluorescent microscopy and the Image-Pro Plus 7.0 software program (Media Cybernetics Inc., Rockville, MD).

## 7. Recombinant MFAP5-increased ovarian cancer cell motility

OVCA432 cells were seeded onto chamber slides in 10% serum RPMI medium. Attached cells were washed with PBS, followed by the addition of serum-free RPMI medium with or without 500 ng/ml recombinant MFAP5 protein (recMFAP5). The cells were then placed in an imaging chamber maintained at 37°C and supplemented with 5% CO<sub>2</sub>. Cell images were taken every 15 minutes for 48 hours using confocal microscopy and the resulting series of

images were analyzed by the MetaMorph Image Analysis software program (Molecular Devices Inc., Sunnyvale, CA) to track the movement of individual cells.

To confirm exogenous MFAP5's effects on ovarian cancer cell motility, motility assay was performed using Boyden chambers with two additional ovarian cancer cell lines: A224 and ALST. Serum-free RPMI medium with or without 50 ng/ml recMFAP5 was incubated with 10 µg/ml control IgG or anti-MFAP5, anti- $\alpha$ V $\beta$ 3, or anti- $\alpha$ 5 antibodies for 1 hour in the wells of 24-well plates. After pre-incubation of medium, A224 or ALST cells ( $5 \times 10^4$ ) were then seeded onto each 8 µm porous cell culture insert (BD Biosciences, San Jose, MA) with serum-free medium and placed into the 24-well plate containing the pre-incubated cell culture medium and incubated for 15 hours. At the end of the experiment, non-migrated cancer cells in the cell culture inserts were removed and the number of cancer cells migrated through the 8 µm pores were quantified by obtaining images of the stained cells from nine random fields of view per membrane using fluorescent microscopy and the Image-Pro Plus 7.0 software program (Media Cybernetics Inc., Rockville, MD)

To evaluate the role of calcium and TNNC1 in cell motility induced by MFAP5, ovarian cancer cells were pretreated with the cell-permeant calcium chelator BAPTA/AM (B-6769; Life Technologies Corp., Grand Island NY) at a concentration of 10 µM for 1 hour or transfected with efficiency-evaluated TNNC1-specific siRNA (Silencer Select# s14271, s224742, s224743; Life Technologies Corp., Grand Island NY) before performing the motility assay.

## **8. Recombinant MFAP5-increased microvascular endothelial cell motility**

To evaluate the role of MFAP5 in angiogenesis, motility assay was performed using Boyden chambers with two microvascular endothelial cell lines: hMEC-1 and TIME. Serum-free MCDB131 and EBM-2 medium with or without 50 ng/mL recMFAP5 was incubated with 10

$\mu\text{g/ml}$  control IgG or anti-MFAP5, anti- $\alpha_v\beta_3$ , or anti- $\alpha_5$  antibodies for 1 hour in the wells of 24-well plates.  $8 \times 10^4$  hMEC-1 or TIME cells were then seeded onto each 3  $\mu\text{m}$  or 8  $\mu\text{m}$  porous cell culture insert respectively (BD Biosciences, San Jose, MA) with serum-free medium and placed into the 24-well plate containing the pre-incubated cell culture medium. After a 4 hours incubation period, endothelial cells were stained with calcein AM (Life Technologies Corp., Grand Island, NY). Non-migrated cancer cells in the cell culture inserts were removed and the number of endothelial cells migrated through the pores were quantified by obtaining images of the stained cells from nine random fields of view per membrane using fluorescent microscopy and the Image-Pro Plus 7.0 software program (Media Cybernetics Inc., Rockville, MD)

To evaluate the role of calcium and LPP in cell motility induced by MFAP5, microvascular endothelial cells were pretreated with the cell-permeant calcium chelator BAPTA/AM (B-6769; Life Technologies Corp., Grand Island NY) at a concentration of 10  $\mu\text{M}$  for 1 hour or transfected with efficiency-evaluated LPP-specific siRNA (Silencer Select #s8271, s8269; Life Technologies Corp., Grand Island NY) before performing the motility assay.

## **9. MFAP5-stimulated ovarian cancer cell and microvascular endothelial cell invasion**

The invasion potential of ovarian cancer cells and microvascular endothelial cells treated with recMFAP5 were evaluated using a Matrigel invasion assay with BD BioCoat Matrigel invasion chambers (BD Biosciences, San Jose, CA) according to the manufacturer's protocol. In brief,  $3 \times 10^4$  A224 / ALST cancer cells or  $5 \times 10^4$  hMEC-1 / TIME endothelial cells were seeded onto an 8  $\mu\text{m}$  porous BD BioCoat Matrigel invasion chamber in serum-free medium and inserted into a BD Falcon TC companion plate with or without 200 ng/ml recMFAP5. Ovarian cancer cells and microvascular endothelial cells were incubated at 37°C for 15 hours and 4 hours respectively. After incubation, cells were then stained with calcein AM, and non-invaded cells in the cell culture inserts were removed. The number of cancer and

endothelial cells invaded through the Matrigel coated porous membrane were quantified by obtaining images of the stained cells from nine random fields of view per membrane using fluorescent microscopy and the Image-Pro Plus 7.0 software program (Media Cybernetics Inc., Rockville, MD).

#### **10. Recombinant MFAP5-induced endothelial barrier disruption and increased permeability of endothelial cell monolayer**

$1 \times 10^4$  hMEC1 or TIME cell were seeded onto each well of E-plate of the xCELLigence system (Roche Applied Bioscience, Indianapolis, IN) and incubated at 37°C for 24 hours to obtain confluent monolayer endothelial cell culture. On the next day, cell culture media in the wells were replenished with serum-free MCDB131 or EBM-2 medium with or without 200ng/mL recMFAP5. Electrical impedance generated by the monolayer endothelial cells sitting on gold electrodes was measured throughout the course of the experiment by the real-time cell analyzer (RTCA) as cell index (CI). Decrease in cell adhesion or monolayer integrity would be indicated by a drop of CI value.

*In vitro* monolayer permeability assay was also performed to verify the observation by the xCELLigence system. 20 mg/mL of FITC-dextran (relative molecular mass 70,000; Sigma-Aldrich Corp. St. Louis, MO) was added to the confluent hMEC-1 or TIME monolayers seeded onto 0.4  $\mu\text{m}$  porous cell culture inserts in the presence or absence of 200 ng/mL recombinant MFAP5. The appearance of fluorescence in the bottom wells of the Boyden Chambers were monitored by analyzing 40  $\mu\text{L}$  medium aliquots in a time course using a FLUO-star Omega microplate reader (BMG Labtech Inc., Cary, NC). The passage of FITC-dextran through the endothelial cell monolayer culture was used to assess the permeability and integrity of the monolayer culture.

## 11. Tube formation assay

100  $\mu$ L of growth factor reduced BD Matrigel (BD Biosciences, San Jose, CA) supplemented with 200 ng/mL recMFAP5, 500 ng/mL recMFAP5 or PBS was coated onto each well of pre-chilled 24-well plate. The 24-well plate was then incubated at 37°C for 1 hour to allow the Matrigel to solidify. After that,  $5 \times 10^4$  hMEC-1 or TIME cells were resuspended in 1 mL of serum free MCDB131 or EBM-2 medium and seeded onto each well of the 24-well plate coated with growth factor reduced BD Matrigel. The assay plate was then incubated at 37°C for 4 hours before the cells were stained with calcein AM (Life Technologies Corp., Grand Island, NY). Endothelial tube formation was examined using a fluorescent microscope and the extent of tube formation among different experimental groups was quantified and compared by using the Angiogenesis module of the Leica MetaMorph Image Analysis software program (Molecular Devices Inc., Sunnyvale, CA).

## 12. *In vivo* angiogenesis assay

*In vivo* angiogenesis assay was performed as previously described.<sup>106,107</sup> 500  $\mu$ L of Matrigel alone or Matrigel supplemented with one of the following: 1) 150 ng/mL basic fibroblast growth factor (bFGF), 2) 200 ng/mL recMFAP5 or 3) 500 ng/mL recMFAP5 was injected subcutaneously into nude mice. When warmed to body temperature, Matrigel polymerizes to form subcutaneous plugs. After 5 days, the mice were sacrificed and Matrigel plugs were excised, fixed in 10% formalin, embedded in paraffin and sectioned. Paraffin sections were stained with anti-CD34 antibody (#GTX28158; GeneTex Inc., Irvine, CA). The extent of tube formation among different experimental groups was quantified and compared using the angiogenesis module of the MetaMorph Image Analysis software program (Molecular Devices Inc., Sunnyvale, CA).



### 13. Derivation of MFAP5-overexpressing NOFs

The telomerase-immortalized human NOF cell line NOF151-hTERT was transduced with lentiviruses packaged with the human MFAP5 open reading frame (#EX-D0360-Lv105; GeneCopoeia, Rockville, MD). Stably transduced cells were selected using complete medium supplemented with 1 µg/ml puromycin for 5 days. MFAP5 overexpression in stably transduced NOFs was validated by Western blot analysis, in which the cell lysate and conditioned medium from the resultant NOF cell line NOF151-LvMFAP5 were compared with those from the mock-transduced control cell line. A proliferation assay was performed using the xCELLigence system (Roche Applied Bioscience, Indianapolis, IN) to ensure that the NOF151-LvMFAP5 and NOF151-hTERT cells had similar growth rates.

### 14. MFAP5 overexpressing fibroblast-stimulated ovarian cancer cell migration and invasion *in vivo*

5 x 10<sup>4</sup> control NOF151 cells or MFAP5-overexpressing NOF151 (NOF151-LvMFAP5) cells resuspended in one part of PBS was mixed with two parts of Matrigel. 500 µL of the resultant cell suspension was injected into the intraperitoneal cavity of anesthetized nude mice and was allowed to form a Matrigel plug attached to the peritoneal wall. On the next day, 1 x 10<sup>6</sup> A224 or OVCA432 cells were injected intraperitoneally into the Matrigel plug bearing mice. Matrigel plugs were harvested from A224- and OVCA432-injected mice at 48 and 72 hours post cancer cell injection respectively. The resected plugs were fixed in formalin and processed for cancer cell migration, invasion and histological evaluation.

## **15. Fibroblast-derived MFAP5 enhanced intratumoral microvessel formation and ovarian tumor growth**

$2 \times 10^6$  of luciferase expressing A224 ovarian cancer cells were injected or co-injected with  $2 \times 10^6$  of either NOF151-LvMFAP5 or the mock transduced NOF151 cells in PBS into each nude mouse subcutaneously. 10 mice were included in each of the control or treatment groups. Five days after cell injection, tumor progression was monitored and quantified by luciferase based imaging using the IVIS® -200 bioluminescence and fluorescence imaging system. (Caliper Life Sciences, Inc., Hopkinton, MA). At day 12, all mice were sacrificed and weighted. The tumor collected were fixed in formalin and processed for histological evaluation.

## **16. Stromal MFAP5 silencing reduced intratumoral microvessel formation and ovarian tumor progression**

$2 \times 10^6$  luciferase expressing A224 ovarian cancer cells resuspended in one part of PBS and two parts of Matrigel were injected intraperitoneally into nude mice. 10 mice were randomized into each of the control and treatment groups. One week after cancer cell injection, chitosan nanoparticles packaged with either 5  $\mu$ g non-targeting scrambled siRNA, mouse mfap5-targeting siRNA 68 or siRNA 69 were injected intravenously into each mouse of the corresponding group at the frequency of twice per week, for 5 weeks. Tumor progression was monitored and quantified by luciferase based imaging using the IVIS® -200 bioluminescence and fluorescence imaging system (Caliper Life Sciences, Inc., Hopkinton, MA). At the end of the experiment, all animals were sacrificed and tumor tissues were harvested. Weights of tumor tissues were recorded, followed by formalin fixation and paraffin tissue block preparation.

## **17. Murine stromal Mfap5 silencing reduced ovarian tumor growth and metastasis *in vivo***

Luciferase labeled OVCA432ip ovarian cancer cells were suspended in 50 µl of Hanks' balanced salt solution and injected directly into the left ovary of anesthetized nude mice through a 1.5 cm incision. One week after tumor cell injection, chitosan nanoparticles packaged with Mfap5-targeting siRNA or non-targeting siRNA were injected intravenously into nude mice twice a week for a total of 7 weeks. 6 weeks after initial injection, tumor progression of each treatment group was quantified by luciferase based imaging using the IVIS® -200 bioluminescence and fluorescence imaging system (Caliper Life Sciences, Inc., Hopkinton, MA). At week 8, animals were sacrificed and necropsy was performed. The number, weight, and location of individual tumor nodules were recorded. Tumor tissues were fixed in formalin and further processed for histological evaluation.

## **18. Transcriptome profiling to identify signaling mechanism underlying MFAP5's effect on ovarian cancer and microvascular endothelial cells**

Total RNA were isolated from OVCA432 cells treated with PBS or 200 ng/ml recMFAP5 and mouse endothelial cells invaded into the recMFAP5 containing Matrigel plugs obtained from the *in vivo* angiogenesis assay. 100 ng of total RNA from each group were used to generate biotin-labeled RNA using the MessageAmp Premier RNA amplification kit (Life Technologies Corp., Grand Island NY) according to the manufacturer's protocol. Biotin-labeled RNA samples from human cancer cells and mouse endothelial cells were then subjected to whole-genome transcriptome profiling using the GeneChip Human Genome U133 Plus 2.0 microarrays and the Genechip mouse genome 430 2.0 array (Affymetrix Inc., Santa Clara, CA) respectively. Differentially expressed genes with expression levels at least 1.5-fold higher than

those of the corresponding controls ( $p < 0.05$ ) were selected for further analyses using the Ingenuity Pathway Analysis software program (Qiagen, Valencia, CA).

### **19. MFAP5 stimulates calcium-dependent F-actin rearrangement**

$5 \times 10^4$  A224, ALST, hMEC-1 or TIME cells were seeded onto 8-well Lab-Tek chamber slides (Thermo Fisher Scientific, Pittsburgh, PA) and serum fasted for 24 hours. After serum starvation, ovarian cancer cells and microvascular endothelial cells were then treated with fresh serum-free medium supplemented with or without 200 ng/ml recMFAP5. After a 24 hours and 4 hours incubation for cancer cells and endothelial cells respectively, cells were fixed with 3.7% formaldehyde and stained with Alexa Fluor 594 phalloidin (Life Technologies Corp., Grand Island, NY) according to the manufacturer's instructions to visualize the F-actin cytoskeleton. Fluorescent microscopy was used to evaluate the MFAP5-induced F-actin cytoskeleton rearrangement in cells.

To evaluate the role of calcium in MFAP5-induced F-actin cytoskeleton rearrangement, ovarian cancer cells and microvascular endothelial cells were pretreated with the cell-permeant calcium chelator BAPTA/AM (B-6769; Life Technologies Corp., Grand Island, NY) for 1 hour before MFAP5 treatment and staining with Alexa Fluor 594 phalloidin. To study the effect of TNNC1 and LPP in F-actin reorganization induced by MFAP5, ovarian cancer cells and microvascular endothelial cells were transfected with TNNC1-specific and LPP-specific siRNA, respectively, before MFAP5 treatment and staining with Alexa Fluor 594-phalloidin.

### **20. Protein fractionation and Western blot analysis of TNNC1 expression in TNNC1 siRNA-transfected cell lines**

Knockdown of TNNC1 protein expression in A224 and ALST cells by siRNA transfection

was confirmed by Western blot analysis. Prior to this analysis, cell pellets were collected from non-targeting scrambled siRNA and TNNC1-targeting siRNA-transfected A224 and ALST cells. Cytoplasmic protein fractions of the protein samples were obtained using the NE-PER nuclear and cytoplasmic extraction reagents (Thermo Fisher Scientific Inc., Waltham, MA) according to the manufacturer's protocol. A polyclonal rabbit anti-human TNNC1 antibody (13504-1-AP; Proteintech, Chicago, IL) was used to determine TNNC1 expression levels in the cytoplasmic protein fractions by Western blot analysis.

## 21. Traction force microscopy

The cell traction force exerted on a flexible substrate impregnated with fluorescent microspheres by A224, ALST or hMEC-1 cells was determined according to measured substrate displacements using the LIBTRC analysis library developed by Dr. Micah Dembo of Boston University.<sup>108-110</sup> In brief, polyacrylamide gel (5% acrylamide and 0.1% Bis-acrylamide, thickness = 75  $\mu\text{m}$ ; Young's modulus = 28  $\text{kN/m}^2$ ) was prepared on glass coverslips with fluorescent microspheres (0.2  $\mu\text{m}$  diameter, yellow-green FluoSpheres; Life Technologies) impregnated under the surface. The surface was then coated with 0.2 mg/ml collagen type I (BD Biosciences, San Jose, CA) after photoactivation of the surface molecular linker sulfosuccinimidyl-6-(4'-azido-2'-nitrophenylamino) hexanoate (sulfo-SANPAH; Pierce Chemical, Dallas, TX). Cells were then seeded and cultured overnight on the prepared substrate. To evaluate the effect of exogenous MFAP5 on the traction force exerted by cancer cells on the substratum, cancer cells were treated with exogenous recMFAP5 and a series of images of individual cancer cells were captured during the course of the experiment. A background image of the fluorescent beads was also taken after the cells were removed from the substrate. The LIBTRC library was then used to track the displacement of microspheres and compute the cell traction force. All images were collected using a TCS SP5 confocal microscope (Leica

Microsystems, Buffalo Grove, IL).

## **22. [Ca<sup>2+</sup>]<sub>i</sub> measurement**

A224, ALST or hMEC-1 cells that grew on collagen-coated Petri dishes with glass bottoms were loaded with Fluo-4 AM in Hank's balanced salt solution for 30 minutes followed by 20 minutes to de-esterify the dye. Fluo-4 AM was excited at 488 nm, and its emission was collected using a bandpass filter at 522/35 nm. Fluorescent images of the cells were collected using a Leica TCS SP5 confocal microscope at 0.25 Hz. Calcium mobilization in cells was quantified by measuring Fluo-4 AM fluorescent signal.

## **23. Immunofluorescence labeling of LPP and focal adhesion markers**

5 x 10<sup>4</sup> hMEC-1 or TIME cells were seeded onto 8-well Lab-Tek chamber slides (Thermo Fisher Scientific, Pittsburgh, PA) and serum fasted for 24 hours. After serum starvation, cells were treated with fresh serum-free medium supplemented with or without 200 ng/ml recMFAP5 for 24 hours. After incubation, cells were fixed with 3.7% formaldehyde and stained with an anti-LPP antibody (1:100; Cell Signaling Technology Inc., Beverly, MA) or an anti-Vinculin antibody (1:100; Life Technologies Corp., Grand Island, NY) at room temperature for 2 hours followed by a 1-hour incubation with the Alexa Fluor-488 Goat Anti-mouse IgG antibody (1:1000; Life Technologies Corp., Grand Island, NY). Slides were then mounted using the ProLong Diamond Antifade Mountant (#P36961, Life Technologies Corp., Grand Island, NY) and fluorescent microscopy was performed to evaluate the expression level and localization of LPP and Vinculin in endothelial cells.

To determine whether MFAP5-induced LPP expression localized at the focal adhesion complexes of endothelial cells, immunolocalization of LPP and one of the following focal

adhesion markers: 1) Vinculin, 2) Paxillin and 3) FAK, was performed by sequential immunostaining using an anti-LPP antibody (1:100; Cell Signaling Technology Inc., Beverly, MA) followed by staining with anti-Vinculin antibody (1: 100; #700062; Life Technologies Corp., Grand Island, NY), anti-Paxillin antibody (1:50; #AF4259; R&D Systems Inc., Minneapolis, MN) or anti-FAK antibody (1:100; #3285; Life Technologies Corp., Grand Island, NY).

To evaluate the role of LPP in focal adhesion formation induced by MFAP5, microvascular endothelial cells were transfected with LPP-specific siRNA, before MFAP5 treatment and staining with anti-LPP antibody and anti-Vinculin antibody.

#### **24. Monoclonal anti-mfap5 antibody attenuated ovarian cancer cell and microvascular endothelial cell motility**

Immortalized normal ovarian fibroblasts, NOF151, or MFAP5 overexpressing fibroblasts, NOF151 LvMFAP5, were seeded onto each well of a 24-well plate ( $1 \times 10^5$  cells /well) in serum-free medium and incubated at 37°C for 3 days. After that, fibroblasts were incubated with 10 µg/mL of control mouse IgG, anti-MFAP5 monoclonal antibody clone 64A or clone 117B for 1 hour. After incubation,  $5 \times 10^4$  hMEC-1 or TIME endothelial cells were seeded onto each 8 µm porous cell culture insert (BD Biosciences, San Jose, MA) in serum-free medium and incubated with the control fibroblasts or MFAP5-overexpressing fibroblasts in the presence of IgG or anti-MFAP5 antibody for 4 hours. Similarly,  $5 \times 10^4$  A224 or ALST ovarian cancer cells in 8 µm porous cell culture inserts were incubated with fibroblasts for 15 hours. To visualize cell migration, endothelial and cancer cells were stained with calcein AM (Life Technologies Corp., Grand Island, NY). Non-migrated cells in the cell culture inserts were removed and the number of cells migrated through the porous cell culture membrane were quantified by obtaining images of the stained cells from nine random fields of view per membrane using fluorescent microscopy and the Image-Pro Plus 7.0 software program (Media

Cybernetics Inc., Rockville, MD).

To evaluate the inhibitory effect of anti-mfap5 antibody clone 130A on mouse endothelial cell motility, motility assay was performed using Boyden chambers with a SV40-transformed mouse endothelial cell line: SVEC4-10 (ATCC; #CRL-2181). Serum-free medium with or without 100ng/mL recombinant mouse mfap5 was pre-incubated with 10 µg/ml control IgG or anti-mfap5 antibody clone 130A for 1 hour in the wells of a 24-well plates. After antibody pre-incubation, 8 µm porous cell culture inserts (BD Biosciences, San Jose, MA) were placed in each of the wells and  $5 \times 10^4$  SVEC4-10 cells were seeded onto the cell culture inserts in serum-free medium and incubated for 4 hours. To visualize cell migration, endothelial and cancer cells were stained with calcein AM (Life Technologies Corp., Grand Island, NY). Non-migrated cells in the cell culture inserts were removed and the number of cells migrated through the porous cell culture membrane were quantified by obtaining images of the stained cells from nine random fields of view per membrane using fluorescent microscopy and the Image-Pro Plus 7.0 software program (Media Cybernetics Inc., Rockville, MD).

## **25. Clone 130A anti-mfap5 antibody suppressed ovarian tumor growth *in vivo***

To study the inhibitory effects of anti-MFAP5 monoclonal antibodies on ovarian tumor progression *in vivo*,  $3 \times 10^6$  luciferase-labeled OVCA432 cells were I.P. injected into nude mice. 1 week after tumor cell injection, mice randomized into the treatment and control group (N=12 per group) were injected twice weekly with 15 mg/kg of anti-MFAP5 antibodies clone 130A and 15 mg/kg of control normal mouse IgG respectively for a total of 6 weeks. During the course of the experiment, tumor progression was monitored by the IVIS® -200 bioluminescence and fluorescence imaging system (Caliper Life Sciences, Inc., Hopkinton, MA)., 100 µL of 10 mg/mL FITC-dextran (relative molecular mass 200,000; Sigma-Aldrich Corp. St. Louis, MO) was injected via tail vein into mice before the mice were sacrificed for the later evaluation of vessel



leakiness. Tumor weight was recorded to evaluate tumor progression and 6 µm frozen tissue sections were prepared from tumor tissues harvested using the Leica CM1850 cryostat (Leica Microsystems, Buffalo Grove IL) for the evaluation of the effect of anti-mfap5 antibody on intratumoral microvessel leakiness by fluorescent microscopy.

## **26. Anti-mfap5 antibody clone 130A increased paclitaxel bioavailability in ovarian tumor tissues**

10 nude mice were intraperitoneally injected with  $3 \times 10^6$  luciferase-labeled OVCA432 cells. At 1 week after cancer cell injection, tumor bearing animals were I.P. injected with 15 mg/kg of control normal mouse IgG or anti-mfap5 antibody clone 130A twice weekly for a total of 4 weeks. 1 mg/kg of Oregon Green 488-conjugated paclitaxel (Life Technologies Corp., Grand Island, NY) was I.V. injected into each of the animals at 1 hour before they were sacrificed. Tumor weight was recorded and 6 µm frozen tissue sections were prepared from tumor tissues harvested using the Leica CM1850 cryostat (Leica Microsystems, Buffalo Grove IL) to evaluate the effects of anti-mfap5 antibody on the bioavailability of paclitaxel.

## **27. Toxicity test on anti-MFAP5 antibodies**

Nude mice were treated with anti-MFAP5 antibody clones 64A, 117B or 130A for the experimental groups and PBS for the control group (N=3 per group) twice weekly for 2 weeks. Complete blood count (CBC) and chemistry panel were performed to measure the levels of 1) albumin, 2) alkaline phosphatase (ALP), 3) alanine aminotransferase (ALT), 4) aspartate aminotransferase (AST), 5) blood urea nitrogen (BUN), 6) creatinine, 7) globulin and 8) total proteins in serum samples collected. In addition, H&E stained tissue sections were examined to

evaluate and identify the possible organ or tissue toxicity due to treatment of anti-MFAP5 antibodies.

## **28. Statistical analysis**

The SPSS 19 (IBM Corp., Armonk, NY) and Prism 5.0 (GraphPad Software, La Jolla, CA) software programs were used to perform statistical tests. All *in vitro* experiments were repeated independently in triplicate. A two-tailed Student *t*-test was used to determine differences in sample means for data with normally distributed means. The Mann-Whitney *U* test was used for analysis of nonparametric data. A p-value less than 0.05 was considered statistically significant.

## **29. Accession numbers**

Data files from the transcriptome profiling analysis were deposited in the Gene Expression Omnibus (GEO; National Center for Biotechnology Information, Bethesda, MD). Transcriptome profiling data for microdissected ovarian tissue samples was assigned the GEO accession number GES40595, and microarray data for MFAP5-treated OVCA432 cells was assigned the GEO accession number GES40643.

## Results

**Specific aim I: The role of CAF derived MFAP5 on ovarian cancer cell growth, motility and invasion potential**

This section is based upon Leung, C.S., Yeung, T.L., Yip, K.P., Pradeep, S., Balasubramanian, L., Liu, J., Wong, K. K., Mangala, L.S., Armaiz-Pena, G. N., Lopez-Berestein, G., Sood, A.K., Birrer, M. J., Mok, S. C., Calcium-dependent FAK/CREB/TNNC1 signalling mediates the effect of stromal MFAP5 on ovarian cancer metastatic potential. *Nature communications* 5, 5092 (2014). doi: 10.1038/ncomms6092, used with permission.

## A. Ovarian cancer associated fibroblasts express high levels of MFAP5

The stromal microenvironment is known to provide a niche that supports tumor growth.<sup>2</sup> To identify mediators produced by the stromal microenvironment that support ovarian tumor growth, transcriptome profiling was performed with RNA extracted from microdissected stromal and epithelial components of ovarian tumor tissues, which included tumor epithelial components (N=33), normal ovarian surface epithelial (OSE) cells (N=6), stromal CAFs (N=33) and normal stromal fibroblasts (N=8). Microdissection was performed as previously described (Fig. 12).<sup>111</sup> Areas with immune cell and blood vessel infiltration were excluded to minimize contamination. Among the differentially expressed genes, we identified 19 upregulated secretory protein coding genes in the stromal component of HGSOE samples (Fig. 13 and Table 1). Microfibrillar-associated protein 5 (MFAP5), which we have shown to be amplified and overexpressed in a subset of ovarian cancer cells,<sup>75</sup> was selected for further validation. Validation by quantitative real-time PCR revealed significantly higher levels of MFAP5 mRNA expression in the cancer stroma than the epithelial components and normal ovarian stroma (Fig. 14). Immunohistochemistry also revealed higher level of MFAP5 protein expression in the cancer-associated stroma, particularly in CAFs, than in ovarian cancer cells (Fig. 15). Western blot analysis confirmed a higher endogenous level of MFAP5 in ovarian CAFs when compared to normal fibroblasts and ovarian cancer cell lines (Fig. 16).

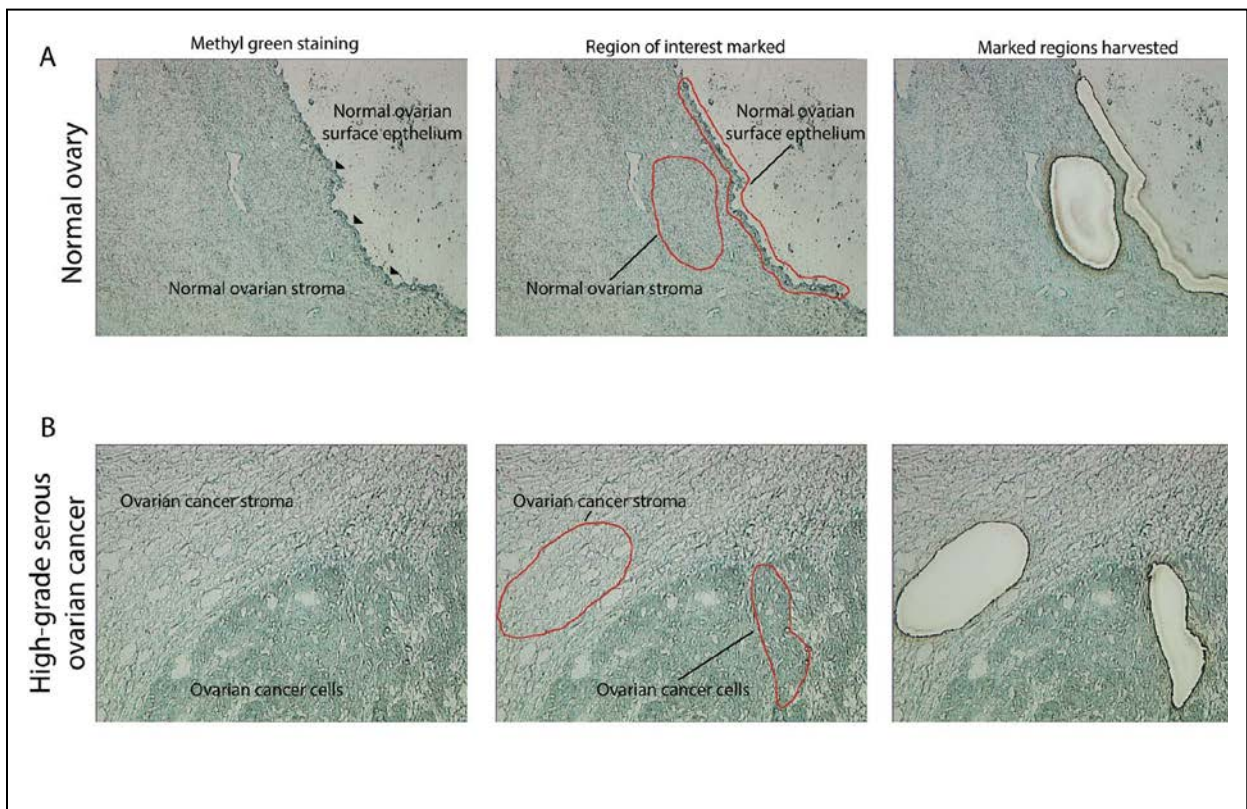


**Fig. 12: Microdissection of (A) normal ovarian tissue and (B) high-grade serous ovarian tumor samples.** After fixation, frozen tissue sections were stained with methyl green to visualize the histologic features (left panels). Stromal and epithelial components in both normal and cancerous tissue were dissected for RNA extraction. During dissection, areas of interest were carefully outlined (middle panels). Areas with immune cell or blood vessel infiltration were avoided to minimize contamination. The areas of interest were recovered from the slides for further processing (right panels). (Yeung, T.L., *et al.* TGF-beta modulates ovarian cancer invasion by upregulating CAF-derived versican in the tumor microenvironment. *Cancer research* **73**, 5016-5028 (2013), Supplementary figure 1)

## B. Overexpression of stromal MFAP5 predicts poor patient survival

To determine the clinical significance of stromal MFAP5 expression, we performed MFAP5 immunolocalization on 130 advanced HGSOC samples. Kaplan-Meier analysis and log-rank test showed that high stromal MFAP5 expression is significantly associated with poor clinical outcomes ( $p < 0.001$ ) (Fig. 17). Patients expressed high (above the median) and low (at or below the median) stromal MFAP5 had a median overall survival duration of 24 months and 54 months respectively. Cox regression analysis with adjustment for age and debulking status

confirmed the prognostic significance of stromal MFAP5 expression (hazard ratio, 2.603;  $p=0.001$ ).

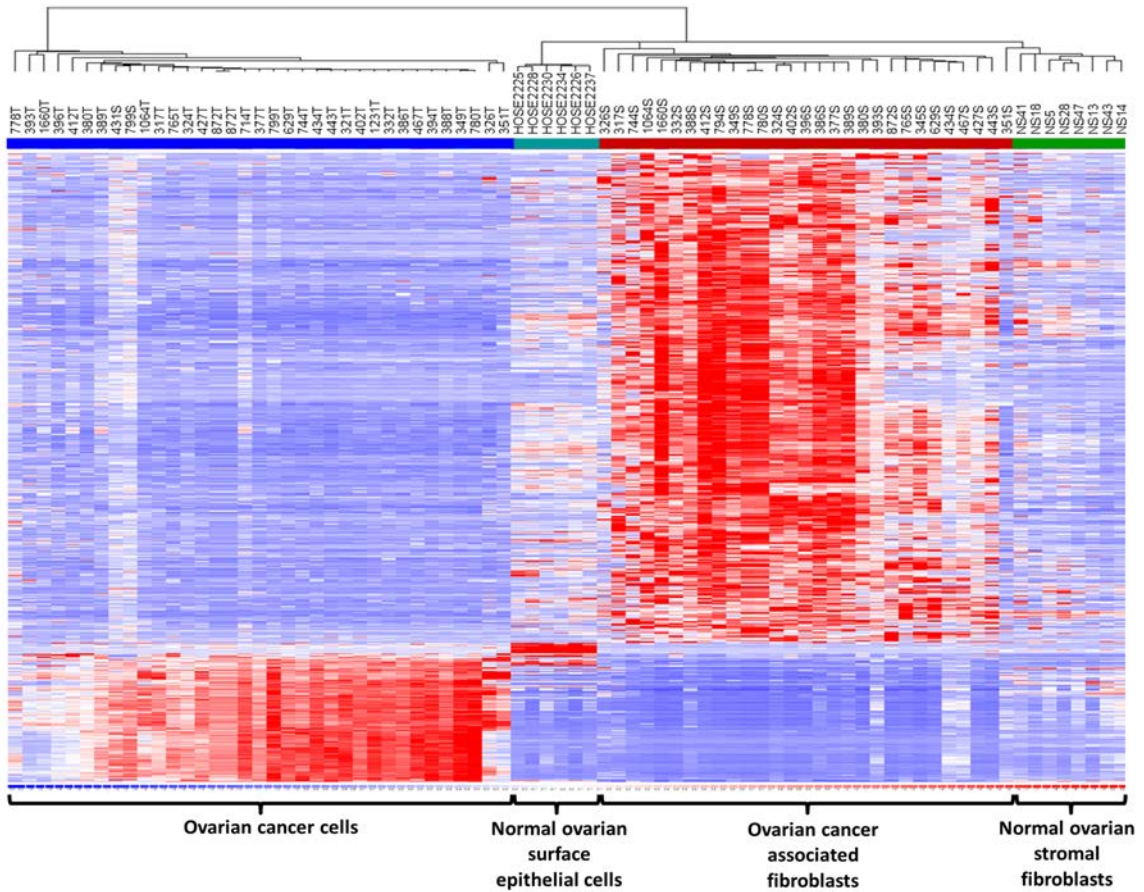


**Fig. 13: Differentially expressed genes in ovarian cancer-associated fibroblasts.** Heat map showing 819 significantly differentially expressed genes among microdissected CAFs and ovarian epithelial tumor samples obtained from 33 patients, normal stromal fibroblasts obtained from 8 normal ovaries, and 6 normal ovarian surface epithelial tissue samples. 19 upregulated secretory protein-coding genes were identified in the CAFs samples.



Probe set	Gene	Accession	Fold change	P-value
223122_s_at	SFRP2: secreted frizzled-related protein 2	AF311912	10.29	0.000082
213764_s_at	MFAP5: microfibrillar-associated protein 5	AW665892	10.54	0.001128
1555778_a_at	POSTN: periostin	AY140646	11.13	0.008831
203570_at	LOXL1: lysyl oxidase-like 1	NM_005576	11.76	0.000043
231993_at	ITGBL1: osteoblast-specific cysteine-rich protein	AK026784	11.89	0.005861
232523_at	MEGF10: multiple EGF-like-domains 10	AU144892	11.98	0.008406
212489_at	COL5A1: collagen, type V, alpha 1	AI983428	12.22	0.000010
209156_s_at	COL6A2: collagen, type VI, alpha 2	AY029208	12.43	0.000000
215446_s_at	LOX: lysyl oxidase	L16895	12.85	0.000013
205479_s_at	PLAU: plasminogen activator, urokinase	NM_002658	13.86	0.000033
206091_at	MATN3: matrilin 3	NM_002381	14.22	0.017423
221731_x_at	VCAN: versican	BF218922	14.85	0.000000
213905_x_at	BGN: biglycan	AA845258	15.21	0.000000
204320_at	COL11A1: collagen, type XI, alpha 1	NM_001854	16.61	0.000017
226930_at	FNDC1: fibronectin type III domain containing 1	AI345957	17.32	0.000003
210511_s_at	INHBA: inhibin, beta A	M13436	20.98	0.000006
218002_s_at	CXCL14: chemokine (C-X-C motif) ligand 14	NM_004887	24.38	0.000089
205713_s_at	COMP: cartilage oligomeric matrix protein	NM_000095	43.14	0.000054
206439_at	EPYC: epiphycan	NM_004950	48.64	0.000561

CAF, cancer-associated fibroblast; FDR, false discovery rate; HOSE, human ovarian surface epithelia; NOF, normal ovarian fibroblast.  
By transcriptome analysis, 19 significantly upregulated secretory protein-coding genes were identified in microdissected CAF samples ( $P < 0.05$ ; t-test and Benjamini-Hochberg FDR multiple testing).

**Table 1: Secretory proteins unregulated in CAFs compared with HOSE, NOFs and ovarian cancer epithelia.**

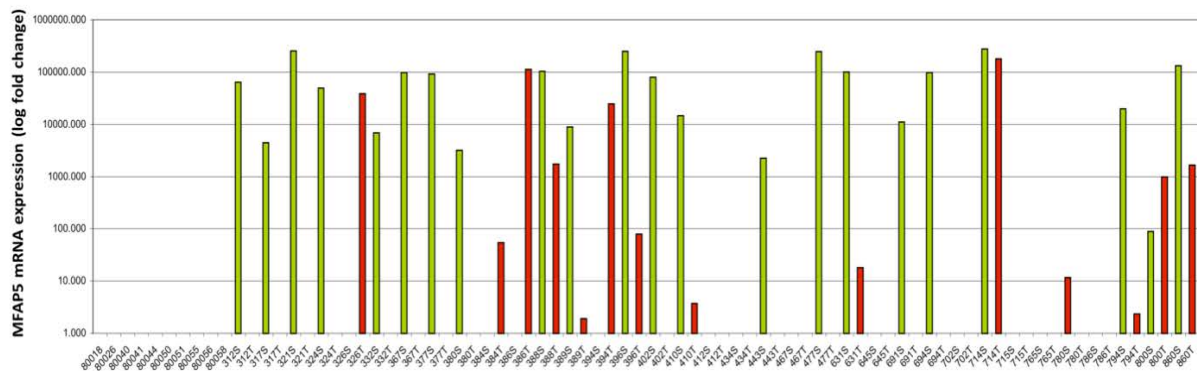


**Fig. 14: Validation of MFAP5 overexpression in ovarian cancer-associated fibroblasts at mRNA level.** Quantitative RT-PCR analysis of RNA isolated from microdissected normal ovarian cortical fibroblasts, and the stromal fibroblastic (S: green bars) and epithelial (T: red bars) components from the same patients are shown. Normal fibroblasts did not have MFAP5 expression. Cancer stromal fibroblasts had significantly higher levels of MFAP5 expression than did those in the epithelial components ( $p < 0.001$ ).



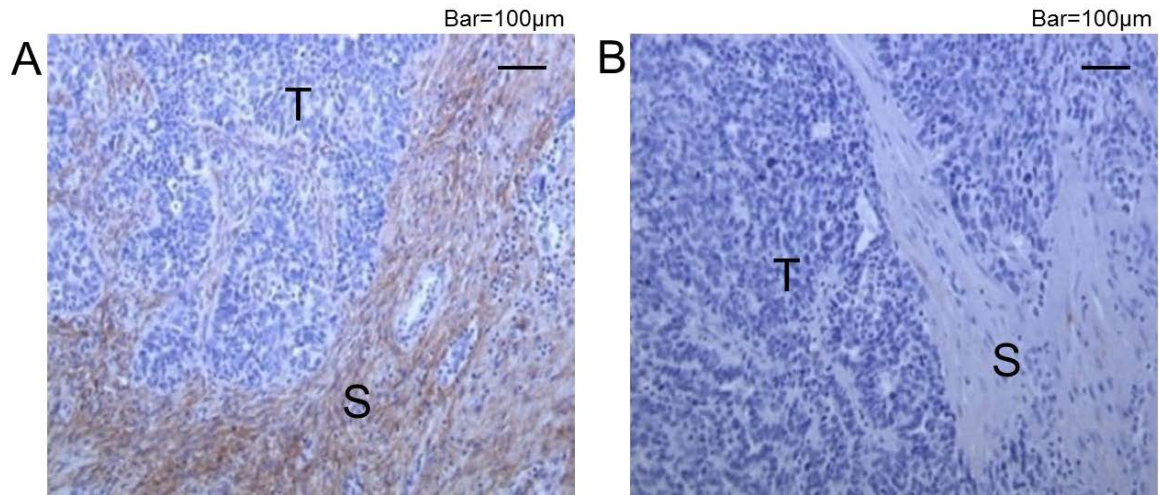


**Fig. 15: Immunolocalization of MFAP5 in advanced stage high-grade serous ovarian tumor tissues.** Representative images for high (A) and low (B) levels of MFAP5 expression in the cancer stroma. S, Cancer stroma; T, epithelial component. Bar = 100 µm.

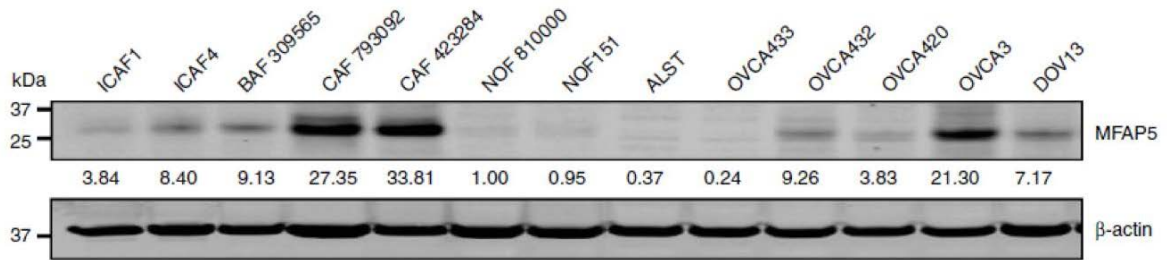


**Fig. 16: Validation of MFAP5 overexpression in ovarian cancer-associated fibroblasts at protein level.** Western blot analysis demonstrated higher levels of MFAP5 expression in CAFs than in NOFs and ovarian cancer cells. Relative normalized protein expression levels were presented.

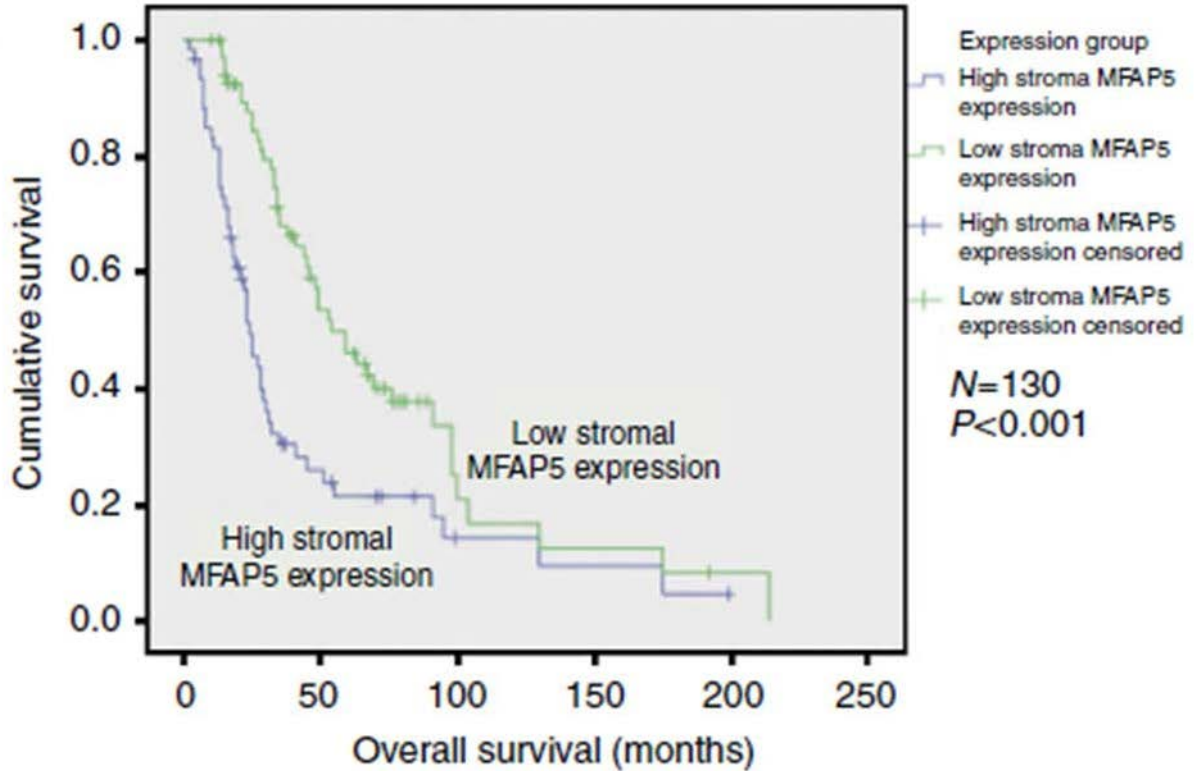


**Fig. 17: Evaluation of clinical significance of MFAP5 overexpression.** Immunolocalization of MFAP5 was performed on 130 advanced HGSOc tissues samples to determine the clinical relevance of stromal MFAP5 expression and HGSOc patient survival. Kaplan-Meier analysis and log-rank test revealed that low stromal MFAP5 expression was significantly associated with a longer overall survival duration than patients who have high stromal MFAP5 expression ( $p < 0.001$ ). Patients with high (above the median) and low (at or below the median) stromal MFAP5 expression levels had a median overall survival duration of 24 months and 54 months respectively.

### C. CAF-derived MFAP5 protein stimulates motility and invasiveness of ovarian cancer cells

Previous studies by our group revealed that MFAP5 could exert its effect on cancer cells in an autocrine manner via binding of its RGD domain to  $\alpha_v\beta_3$  integrin. To determine CAF-derived MFAP5's role on ovarian cancer progression, CAFs expressing high levels of MFAP5 were co-cultured with A224 and ALST ovarian cancer cells which have undetectable levels of endogenous MFAP5 and high levels of  $\alpha_v\beta_3$  integrin expressions (Fig. 18). Experimental results

demonstrated that anti-MFAP5 and anti- $\alpha_v\beta_3$  integrin antibody attenuated the stimulatory effect of MFAP5 on cancer cell motility ( $p < 0.001$ ) (Fig. 19).

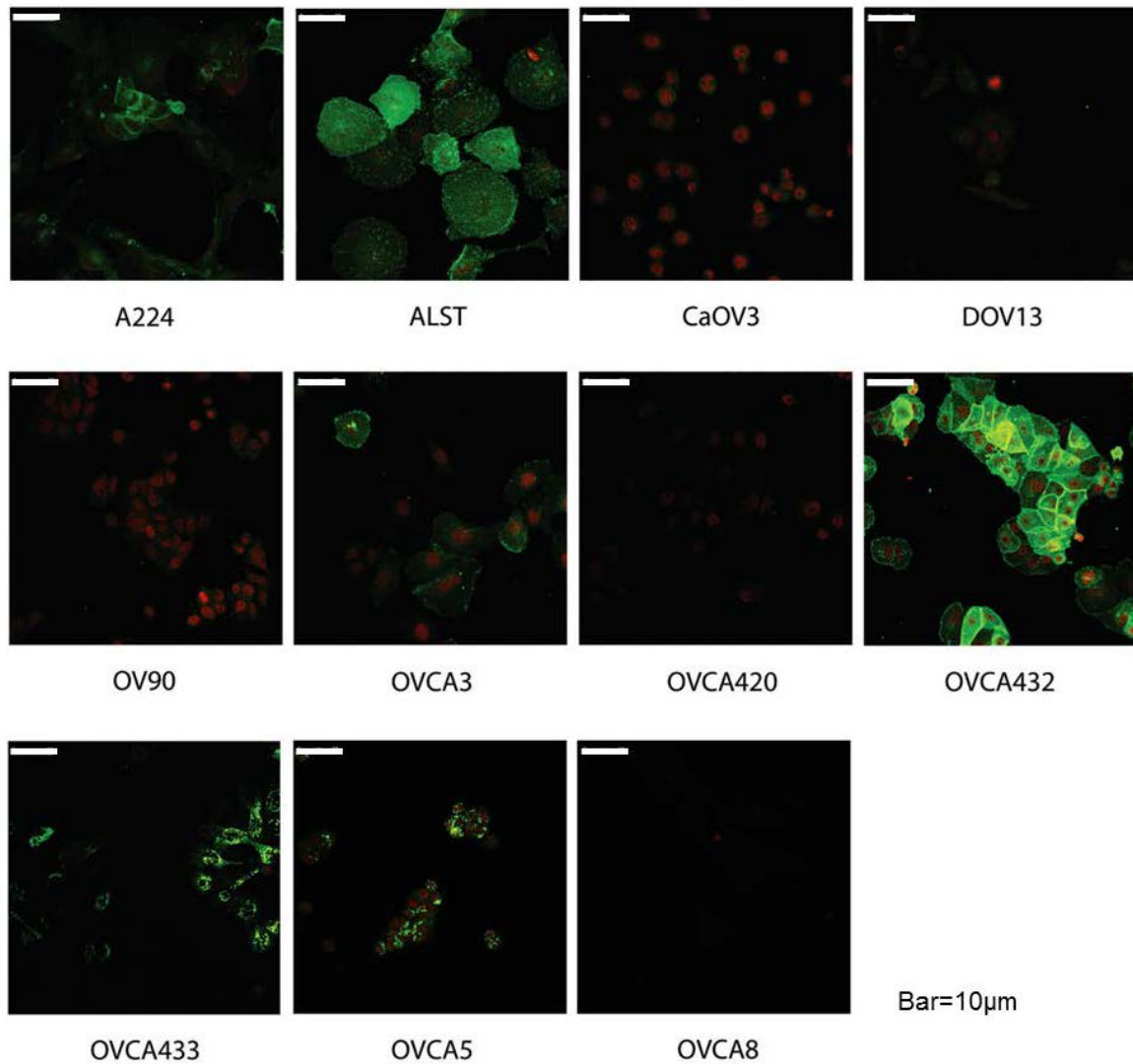


**Fig. 18: Immunocytochemical analysis on the differential expression of  $\alpha_v\beta_3$  integrin receptor in a panel of HGSOc cell lines.** 3  $\alpha_v\beta_3$  integrin expressing ovarian cancer cell lines: A224, ALST and OVCA432 were selected for the functional characterization of MFAP5. Green:  $\alpha_v\beta_3$  integrin; Red: nuclei.

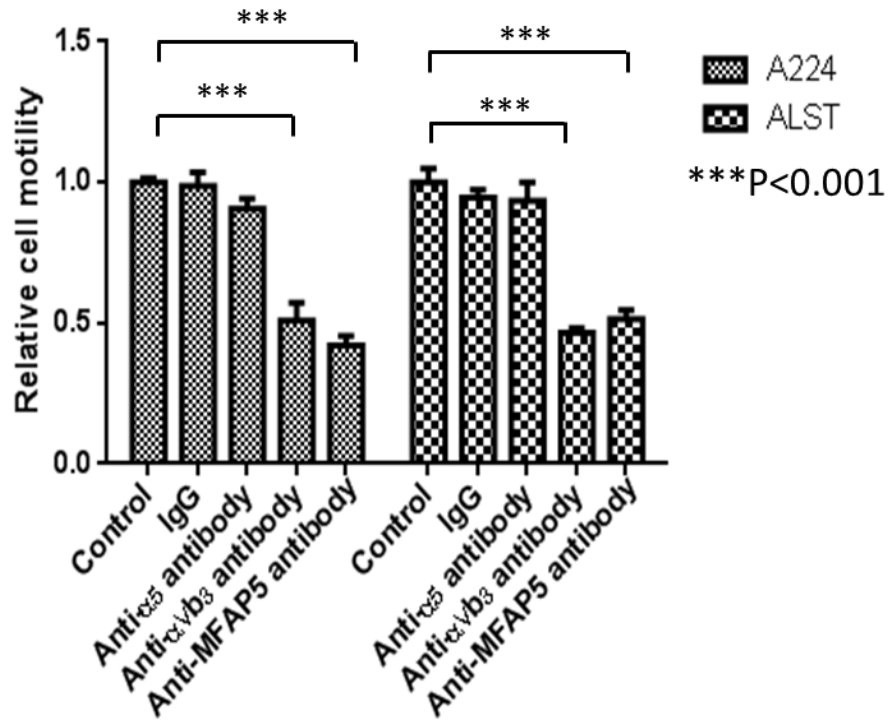


**Fig. 19: Relative motility of ovarian cancer cells when co-cultured with CAF793092 primary ovarian CAFs in the presence of different antibodies.** Control IgG, and anti- $\alpha_5$  antibodies did not affect cancer cell motility, while anti- $\alpha_v\beta_3$  and anti-MFAP5 antibodies attenuated cancer cell motility in the co-culture system (mean  $\pm$  SD of 3 independent experiments;  $p < 0.001$ ).

Real-time imaging of HGSOc cell line OVCA432 treated with purified recombinant MFAP5 protein (recMFAP5) revealed that exogenous recMFAP5 increased OVCA432 cell motility (Fig. 20). To further validate the motility-stimulating effects of exogenous MFAP5, Boyden chamber based motility assays were performed on A224 and ALST cell lines. Increased number of migrated cancer cells was observed in both recMFAP5-treated cell lines. Presence of anti- $\alpha_v\beta_3$  antibody attenuated the stimulatory effect of MFAP5 on cell motility ( $p < 0.01$ ) (Fig. 21). Data from the co-culture studies and exogenous MFAP5 treatment confirmed that the stimulatory effect of MFAP5 on ovarian cancer cell motility is mediated by its binding to the  $\alpha_v\beta_3$  integrin receptor.

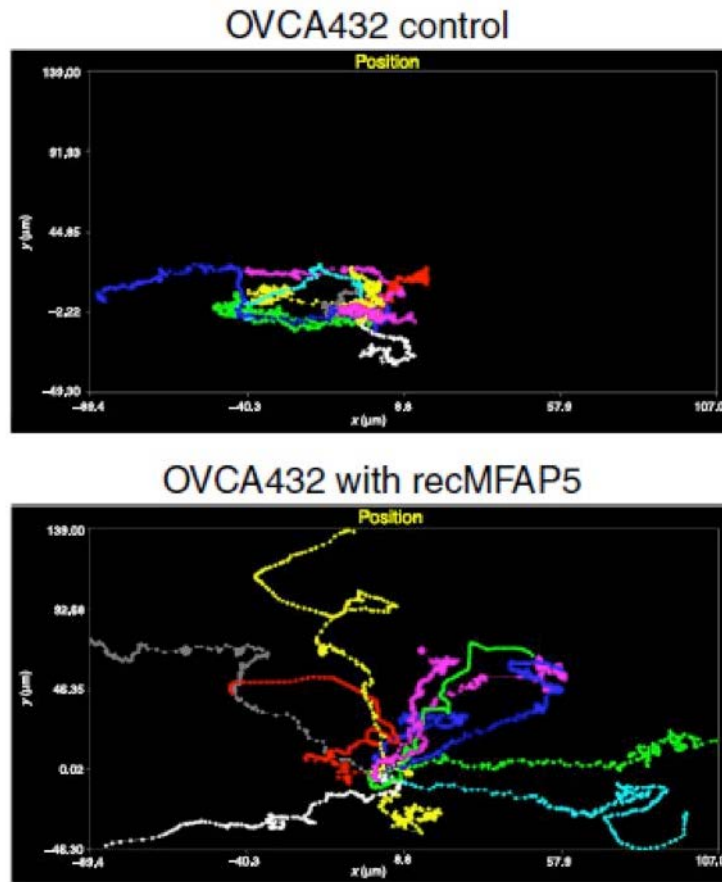


**Fig. 20: Exogenous MFAP5 enhanced OVCA432 cell motility.** A series of images obtained from treatment of OVCA432 cells with recombinant MFAP5 protein in a temperature controlled imaging chamber for 48 hours was analyzed using the MetaMorph Image Analysis software program for tracking of the movement of individual cells.

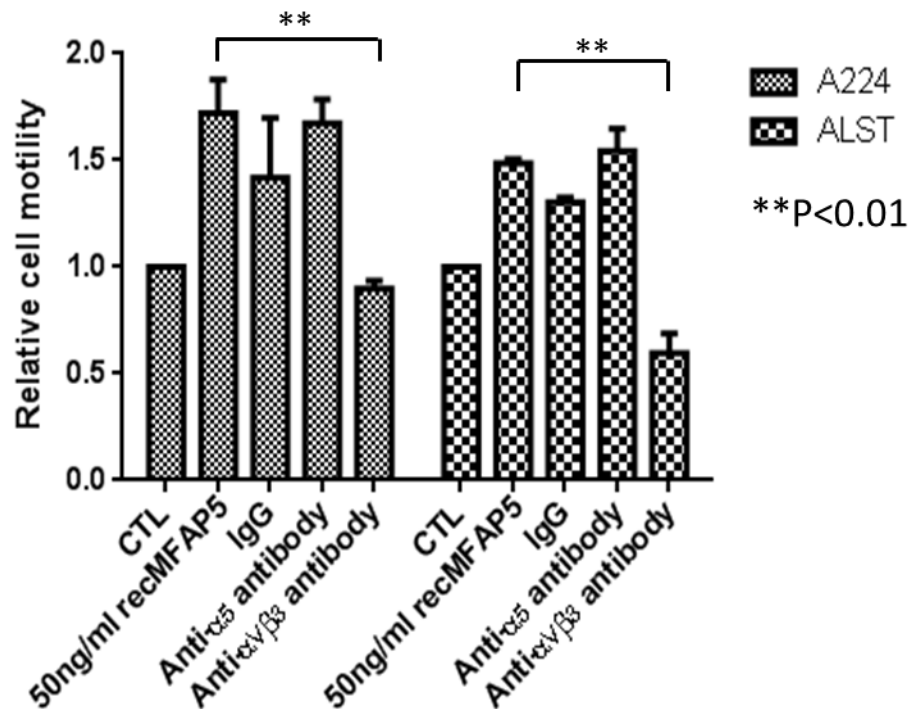


**Fig. 21: Exogenous MFAP5 enhanced ovarian cancer cell motility in Boyden chambers.** Relative motility of cancer cells was evaluated after treatment with recombinant MFAP5 in the presence of control IgG, anti- $\alpha_5$  or anti- $\alpha_v\beta_3$  antibodies compared with antibody-free controls, the presence of anti- $\alpha_v\beta_3$  antibodies significantly abrogated MFAP5-induced cell motility (mean  $\pm$  SD of 3 independent experiments;  $p < 0.01$ ).

In addition, A224 and ALST cells seeded onto Matrigel matrix with recMFAP5 resulted in three times the number of cells invaded through the matrix when compared to the control (Fig. 22), suggesting that MFAP5 also stimulated invasion potential of ovarian cancer cells.



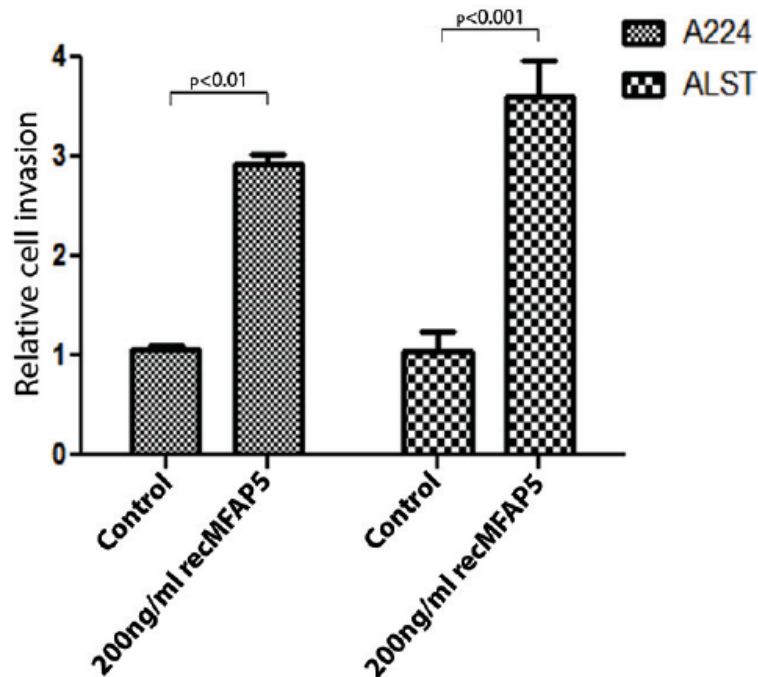


**Fig. 22: Exogenous MFAP5 enhanced ovarian cancer cell invasiveness.** Invasion assay using Matrigel invasion chamber showed that recombinant MFAP5 enhanced ovarian cancer cell invasiveness (mean  $\pm$  SD of 3 independent experiments;  $p < 0.001$ ).

#### D. CAF-derived MFAP5-stimulated motility and invasion potential of ovarian cancer cells *in vivo*

To determine the effects of exogenous MFAP5 on ovarian tumor growth *in vivo*, a MFAP5-overexpressing NOF cell line was created. Overexpression of MFAP5 was confirmed by Western blot analysis (Fig. 23). Cell proliferation assay demonstrated similar proliferation rates of MFAP5-overexpressing NOFs and mock-transduced control NOFs (Fig. 24). For the *in vivo* study, fibroblasts embedded Matrigel plugs were I.P. implanted into nude mice followed by cancer cell injection (Fig. 25A). Matrigel plugs harvested were double-stained for cytokeratin 18 and MFAP5. Results showed that more cancer cells were found in Matrigel plugs embedded with MFAP5-overexpressing fibroblasts than those embedded with control fibroblasts (Figs. 25B and 25C), suggesting that stromal MFAP5 promoted ovarian cancer cell migration and invasion into the Matrigel plugs.

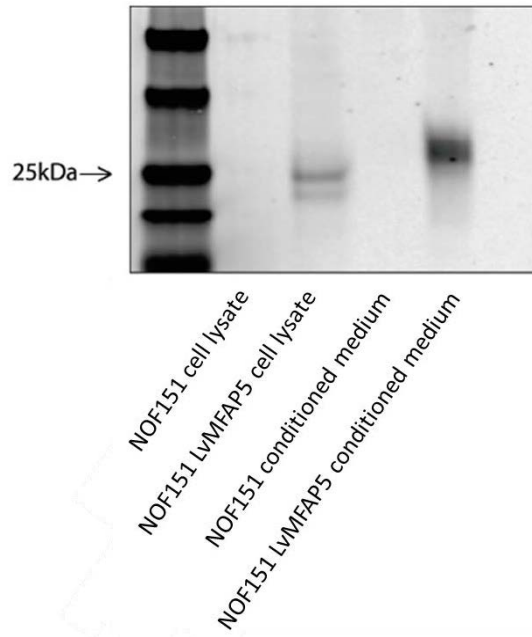


**Fig. 23: Validation of MFAP5-overexpressing fibroblast line generated.** Overexpression and secretion of MFAP5 were validated by Western blot detection of the target protein in the lysate and conditioned media for NOFs overexpressing MFAP5 (NOF151-LvMFAP5 cells).

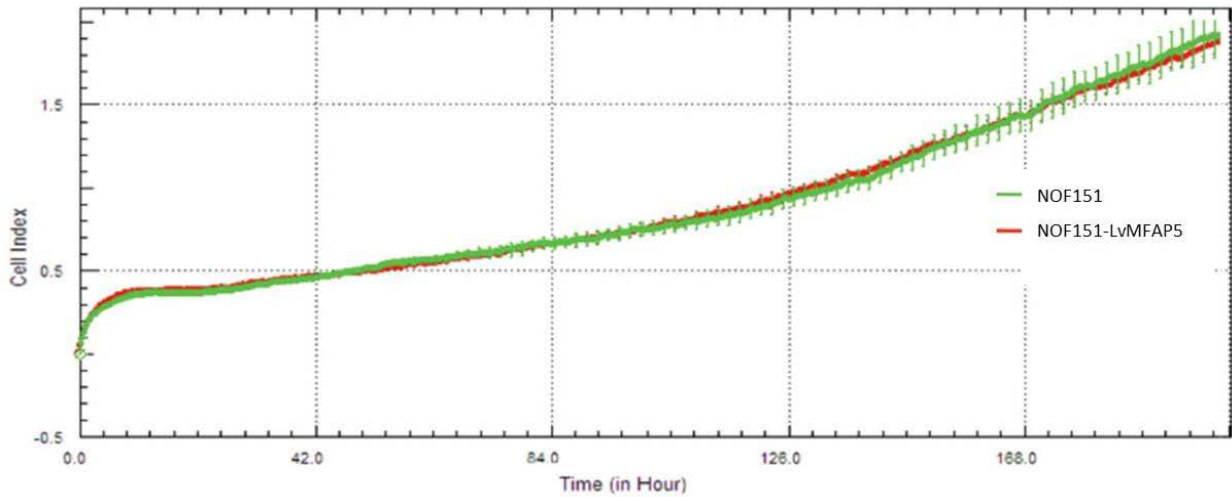


**Fig. 24: Growth rate of MFAP5-overexpressing fibroblasts compared to parental fibroblast line.** Real time monitoring of cell proliferation rate showing that NOF151-LvMFAP5 cells had a proliferation rate comparable with that of the corresponding control cell line, NOF151 (mean  $\pm$  SD of 3 independent experiments).



### **E. *In vivo* stromal Mfap5 silencing reduced ovarian tumor growth and metastasis**

To evaluate the effect of stromal MFAP5 silencing in ovarian cancer metastasis, we silenced murine stromal Mfap5 in an orthotopic mouse model of ovarian carcinoma<sup>112,113</sup> by intravenous injection of Mfap5-targeting siRNAs incorporated chitosan nanoparticles (CH-NP) (Fig. 26A). The efficacy of three siRNA sequences on murine Mfap5 silencing was evaluated in mouse fibroblasts (Fig. 26B). Two Mfap5-targeting siRNAs and a non-targeting sequence were packaged with CH-NP and delivered via tail vein to luciferase labeled cancer cells bearing nude mice throughout the course of the experiment. Significantly lower luciferase activity was detected in Mfap5 knockdown groups compared to the control group at week 6 (Fig. 26C). At the end point of the study, necropsy revealed amelioration of cancer metastasis in the stromal Mfap5 silenced groups when compared to the control group while the primary tumor burden between groups had no significant difference (Figs. 26D and 26E). Mfap5 siRNAs/CH-NP resulted in a significant decrease in the total number of tumor nodules ( $p < 0.001$ ), tumor weight ( $p < 0.001$ ) and volume of ascites ( $p < 0.001$ ) (Fig. 26F), suggested that stromal Mfap5 silencing inhibited ovarian tumor growth and metastatic spread. Immunostaining was performed on paraffin sections of tumor tissue harvested to validate *in vivo* silencing of murine stromal Mfap5 (Fig. 26G).

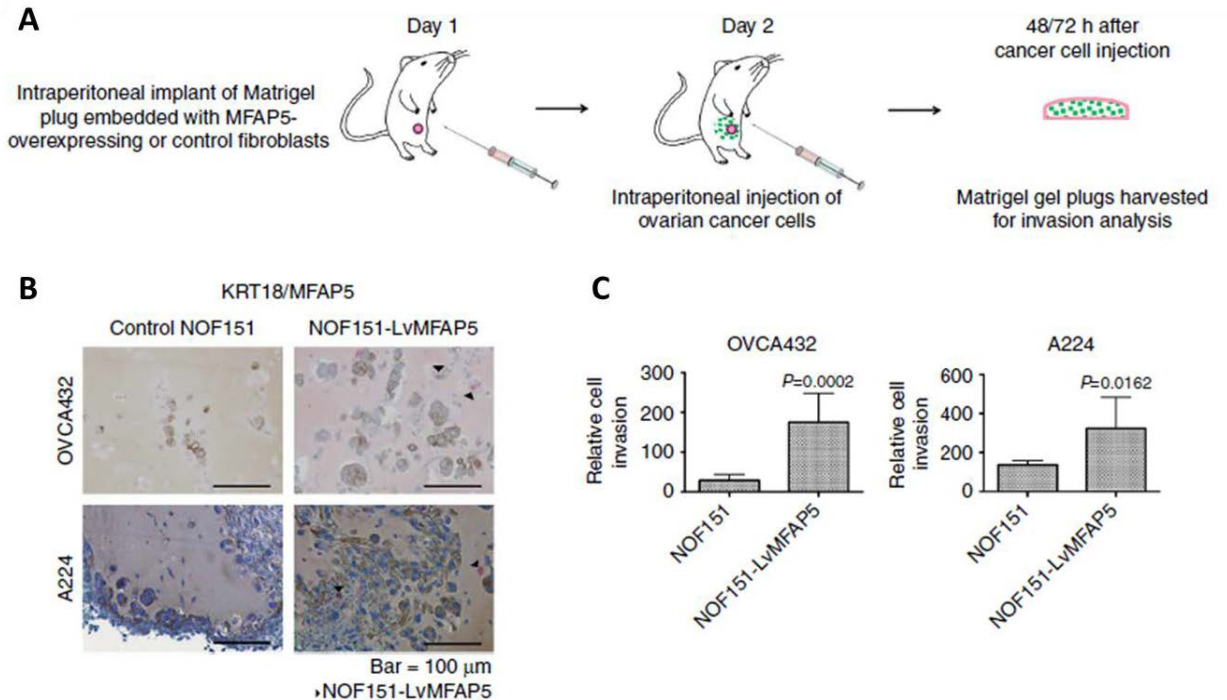


**Fig. 25: Stromal MFAP5 stimulated motility and invasion of ovarian cancer cells *in vivo*.** (A) A schematic diagram showing the procedures of using intraperitoneally implanted Matrigel plugs to evaluate the effects of MFAP5 on invasion potential of ovarian cancer cells. (B and C) Immunolocalization of MFAP5 (red signal) and cytokeratin 18 (brown signal) on paraffin sections Matrigel plugs collected from the peritoneal cavities of mice. The invaded cancer cells with cytokeratin 18 staining were quantified using the Image-Pro Plus software program (mean  $\pm$  SD; N = 10 Matrigel plugs per treatment group for each cell line;  $p=0.0002$  and  $0.0162$  for OVCA432 and A224 cells respectively). Staining for MFAP5 showed that MFAP5 positive cells were found only in Matrigel plugs embedded with MFAP5 overexpressing fibroblasts, suggesting that stromal MFAP5 promoted ovarian cancer cell invasion into the plugs implanted.

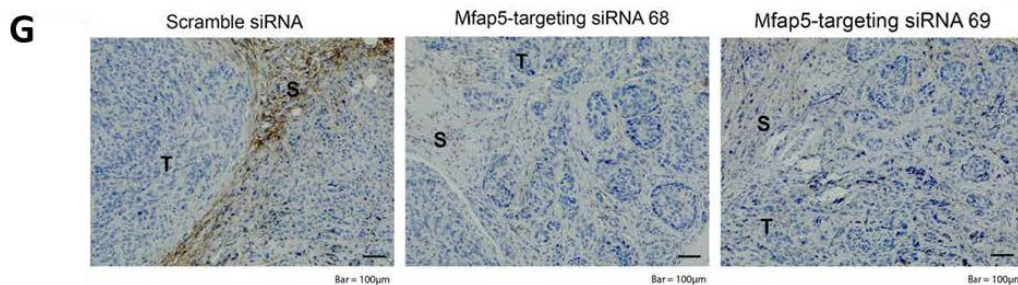
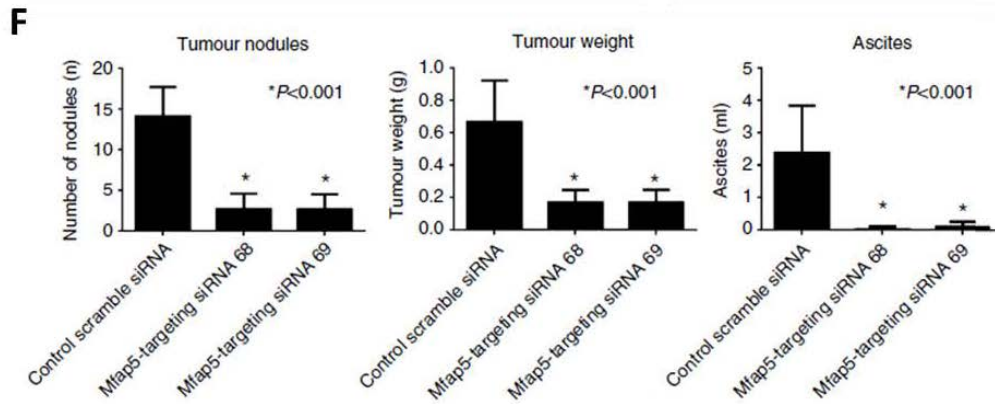
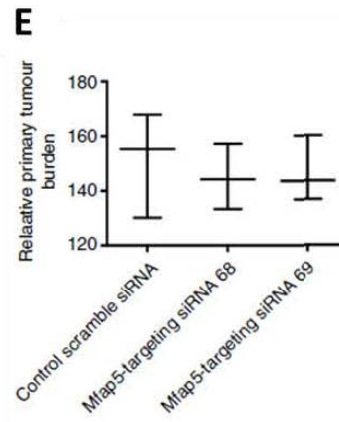
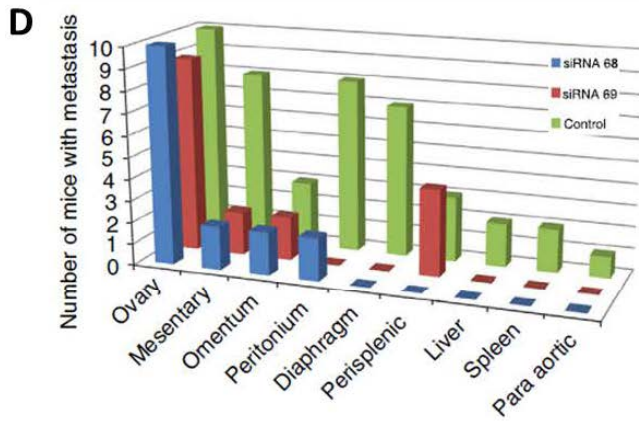
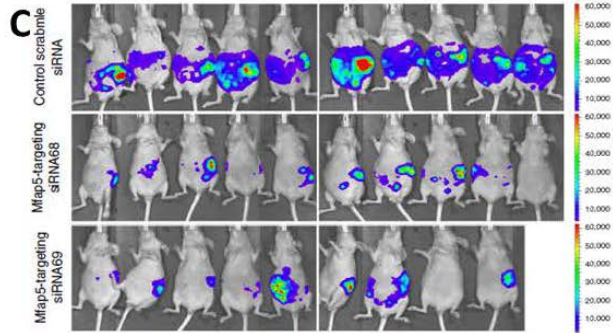
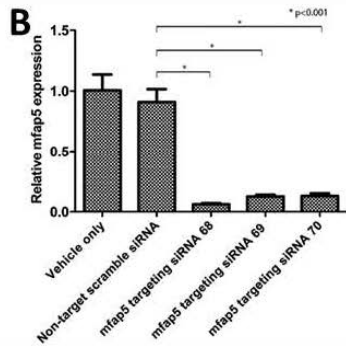
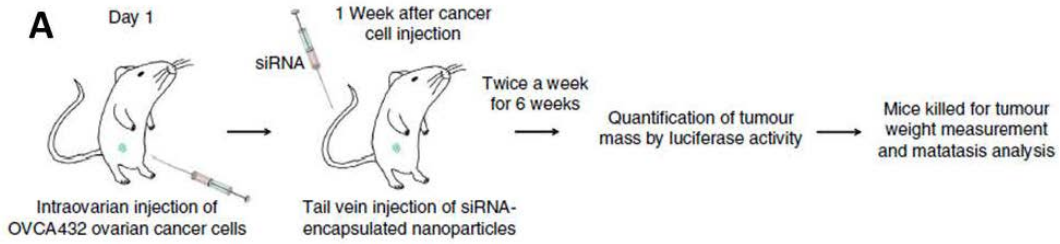


**Fig. 26: *In vivo* stromal Mfap5 silencing reduced ovarian tumor growth and metastasis.** (A) A schematic diagram showing the procedures of using intraovarian tumor injection model to evaluate the effects of MFAP5 on invasion and metastatic potential of ovarian cancer cells. (B) Quantitative RT-PCR data revealing efficient knockdown of stromal *Mfap5* expression in murine fibroblasts by *Mfap5*-specific siRNAs (mean  $\pm$  SD of 3 independent experiments). (C) Luciferase labeled ovarian cancer cells were injected into left ovary of nude mice and luminescence was measured at week 6. Luciferase activities were significantly weaker in stromal *Mfap5* silenced groups when compared to the control siRNA groups (N=9-10 per treatment group). (D) Reduced metastatic spread of cancer cells within the abdominal cavity was observed in the *Mfap5* siRNA encapsulated chitosan nanoparticles treated groups when compared to the control group. (E) Primary tumor burden was quantified by measuring the primary tumor area in the ovaries using images of haematoxylin and eosine tissue sections prepared from tumors harvested from the control scramble siRNA treatment groups and two *Mfap5*-targeting siRNA treatment groups. Similar primary tumor burdens were observed in the control and *Mfap5*-targeted animal groups based on Mann–Whitney U-tests. (F) Significantly reduced number of tumor nodules, tumor weight and ascites volume were observed in the *Mfap5* knockdown groups when compared with the control siRNA group after necropsy (mean  $\pm$  SD; n=9-10 per treatment group;  $p < 0.001$ ). (G) Tumor tissues were fixed in formalin and embedded with paraffin followed by immunolocalization of *Mfap5* to confirm the successful knockdown of stromal *Mfap5* expression. S, Stroma; T, Tumor; Bar=100  $\mu$ m.

#### **F. Transcriptome profiling identified calcium-dependent signaling pathway activation and troponin C type 1 upregulation in MFAP5-treated ovarian cancer cells**

Transcriptome profiling on recMFAP5-treated and untreated OVCA432 cells followed by pathway analysis identified a set of up-regulated motility-promoting genes associated with calcium signaling in recMFAP5-treated cells (Figs. 27 and 28). Among them, troponin C type 1 (TNNC1) was chosen for further studies. TNNC1 contains a calcium-binding subunit and facilitates the interaction between actin and myosin in skeletal and cardiac muscle cells and the formation of stress fibers, suggesting that it may play a key role in mediating MFAP5's stimulatory effect on ovarian cancer cell motility. We performed quantitative RT-PCR analysis on five MFAP5-treated ovarian cancer cell lines and observed a significant increase of TNNC1 expression in all of them (Fig. 29). Results from motility assays revealed that silencing of

TNNC1 by TNNC1-targeting siRNA abolished MFAP5's stimulatory effect on A224 and ALST cell motility (Fig. 30), suggested that TNNC1 is the effector protein for MFAP5-enhanced cancer cell motility. In addition, F-actin staining showed that recMFAP5 treatment led to an increased density and more organized F-actin cytoskeleton in ovarian cancer cells (Fig. 31), while these effects were abrogated in TNNC1-targeting siRNAs transfected cells (Fig. 32) suggested that MFAP5 stimulated cell motility through induction of TNNC1 expression and F-actin cytoskeleton reorganization.

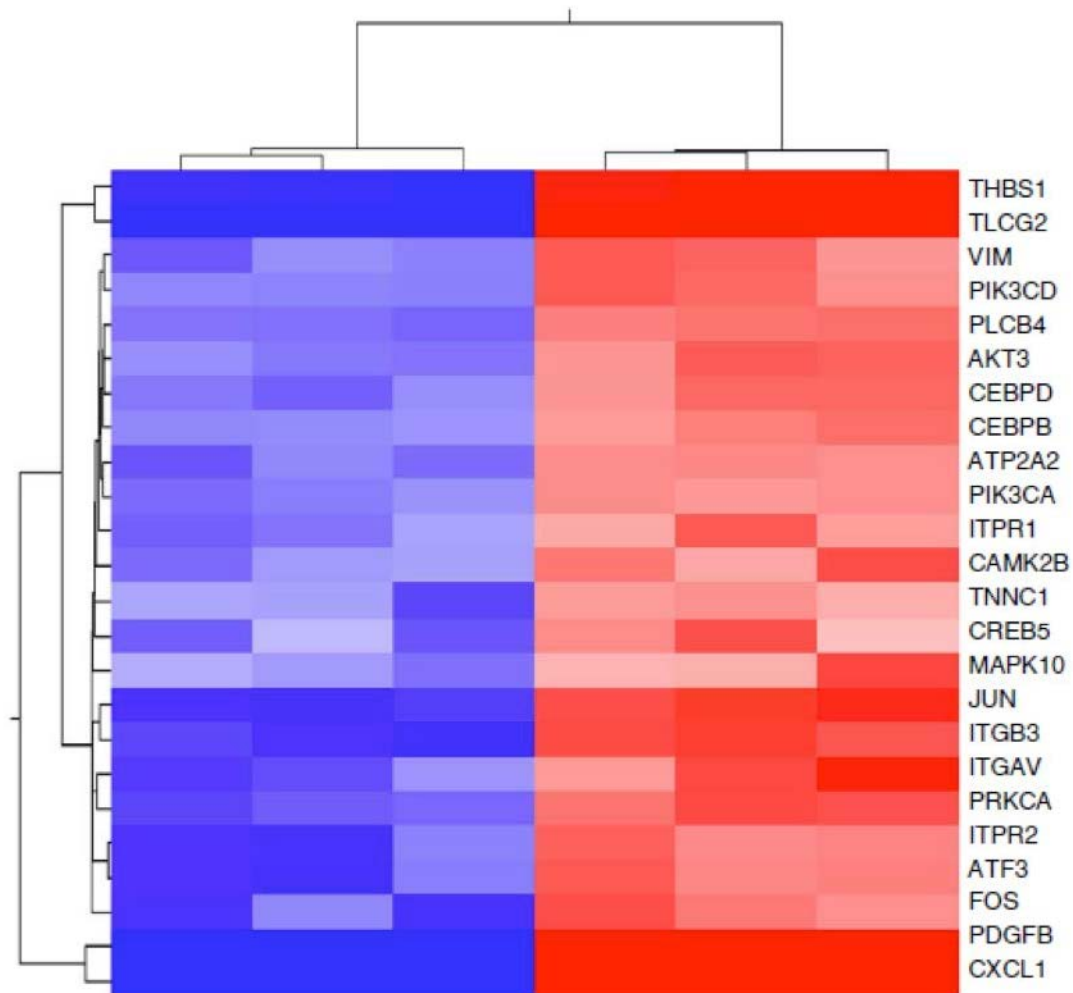


**Fig. 27: Motility-promoting genes upregulated by MFAP5 in ovarian cancer cells.** Heat map showing motility-promoting genes associated with calcium signaling whose expressions were upregulated in MFAP5-treated OVCA432 cells. Among them, TNNC1 was chosen for follow up evaluations.



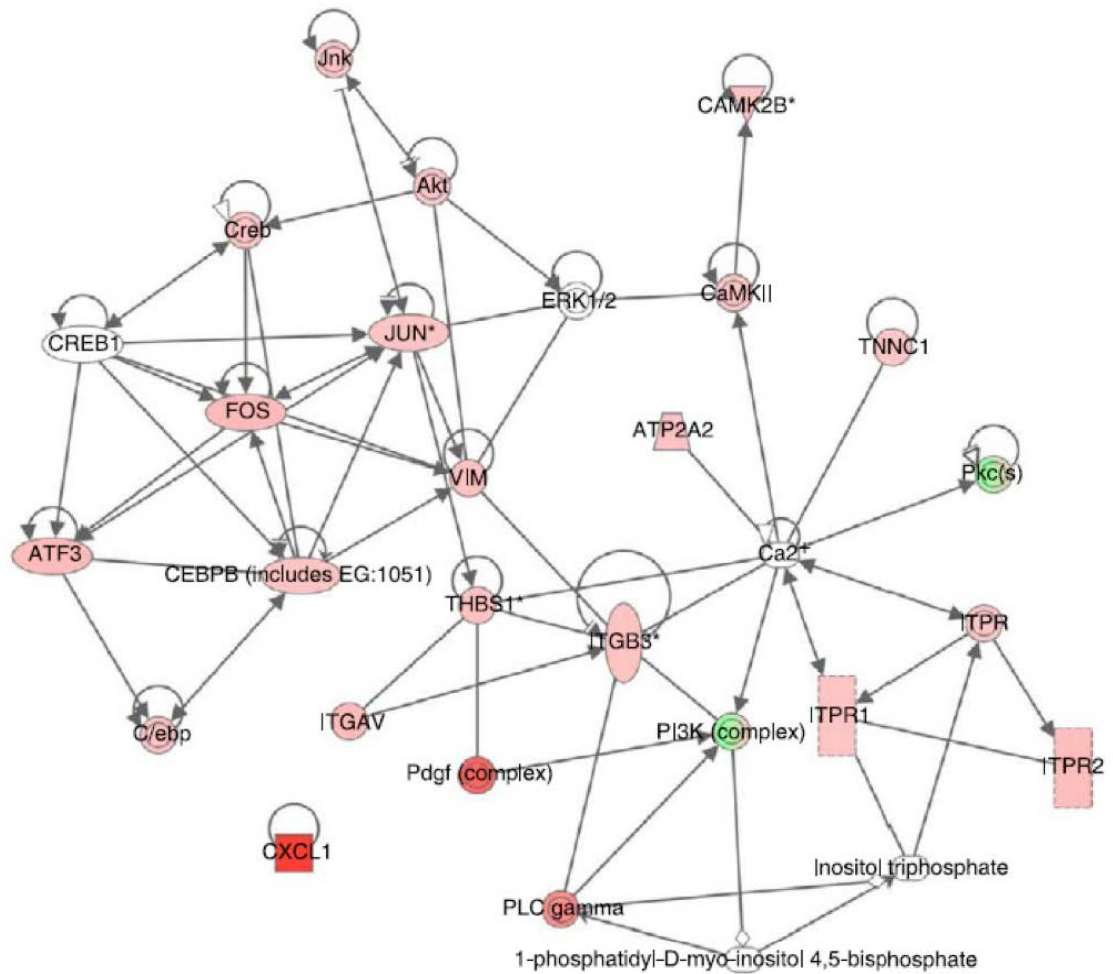


**Fig. 28: Pathway analysis of genes upregulated by MFAP5.** Interaction network of motility promoting and calcium signaling related genes whose expressions were upregulated in MFAP5-treated OVCA432 cells was identified using the Ingenuity Pathway Analysis software program (Ingenuity Systems, Redwood City, California).

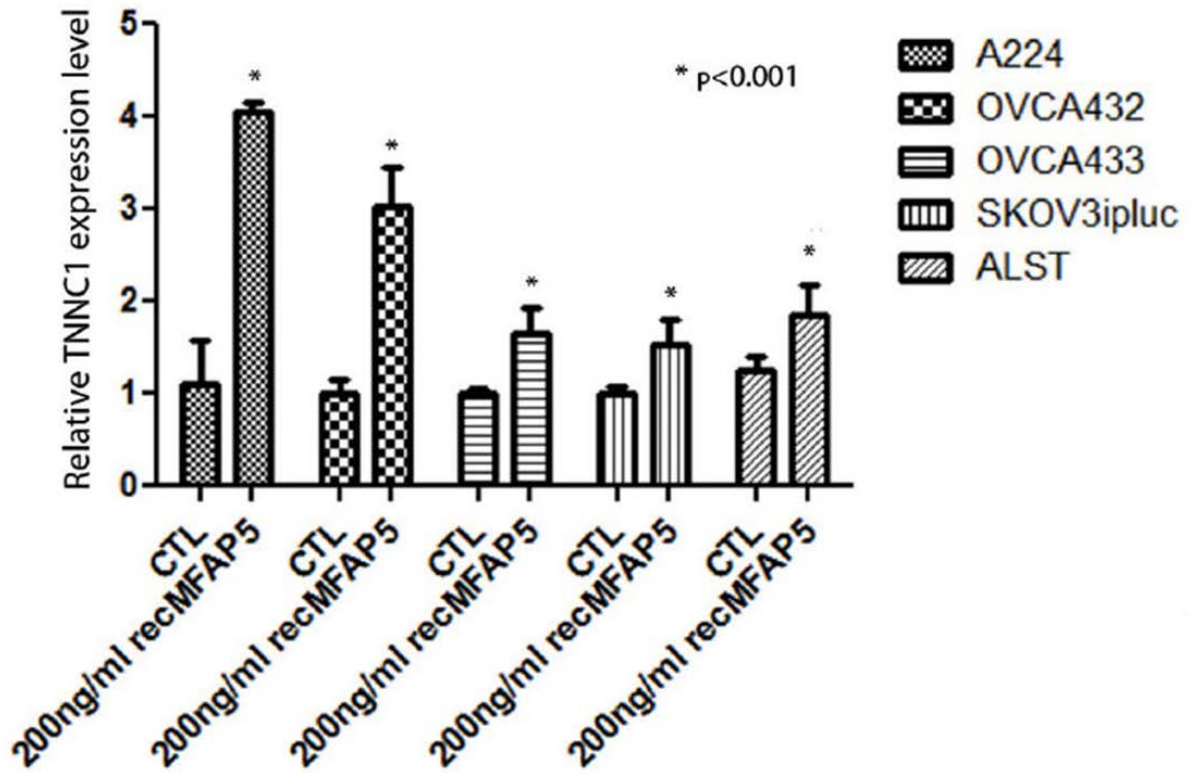


**Fig. 29: Validation of TNNC1 upregulation in recMFAP5-treated cancer cells by quantitative RT-PCR.** Upregulation of TNNC1 mRNA expression in five serous ovarian cancer cell lines after MFAP5 treatment (mean  $\pm$  SD of 3 independent experiments;  $p < 0.001$ ).

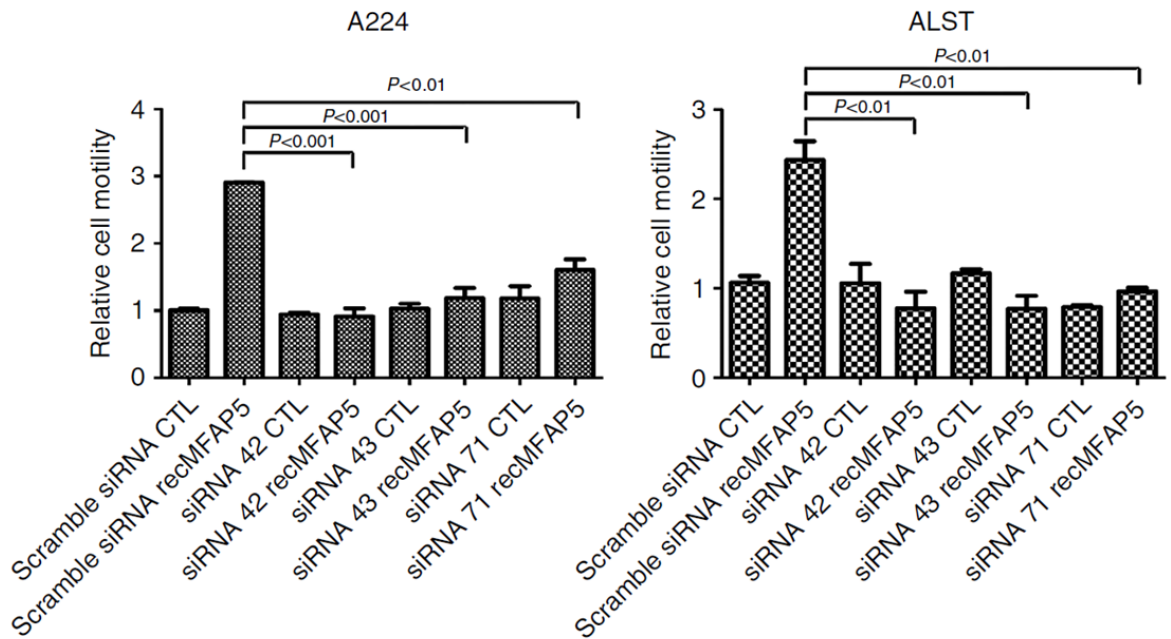


**Fig. 30: Evaluation of the role of TNNC1 in MFAP5 induced ovarian cancer cell motility.** Abrogation of MFAP5's stimulatory effect on ovarian cancer cell motility by knockdown of TNNC1 expression using TNNC1-targeting siRNAs and a scrambled non-targeting siRNA as control (mean  $\pm$  SD of 3 independent experiments).

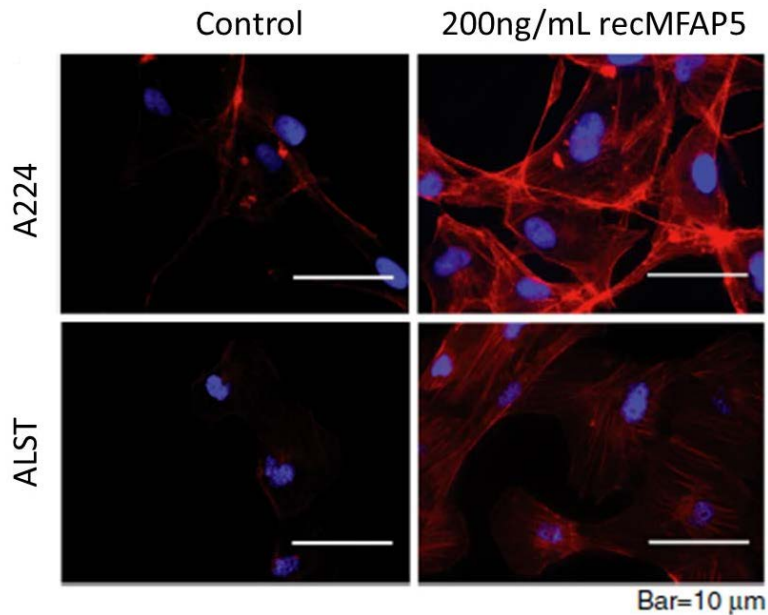


**Fig. 31: Fluorescent labeling of F-actin in MFAP5-treated ovarian cancer cells.** MFAP5-induced F-actin rearrangement and activated stress fiber formation in A224 and ALST cells was visualized by immunofluorescence. Red: F-actin; Blue: nuclei.



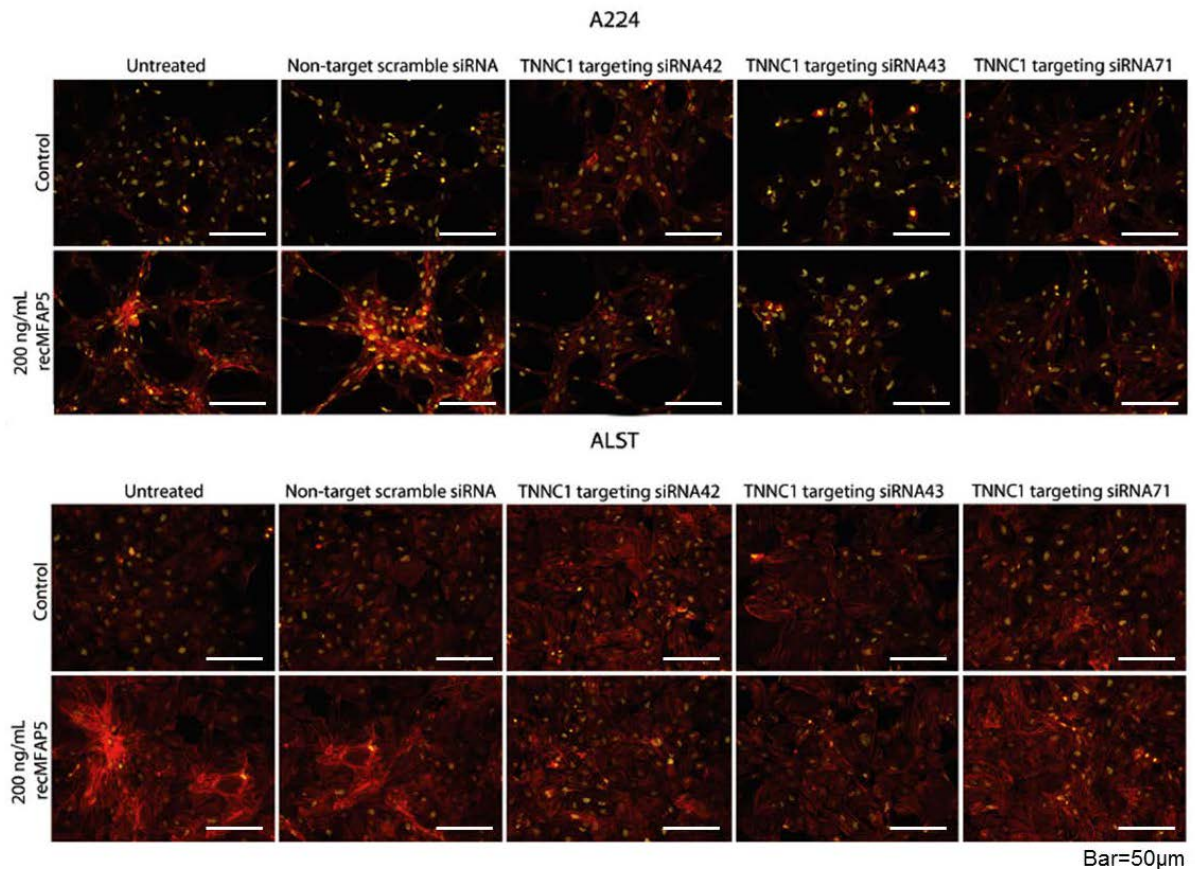


**Fig. 32: MFAP5 induced increase in density and rearrangement of F-Actin cytoskeleton were abrogated by siRNA silencing of TNNC1 in A224 and ALST cells.** Immunofluorescence was used to visualize the actin cytoskeleton of ovarian cancer cells. While MFAP5 treatment increased density and promoted rearrangement of actin cytoskeleton in both cell lines, the effects of MFAP5 were abrogated by knockdown of TNNC1 using siRNA. Red: F-actin; Yellow: nuclei.

### **G. MFAP5's effects on motility is mediated via calcium mobilization and increased traction force in ovarian cancer cells**

Transcriptome profiling and pathway analysis data suggest that cytosolic calcium mobilization is integral to MFAP5's effect on ovarian cancer motility. The observations that MFAP5's motility stimulatory effect was attenuated and F-actin reorganizing effect was abrogated in calcium chelator BAPTA/AM preloaded cancer cells (Fig. 33), suggested that calcium signaling is involved in modulating MFAP5's functions. Using calcium dye Fluo-4 AM and confocal fluorescence microscopy, we observed that exogenous MFAP5 mobilized

intracellular  $\text{Ca}^{2+}$  in A224 and ALST cells (Fig. 34). Further evaluation on the mechanisms involved in calcium mobilization in ALST cells showed that treatment with the L-type  $\text{Ca}^{2+}$  channel blocker nifedipine attenuated but did not abolish MFAP5-induced calcium mobilization (Fig. 35A). Besides, L-type calcium channel opener BAYK8644 triggered calcium mobilization in ALST cells (Fig. 35B), suggesting that MFAP5 induced exogenous  $\text{Ca}^{2+}$  entry via the L-type voltage-gated channel, although other channels may be involved. Also, treatment with the  $\text{IP}_3$  receptor inhibitor xestospongin C but not the ryanodine receptor blocker attenuated MFAP5-induced calcium mobilization, suggesting that  $\text{IP}_3$ -sensitive  $\text{Ca}^{2+}$  stores are mobilized by MFAP5 (Figs. 35C and 35D). Because  $\text{IP}_3$ -sensitive  $\text{Ca}^{2+}$  store depletion can trigger store-operated  $\text{Ca}^{2+}$  entry (SOCE) and is a common entry pathway in nonexcitable cells, we evaluated whether a transient receptor potential channel antagonist, SKF96365, could abrogate SOCE activated by thapsigargin in ALST cells. The result confirmed that an exogenous  $\text{Ca}^{2+}$  entry mechanism resembling store-operated calcium entry was present in ALST cells (Fig. 35E).

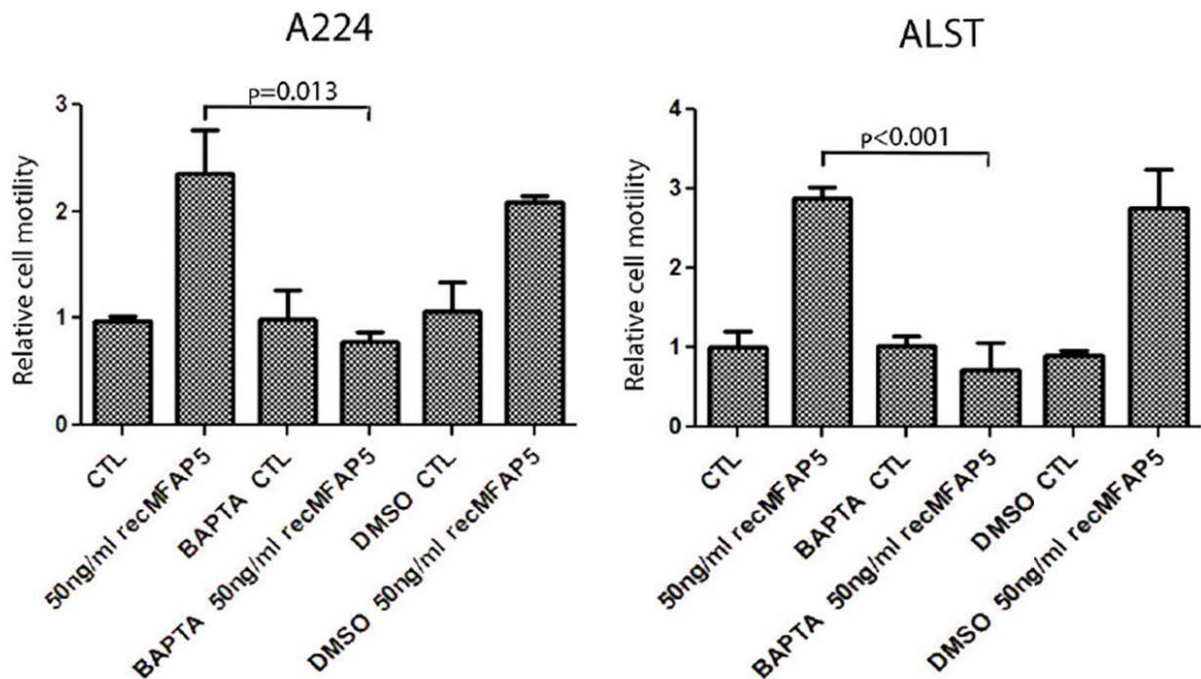


**Fig. 33: Evaluation of the role of calcium signaling in MFAP5 induced ovarian cancer cell motility.** Stimulatory effect of MFAP5 on ovarian cancer cell motility was attenuated by the cell-permeant calcium chelator BAPTA/AM but not by the solvent control DMSO (mean  $\pm$  SD of 3 independent experiments).

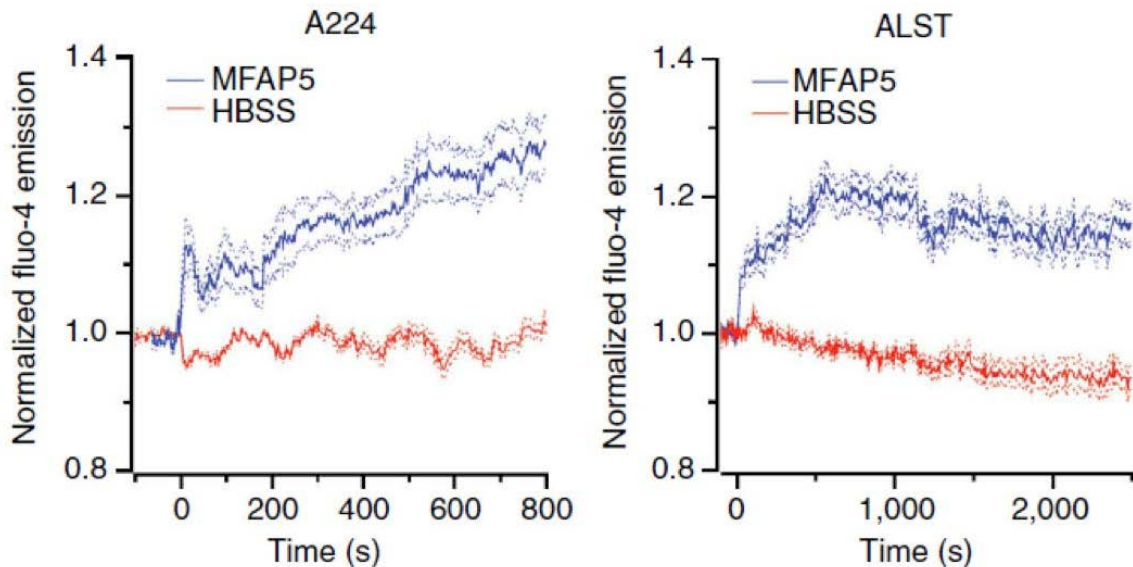


**Fig. 34: The mean normalized time course of  $Ca^{2+}$  mobilization in A224 and ALST cells induced by MFAP5.** Hank's balanced salt solution with or without MFAP5 or was added to the bath of cells at  $t=0$  followed by the monitor of  $Ca^{2+}$  mobilization (mean  $\pm$  SEM of 10 independent experiments for each treatment group).

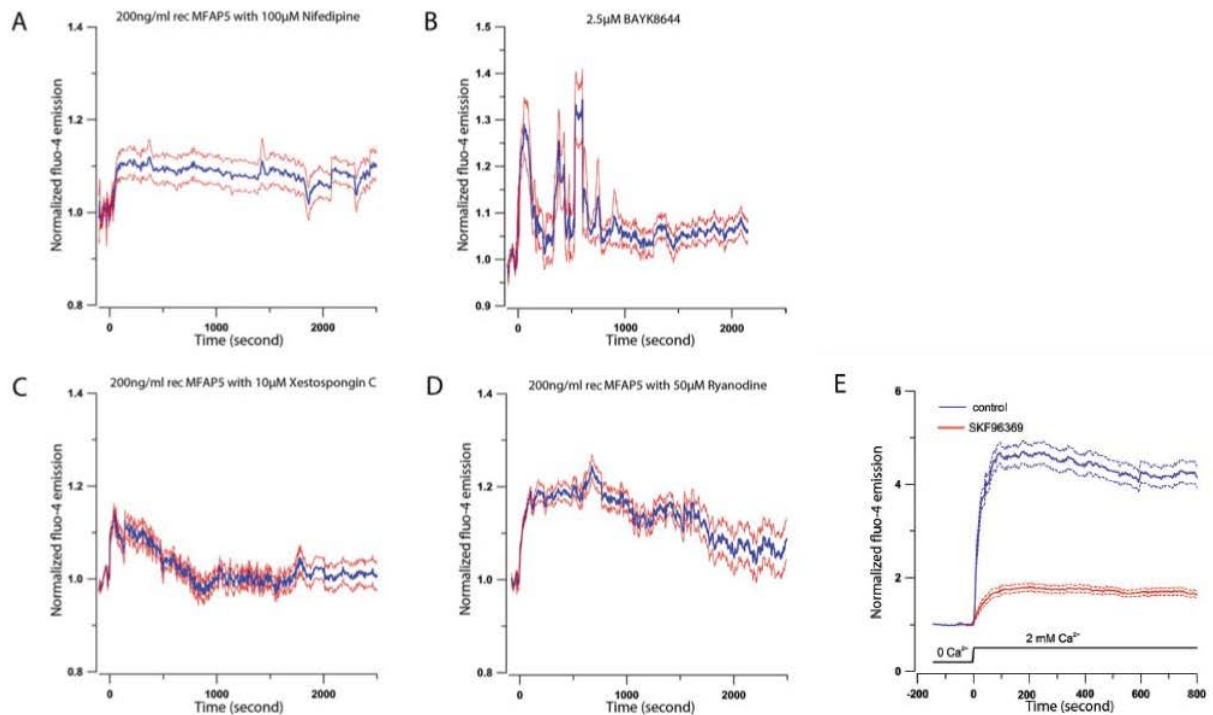


**Fig. 35: Calcium influx in ovarian cancer cells induced by MFAP5 treatment in the presence of different channel blockers.** (A) Mean normalized time course of  $\text{Ca}^{2+}$  mobilization in ALST cells induced by recombinant MFAP5 (200 ng/ml) in the presence of nifedipine (100  $\mu\text{M}$ , 30 minutes of preincubation). (B) Mean normalized time course of  $\text{Ca}^{2+}$  mobilization in ALST cells induced by BAYK8644 (2.5  $\mu\text{M}$ ). (C) Mean normalized time course of  $\text{Ca}^{2+}$  mobilization in ALST cells induced by recombinant MFAP5 (200 ng/ml) in the presence of the IP3 receptor inhibitor xestospongin C (10  $\mu\text{M}$ , 30 minutes of preincubation). (D) Mean normalized time course of  $\text{Ca}^{2+}$  mobilization in ALST cells induced by recombinant MFAP5 (200 ng/ml) in the presence of ryanodine (50 $\mu\text{M}$ , 30 minutes of preincubation). (E) Activation of store-operated calcium entry by thapsigargin in ALST cells. ALST cells were incubated with 20  $\mu\text{M}$  thapsigargin in the absence of extracellular  $\text{Ca}^{2+}$  for 25 minutes. Subsequent addition of 2 mM  $\text{Ca}^{2+}$  to the medium resulted in rapid extracellular  $\text{Ca}^{2+}$  entry, which was inhibited by treatment with 50  $\mu\text{M}$  SKF96365. Dotted lines, standard errors.

Since calcium mobilization has been linked to increased cell traction force and cell motility,<sup>114,115</sup> we therefore used traction force microscopy to evaluate MFAP5's effects on cancer cells' traction force generation. RecMFAP5 exposure induced amplitude increase and cell traction force redistribution in A224 and ALST cells (Figs. 36A and 36B), suggested that directional traction force induction is the physical mechanism of MFAP5-enhanced motility and invasion potential. Furthermore, TNNC1 silencing abrogated the amplitude increase of traction force induced by MFAP5 (Fig. 37), suggested that TNNC1 is the key molecule involved in



traction force induction by MFAP5.

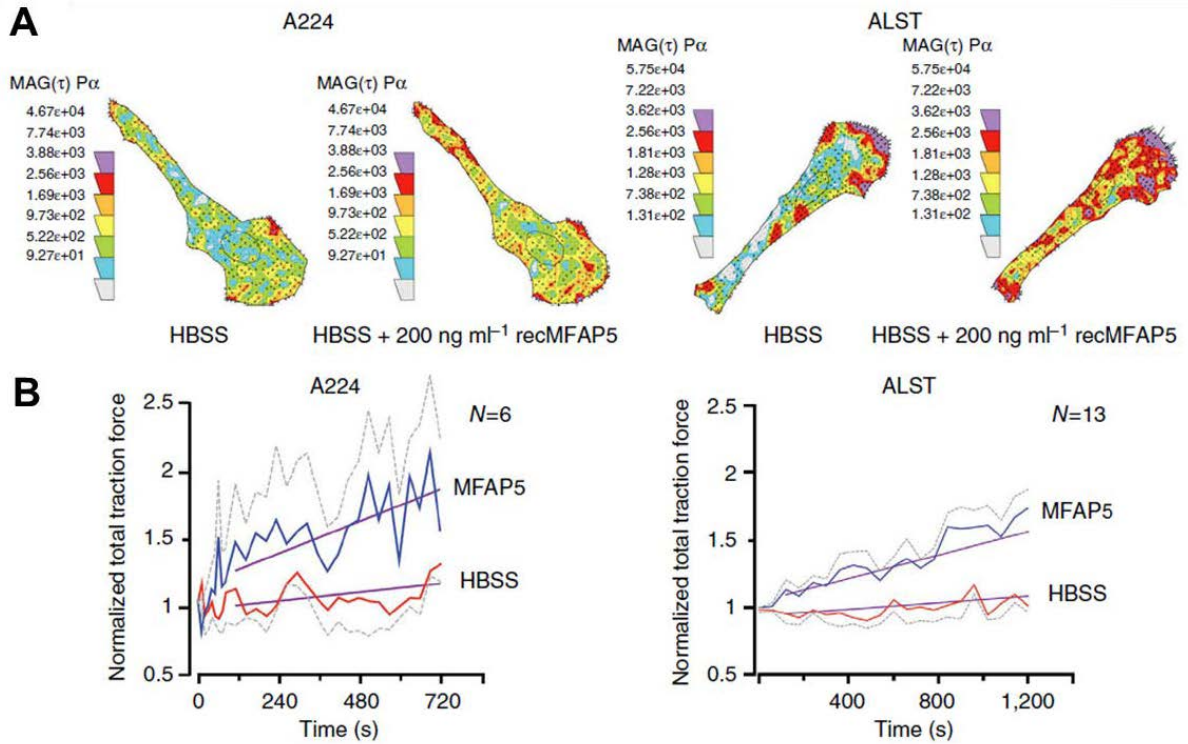


**Fig. 36: Traction force induction by MFAP5 in ovarian cancer cells. (A)** Cell traction force maps of A224 and ALST cells before and after exposure to MFAP5. **(B)** The normalized total traction force exerted by A224 and ALST cells induced by MFAP5. (Mean  $\pm$  SEM of 10 independent experiments for each treatment group).

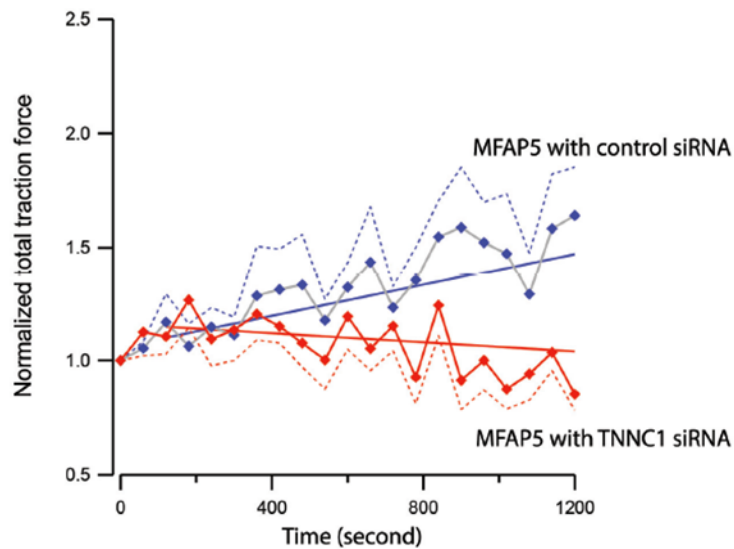


**Fig. 37: The effect of TNNC1 silencing on traction force generation in ovarian cancer cells.** Silencing of TNNC1 expression by siRNAs attenuated the increase in total traction force exerted by ALST cells to the substratum in the presence of exogenous MFAP5 (mean  $\pm$  SEM of 10 independent experiments for each treatment group).

#### H. TNNC1 upregulation by MFAP5 was mediated through the activation of calcium-dependent FAK/CREB/TNNC1 signaling pathway

Western blot analysis of key signaling molecules implicated in calcium-dependent pathways and TNNC1 transcriptional regulation demonstrated increases in p-FAK (Y861), p-PLC- $\gamma$ 1 (Y783), p-PKC $\theta$  (T538), p-ERK1/2 (T202/Y204), p-CREB (S133), total Jun, and p-Jun (S63, S73 and S243) expression in MFAP5-treated cancer cells (Figs. 38A and 38B). Based on our results, we hypothesized that binding of MFAP5 to  $\alpha_v\beta_3$  integrin activates FAK. FAK activation activates PLC- $\gamma$ 1 and PKC $\theta$ , which regulate Ca<sup>2+</sup> influx. Ca<sup>2+</sup> mobilization leads to ERK1/2 phosphorylation and subsequent cAMP response element-binding protein (CREB) activation. Translocation of activated CREB to the nucleus leads to c-Jun transcription via binding of activated CREB to cAMP-response element (CRE) in the c-Jun promoter, which then upregulates TNNC1 expression. Increased TNNC1 protein level thereby enhances stress fiber formation and cell motility (Fig. 39).

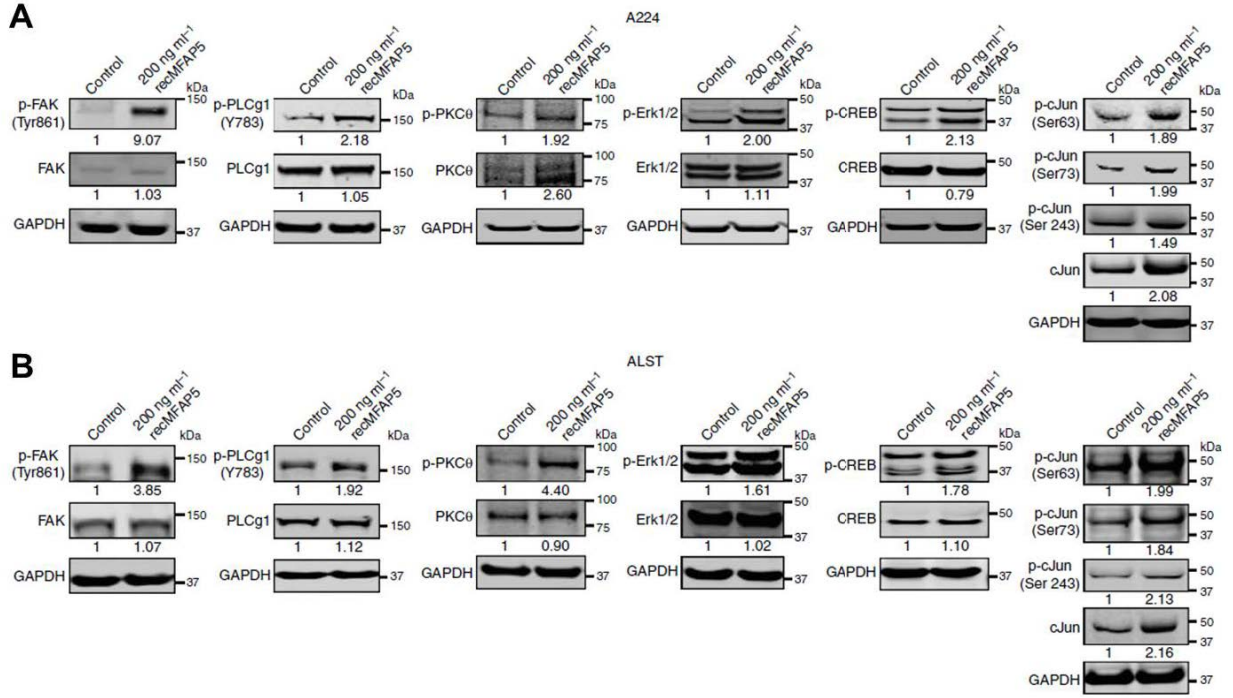


**Fig. 38: Western blot analyses on proteins isolated from MFAP5-treated A224 and ALST ovarian cancer cells. (A)** Treatment of exogenous MFAP5 increased p-FAK (Y861), p-PLC-γ1 (Y783), p-PKCθ (T538), p-ERK1/2 (T202/Y204), p-CREB (S133), total Jun, and p-Jun (S63, S73 and S243) expressions in A224 ovarian cancer cells. **(B)** Treatment of exogenous MFAP5 increased p-FAK (Y861), p-PLC-γ1 (Y783), p-PKCθ (T538), p-ERK1/2 (T202/Y204), p-CREB (S133), total Jun, and p-Jun (S63, S73 and S243) expressions in ALST ovarian cancer cells. Relative normalized protein expression levels with respect to the corresponding control were presented.

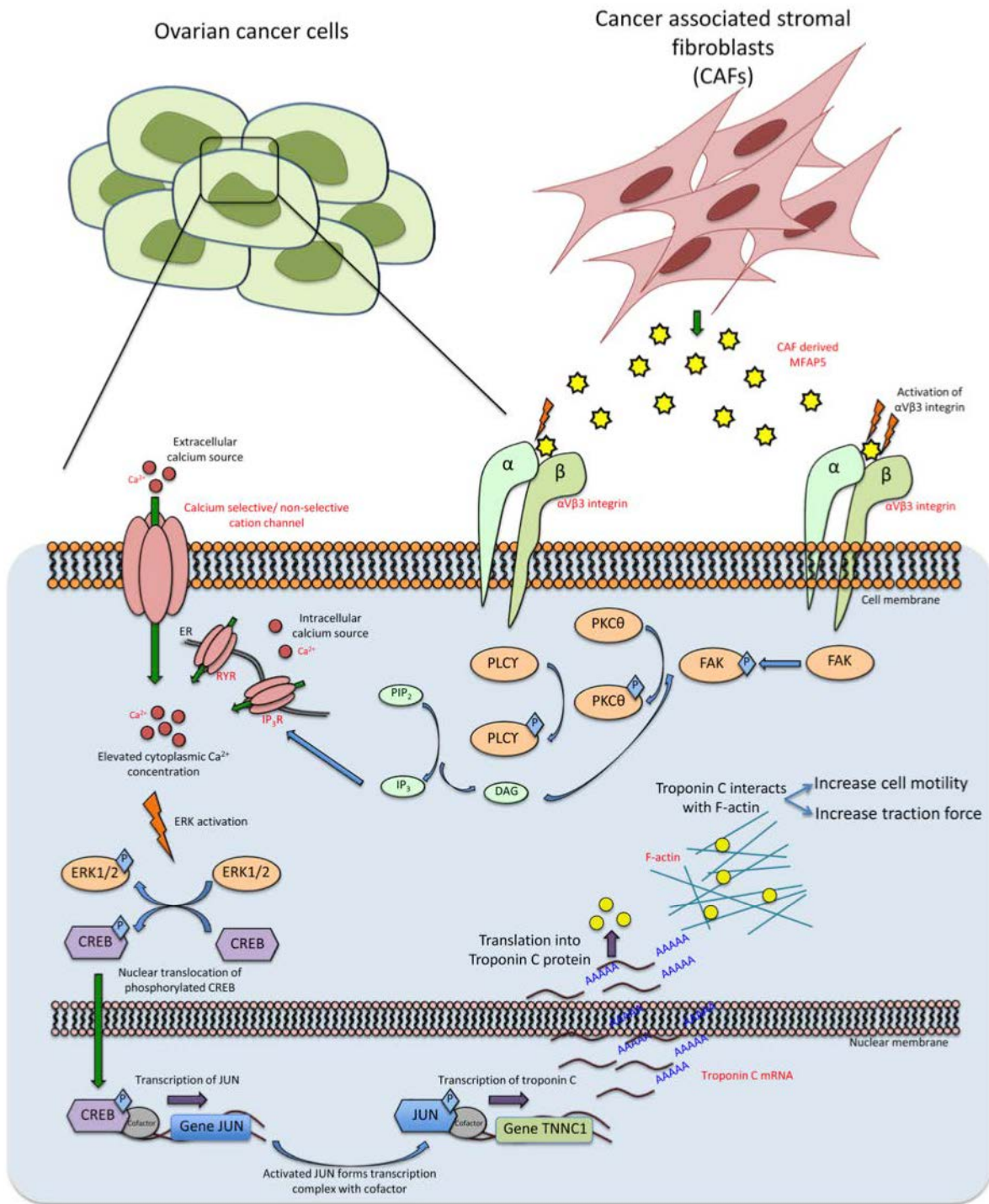


**Fig. 39: Molecular mechanism by which MFAP5 induces ovarian cancer cell motility and invasion potential.** A graphical summary of the molecular signaling events involved in MFAP5-mediated ovarian cancer cell motility and invasiveness.



To test the hypothesis, Western blot analyses were performed. Pretreatment with the anti- $\alpha_v\beta_3$  integrin antibody abrogated MFAP5-induced FAK and PLC- $\gamma$ 1 phosphorylation (Fig. 40) suggested that  $\alpha_v\beta_3$  integrin is responsible for MFAP5-induced FAK and PLC- $\gamma$ 1 phosphorylation. Previous studies showed that PLC- $\gamma$ 1 phosphorylation is stimulated by both  $\alpha_v\beta_3$  engagement and formation of FAK/ $\alpha_v\beta_3$  complex.<sup>116,117</sup> We therefore treated cancer cells with an FAK inhibitor to determine whether MFAP5-induced PLC- $\gamma$ 1 phosphorylation is FAK-dependent. Results demonstrated that phosphorylation of p-PLC- $\gamma$ 1 was attenuated in inhibitor pretreated cells (Fig. 41), suggested that MFAP5-induced pPLC- $\gamma$ 1 phosphorylation is FAK-dependent.

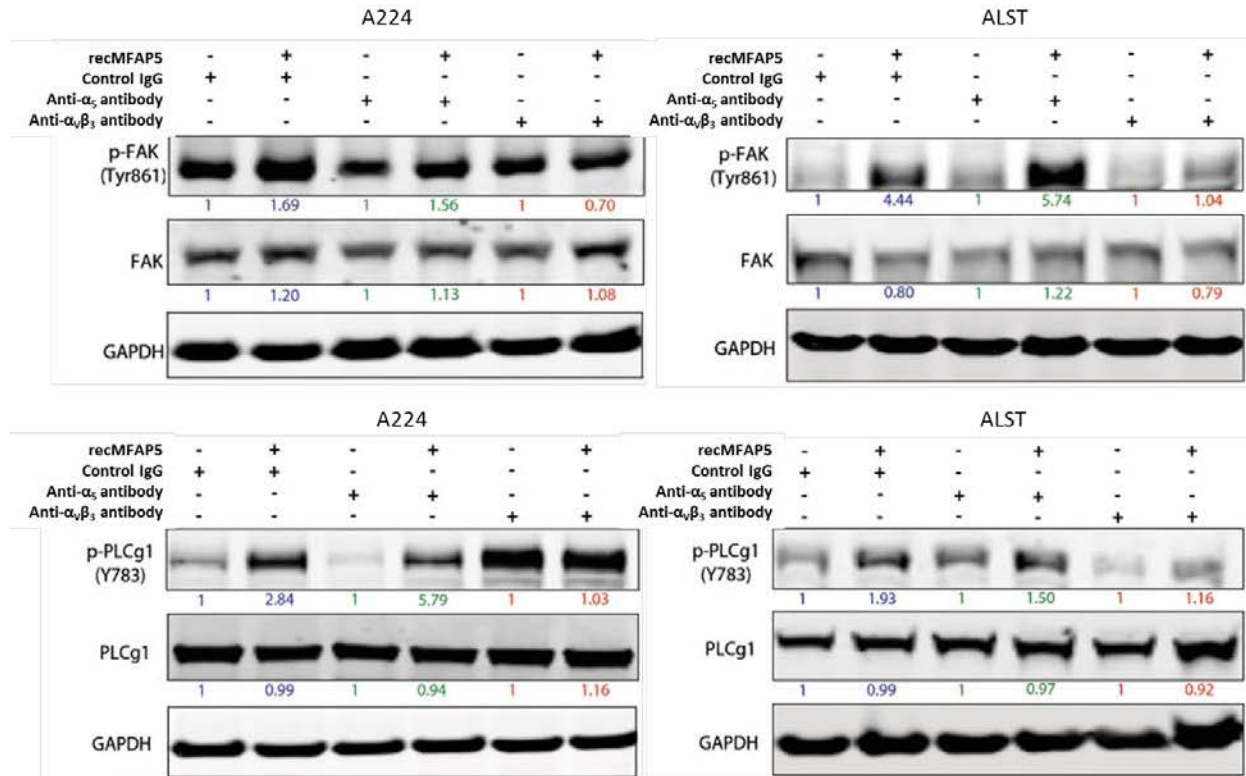


**Fig. 40: Western blots showing blockade of  $\alpha_v\beta_3$  integrin attenuated MFAP5 stimulated FAK and PLC- $\gamma$ 1 phosphorylation.** Pretreatment of A224 and ALST ovarian cancer cells with an anti- $\alpha_v\beta_3$  integrin antibody abrogated MFAP5's effect on FAK and PLC- $\gamma$ 1 phosphorylation, whereas pretreatment with an anti- $\alpha_5$  antibody and IgG had no effect.

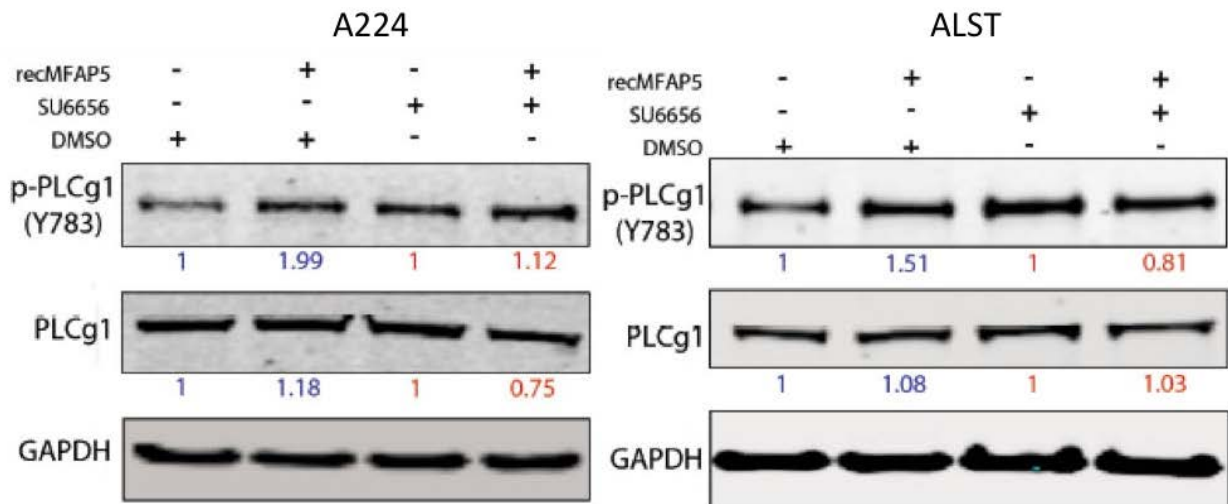


**Fig. 41: Western blots showing FAK inhibitor abrogated MFAP5 stimulated PLC-γ1 phosphorylation.** Increased p-PLC-γ1 expression in MFAP5-treated A224 and ALST cells was observed in the presence of solvent control DMSO but not in the presence of an FAK inhibitor SU6656.

Next, we sought to determine whether  $Ca^{2+}$  mobilization in MFAP5-treated ovarian cancer cells is dependent on p-FAK-mediated PLC-γ1 and PKCθ phosphorylation. Previous studies demonstrated that p-FAK induces PKCθ phosphorylation by activating PLC-γ1.<sup>118</sup> Activated PLC-γ1 increases the hydrolysis of intracellular phosphatidylinositol-4, 5-bisphosphate to form two products:  $IP_3$  and DAG.  $IP_3$  induces endogenous  $Ca^{2+}$  release from the endoplasmic reticulum via  $IP_3$  receptors, whereas DAG induces PKCθ phosphorylation and activation. Furthermore, p-PKCθ directly mobilizes  $Ca^{2+}$ .<sup>119,120</sup> To determine whether PKCθ activation is mediated by p-FAK in MFAP5-treated cells, Western blot analysis of p-PKCθ was performed. p-PKCθ level increased in MFAP5-treated cells only in the absence of the FAK inhibitor (Figs. 42). To determine whether the  $Ca^{2+}$  mobilization observed in MFAP5-treated cells was mediated via PKCθ activation, cells were treated with MFAP5 with or without a PKCθ inhibitor. PKCθ inhibitor decreased but did not eliminate  $Ca^{2+}$  mobilization (Fig. 43A), suggesting that  $Ca^{2+}$  mobilization is mediated only in part by PKCθ activation. To determine whether PLC activation is involved in  $Ca^{2+}$  mobilization, we studied the effect of PLC inhibitor

U73122 on  $Ca^{2+}$  mobilization in MFAP5-treated cells. PLC inhibition effectively suppressed  $Ca^{2+}$  mobilization (Fig. 43B), suggesting that PLC activation is the major signaling event involved in MFAP5-mediated  $Ca^{2+}$  mobilization. However, Western blot analysis revealed that PLC inhibitor abolished phosphorylation of PKC $\theta$  and PKC $\theta$  inhibitor abolished phosphorylation PLC- $\gamma$ 1 (Fig. 44), indicated that activation of PLC and PKC are interdependent and affect  $Ca^{2+}$  mobilization in MFAP5-treated cancer cells.

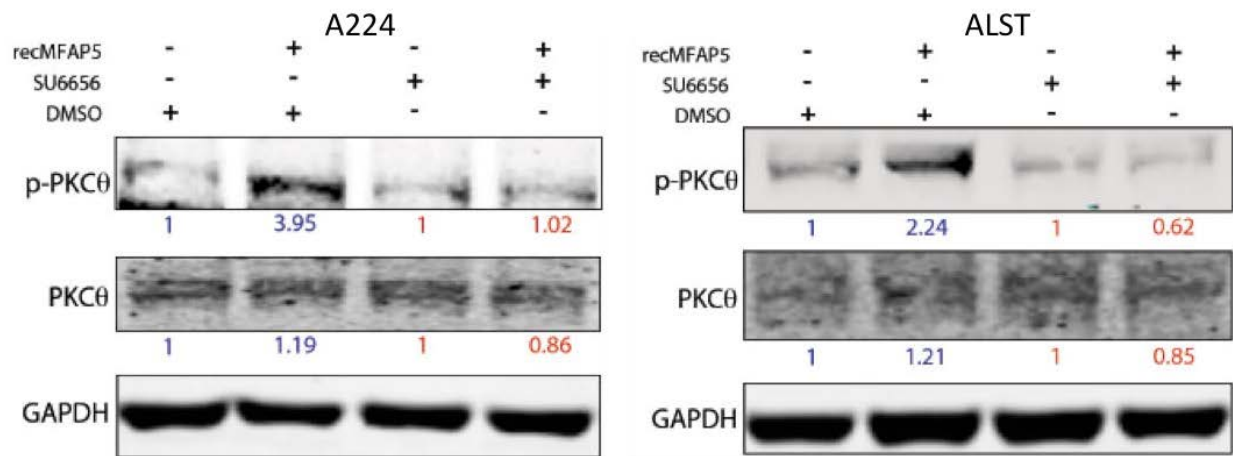


**Fig. 42: Western blots showing FAK inhibitor abrogated MFAP5 stimulated PKC $\theta$  phosphorylation.** Increased p-PKC $\theta$  expression in MFAP5-treated A224 and ALST cells was observed in the presence of solvent control DMSO but not in the presence of an FAK inhibitor.

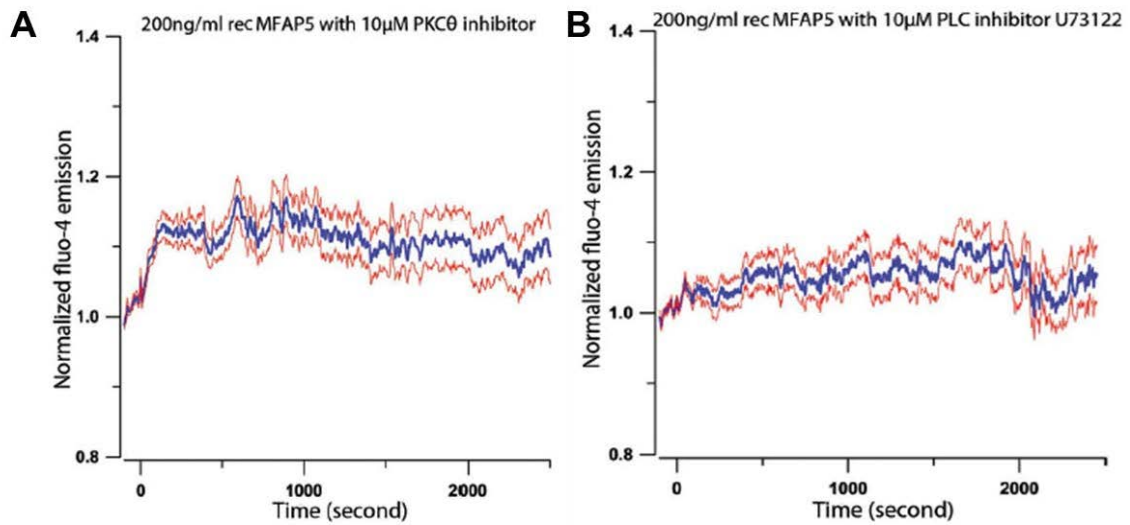


**Fig. 43: Effects of PKC $\theta$  and PLC inhibitors on calcium influx induced by recombinant MFAP5.** (A) Mean normalized time course of Ca<sup>2+</sup> mobilization in ALST cells induced by recombinant MFAP5 (200 ng/ml) in the presence of a PKC $\theta$  pseudosubstrate inhibitor (10  $\mu$ M, 30 minutes of preincubation). (B) Mean normalized time course of Ca<sup>2+</sup> mobilization in ALST cells induced by recombinant MFAP5 (200 ng/ml) in the presence of the PLC inhibitor U73122 (10  $\mu$ M, 30 minutes of preincubation). Red lines indicate standard errors. (Mean  $\pm$  SEM of 10 independent experiments).

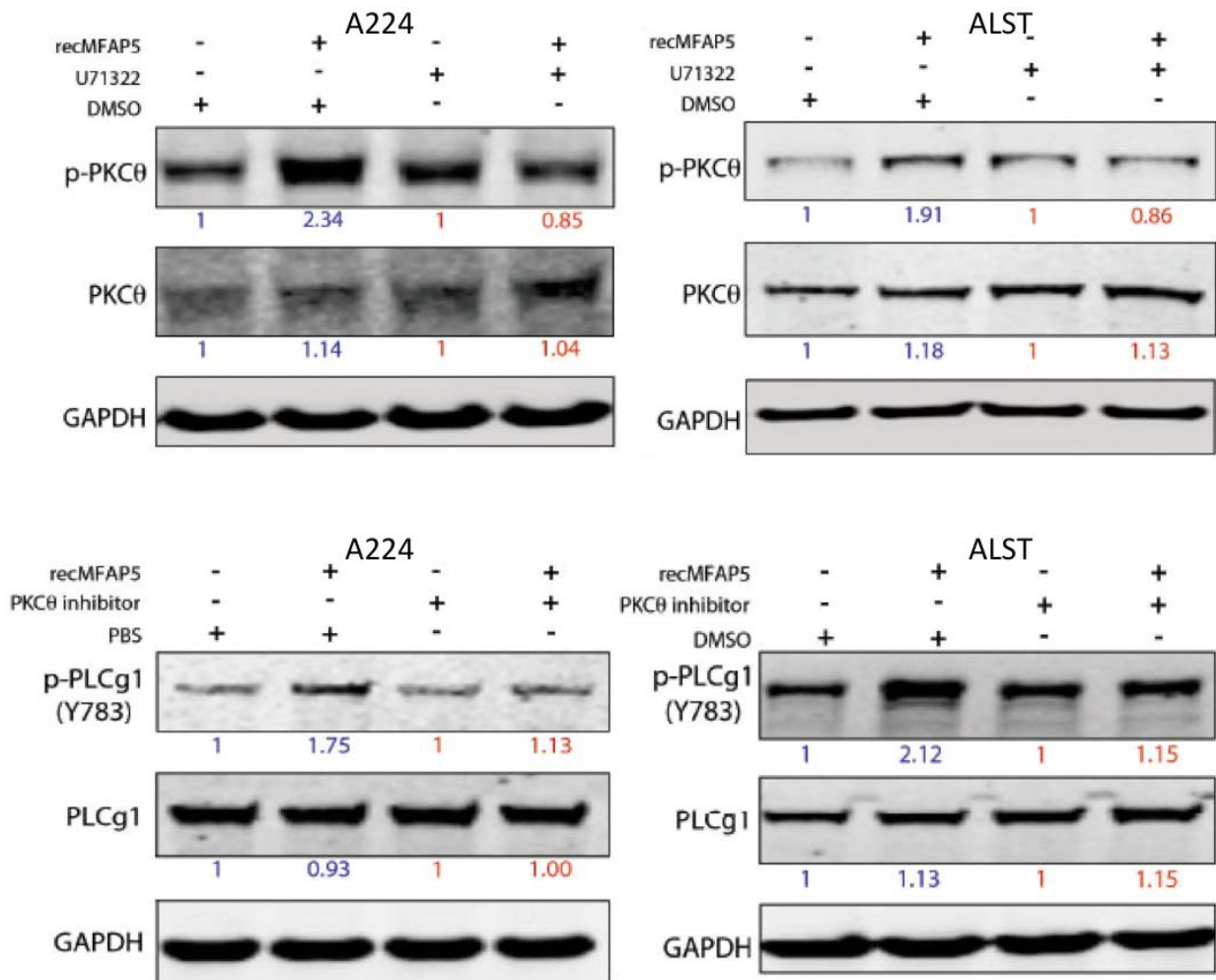


**Fig. 44: Western blots showing the effects of PKCθ and PLC inhibitors on PLC-γ1 and PKCθ phosphorylation respectively.** The PLC inhibitor U71322 abolished upregulation of p-PKCθ expression and the PKCθ inhibitor attenuated upregulation of p-PLC-γ1 expression in MFAP5-treated A224 and ALST cells.

To determine whether MFAP5-induced  $Ca^{2+}$  mobilization activates FAK via a feedback loop, we evaluated the effect of  $Ca^{2+}$  chelator BAPTA/AM on MFAP5-induced FAK phosphorylation. MFAP5-induced FAK phosphorylation was abrogated in BAPTA/AM-loaded cells, suggested that this phosphorylation is  $Ca^{2+}$ -dependent (Fig. 45).

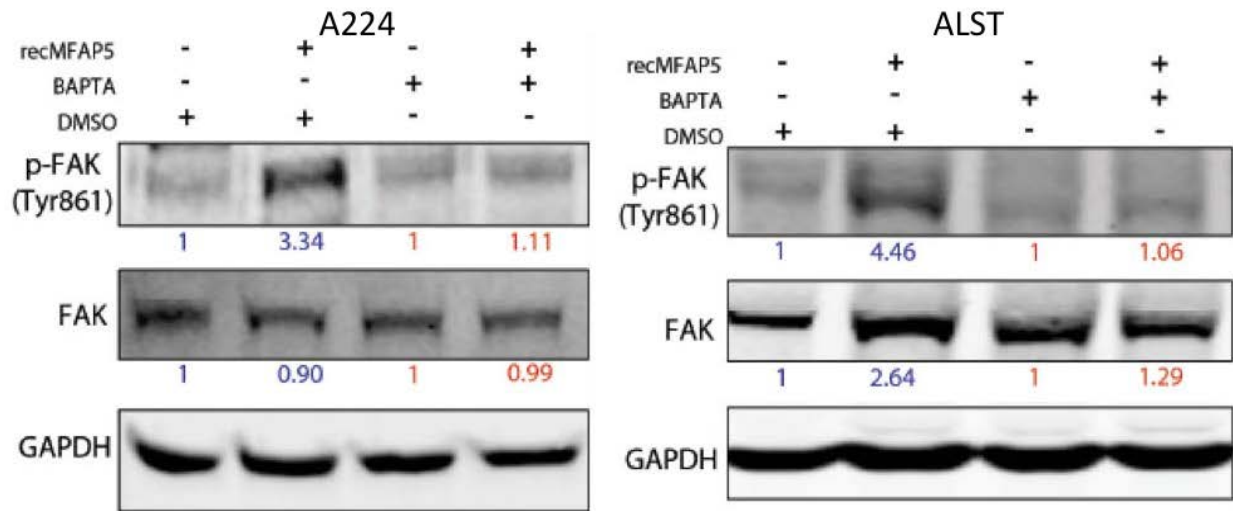


**Fig. 45: Western blots showing the effects of calcium chelation on FAK phosphorylation.** MFAP5-induced FAK phosphorylation was not observed in BAPTA/AM-loaded A224 and ALST cells.

ERK1/2 and CREB phosphorylation induced by recMFAP5 was attenuated in cells preloaded with  $\text{Ca}^{2+}$  chelator BAPTA/AM (Fig. 46), and in cells pretreated with PKC $\theta$  inhibitor, and PLC inhibitor U73122 (Figs. 47), suggested that MFAP5-induced ERK and CREB activation is calcium-dependent and mediated via  $\alpha_v\beta_3$  integrin/FAK/PKC $\theta$ - and  $\alpha_v\beta_3$  integrin/FAK/PLC- $\gamma$  activation.



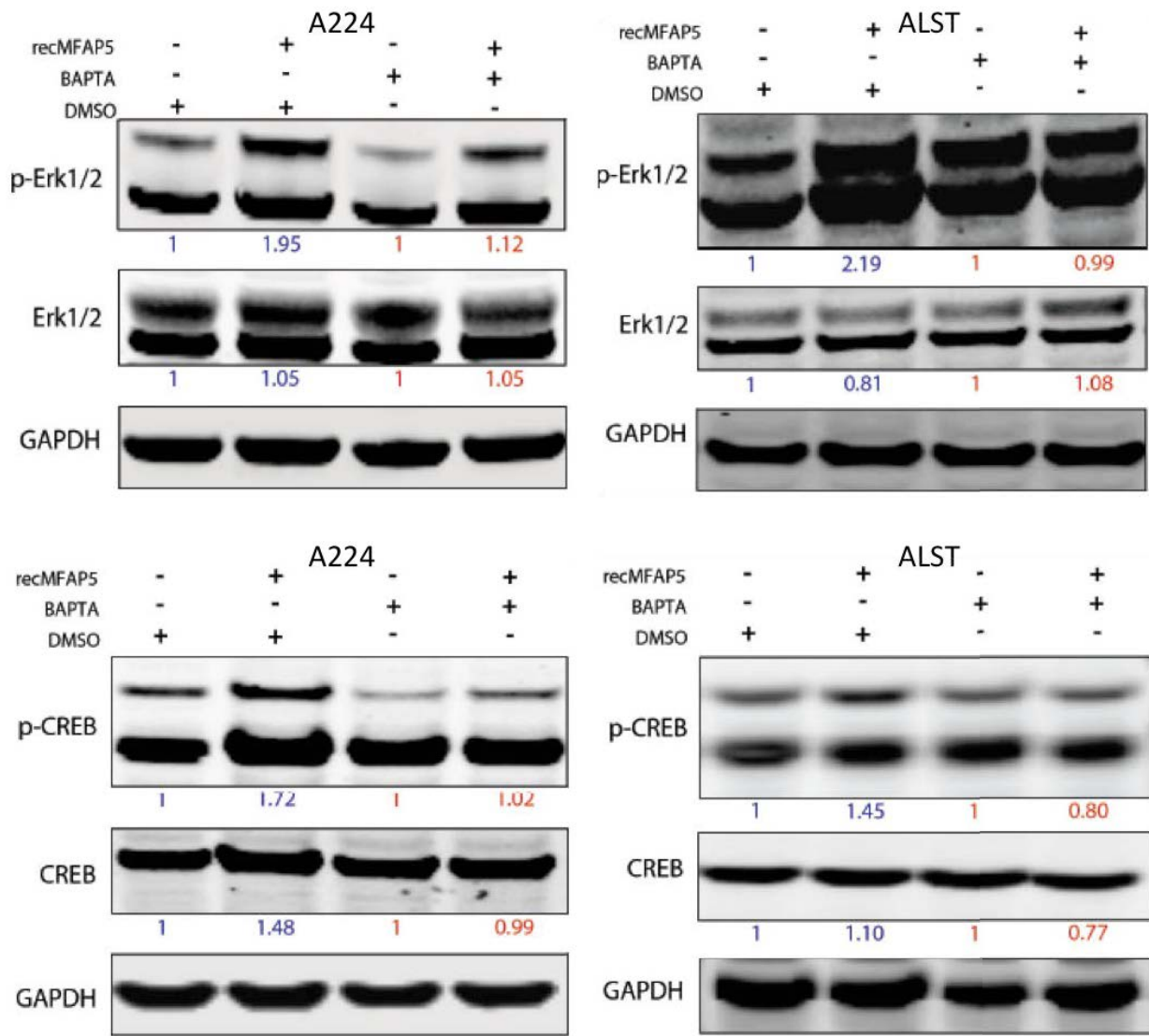


**Fig. 46: Western blots showing the effects of calcium chelation on ERK and CREB phosphorylations.** Phosphorylation of ERK1/2 and CREB after recMFAP5-based treatment was attenuated in BAPTA/AM-loaded A224 and ALST cells.

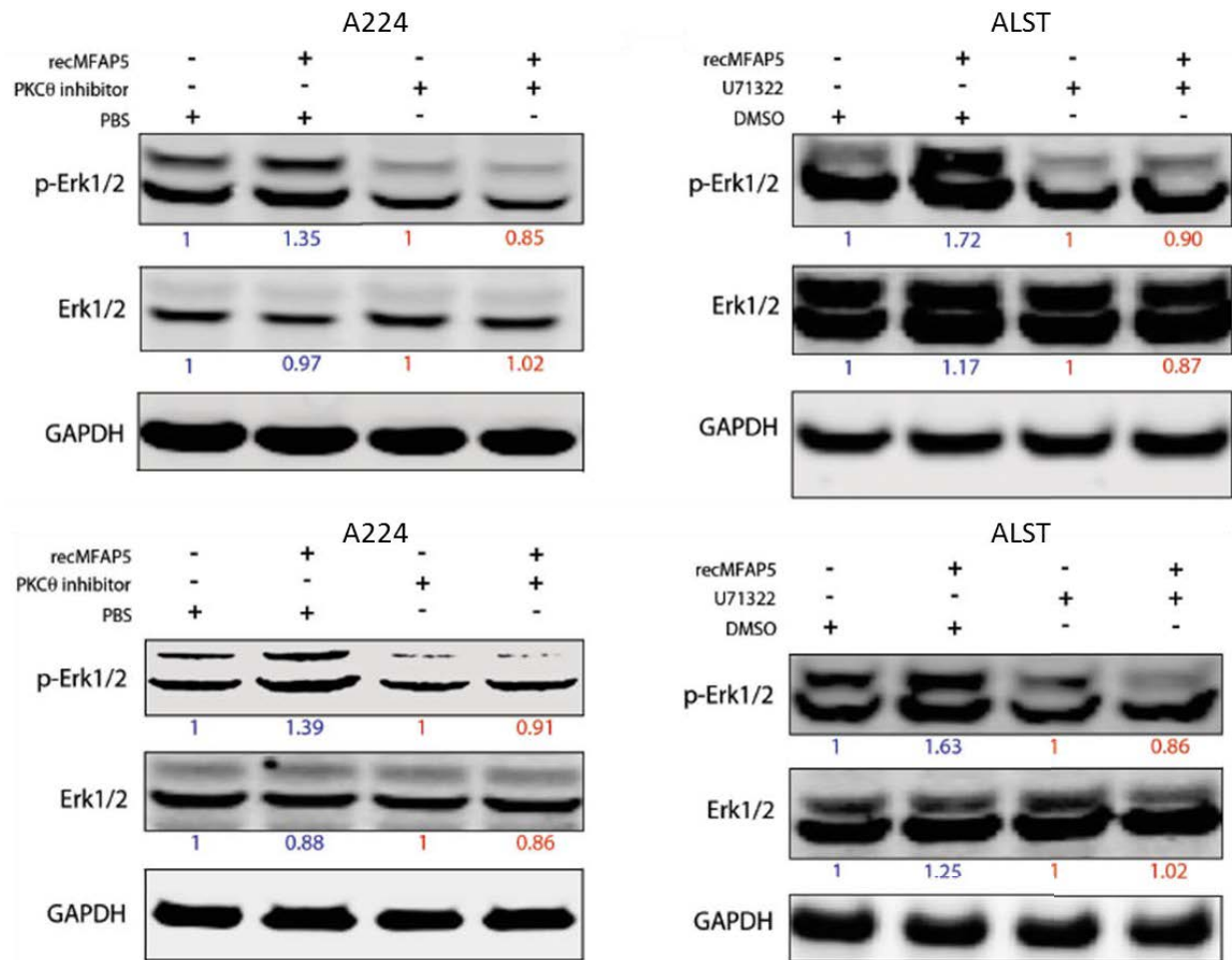


**Fig. 47: Western blots showing the effects of PKCθ and PLC inhibitors on ERK phosphorylation.** Application of a PKCθ pseudosubstrate inhibitor or PLC inhibitor (U73122) abrogated phosphorylation of ERK1/2 in MFAP5-treated A224 and ALST cells.

CREB is known to be activated by ERK.<sup>121</sup> To determine whether MFAP5 activates CREB through ERK, the effect of ERK1/2 inhibitor on MFAP5-induced CREB activation was evaluated. Pretreatment of cancer cells with ERK1/2 inhibitor abolished upregulation of p-CREB expression, suggesting that MFAP5 activates CREB through ERK (Fig. 48). CREB, together with co-activators, contributes to target gene transcription in response to Ca<sup>2+</sup> and via binding to the CRE. Our data demonstrated upregulation of c-Jun, which contains a CRE in its promoter, in MFAP5-treated cells. Also, promoter analysis revealed that the TNNC1 promoter consisted of potential AP-1 binding sites (Fig. 49), suggested that transcriptional upregulation



of TNNC1 expression is mediated by CREB-mediated c-Jun expression. To verify that, we evaluated the effects of CBP/CREB interaction inhibitor and c-Jun inhibitor SP600125 on MFAP5-treated cells. Results demonstrated that CBP/CREB interaction inhibitor attenuated the upregulation of p-c-Jun (Fig. 50) while SP600125 abrogated the upregulation of TNNC1 (Fig. 51). MFAP5-induced TNNC1 mRNA expression was abrogated in BAPTA/AM, CBP/CREB interaction inhibitor, and c-Jun inhibitor pretreated cells (Fig. 52). These data confirmed that the increase of TNNC1 expression induced by MFAP5 is calcium-dependent and mediated via upregulation of c-Jun by CREB activation.

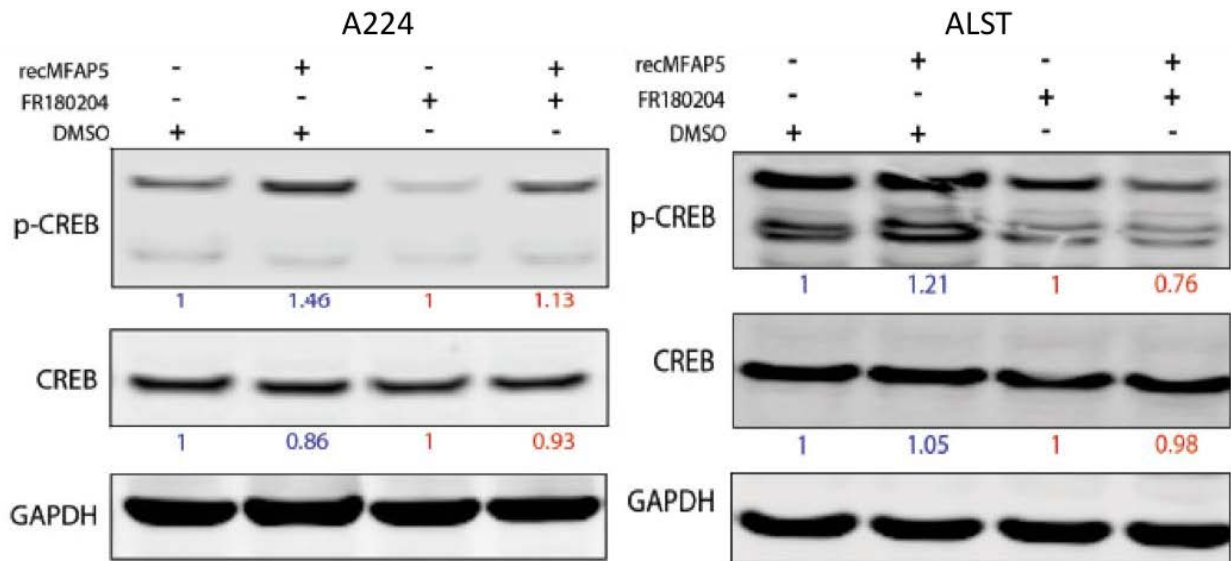


**Fig. 48: Western blots showing the effects of ERK1/2 inhibitor on CREB phosphorylation.** Pretreatment of ovarian cancer cells with the ERK1/2 inhibitor abolished the upregulation of p-CREB expression in MFAP5-treated A224 and ALST cells.

### Human TNNC1 promoter

```

-1500 GCCCCCGGCCCCCGCCCGCCGTCGCCCCCGCCGCGCGCTGCGCCGCCATCTTGCCCCCG -1441
-1440 CCTTCTTCCTGCGCCCTCGCCCCGCCCCCGCGCTGACTGACAGGGGCCACTCAGGGCGC -1381
                                     AP1 binding site 1
-1380 GCGTGCAGAGGTGCTCGCTTGCCTAATCTACCTGCGTGGCGCCGCCGGCGGTACCCTGCAC -1321
-1320 AGCCTGCTAGAAACTGAGACCCCGGGTGGTGACAGCTCTGGGCATGCCCCCTGGGTCTCTC -1261
-1260 GGGAAAGAGGGGACAGAAGGTCCCGAGTCTCCAGGCCACACGAAGCAAGTCACTGCTCTT -1201
                                     AP1 binding site 2
-1200 CCTGGCCTCAGTTTACTCCTCCTGATAAAGGAGGCCATAAATAGTGCCTCACCTGGCTGTT -1141
-1140 GGGCTCTTTCTCTTTAGGCAAGGCAGGTGAGAGGGGAAAATAGGACCTGTGCTTACCGC -1081
-1080 CGGAGCAGGGCGAGAGTGATTCTGGGCCAGTTCTGAACCTCTCTGAGATTCCGAGATCTC -1021
                                     AP1 binding site 3
-1020 TTGTCAGTGGGGCTTCTGGACAACCTGAGTGGGTGATTGATGCCCGGCCAGCACGCAGT -961
-960 AGTGCTCGAGGCAGGGAGCGTGTATTATCAAGAGGGATAAACTTGATACGAACTCTGTACG -901
-900 AAGGAAGGTGTAGGTGGATGGAGGGGTGTGTGCTGCCACTGAGCACAAGAACCACCGGG -841
-840 GTGGCCTGCCAAAGTTCAAAACGAGGGAGACAGGTTGATCTGGACCCAGGAACTACAGTG -781
-780 CTGAATCCTAAACCGGGGAAAGATGAGACCTAGAAGAGGGAGGTGTAACCTAATTGGAG -721
-720 GGTGAGGAGGGAAAAGAGCCTGCCACAGATGGGGCATCTATAGGGGTGCTGTTGAATAACT -661
-660 GAGAGCAGCTGACTTAAGCCCAGTGGGTACTTCTCCCTGGGCAGATGGGAGGTCTGGG -601
                                     AP1 binding site 4
-600 ACAGGCTCCTCTGGCAGAAGGGCTCCTGGCCACCCTGTCCCTAAGGTGGGTCAGTCACTTC -541
-540 CTCCTTCACCAGTTCACAGCATCTTACTATGAGCTTGGCATTTCGAGGCTTCTCTTGGCA -481
-480 GGGCCCTGCACTCCTAGCCTCTCCTTGACATTGCACCCCATTCAGAGAGGTTTAGTT -421
                                     AP1 binding site 5
-420 AAAGGCGGGGTTACCAAGTCAGTCAGATCTTGGGCAAGTCACCCTCCTCCAGAGCCTC -361
-360 AGTTTCTTATCTGGAAAGTGGAGGTGATGGCAACCCGCCAACCTGGTGGATGGGAGCC -301
-300 TGAGCTGTTGTGTGCACCTTGCCTGGGGCCACGACTTTGTAGCTCCTGTCCTGCACTG -241
-240 GGCTTATGTTTTCATTCATTCCAGAAACCTTTTCAGAGAGTCCCTTTGGGGAGTGTGGG -181
-180 GACAGGAGGGAAAAGAAACCTGGTCCCTGTAGCCGTTTCGTCTGCTCCCTGCCCTGGGCAGA -121
-120 GGACGTGGGACTCAGGCCAGCCTGAGATCACTGGGACCAGAGGAGGGGCTGGAGGATAC -61
-60 TACACGCAGGGGTGGGCTGGGCTGGGCTGGGCTGGGCCAGGAATGCAGCGGGGCAGGGCT -1
Transcription start site                               Start codon
1 A TTTAAGTCAAGGGCCGGCTGGCAACCCAGCAAGCTGTCTGTGAGCCGCCAGCATGGA 60
  
```

### Positional weight matrix



**Fig. 49: Promoter analysis revealed multiple potential AP-1 binding sites in the TNNC1 promoter.** The nucleotide sequence of the TNNC1 promoter from 1500 base pairs upstream the transcription start site was analyzed using the Biobase ExPlain Analysis Platform (Biobase Biological Databases, Wolfenbüttel, Germany). Five potential AP-1 binding sites were identified. The AP-1 transcription factor is a dimeric protein composed of proteins from the c-Jun and c-Fos families. The result suggested that MFAP5-induced TNNC1 upregulation may be regulated through upregulation of c-Jun expression and AP-1 transcription activation.

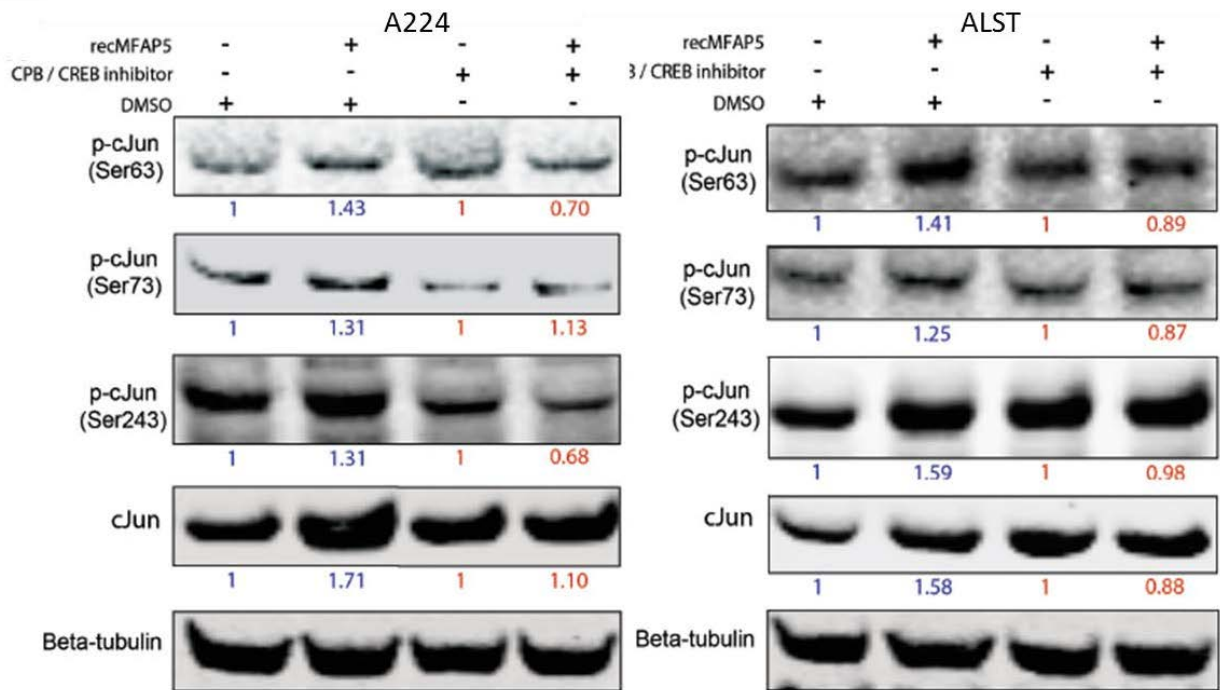


**Fig. 50: Western blots showing the effects of CBP/CREB interaction inhibitor on c-Jun and p-c-Jun expressions.** Pretreatment with the CBP/CREB interaction inhibitor attenuated the upregulation of total c-Jun and p-c-Jun expression induced by MFAP5 in A224 and ALST cells.

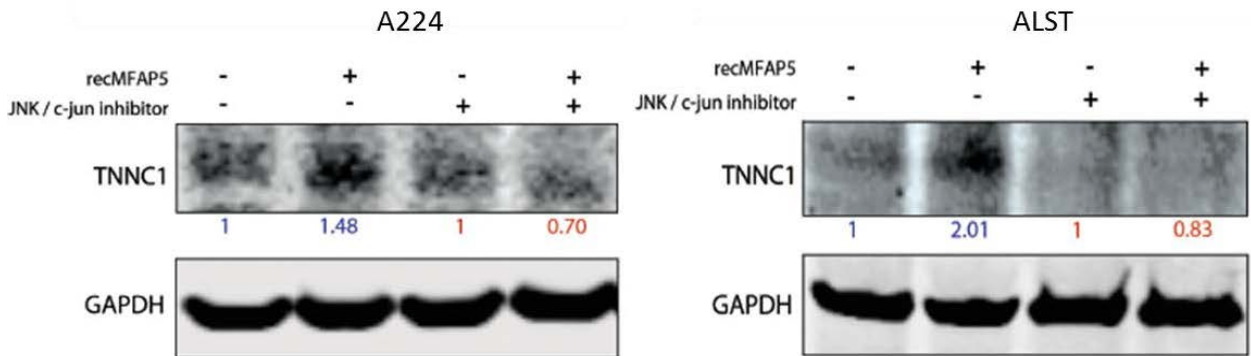


**Fig. 51: Western blots showing the effect of c-Jun inhibitor on MFAP5 induced TNNC1 overexpression.** Pretreatment with the c-Jun inhibitor abrogated the upregulation of TNNC1 expression induced by exogenous MFAP5 in A224 and ALST cells.

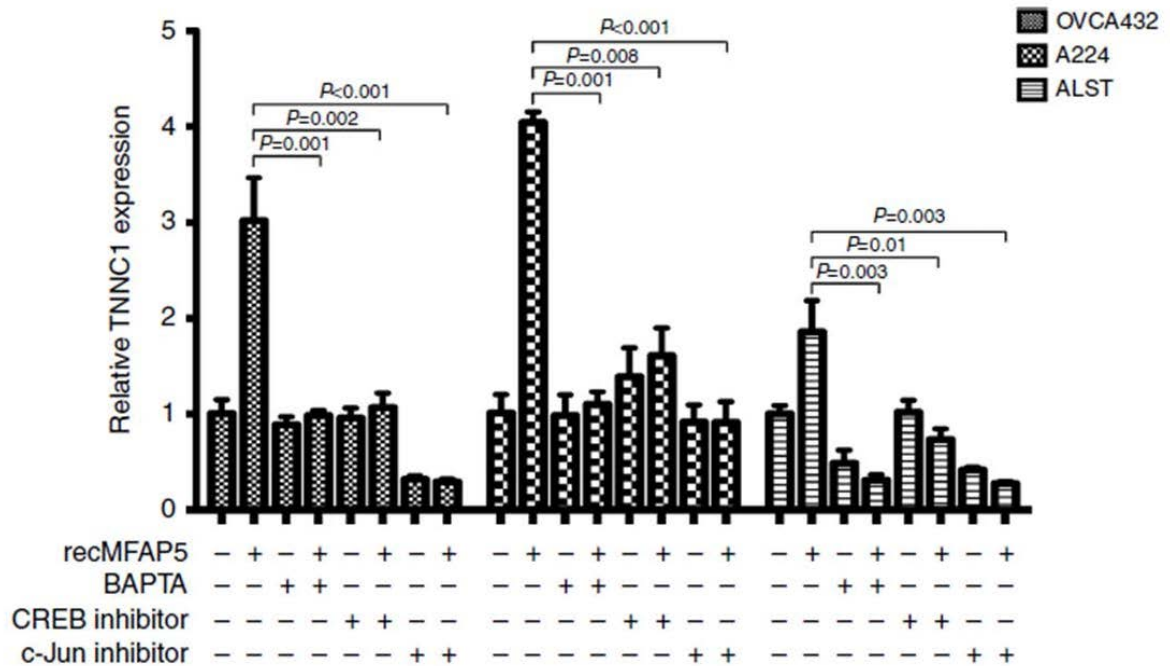


**Fig. 52: TNNC1 expression in ovarian cancer cells after pretreatment with calcium chelator and different inhibitors.** Abrogation of MFAP5-induced increase in TNNC1 mRNA expression in A224, ALST, and OVCA432 cells after pretreatment with cell-permeant calcium chelator BAPTA/AM, a CBP/CREB inhibitor, or a c-Jun inhibitor (mean  $\pm$  SD of 3 independent experiments).

To validate the activation of ERK signaling and upregulation of TNNC1 by MFAP5 *in vivo*, immunostaining of p-ERK1/2 and TNNC1 was performed on paraffin-embedded sections of Matrigel plugs from the previously described animal study. We observed higher p-ERK1/2 and TNNC1 expression in cancer cells in the Matrigel plugs embedded with MFAP5-overexpressing fibroblasts than in control Matrigel plugs (Fig. 53).

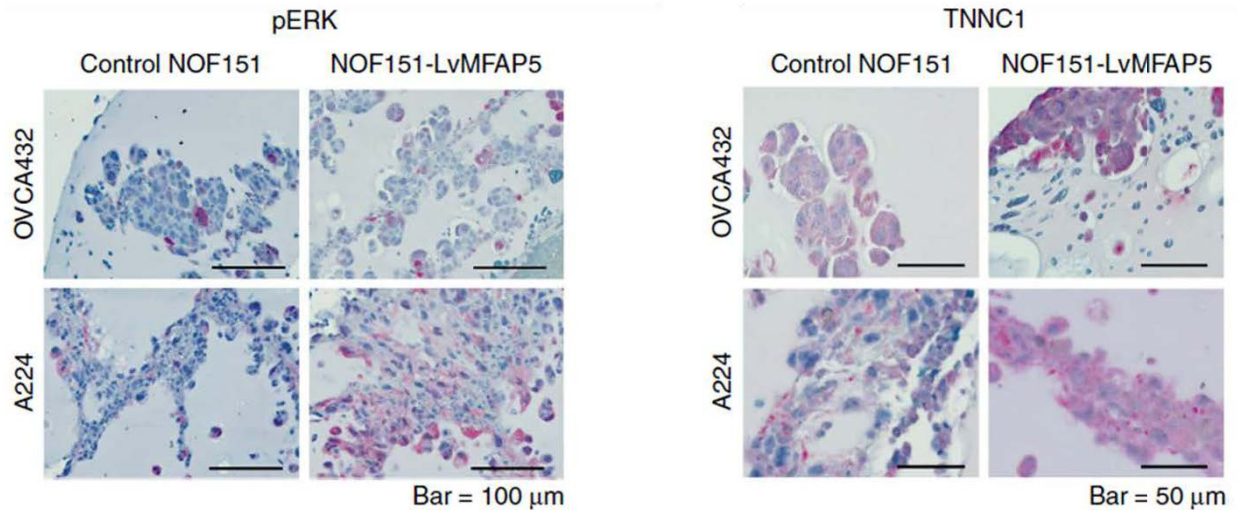
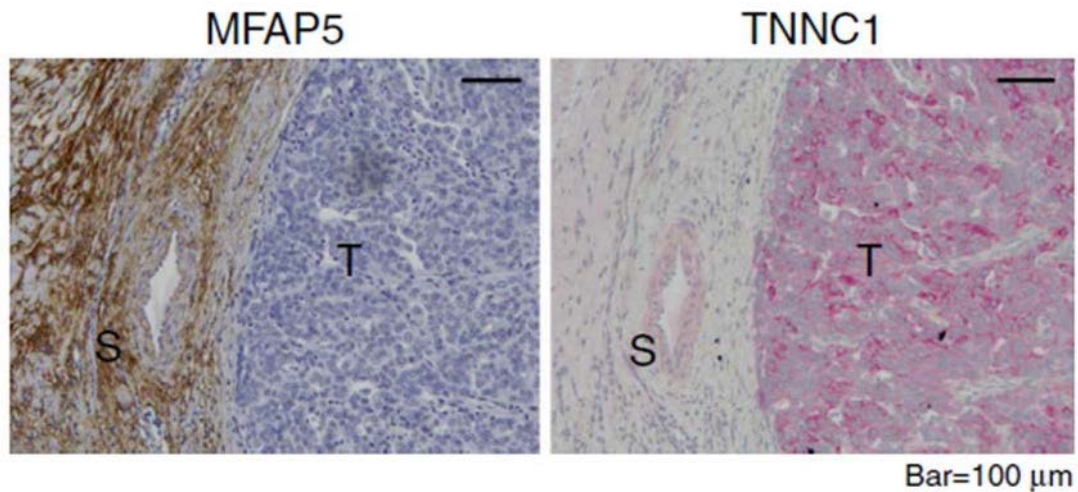


**Fig. 53: Validation of pERK and TNNC1 overexpressions in MFAP5 overexpressing fibroblasts embedded Matrigel plugs.** Immunolocalization of p-ERK1/2 and TNNC1 in paraffin tissue sections of Matrigel plugs collected from the peritoneal cavities of mice demonstrating that the effects of stromal MFAP5 on cancer cell motility and invasion potential were mediated by upregulation of p-ERK1/2 and TNNC1 expression.

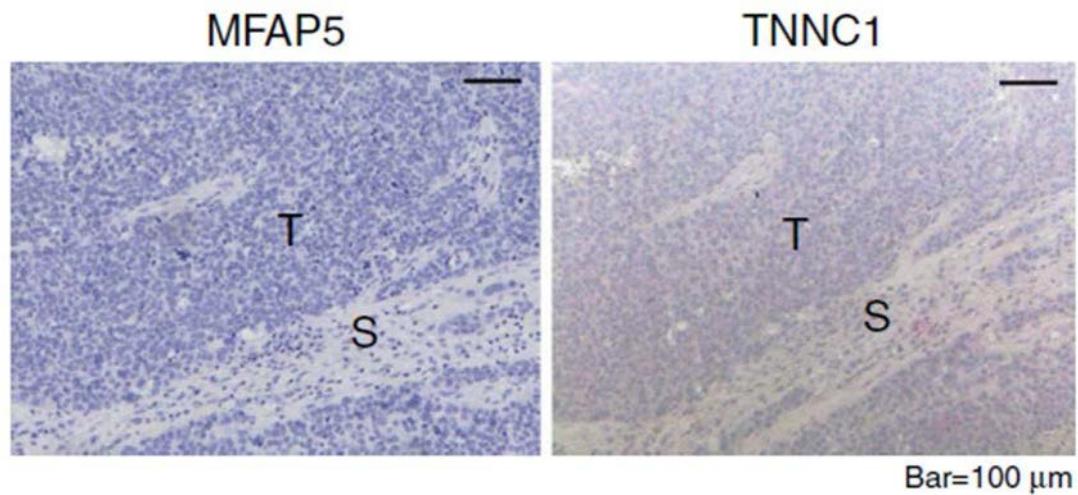
#### I. Correlation between tumor TNNC1 and stromal MFAP5 expression in human HGSOc samples revealed the clinical relevance of TNNC1

The relationship between tumor TNNC1 and stromal MFAP5 expression in 107 HGSOc tumor samples was evaluated by immunohistochemistry (Fig. 54) and a significant positive correlation between tumor TNNC1 and stromal MFAP5 expression ( $r=0.515$ ,  $p<0.001$ ) was observed (Fig. 55). Furthermore, Kaplan-Meier analysis and log-rank test revealed that low tumor TNNC1 expression was significantly associated with an improved survival ( $p=0.018$ ) (Fig. 56). Cox regression analysis adjusted for age and debulking status (hazard ratio: 1.705;  $p=0.029$ ) confirmed the prognostic significance of tumor TNNC1 expression.





High stromal MFAP5/high tumour TNNC1



Low stromal MFAP5/low tumour TNNC1

**Fig. 54: Correlation between stromal MFAP5 and TNNC1 expressions in ovarian tumor samples.** Immunolocalization of TNNC1 and MFAP5 in advanced-stage HGSOC tumor sections revealing a positive correlation between high stromal MFAP5 and high tumor TNNC1 expression. S, stroma; T, tumor. Bar=100  $\mu$ m.

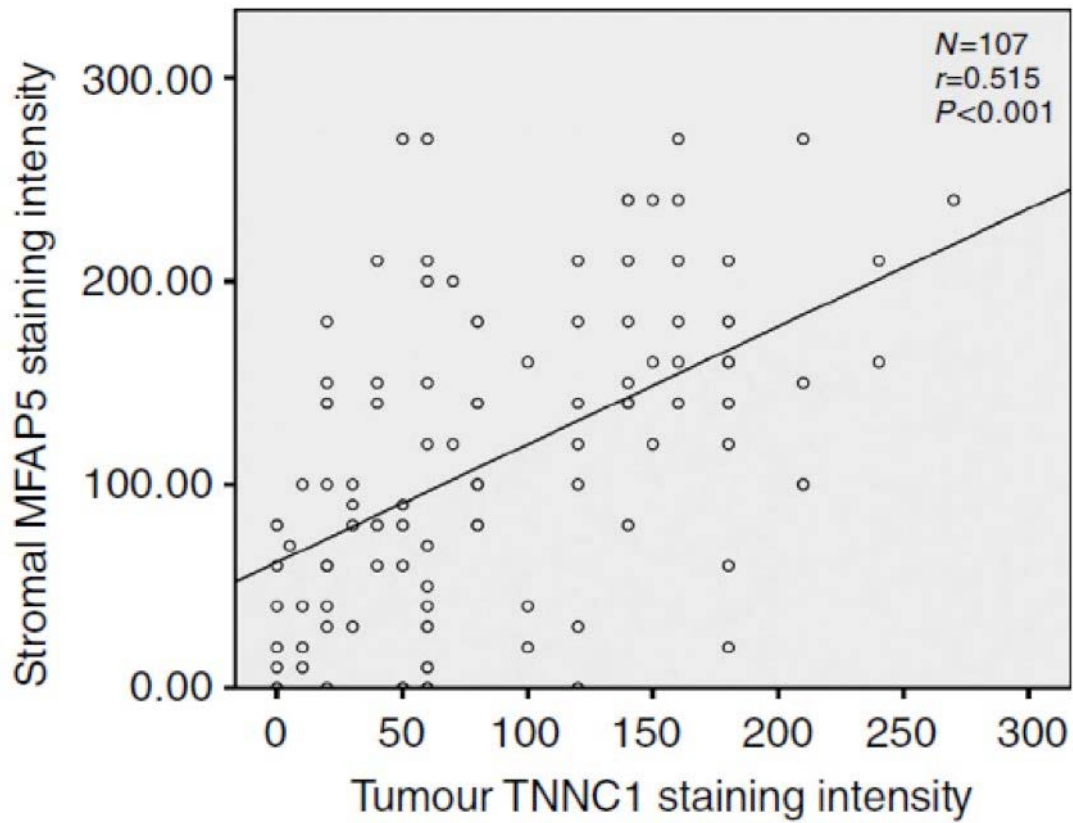


**Fig. 55: Spearman's rank correlation analysis between stromal MFAP5 and tumor TNNC1 expressions.** Positive correlation between stromal MFAP5 expression and tumor TNNC1 expression in HGSOc tissue samples was observed ( $N=107$ ;  $r=0.515$ ;  $p<0.001$ ).

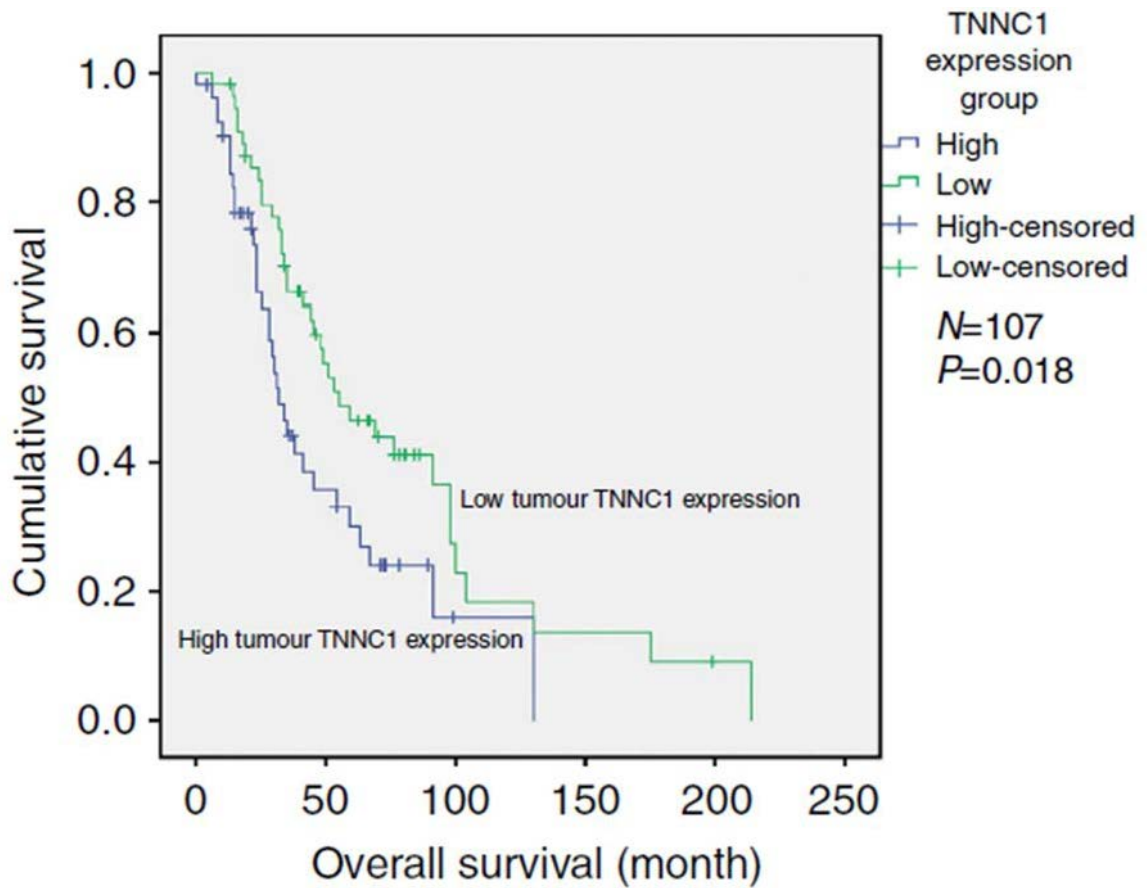


**Fig. 56: Kaplan-Meier analysis of the clinical significance of tumor TNNC1 expression with 107 FFPE tumor samples obtained from HGSOC patients. Low tumor TNNC1 expression is significantly correlated to better overall survival of HGSOC patients (N=107; p=0.018).**



**Specific aim II: The pro-angiogenic roles of stromal MFAP5 in ovarian cancer progression**

**A. Pro-angiogenic MFAP5 stimulates endothelial cell motility potential and permeability**

Increased microvessel density has been shown to be a poor prognostic marker for different types of tumors including ovarian cancer.<sup>10-13,112</sup> Staining data showed that expression of stromal MFAP5, which previously found to be significantly associated with poor patient survival, is significantly associated with CD31<sup>+</sup> microvessel density in HGSOC (Fig. 57).

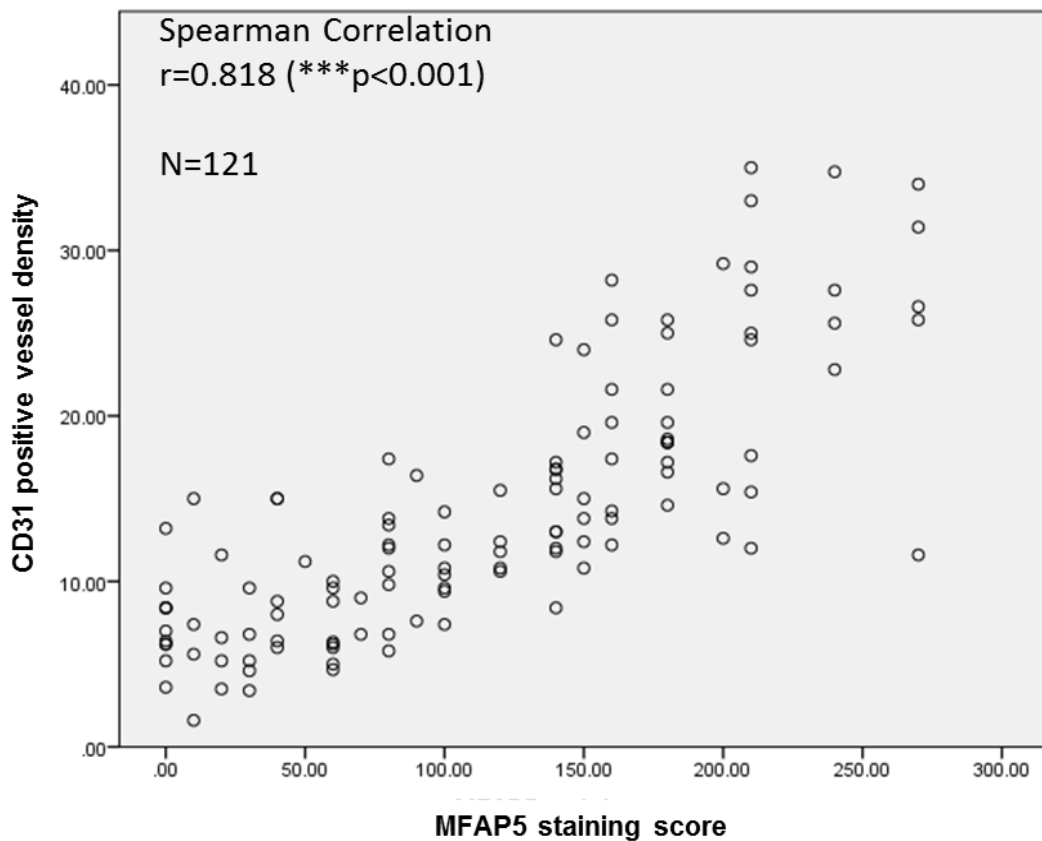


**Fig. 57: Spearman's rank correlation analysis between stromal MFAP5 and CD31 positive vessel density in HGSOC patient samples.** Positive correlation between stromal MFAP5 expression and CD31 positive vessel density was observed in HGSOC tissue samples (N=121; r=0.818; p<0.001).

We further evaluate the role of MFAP5 in angiogenesis by treating human

microvascular endothelial cells (hMEC-1) and telomerase immortalized microvascular endothelial (TIME) cells with exogenous MFAP5 protein. The results showed that while there was no effect of MFAP5 on endothelial cell proliferation rates, there was a significant increase of motility in cells treated with MFAP5, which was abrogated by the presence of anti- $\alpha_v\beta_3$  integrin antibody but not by the  $\alpha_5$  antibody or control IgG (Fig. 58), suggested that  $\alpha_v\beta_3$  integrin mediated the effects of MFAP5 on endothelial cell motility. In addition, by Boyden Chamber assay with porous cell culture inserts coated with Matrigel, we showed three folds increase in the numbers of hMEC-1 and TIME cells invaded through the matrix in recMFAP5 treated wells when compared to the control (Fig. 59), suggesting that MFAP5 also stimulated invasion potential of microvascular endothelial cells.

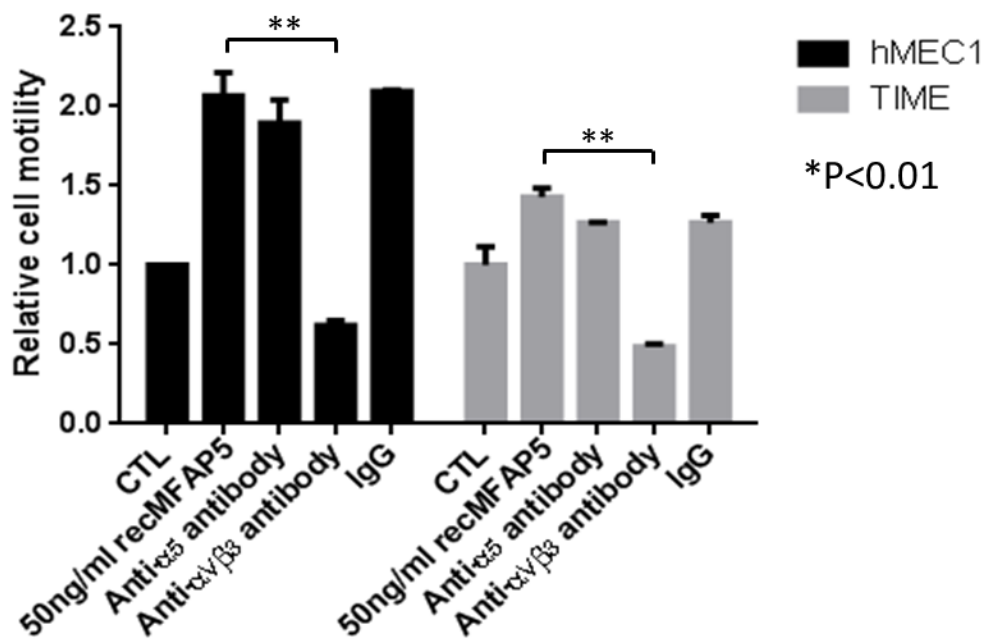


**Fig. 58: Attenuation of MFAP5-induced microvascular endothelial cell motility by the presence of anti- $\alpha_v\beta_3$  antibodies.** Relative motility of microvascular endothelial cells was evaluated after treatment with recombinant MFAP5 in the presence of control IgG, anti- $\alpha_5$  or anti- $\alpha_v\beta_3$  antibodies compared with antibody-free controls (mean  $\pm$  SD of 3 independent experiments;  $p < 0.01$ ).

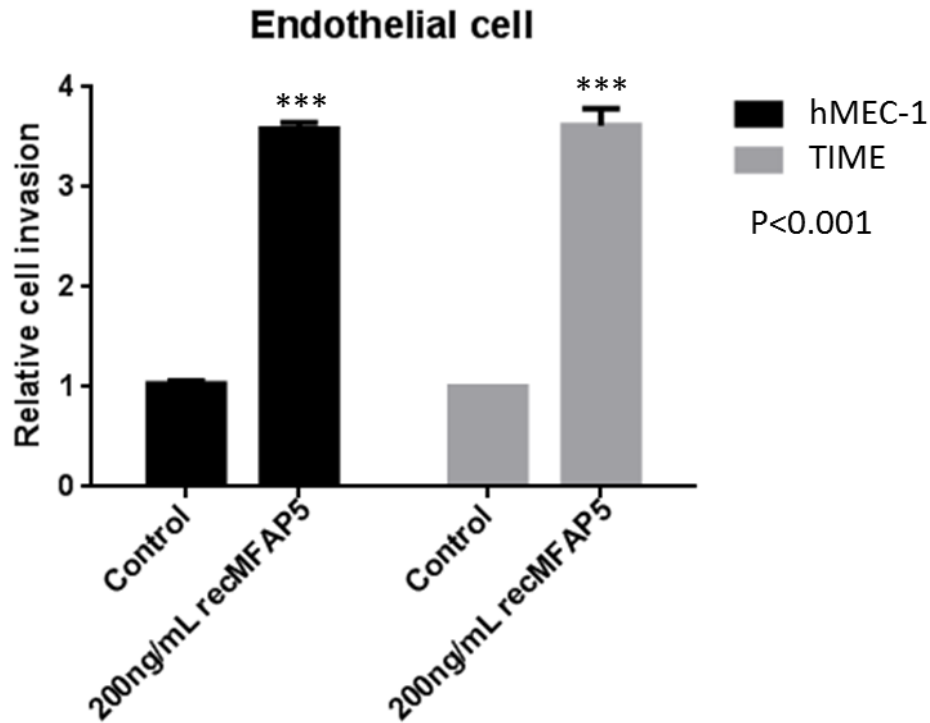


**Fig. 59: Exogenous MFAP5 promoted microvascular endothelial cell invasiveness.** Invasion assay using Matrigel invasion chamber showed that recombinant MFAP5 protein enhanced microvascular endothelial cell invasiveness (mean  $\pm$  SD of 3 independent experiments;  $p < 0.001$ ).

Furthermore, tube formation assay demonstrated enhanced tubular network formation by hMEC-1 and TIME cells seeded on Matrigel containing recMFAP5 when compared to the control Matrigel in a dose-dependent manner (Fig. 60). Further analysis using the angiogenesis module of the Metamorph Imaging Analysis software program confirmed that there were significantly increased in the total tube length, total tube area, number of segment and number of branch point in TIME cells seeded onto MFAP5 containing Matrigel in a dose-dependent manner when compared with those seeded onto PBS containing Matrigel ( $p < 0.05$ ) (Fig. 61). These data further support the pro-angiogenic roles of MFAP5.

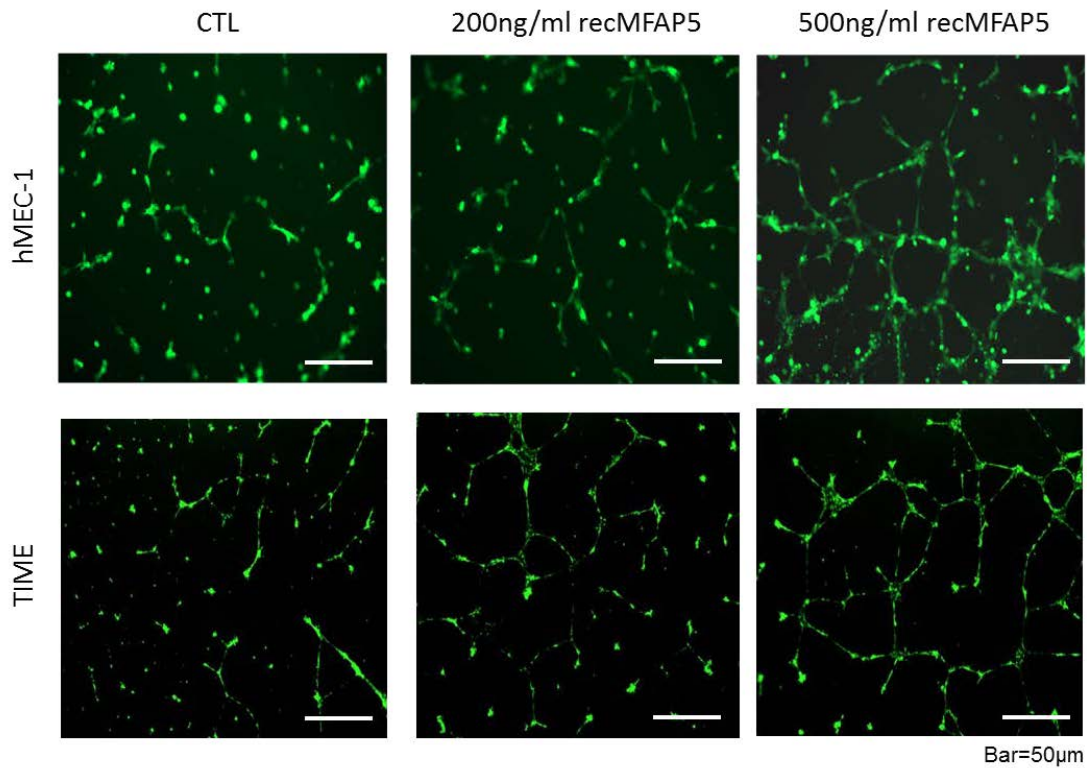


**Fig. 60: *In vitro* tube formation assay on MFAP5 treated microvascular endothelial cells.** Tube formation assay on hMEC-1 and TIME showing more extensive tubular structure formation on Matrigel mixed with recMFAP5 in a dose dependent manner when compared to control.

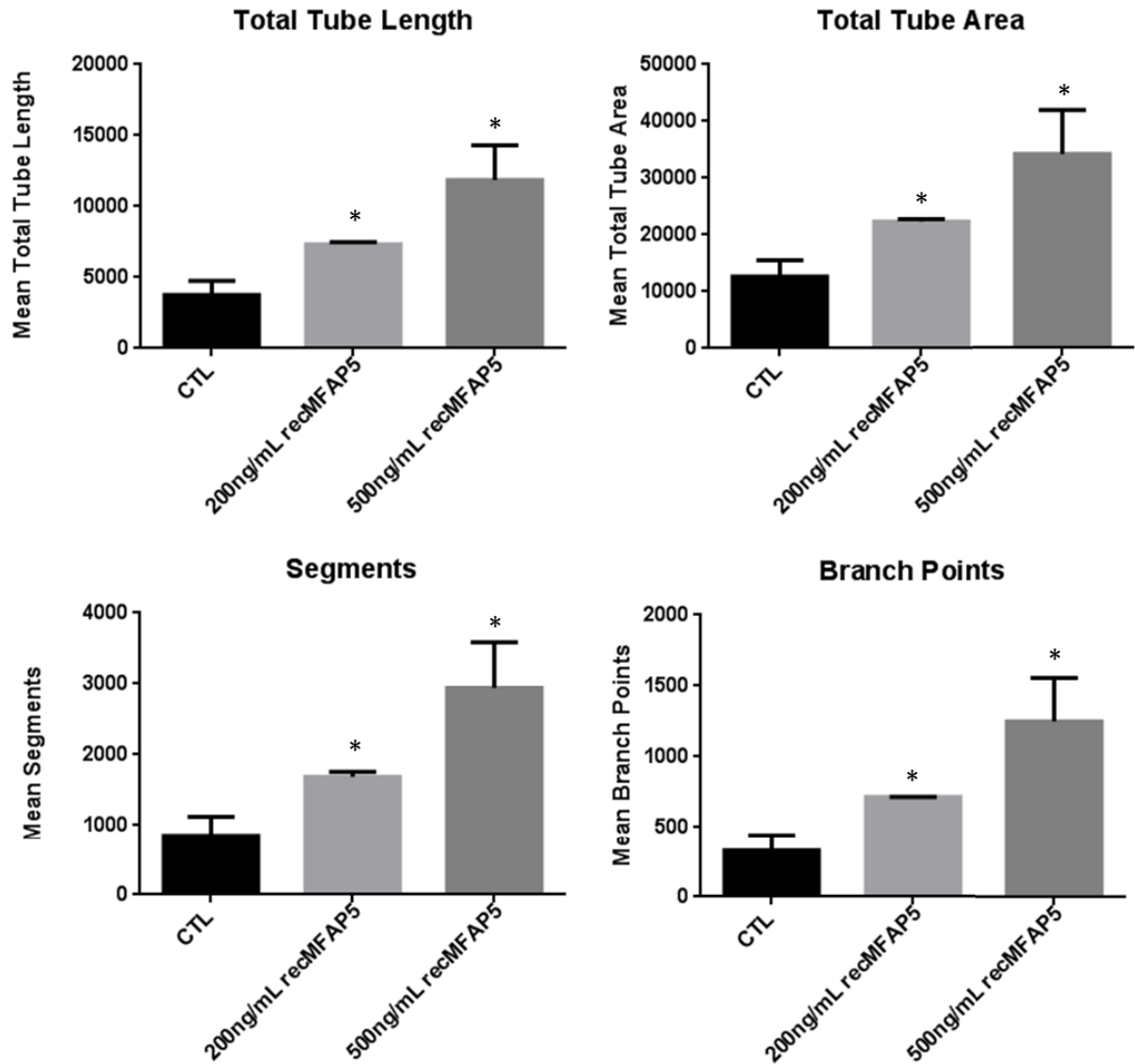


**Fig. 61: Quantitative analysis for *in vitro* tube formation assay.** Quantitative analysis using the Leica Metamorph Angiogenesis Module showed that there were significantly increased in the total tube length, total tube area, number of segment and number of branch point in TIME cells seeded onto MFAP5 containing Matrigel in a dose-dependent manner compared with those seeded onto Matrigel reconstituted with PBS ( $p < 0.05$ ).

In addition, blood vessel leakiness in tumors has been shown to facilitate excessive fluid loss from the vasculature to the interstitial space, which increases the interstitial pressure and reduces blood flow. This will negatively affect the distribution of systemically administrated drugs in solid tumor.<sup>122</sup> To evaluate the effect of MFAP5 on endothelial cell monolayer

permeability *in vitro*, hMEC-1 or TIME cells were seeded onto to the E-plate of the xCELLigence system to obtain confluent monolayer cultures for the impedance measurement by the RTCA analyzer in the presence or absence of MFAP5. The results showed that there was a significant decrease in impedance in MFAP5-treated endothelial cell monolayer cultures suggested that there was a disruption of the endothelial monolayer integrity by MFAP5 treatment (Fig. 62). To further validate such observation, we performed an *in vitro* permeability assay by measuring the traversing of FITC-labeled dextran (relative molecular mass 70,000) through the hMEC-1 and TIME monolayers growing on 0.4 $\mu$ m porous cell culture membrane in the presence or absence of recombinant MFAP5 protein. The result showed that MFAP5 increased passage of the fluorescent-labeled dextran from the cell culture insert to the bottom wells. (Fig. 63)

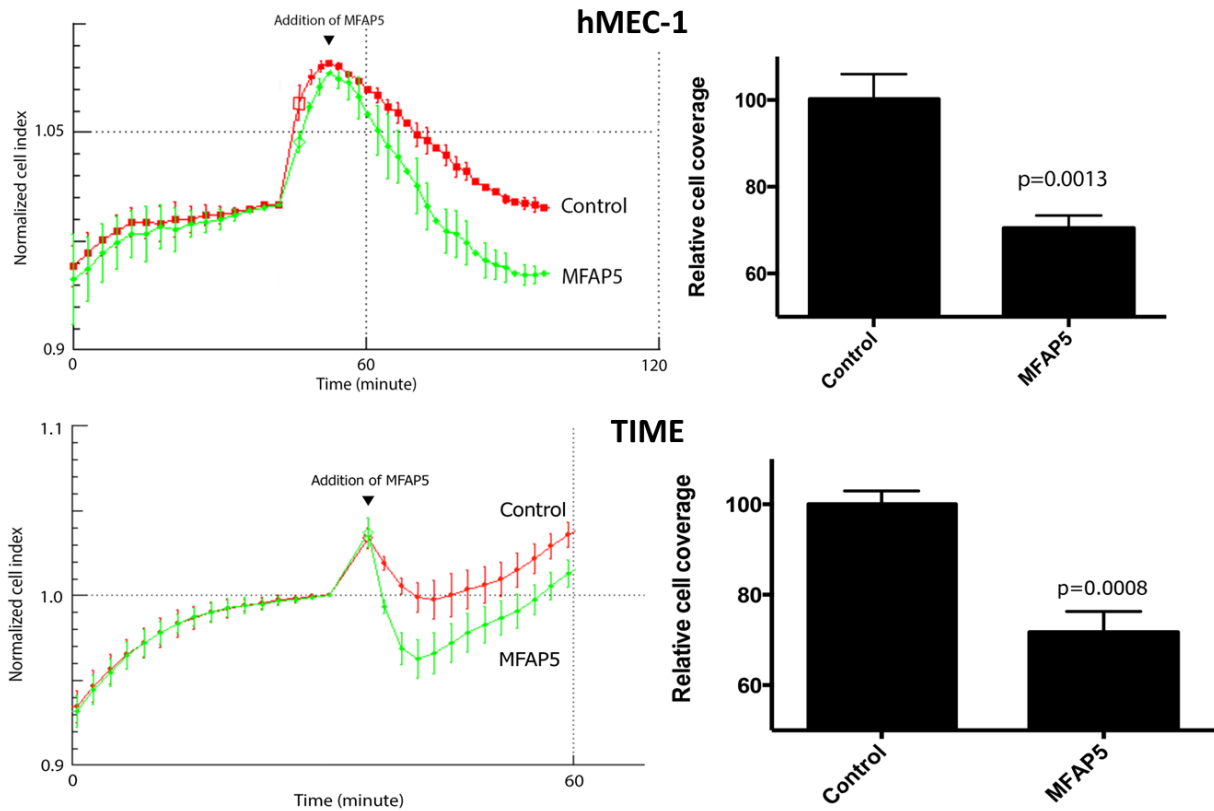


**Fig. 62: Permeability assay using the xCELLigence system.** Impedance measurement by the xCELLigence system in the presence of MFAP5 showed that there were significant decreases in the impedance of hMEC-1 and TIME monolayers when compared to the control, suggesting that there was a disruption of the endothelial cell monolayer integrity by the presence of MFAP5.

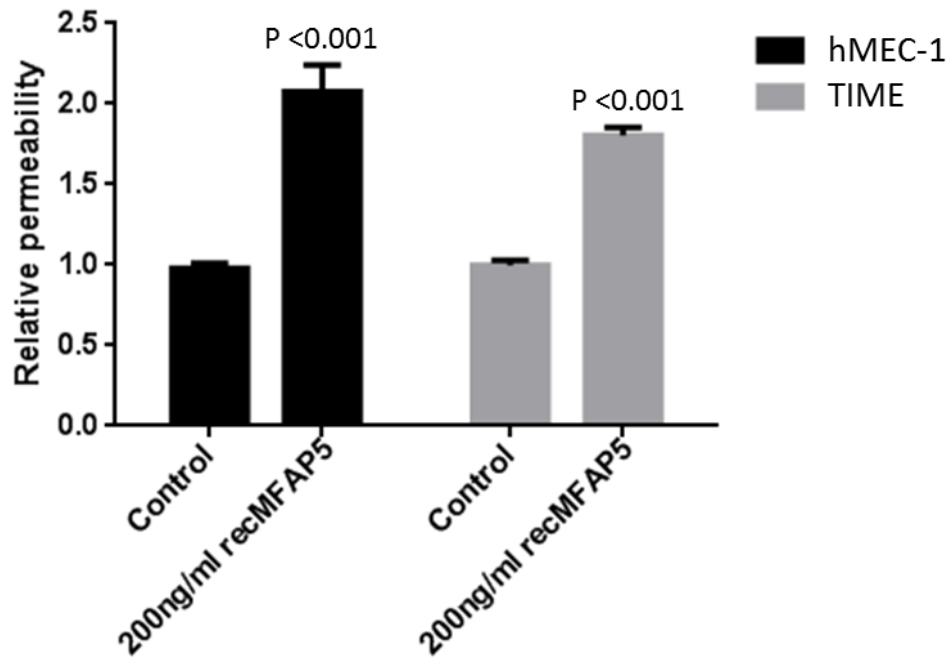


**Fig. 63: Permeability assay using Boyden chambers.** Treatment with recombinant MFAP5 protein facilitated the passage of FITC-labeled dextran (relative molecular mass 70,000) through the hMEC-1 and TIME monolayer cultures growing on the 0.4 $\mu$ m porous cell culture membrane to the bottom wells.

### B. Stromal MFAP5 enhanced matured intratumoral microvessel formation

To evaluate the roles of MFAP5 in angiogenesis *in vivo*, A224 ovarian cancer cells were co-injected subcutaneously with either MFAP5-overexpressing NOFs or control NOFs. The results showed a significant increase in tumor size and weight as well as the number of CD34<sup>+</sup> microvessels in the tumor tissue with high stromal MFAP5 expression level (Fig. 64), suggesting that stromal MFAP5 facilitated tumor angiogenesis *in vivo*, which could subsequently lead to increased tumor growth. In addition, immunostaining of pericyte marker, NG2, was performed on paraffin sections of tumor tissue harvested. The result showed significantly increased pericyte coverage in MFAP5-overexpressed tumors, suggested that MFAP5 stimulates the formation of matured intratumoral microvessels (Fig. 65).



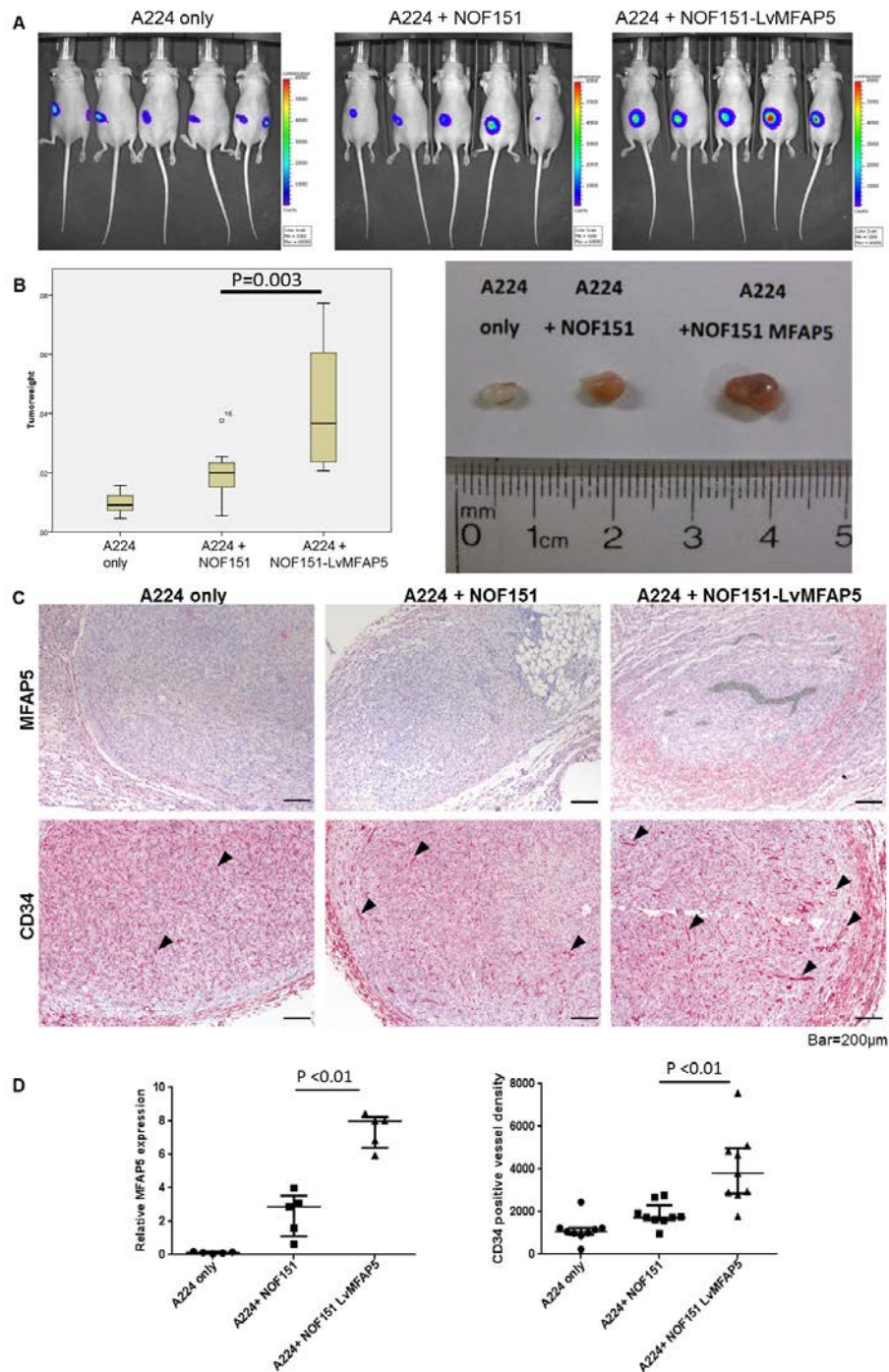


**Fig. 64: The effects of stromal MFAP5 on ovarian cancer cells growth *in vivo*.** (A) Tumor growth for each treatment groups was quantified. (B) Significant increased tumor growth was observed when A224 cells were co-cultured with MFAP5 overexpressing fibroblasts *in vivo* ( $p=0.003$ ). Box represents the interquartile range of the records and the line across the box indicates the median. Whiskers indicate the highest and lowest values among the records that are no greater than 1.5 times the interquartile range. Outliers (indicated by numbered circles) are cases with values between 1.5 and 3 times the interquartile range. (C) Immunolocalization of MFAP5 and CD34. Arrows indicate microvessels. (D) MFAP5 and CD34 staining on tissue sections were quantified ( $p < 0.01$ ). For scatter plots, upper and lower bars indicate the interquartile range of the records, and the middle line indicates the median.

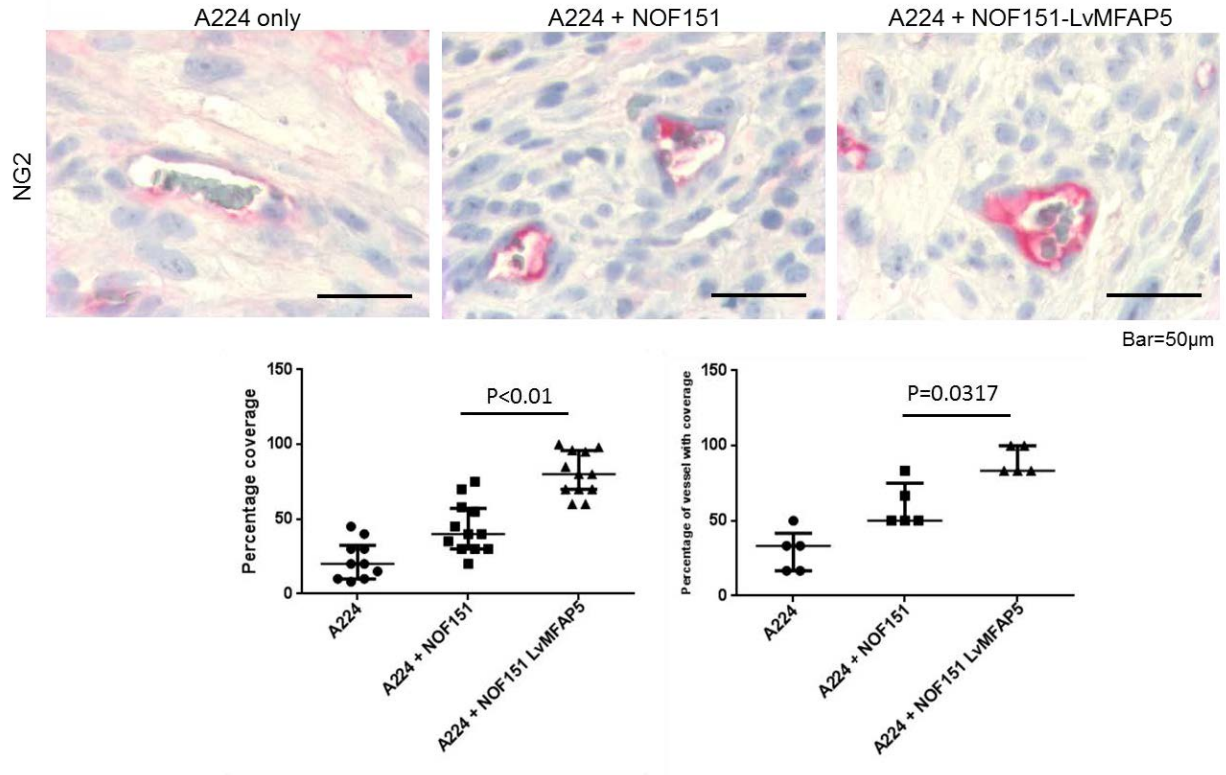


**Fig. 65: The effect of stromal MFAP5 on pericyte coverage on intratumoral microvessels.** Immunostaining of pericyte marker, NG2, on paraffin sections of tumor tissue harvested showed significantly increased pericyte coverage in MFAP5 overexpressed tumors, suggesting that MFAP5 stimulates the formation of matured intratumoral microvessels. Quantification analysis was performed using the Image Pro PLUS 7.0 software. For scatter plots, upper and lower bars indicate the interquartile range of the records, and the middle line indicates the median.

To further delineate the roles of MFAP5 in angiogenesis *in vivo*, the numbers of microvessels infiltrating the Matrigel plugs reconstituted with different concentration of recMFAP5 and implanted subcutaneously in nude mice were quantified. The results showed a significant increase in the total tube length, total tube area, number of segments and number of nodes of CD34<sup>+</sup> microvessels in Matrigel reconstituted with recMFAP5 in a dose-dependent

manner when compared to the control (Figs. 66 and 67). These data further support the promoting effects of MFAP5 on tumor angiogenesis.

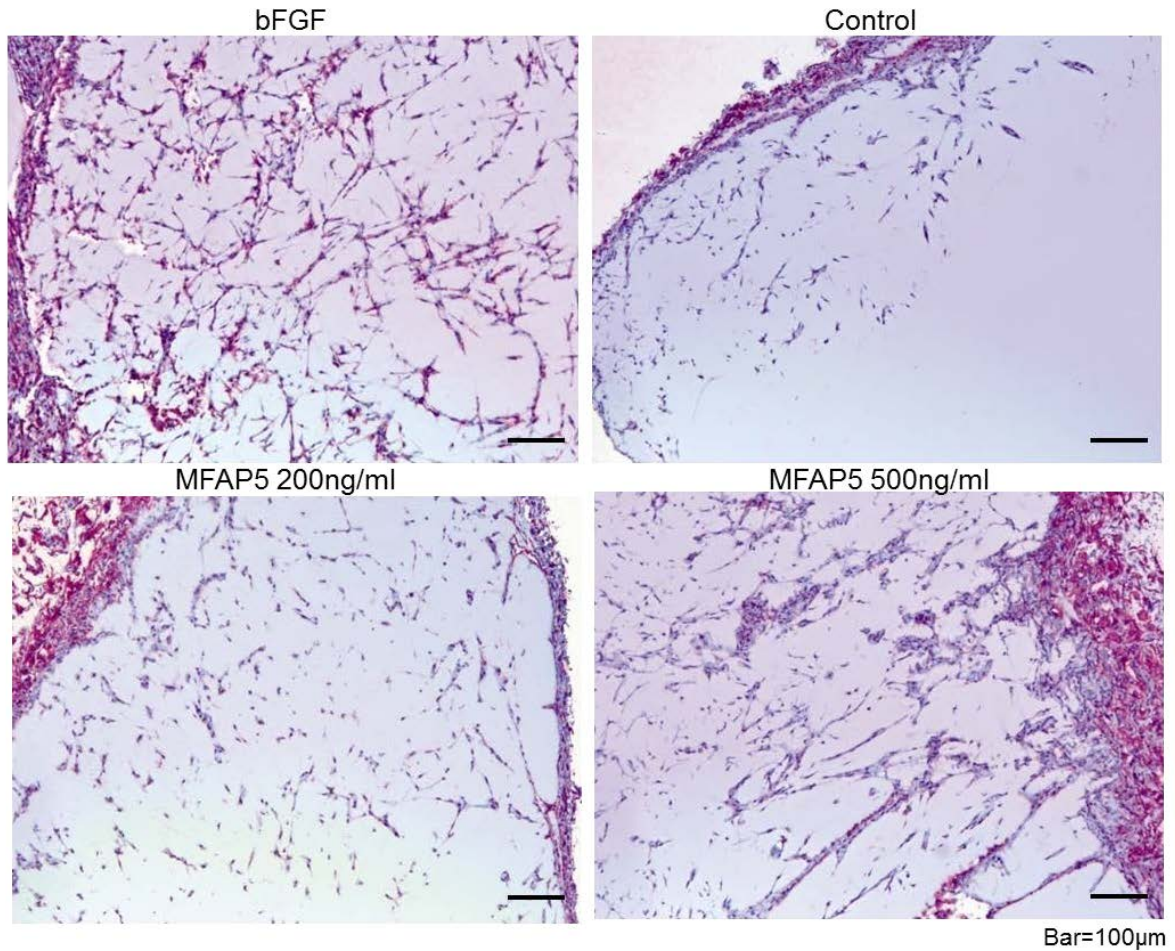


**Fig. 66: Effects of MFAP5 on tube formation of endothelial cells was demonstrated by *in vivo* angiogenesis assay.** More extensive tubular network structures were observed in Matrigel reconstituted with recMFAP5 in a dose dependent manner. bFGF, a known pro-angiogenic protein, was used a positive control.



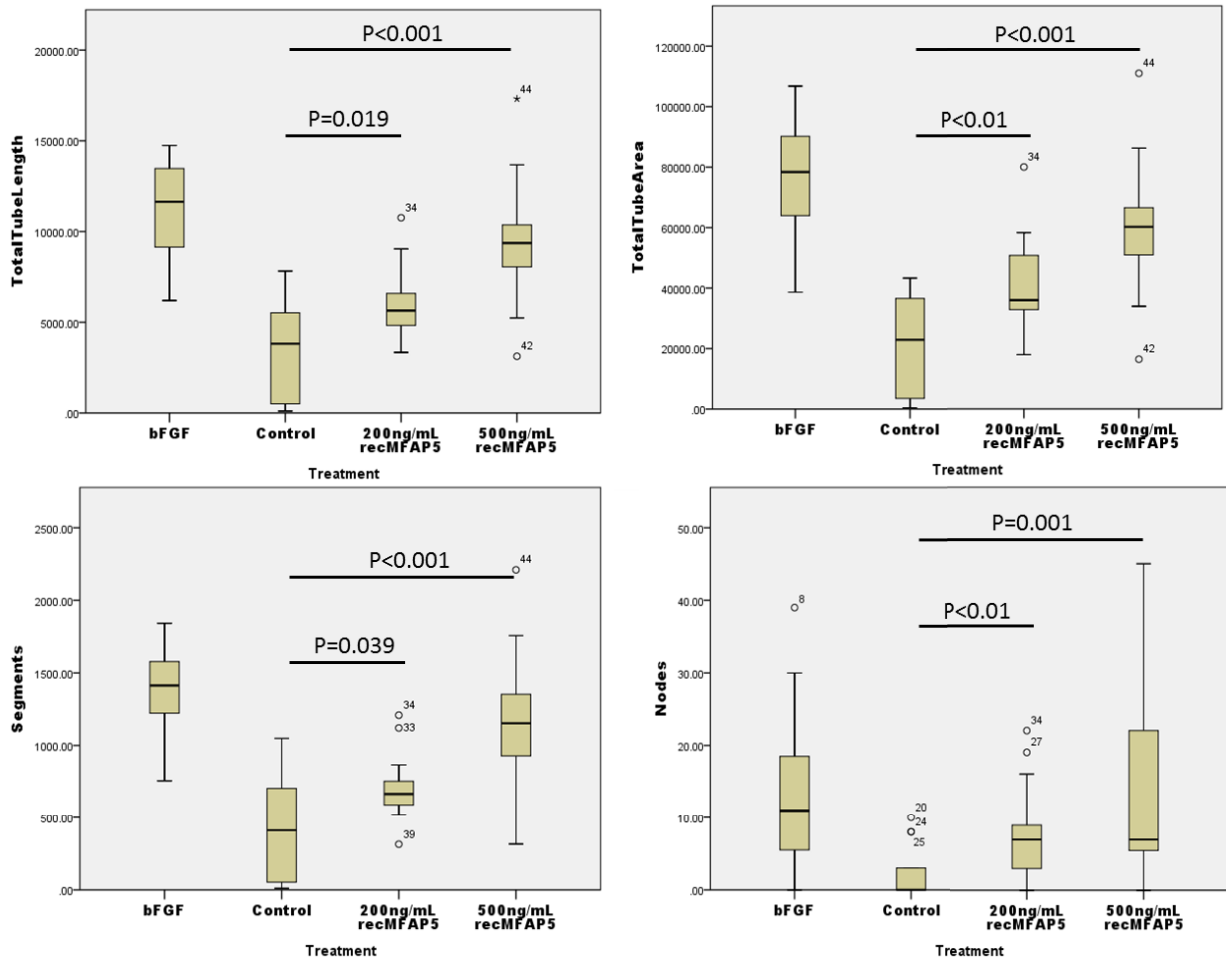


**Fig. 67: Quantitative analysis for *in vivo* angiogenesis assay.** The phenotypes of microvessels infiltrating the Matrigel reconstituted with different concentration of MFAP5 and implanted subcutaneously in nude mice were quantified using the angiogenesis modules of the MetaMorph Image Analysis software program. The results showed a significant increase in the total tube length, total tube area, number of segments and number of nodes in tubular structures formed in the presence of MFAP5 recombinant protein compared to the control in a dose dependent manner ( $p < 0.05$ ). For each boxplot, the box represents the interquartile range of the records and the line across the box indicates the median. Whiskers indicate the highest and lowest values among the records that are no greater than 1.5 times the interquartile range. Outliers (indicated by numbered circles) are cases with values between 1.5 and 3 times the interquartile range. Extremes (indicated by numbered asterisks) are cases with values more than 3 times the interquartile range.

### **C. Silencing of MFAP5 reduces intratumoral microvessel density and inhibits ovarian tumor progression**

To evaluate the feasibility of targeting stromal MFAP5 as a therapeutic approach for ovarian cancer, the effect of silencing stromal mfap5 expression in nude mice by injecting chitosan nanoparticles packaged with mfap5-targeting siRNA was determined. The efficacy of siRNA sequences on mfap5 silencing was first evaluated by knocking down the target gene in mouse fibroblast (Fig. 26B). Three siRNA sequences were tested and two of them that showed the highest efficiency together with a non-targeting scrambled sequence were incorporated into chitosan nanoparticles and delivered twice a week via tail vein injection into A224 ovarian cancer cells bearing nude mice. Three weeks after initial injection, tumor progression in each of the treatment groups was quantified using the IVIS-200 bioluminescence and fluorescence imaging system (Caliper Life Sciences, Inc., Hopkinton MA). Significant lower luciferase activity was detected in mfap5 knockdown groups when compared to the control group (Fig. 68). At week 6, the animals were sacrificed and tumor tissues were harvested and weighted. Significantly lower tumor weights were observed in the mfap5 knockdown groups when compared to the scrambled siRNA-treated group ( $p < 0.001$ ) (Fig. 69). Immunolocalization of mfap5 and CD34 on the tumor paraffin tissue sections showed lower stromal mfap5 expression and lower CD34<sup>+</sup> microvessel density in mfap5 knockdown groups when compared to the controls, confirming the successful knockdown of mfap5 and reduction of intratumoral microvessels by mfap5-targeting siRNAs delivered by nanoparticles (Fig. 70). Immunostaining of CD34<sup>+</sup> microvessels on tumor paraffin tissue sections obtained from an intra-ovarian cancer cell injection animal model also demonstrated a significant decrease in CD34<sup>+</sup> intratumoral vessel density in tumors from stromal mfap5 knockdown animals (Fig. 71).

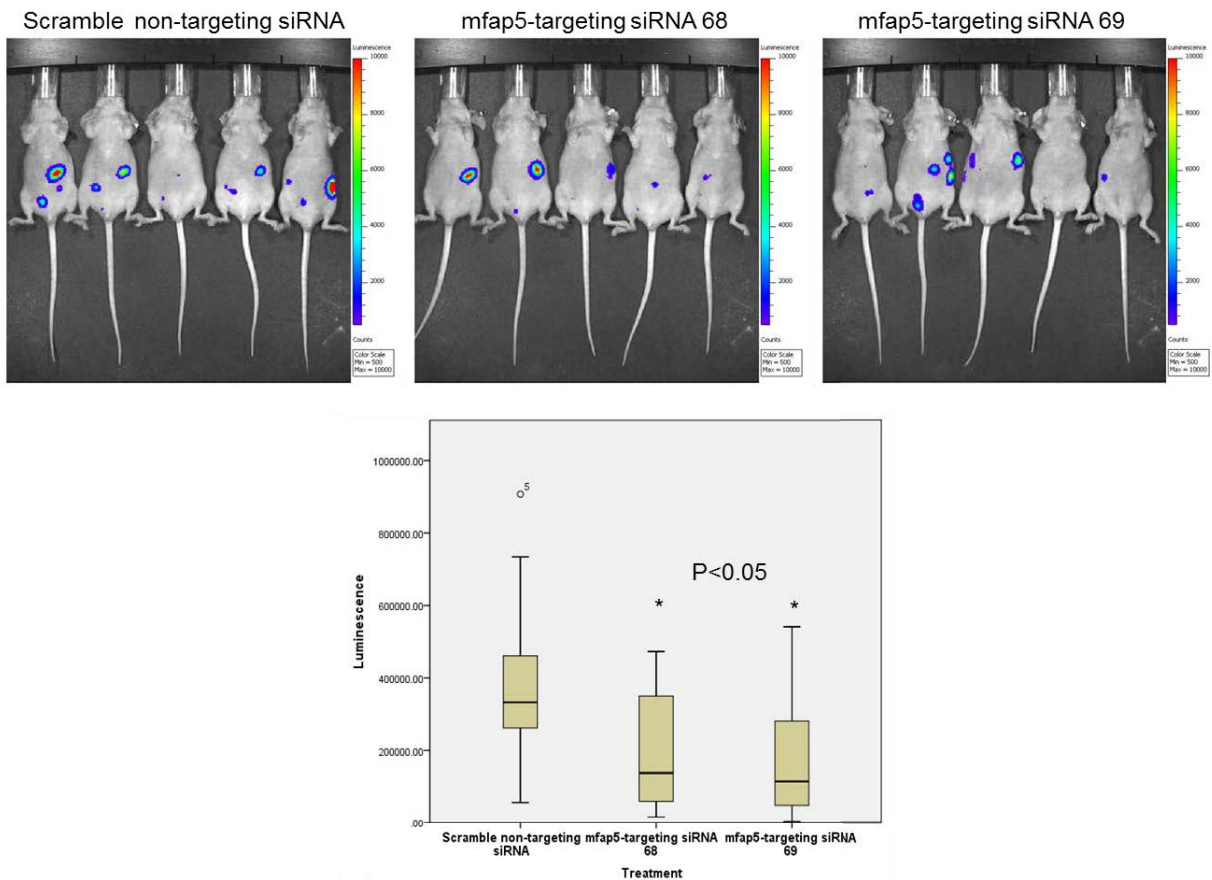


**Fig. 68: Luminescence imaging of tumor volume in mice treated with control siRNA or mfap5-targeting siRNAs encapsulated chitosan nanoparticles.** Tumor volume of each treatment group was quantified by the IVIS-200 bioluminescence and fluorescence imaging system (Caliper Life Sciences, Inc., Hopkinton MA). Significant lower luciferase activity was detected in mfap5 knockdown groups when compared to the control group ( $p < 0.05$ ). For each boxplot, the box represents the interquartile range of the records and the line across the box indicates the median. Whiskers indicate the highest and lowest values among the records that are no greater than 1.5 times the interquartile range. Outlier (indicated by numbered circle) is case with values between 1.5 and 3 times the interquartile range.

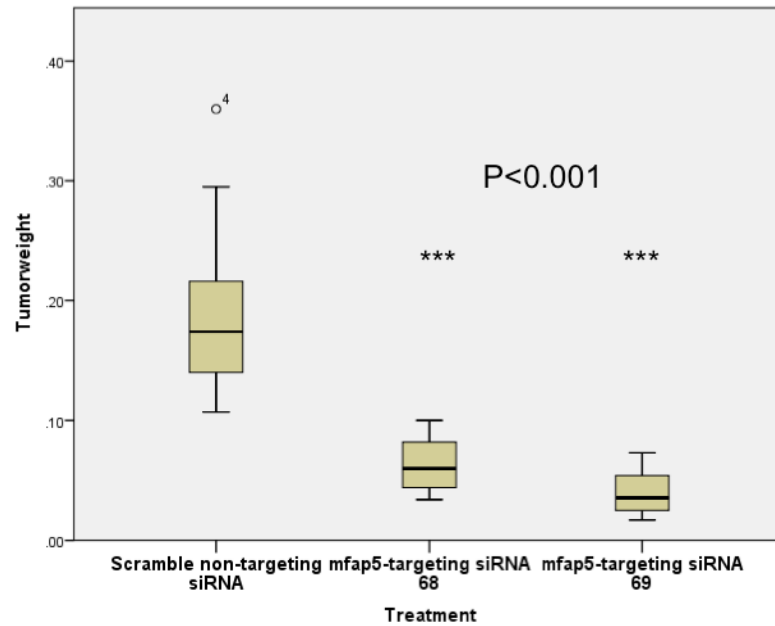


**Fig. 69: Tumor weight of mice injected with control siRNA or mfap5-targeting siRNAs encapsulated chitosan nanoparticles.** After 6 weeks of injection, the animals were sacrificed and tumors were removed and weighted. Significantly lower tumor weights were observed in the mfap5 knockdown groups when compared to the scrambled siRNA group ( $p < 0.001$ ). For each boxplot, the box represents the interquartile range of the records and the line across the box indicates the median. Whiskers indicate the highest and lowest values among the records that are no greater than 1.5 times the interquartile range. Outlier (indicated by numbered circle) is case with value between 1.5 and 3 times the interquartile range.



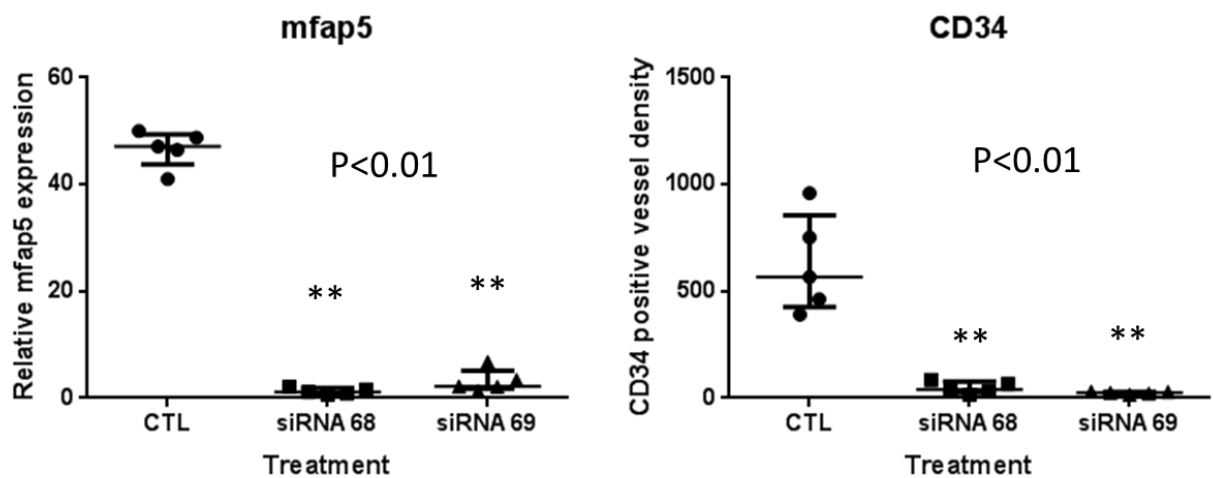
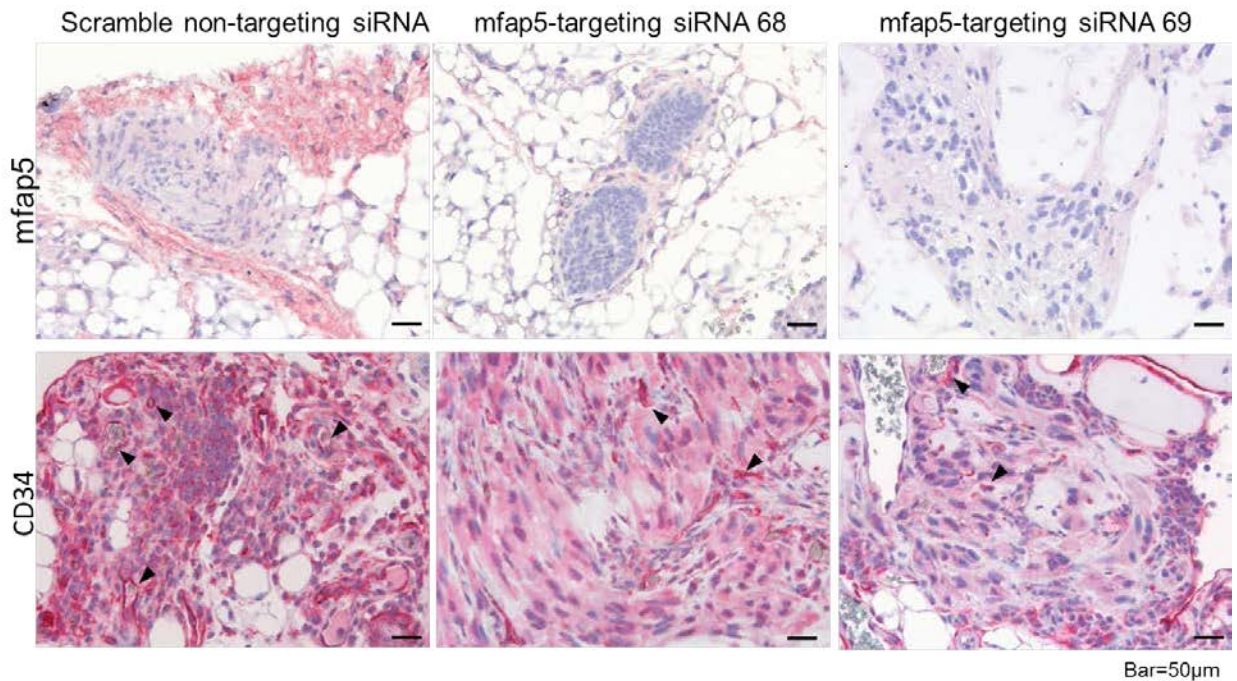


**Fig. 70: Validation of stromal mfap5 silencing by mfap5-targeting siRNAs encapsulated nanoparticles and evaluation of mfap5 knockdown on intratumoral microvessel density.** Immunolocalization for mfap5 and CD34 on the tumor paraffin tissue sections were performed and quantified by the Image Pro-Plus 7.0 software. The results showed lower stromal mfap5 expression and lower CD34<sup>+</sup> microvessels density in mfap5 knockdown groups and confirmed the successful knockdown of mfap5 and reduction of intratumoral microvessel density by the mfap5-targeting siRNAs delivered by nanoparticles (p<0.001). On CD34 staining micrographs, arrows indicate microvessels. For scatter plots, upper and lower bars indicate the interquartile range of the records, and the middle line indicates the median.

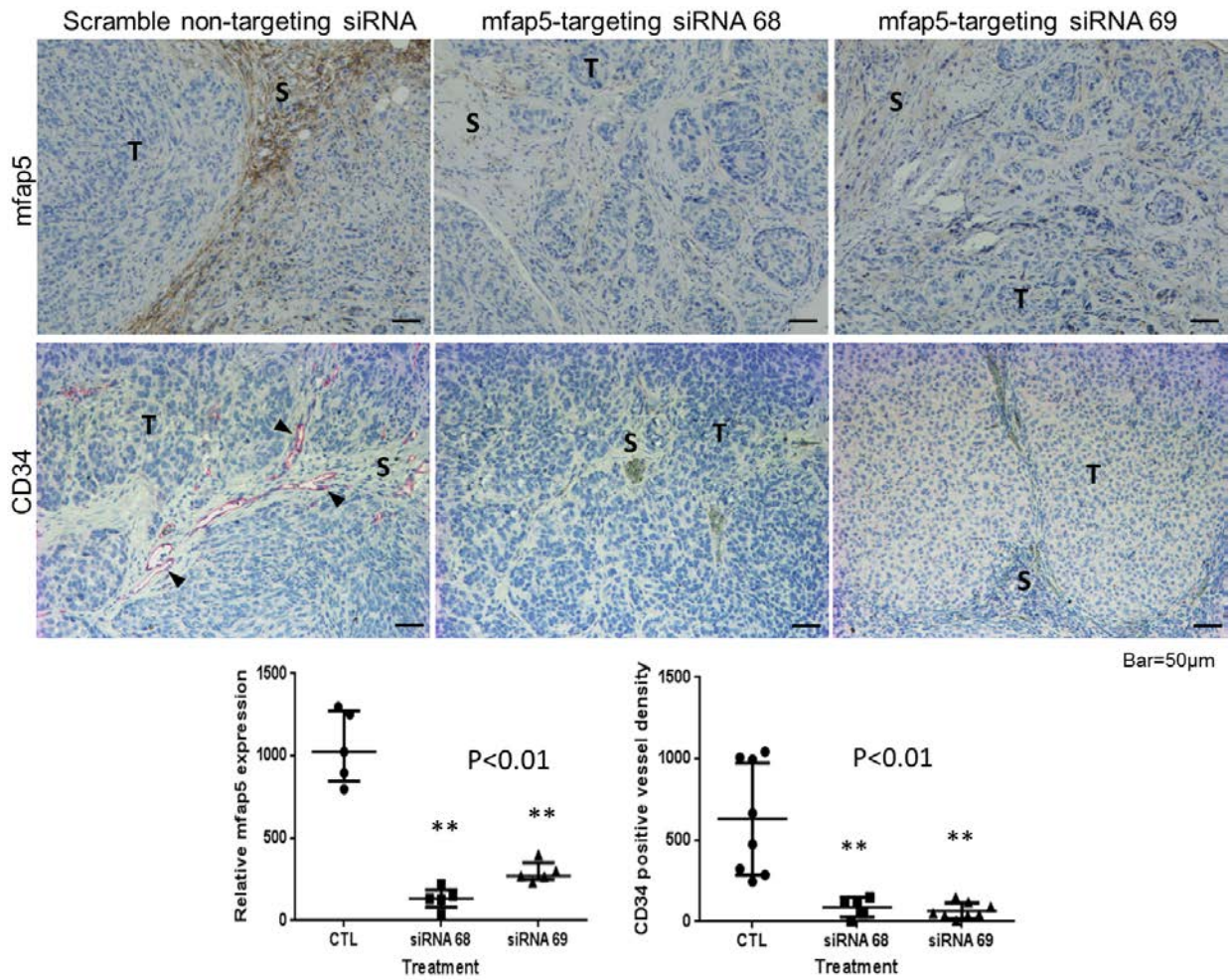


**Fig. 71: The effect of stromal mfap5 silencing on intratumoral microvessel density in an intraovarian cancer cell injection animal model.** Immunostaining for stromal mfap5 and CD34<sup>+</sup> microvessels was performed on tumor paraffin tissue sections and quantified by Image Pro-Plus 7.0 software. The result demonstrated a significant decrease in CD34<sup>+</sup> intratumoral vessel density in mfap5 silenced tumors ( $p < 0.01$ ). For scatter plots, upper and lower bars indicate the interquartile range of the records, and the middle line indicates the median.

#### D. MFAP5 induces endothelial cell stress fiber formation in a calcium-dependent manner

Capillary endothelium permeability and endothelial cell motility have been shown to be influenced by mechanical forces conveyed by the extracellular matrix,<sup>123-128</sup> suggesting that

increased traction force by MFAP5 may attribute to the increase in motility potential and permeability of the endothelial cells. To determine whether traction force induction plays a role in MFAP5 induced angiogenesis in ovarian cancer tissue, hMEC-1 cells were grown on a collagen-I coated polyacrylamide substratum impregnated with fluorescent beads, and the displacement of fluorescent beads in the presence or absence of recombinant MFAP5 were tracked with the algorithm developed by Munevar and colleagues.<sup>129</sup> The results showed that exogenous recombinant MFAP5 protein significantly increased traction force in hMEC-1 cells when compared with those treated with HBSS only (Fig. 72). In addition, we demonstrated that MFAP5 treated endothelial cells showed a significant increase in stress fibers (Fig. 73) and focal adhesion (Fig. 74) formation, suggesting that MFAP5 may increase cytoskeleton tension, which subsequently lead to endothelial cell contraction and increase its cell motility.

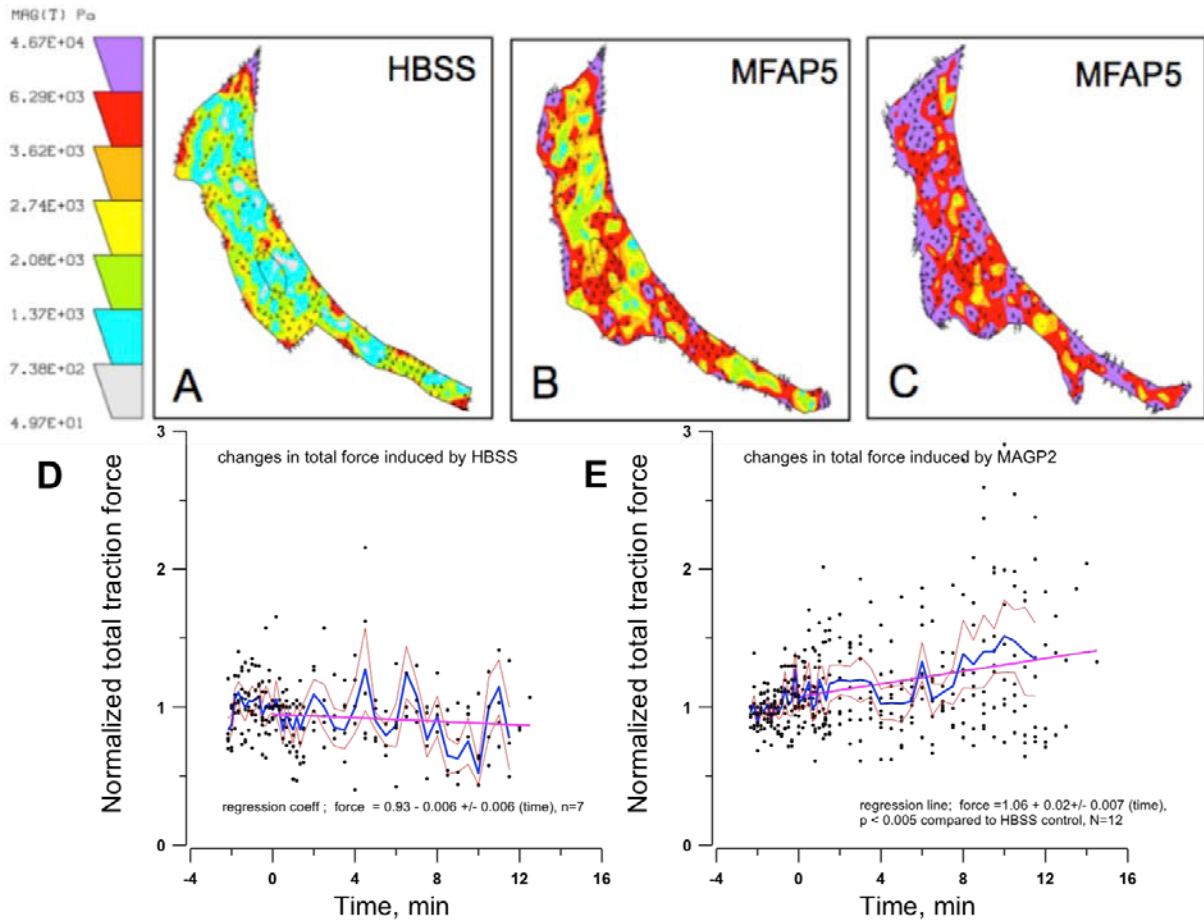


**Fig. 72: Traction force induction by MFAP5 in microvascular endothelial cells.** Traction force maps showing distribution of traction forces (purple color denotes highest force) in hMEC-1 cells treated with control HBSS (A) and recMFAP5 (B & C). Regression lines (purple) showing a significant difference in regression coefficient between HBSS (D) and MFAP5 (E) treated cells.  $P < 0.005$  based on F-ratio. HBSS or recMFAP5 was added at  $t=0$ .



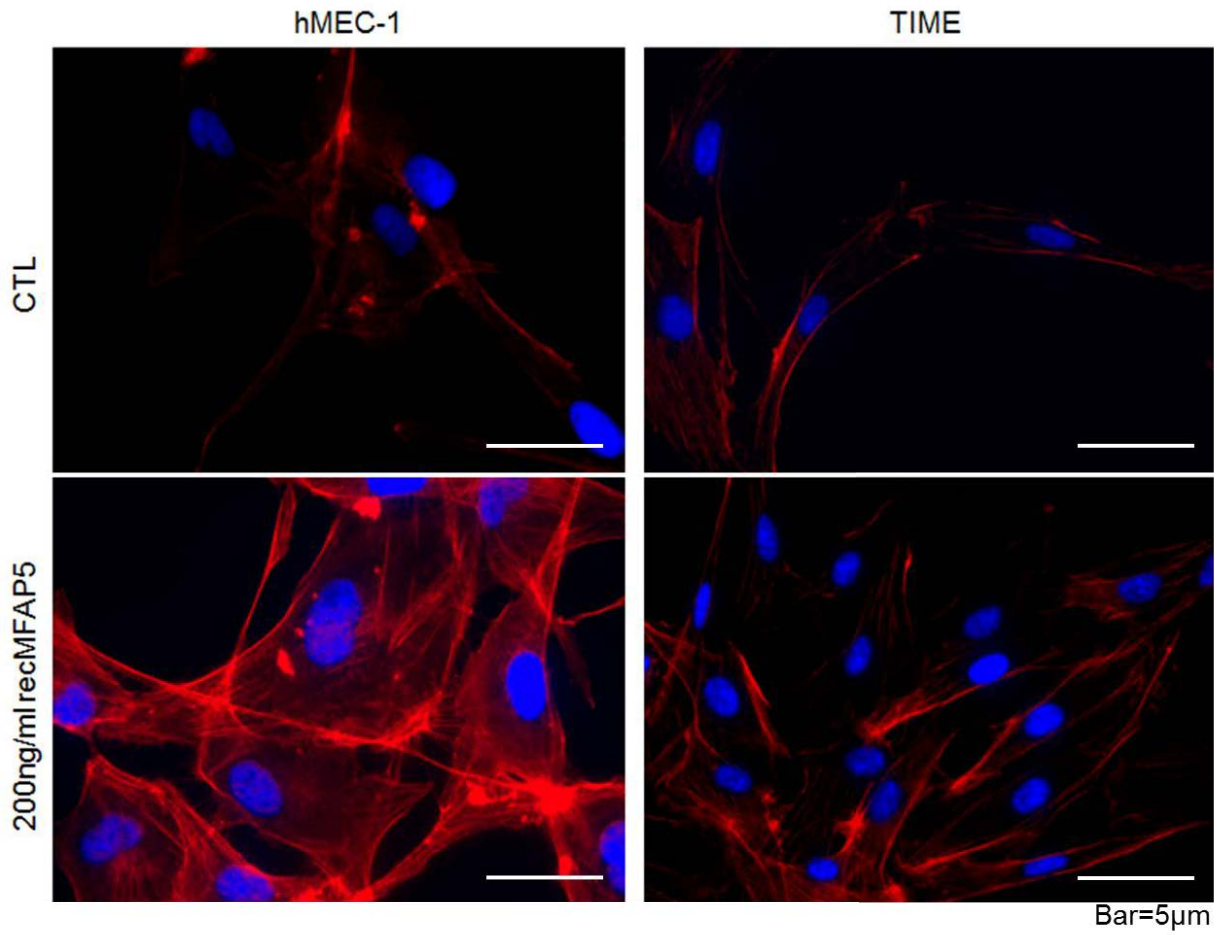


**Fig. 73: Fluorescent labeling of F-actin in MFAP5 treated microvascular endothelial cells.** Confocal microscopy showing increased stress fiber formation in endothelial cell lines hMEC-1 and TIME treated with exogenous MFAP5 protein. Red: F-actin; Blue: nuclei.

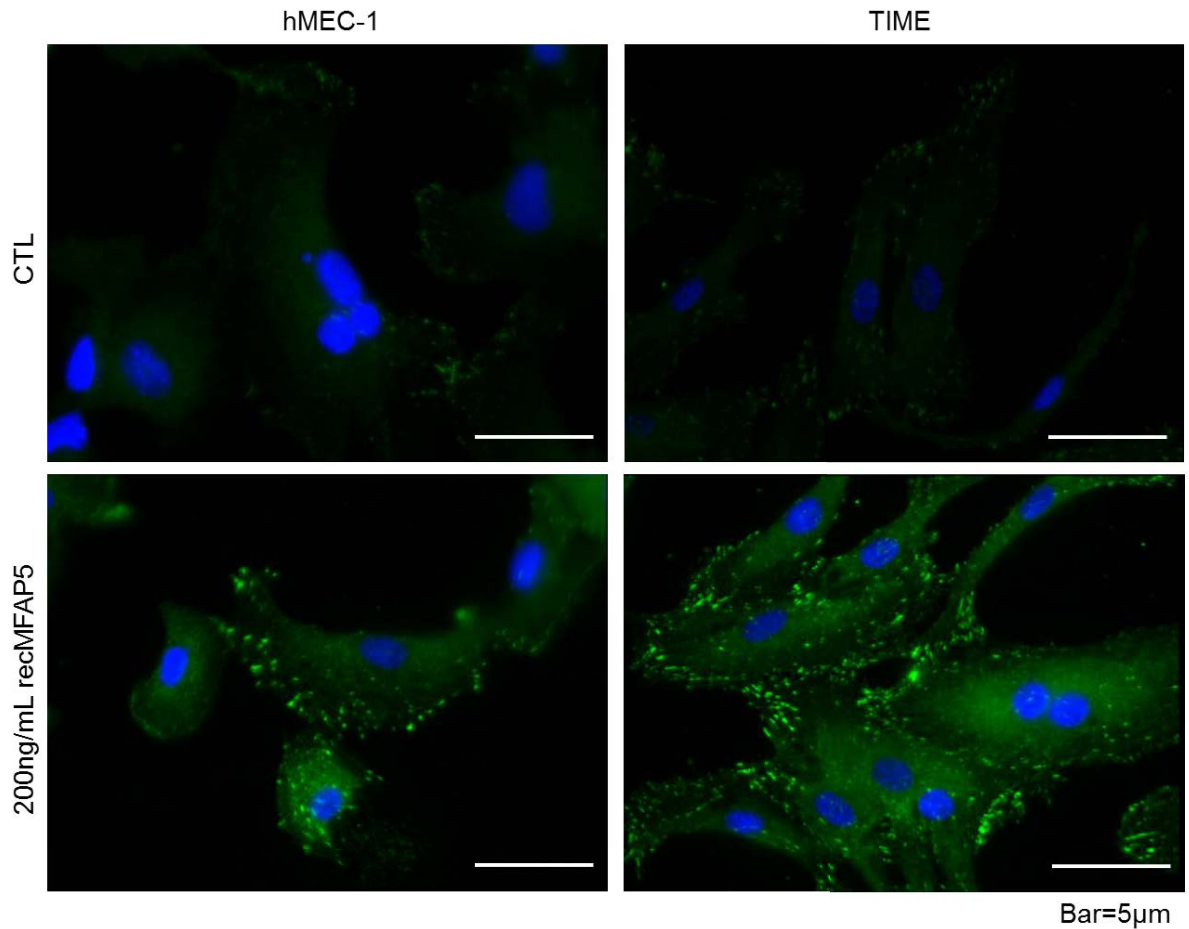


**Fig. 74: Exogenous MFAP5 stimulated focal adhesion formation in microvascular endothelial cells.** By immunolocalization of focal adhesion marker, vinculin and confocal microscopy, increased focal adhesion complex formation in recMFAP5-treated hMEC-1 and TIME endothelial cells was demonstrated. Green: vinculin; Blue: nuclei.

Since calcium has been shown to induce spatially coordinated increases in traction force during the movement of keratinocytes,<sup>114</sup> we also evaluated whether the effect of MFAP5 on endothelial cell motility and permeability is  $\text{Ca}^{2+}$  dependent. The results showed that MFAP5's stimulatory effect on endothelial cell motility (Fig. 75) and stress fiber formation (Fig. 76) was abrogated by pre-loading the cells with permeant calcium chelator, BAPTA/AM, suggesting that calcium signaling is involved in modulating MFAP5's function. Using the calcium dye Fluo-4 AM and confocal fluorescence microscopy, we observed that exogenous

MFAP5 mobilized intracellular  $Ca^{2+}$  in hMEC-1 cells (Fig. 77A), which further demonstrated that calcium signaling is involved in the stimulatory effect of MFAP5 on endothelial cells. The use of  $IP_3$  receptor inhibitor Xestospongin C (XC) but not a ryanodine receptor blocker attenuated MFAP5-induced calcium mobilization, suggesting that MFAP5 induces calcium release via the  $IP_3$  receptor instead of the ryanodine receptor (Fig. 77B & 77C). Furthermore, activation of SOCE by thapsigargin in hMEC-1 was inhibited by treatment with a transient receptor potential channel antagonist, SFK96365, (Fig. 77D) suggesting that an exogenous  $Ca^{2+}$  entry mechanism resembling SOCE was present in hMEC-1 cells.

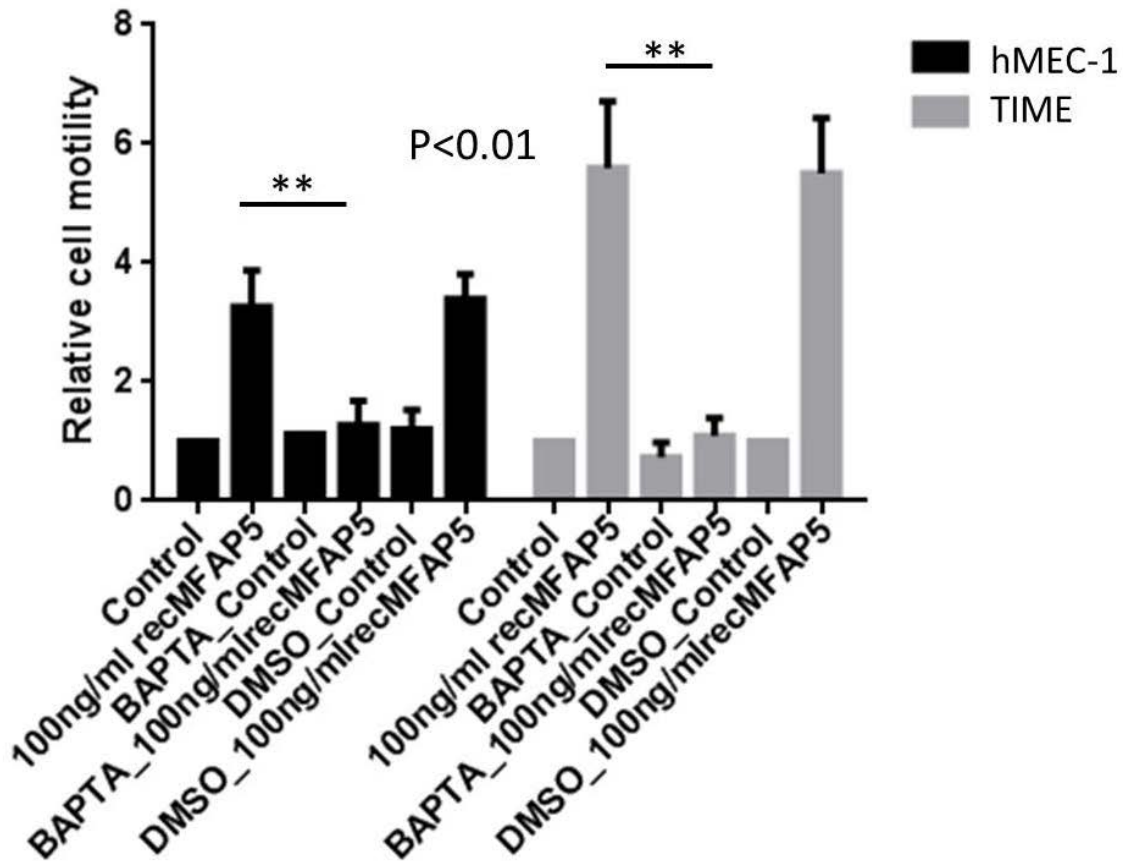


**Fig. 75: Evaluation of the roles of calcium signaling in MFAP5 induced microvascular endothelial cell motility.** Stimulatory effect of recMFAP5 on endothelial cells motility was blocked by calcium chelator, BAPTA, but not by the control solvent, DMSO. Data represents the mean  $\pm$  SD of three independent experiments. ( $p < 0.01$ )



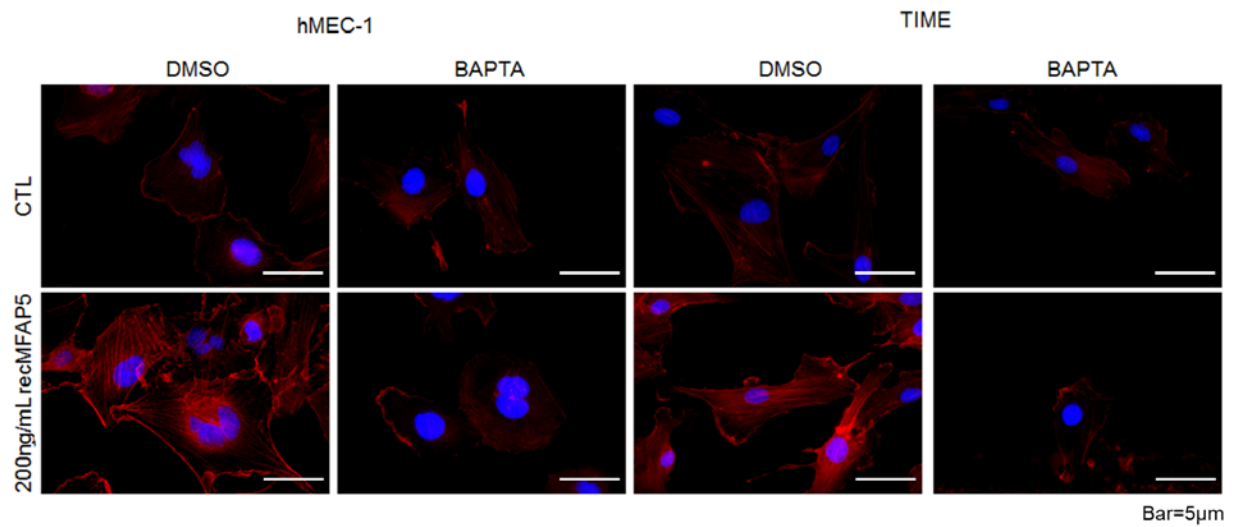


**Fig. 76: Evaluation of the roles of calcium signaling in MFAP5 induced stress fiber formation in microvascular endothelial cells.** Confocal microscopy data showed that stimulatory effect of recMFAP5 on endothelial cells stress fiber formation was blocked by calcium chelator, BAPTA, but not by the control solvent, DMSO. Red: F-actin; Blue: nuclei.

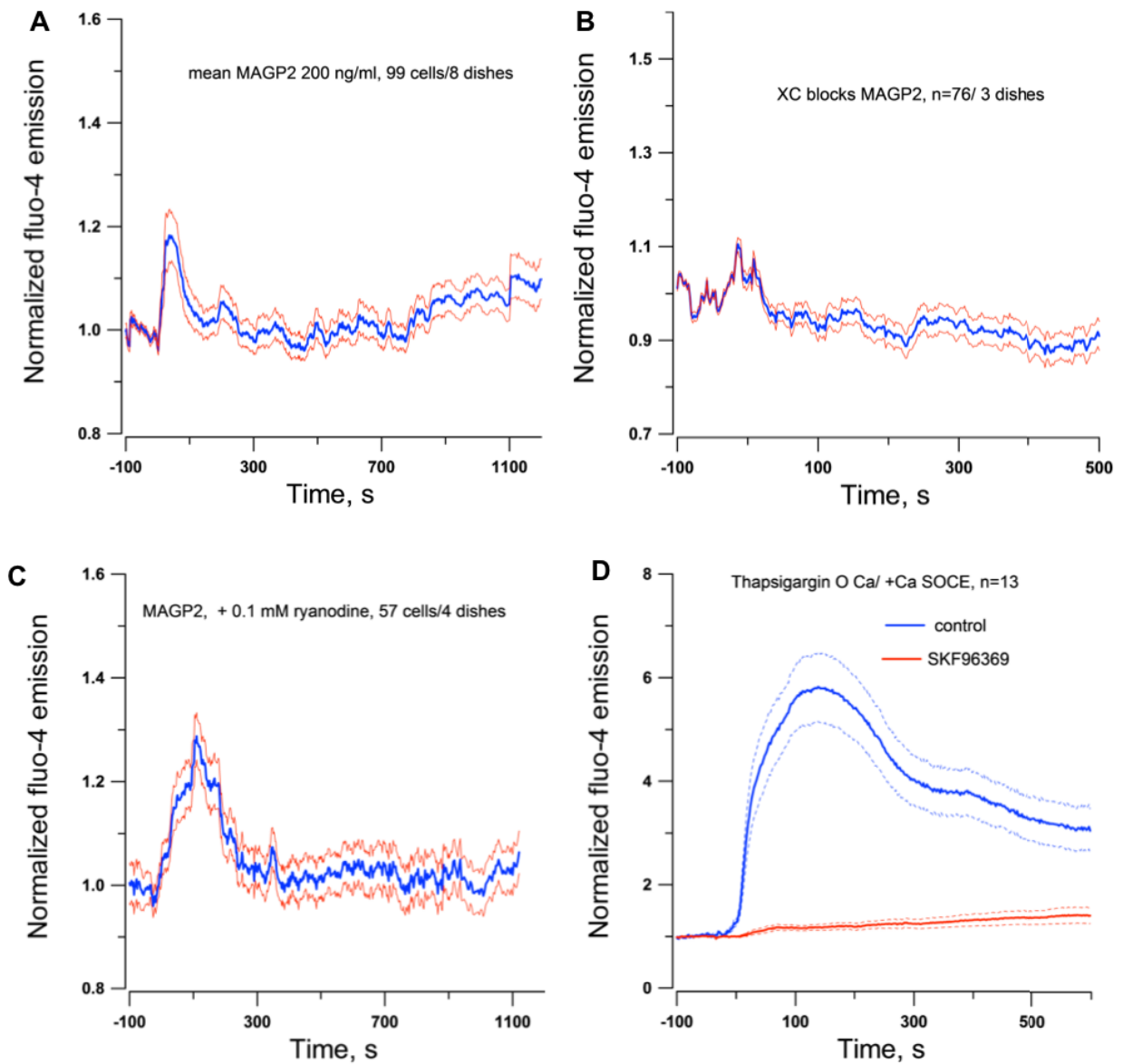


**Fig. 77: Calcium influx induced by recombinant MFAP5 protein in the absence or presence of channel blockers in microvascular endothelial cells.** (A) Mean normalized time course of  $\text{Ca}^{2+}$  mobilization in hMEC-1 cells induced by recombinant MFAP5 (200 ng/ml). (B) Mean normalized time course of  $\text{Ca}^{2+}$  mobilization in ALST cells induced by recombinant MFAP5 (200 ng/ml) in the presence of the  $\text{IP}_3$  receptor inhibitor xestospongine C (10  $\mu\text{M}$ , 30 minutes of preincubation). (C) Mean normalized time course of  $\text{Ca}^{2+}$  mobilization in hMEC-1 cells induced by recombinant MFAP5 (200 ng/ml) in the presence of ryanodine (50 $\mu\text{M}$ , 30 minutes of preincubation). (D) Activation of store-operated calcium entry by thapsigargin in hMEC-1 cells by incubating cells with 20  $\mu\text{M}$  thapsigargin in the absence of extracellular  $\text{Ca}^{2+}$  for 25 minutes. Subsequent addition of 2 mM  $\text{Ca}^{2+}$  to the medium resulted in rapid extracellular  $\text{Ca}^{2+}$  entry, which was inhibited by treatment with 50  $\mu\text{M}$  SKF96365. Dotted lines, standard errors.

## **E. MFAP5 induces LPP upregulation and increases focal adhesion assembly**

To further delineate the underlying molecular mechanisms by which MFAP5 modulates endothelial cell motility and monolayer permeability, transcriptome profiling and pathway analyses were performed on RNA isolated from microvessels infiltrating the Matrigel I.P. implanted in mice mentioned in Fig. 66. Focusing on genes that have been shown to be associated with cell-cell, and cell-substrate cytoskeleton interactions, we identified LIM domain containing preferred translocation partner in lipoma (LPP) as the most significant up-regulated gene in microvessels infiltrated the Matrigel reconstituted with MFAP5 when compared to those with PBS and in microvascular endothelial cells treated with exogenous MFAP5 protein when compared to the control (Fig. 78). Endothelial cells treated with exogenous MFAP5 protein showed a significant increase in LPP mRNA and protein levels when compared with those treated with PBS (Fig. 79). Immunofluorescent microscopy confirmed increased LPP expression particularly in the focal adhesions at cell periphery and co-localized with other focal adhesion proteins when the endothelial cells were treated with exogenous recMFAP5 compared with the control (Figs. 80 and 81). Furthermore, transfecting LPP-targeting siRNAs into MFAP5 treated endothelial cell lines hMEC-1 and TIME completely abrogated the effect of MFAP5 on cell motility (Fig. 82), suggesting that LPP is the key downstream effector molecule involved in MFAP5-modulated endothelial cell motility.

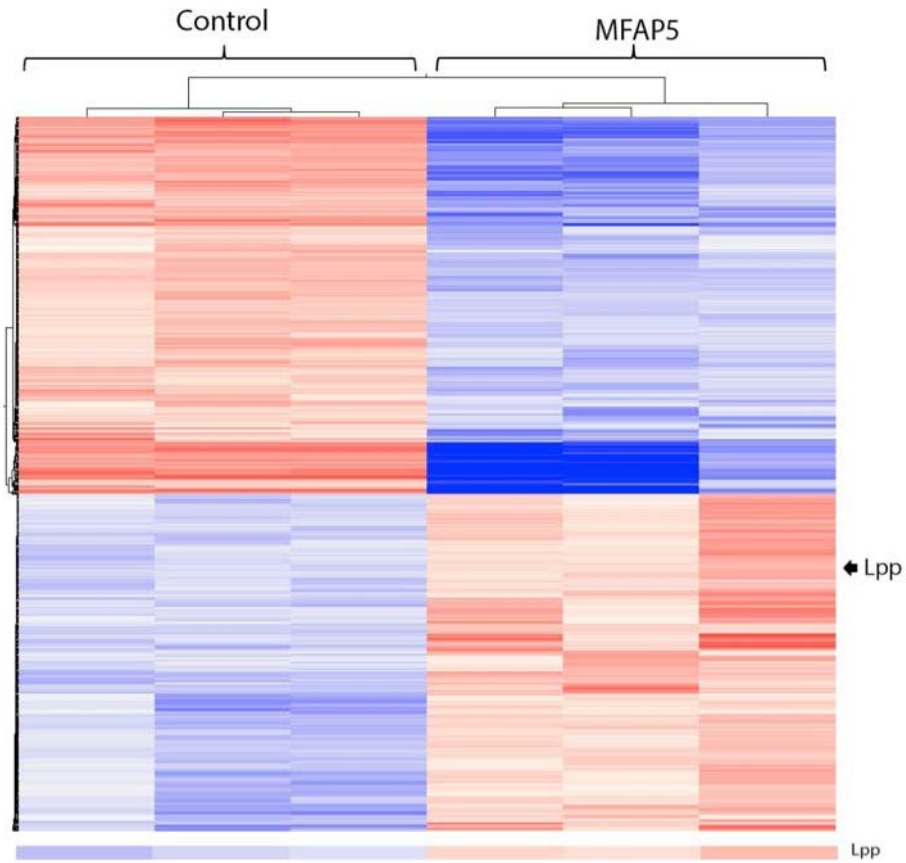


**Fig. 78: Heat map showing differential expressed genes in endothelial cells retrieved from *in vivo* angiogenesis assay.** Result showed that LPP is one of the significantly overexpressed genes in endothelial cells invaded into recMFAP5 reconstituted Matrigel compared to those invaded into control Matrigel retrieved from *in vivo* angiogenesis assay.

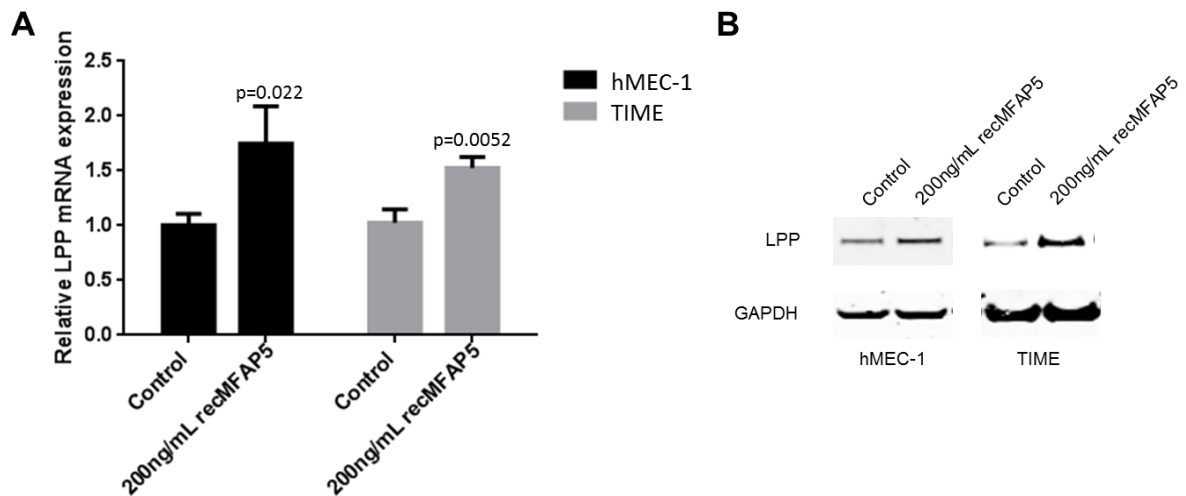


**Fig. 79: Validation of LPP upregulation induced by MFAP5.** Upregulation of LPP in MFAP5 treated endothelial cells was validated (A) at mRNA level by quantitative RT-PCR and (B) at protein level by western blot.

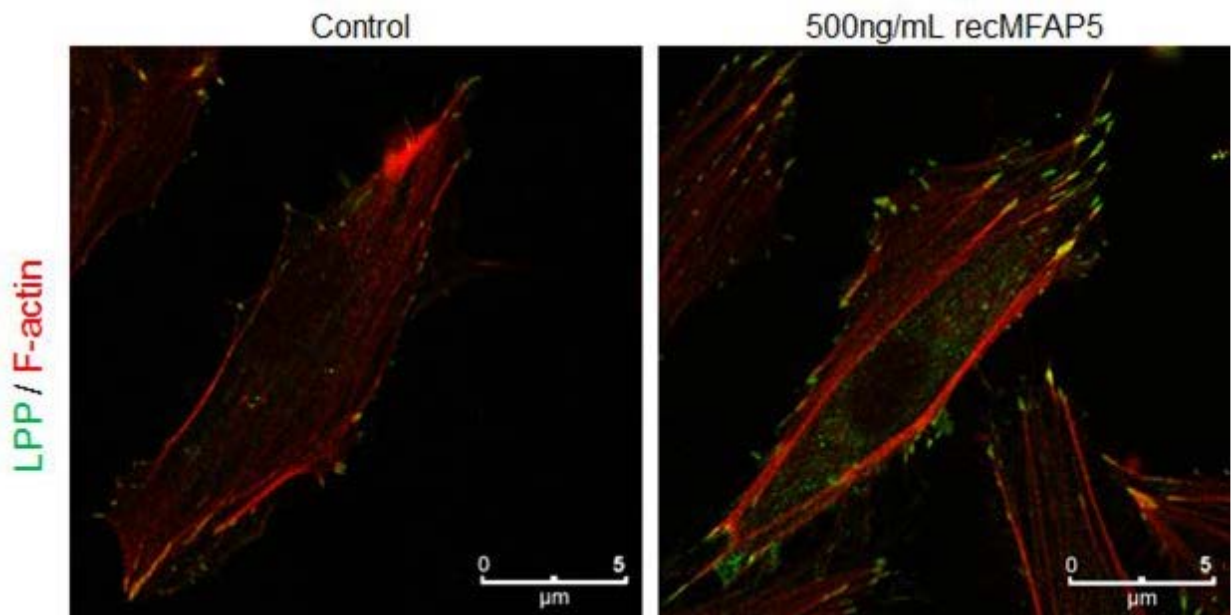


**Fig. 80: Immunolocalization of LPP in recMFAP5 treated microvascular endothelial cells.** Immunofluorescent microscopy showed increased LPP expression particularly at cell periphery connecting to the actin cytoskeleton. Red: F-actin; Blue: nuclei.

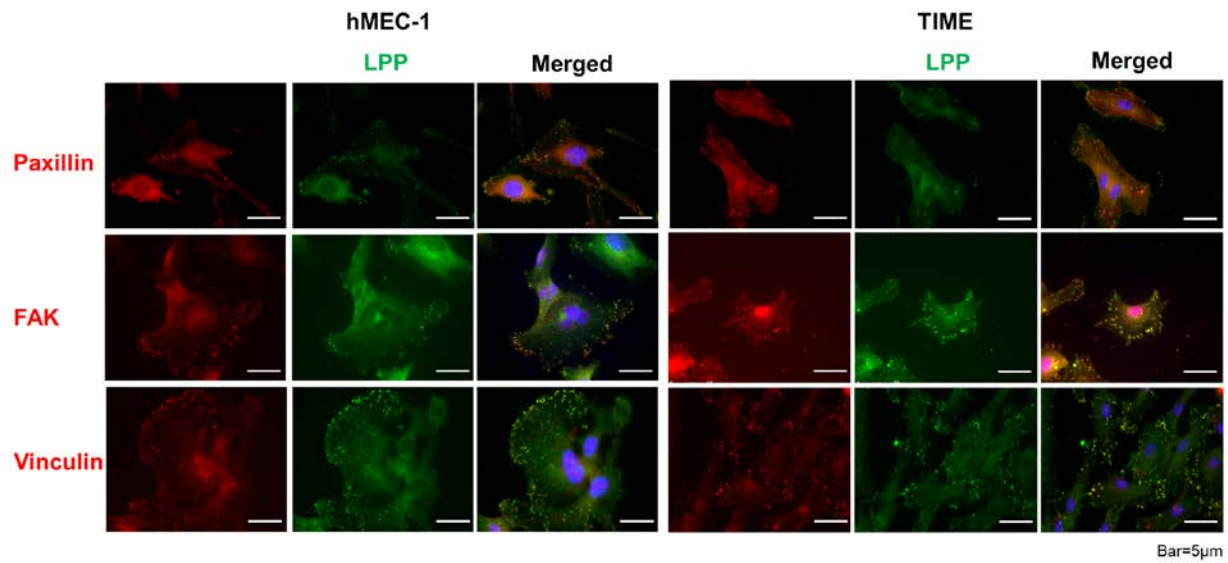


**Fig. 81: Co-localization of LPP with focal adhesion proteins in microvascular endothelial cells.** Immunofluorescent microscopy demonstrated increased LPP expression co-localized with other focal adhesion proteins when the endothelial cells were treated with exogenous MFAP5. Red: focal adhesion proteins; Green: LPP; Blue: Nuclei.

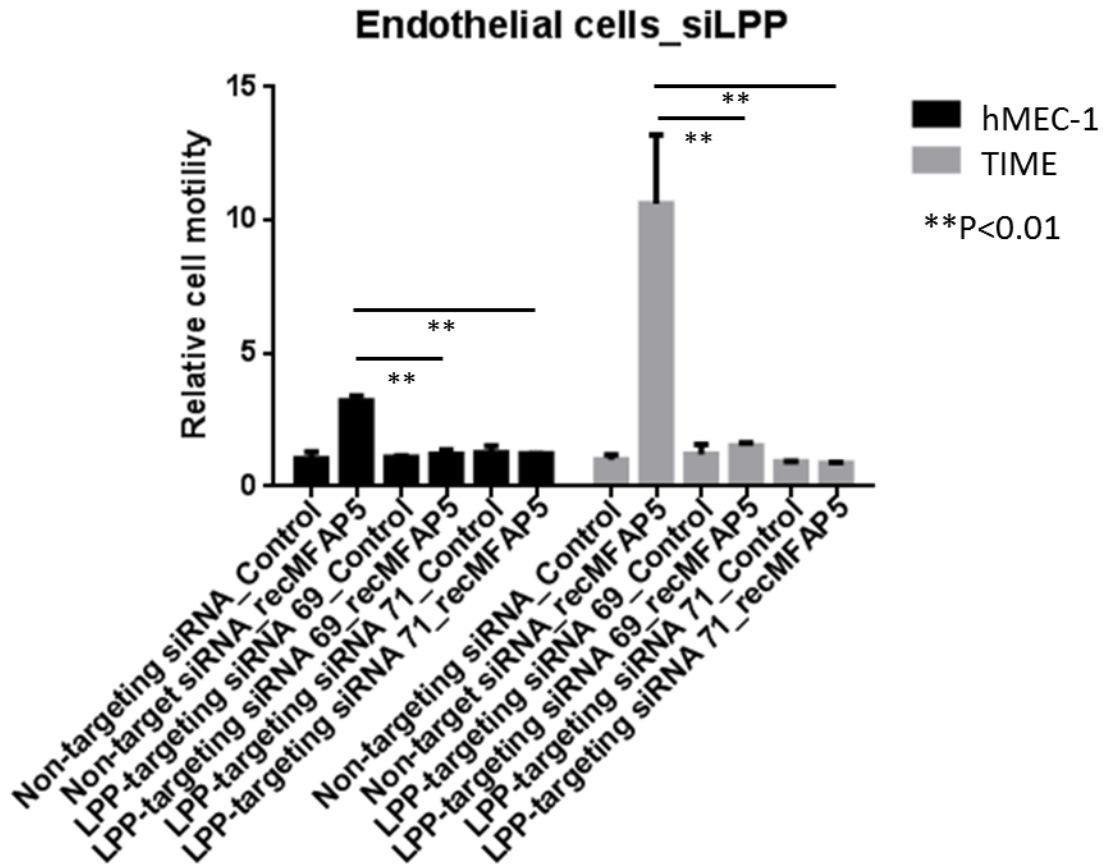


**Fig. 82: The effect of LPP silencing on MFAP5 stimulated microvascular endothelial cell motility.** Stimulatory effect of recMFAP5 on endothelial cells motility was blocked by LPP targeting siRNAs but not by non-targeting scrambled siRNA. Data represents the mean  $\pm$  SD of three independent experiments. ( $p < 0.01$ )

To evaluate whether LPP modulates the effects of MFAP5 on tumor angiogenesis and vessel permeability, tube formation assay was performed in the presence or the absence of MFAP5 with microvascular endothelial cells transfected with LPP-targeting siRNAs or scrambled non-targeting siRNA. Results showed that exogenous MFAP5 protein induced increase in total tube length, total tube area, number of segments and number of branch points were abrogated when cells were transfected with LPP-targeting siRNAs but not with the control non-targeting siRNA (Figs. 83 and 84). Besides, silencing of LPP attenuated the stimulatory



effect of MFAP5 on F-actin cytoskeleton reorganization (Figs. 85 and 86), focal adhesion formation (Figs. 87 and 88) and monolayer permeability (Fig. 89). These data suggest that MFAP5 up-regulates LPP, which leads to an increase in focal adhesion, stress fibers formation and traction force in cells, and subsequently increases endothelial cell motility potential and allows contractile forces to be set up to pull apart the inter-endothelial cell junctions and thus increases permeability.

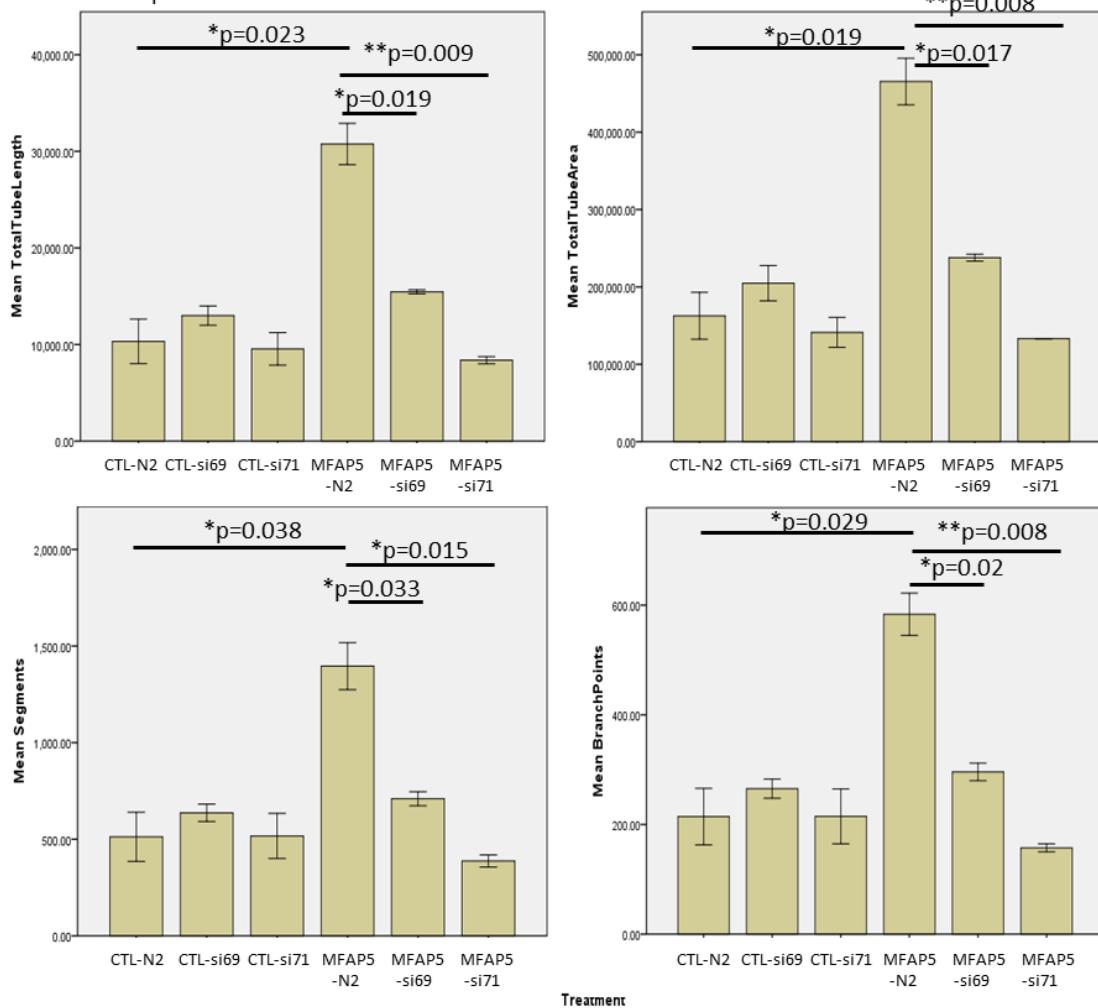
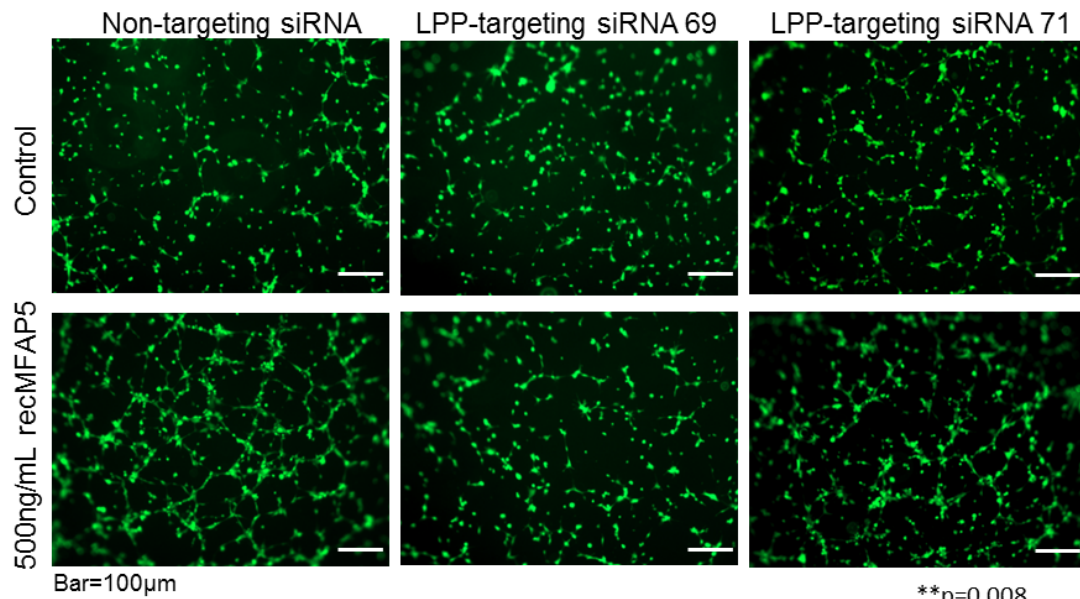


**Fig. 83: The effect of LPP silencing on tube formation in recMFAP5-treated hMEC-1 cells.** Exogenous MFAP5 protein induced significant increase in total tube length, total tube area, number of segments and number of branch points in hMEC-1 cells. Such induction was abrogated in LPP-targeting siRNAs (si69, si71) transfected cells but in control non-targeting siRNA (N2) transfected cells. Error bars: +/- 1SEM.

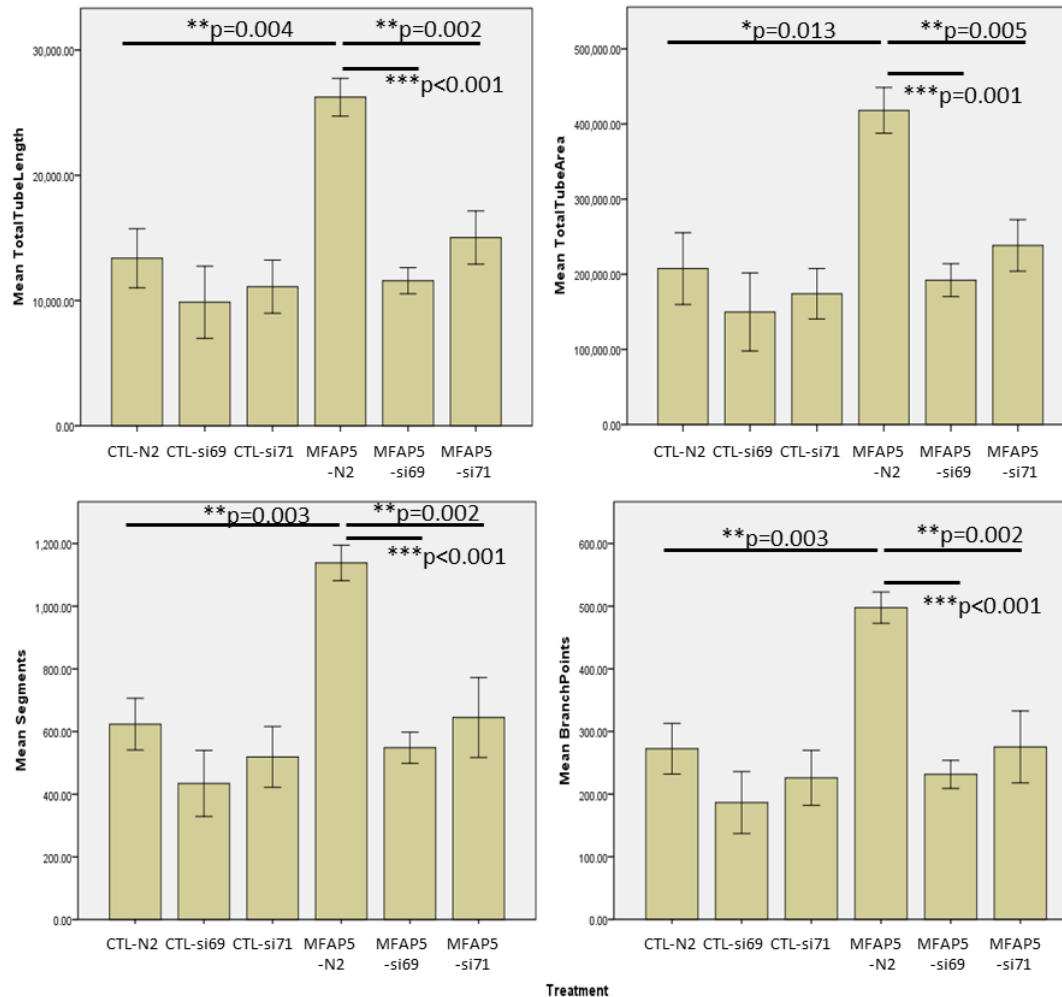
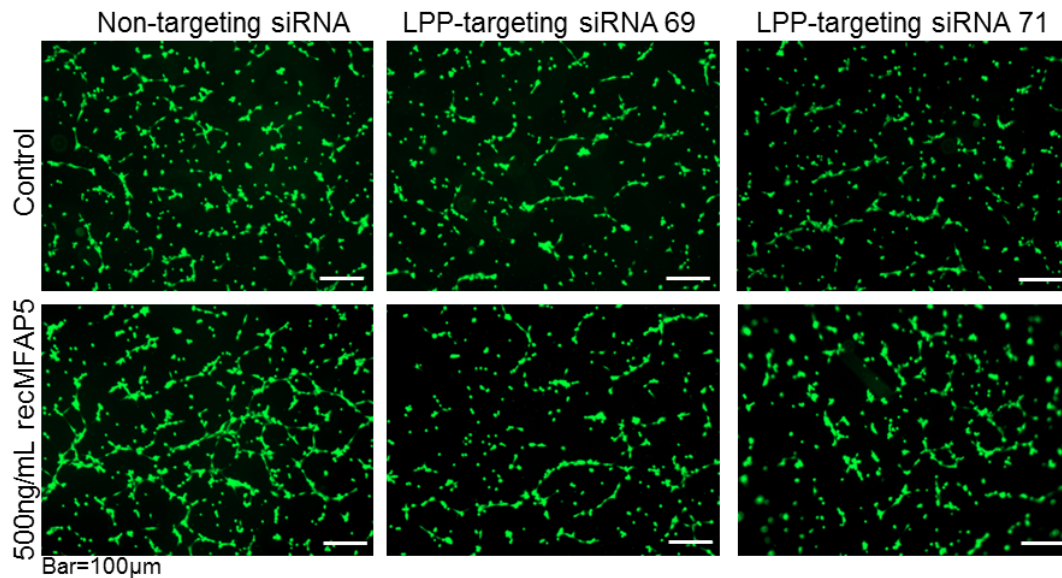


**Fig. 84: The effect of LPP silencing on tube formation in recMFAP5-treated TIME cells.** Exogenous MFAP5 protein induced significant increase in total tube length, total tube area, number of segments and number of branch points in TIME cells. Such induction was abrogated in LPP-targeting siRNAs (si69, si71) transfected cells but in control non-targeting siRNA (N2) transfected cells. Error bars: +/- 1SEM.

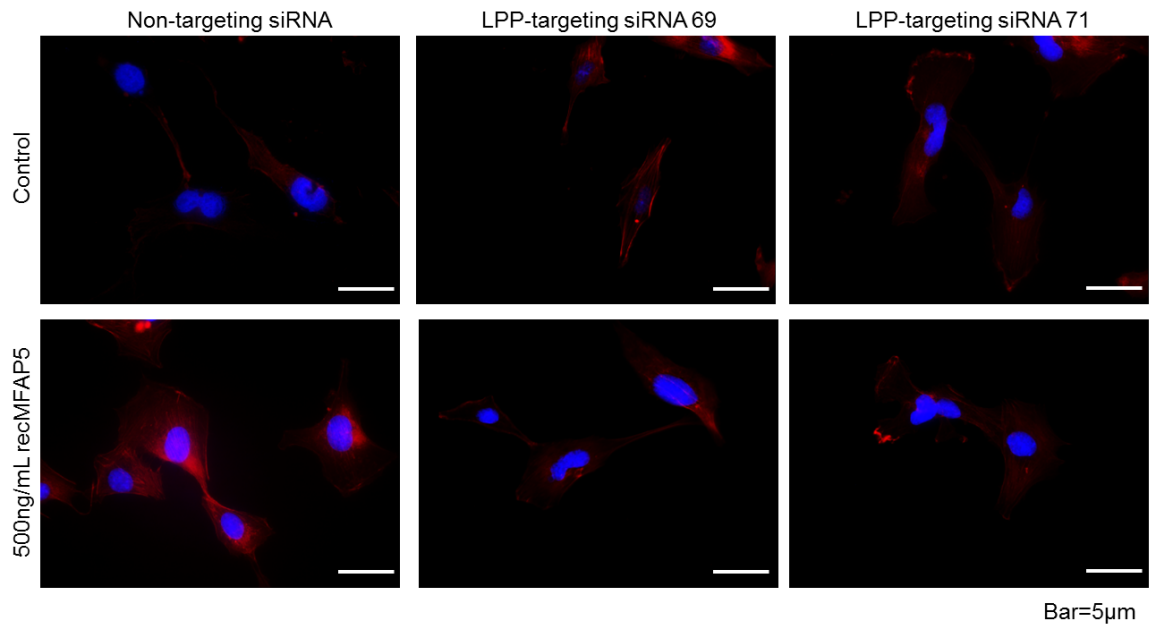


**Fig. 85: The effect of LPP silencing on stress fiber formation in recMFAP5-treated hMEC-1 cells.** Stimulatory effect of MFAP5 on F-actin cytoskeleton reorganization was attenuated by silencing of LPP by LPP-targeting siRNAs but not by the control non-targeting siRNA in hMEC-1 cells. Red: F-actin; Blue: nuclei.

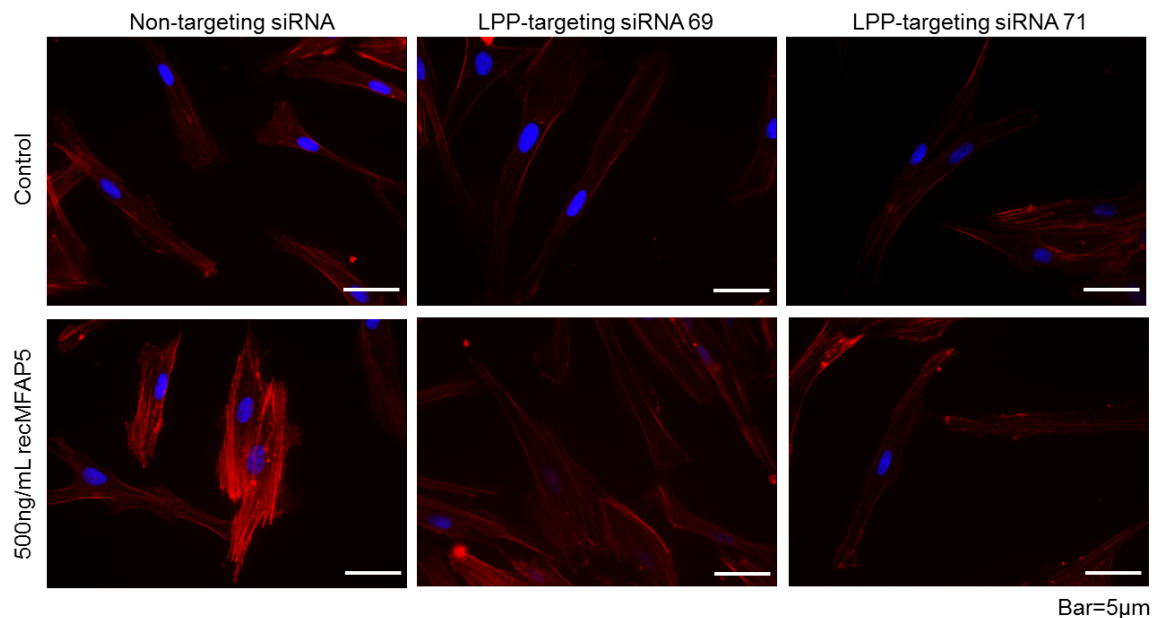


**Fig. 86: The effect of LPP silencing on stress fiber formation in recMFAP5-treated TIME cells.** Stimulatory effect of MFAP5 on F-actin cytoskeleton reorganization was attenuated by silencing of LPP by LPP-targeting siRNAs but not by the control non-targeting siRNA in TIME cells. Red: F-actin; Blue: nuclei.

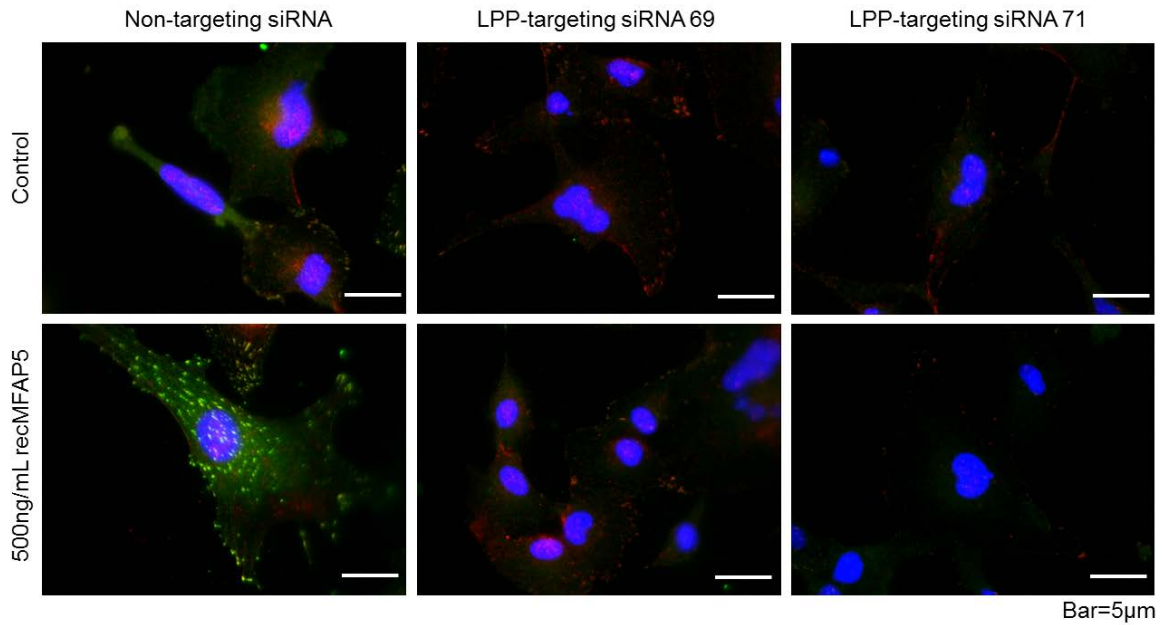


**Fig. 87: The effect of LPP silencing on focal adhesion formation in recMFAP5-treated hMEC-1 cells.** Focal adhesion formation induced by exogenous MFAP5 in hMEC-1 cells was abrogated by LPP silencing by LPP-targeting siRNAs but not by the control non-targeting siRNA. Green: LPP; Red: Vinculin; Blue: nuclei.

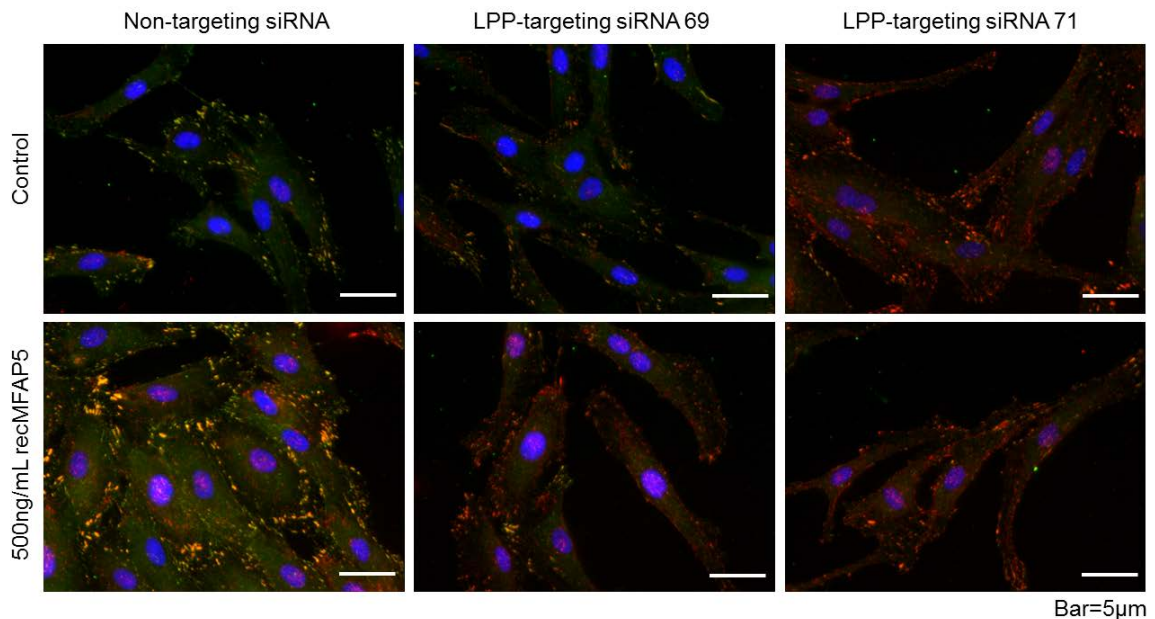


**Fig. 88: The effect of LPP silencing on focal adhesion formation in recMFAP5-treated TIME cells.** Focal adhesion formation induced by exogenous MFAP5 in TIME cells was abrogated by LPP silencing by LPP-targeting siRNAs but not by the control non-targeting siRNA. Green: LPP; Red: Vinculin; Blue: nuclei.

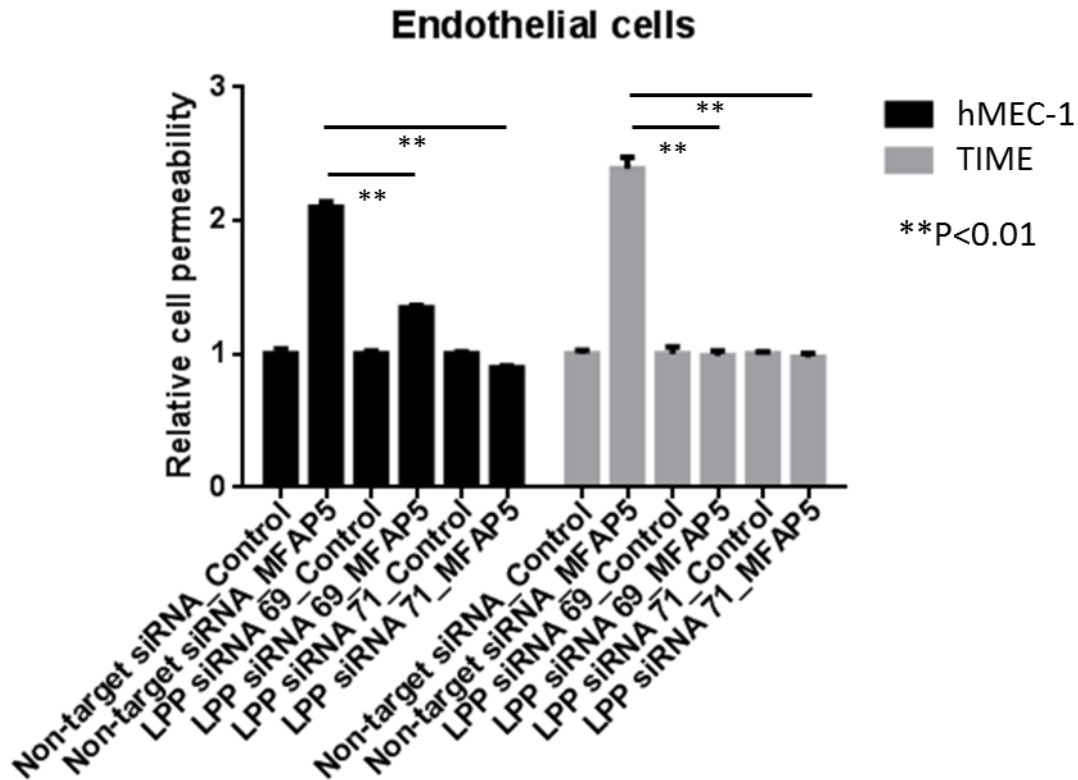


**Fig. 89: The effect of LPP silencing on MFAP5-induced monolayer permeability in microvascular endothelial cells.** MFAP5 induced permeability of endothelial cell monolayer was abolished by transfecting hMEC-1 and TIME cells with LPP specific siRNA compared to control. (p<0.01)

#### **F. Calcium-dependent FAK/ERK/LPP signaling pathway modulates MFAP5-induced endothelial cell motility and permeability**

MFAP5 contains an RGD motif that has been shown to mediate adhesion and spreading of fetal bovine aortic smooth muscle cells, ear cartilage chondrocytes, arterial endothelial cells, human skin fibroblasts and osteoblasts through the  $\alpha_v\beta_3$  integrin.<sup>74</sup> In addition, our data using hMEC-1 and TIME also demonstrated that anti- $\alpha_v\beta_3$  integrin antibody could abrogate MFAP5-mediated effects on endothelial cell motility (Fig. 58). These data suggest that  $\alpha_v\beta_3$  integrin is a major receptor for MFAP5 and MFAP5 may play a role in  $\alpha_v\beta_3$  integrin-



mediated angiogenesis.<sup>130</sup> In addition,  $Ca^{2+}$  mobilization has been shown to be involved in integrin signaling and cell migration<sup>131-133</sup> and our data showed that pre-loading microvascular endothelial cells with cell permeant calcium chelator, BAPTA/ AM, abrogated the stimulatory effect of MFAP5 on endothelial cell motility (Fig. 75). These suggest that calcium signaling is involved in the effect of MFAP5 on endothelial cells. Lastly, our data indicated that LPP is a key downstream effector molecule that may play a role in modulating the effect of MFAP5 on endothelial cell motility and permeability, therefore we hypothesize that binding of MFAP5 to  $\alpha_v\beta_3$  integrin may activate calcium dependent signaling pathways, which transcriptionally up-regulate LPP expression and subsequently increase motility and permeability in endothelial cells.

To test these hypotheses, we first examined the promoter sequence of LPP. We identified multiple AP1 bindings, suggesting that LPP may be regulated by c-Fos/c-Jun (Fig. 90). Then focusing on genes that have been implicated in mediating cell motility and calcium signaling, we identified a significant increase in p-FAK(Y861), p-PLC- $\gamma$ 1 (Y783), p-PKC $\theta$  (T538), p-ERK1/2 (T202/Y204), p-MLC2 (T18/S19), p-CREB (S133), cJun and p-cJun (S73) expression in microvascular endothelial cells treated with MFAP5, which may lead to up-regulation of LPP and subsequently increased cell motility and permeability (Fig. 91).



LPP promoter							
-1500	AACAGAACCA	CCGGGAAGCC	AAGATGTGGT	ACTTGGATTC	CCATCTCGGA	GCACCTCCTA	-1441
-1440	TATCCCGACA	CACCATTTCC	CCTAGTGTCT	GATCTCTCTT	TCTCCTCCTT	TAATTCAGTC	-1381
						API binding site 1	
-1380	TGGAGTCATT	TTAGATCAGA	TTCATTCTCTG	ATTGGCTTCA	CTGCTCCAAC	TTAGTCATCA	-1321
-1320	CAGAACCTTA	GGGTGGAAT	CCATGTTACA	AGTTAAACTG	AGCAATTCAC	CCCCACTTTT	-1261
		API binding site 2					
-1260	CCTGACAACA	GTGTTCTCTT	GAGAGTCTGG	TTTTATCTCTG	AGTCTTCCAG	CCCGGTGTCT	-1201
-1200	GTGCCCATGA	AGGACTCATG	CCAAATTACA	TTCTCAGGAG	GACTCCCAGA	CCAAGAGACT	-1141
-1140	CTGGGCTTGG	GCGTGAGAGA	CTTGGGGCTG	TTCTTTTTTCT	TTTTTTTTTTT	TTGAGAAGAA	-1081
			API binding site 3				
-1080	GTTTCACTCT	TATTGCCAG	GCTGACATGG	AGTTTCACTC	TTATTGCCCA	GGCTGGAGTG	-1021
		API binding site 4					
-1020	CAATGGCACA	GTCATGGCTC	ACTGCAACCT	CCGCCTCCCG	GTTTCAAGTG	ATACTCTGTC	-961
-960	CTCAGCCTCC	CAAGTAGCTG	GGATTACAGG	CACACACCAC	CATGCCTGGC	TAATTTTTTGT	-901
						API binding site 5	
-900	ATTTTTAGTA	GAGACCAGTT	TTCACCATGT	TGCCCAGGCT	GGTCTTGAAC	TCCTGACCTC	-841
						API binding site 6	
-840	AGGTGATCCT	CCCGCCTTGG	TCTCCCAAAG	TGCTGGGATT	ACAGGTGTGA	GCCACTGTGC	-781
-780	CCGGCCGAGA	GGAGTTGTTT	TGAGACTCAC	CTGCCATCAT	AGGAACCATA	GCTTAAATTC	-721
-720	TTGTGACCTT	TTCAGGTGCA	TCTCCCAAAA	TATCTCCCTT	CCACCAAATT	AATGATTTAT	-661
-660	TTCATAAATT	TAGTTGCATT	CTGGATGGTC	TCATTCTTAA	GATGAGCTTA	AAGCCTTCA	-601
-600	GACCAGTCAC	TTCTTGTGTT	GGGGTGGAGG	AGGTTTTTTC	CTGGAATAGG	ACAGTGTATG	-541
-540	GAAGGTTGA	GAATCCACTT	CTTTAGCGGT	TAATAATTTA	CTCCGAGTAA	GGAATCTTTT	-481
-480	GTTAAAGTGG	GGCATGTTCT	TCAAGTGCCA	GAGAAGAGAG	AAGGGTGATT	TTTCTGACAT	-421
						API binding site 7	
-420	CCTCCAGCCT	GCTTCTCCAT	ATTTGGAAAT	GTTTACCCAC	CAGGCTGATC	TATTGGAAGA	-361
-360	GAGGGAGGTG	ACTCAGGGTT	TAGGAGAAAG	AGGATTTGAA	TTCTTGTTTC	CAGAAACAAA	-301
-300	GTCGTCCCCC	CACCCTGCCC	CCACCCTTCC	CCCTTCATTC	CTCTGTCCCT	TGTTCTGGAA	-241
-240	GCTGAGGCGA	GAATGTCTCA	GTTCGTGTTCC	CTTCAGGCTT	CGAGACCACC	GCCTTGCTGT	-181
-180	GTCCCGTAGT	GGACTGAGGG	CCTGCAAGAG	GGAGTGAGGG	CTAGTGAGAG	GCCAGCTGCC	-121
-120	TGTGGGGGCT	GGACATCGTG	TGAGTACATC	ATTACTGCCA	TTTCTGCTCA	CAGACCTGGG	-61
						API binding site 8	
-60	GCTTACAGCC	TGTGGGCTGG	CTCACCTGCA	TGGTGATGGG	ACACGTTGCT	GGGAGTGCTG	-1
						Transcription start site	
1	GTCACTTTTA	TTTGGGGGTG	TGGACAGCTG	CTTTCCAGG	GGAGTACTTC	TTACAGTGGG	60
						Start codon	
241	CCAACAATGT	CTCACCATC	TTGGCTGCCA	CCAAAAGCA	CTGGTGAGCC	CCTCGGCCAT	300

**Fig. 90: Transcription factor binding site analysis on LPP promoter sequence.** Multiple AP1 binding sites were identified with the 1500 base pairs upstream the LPP transcription start site. Analysis result suggested that increased c-Fos/c-Jun expression may transcriptionally upregulate LPP.

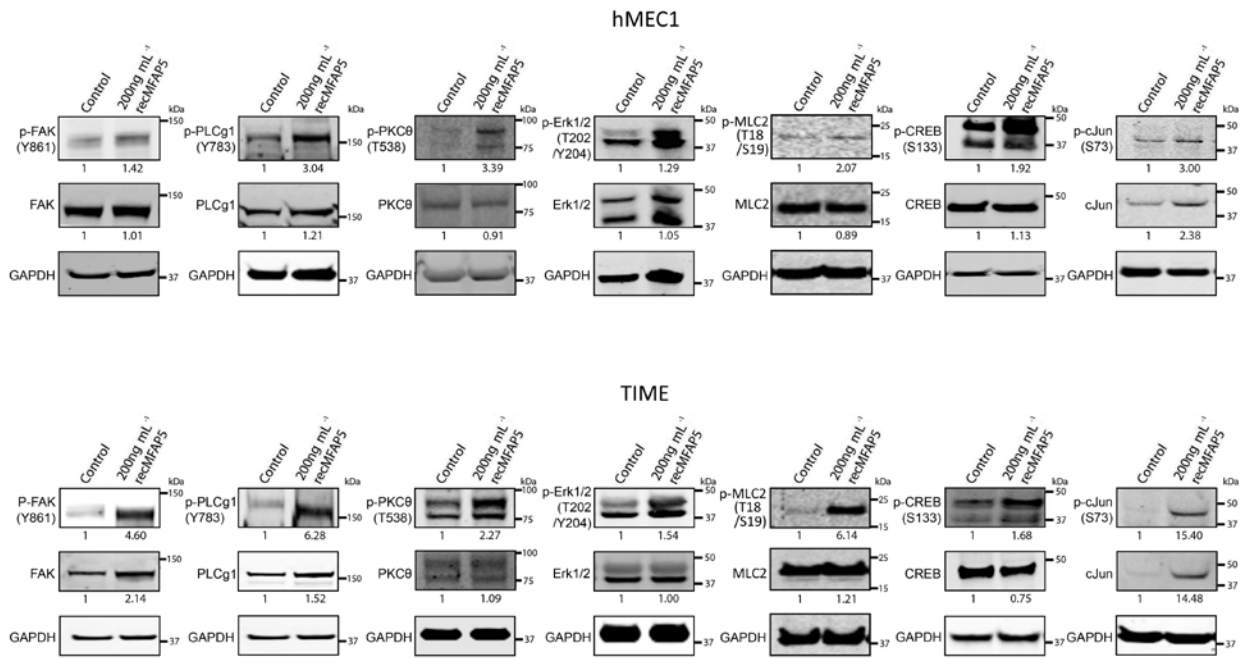


**Fig. 91: Western blot analyses on proteins isolated from MFAP5-treated hMEC-1 and TIME cells.** Western blot analyses identified a significant increase in p-FAK(Y861), p-PLC- $\gamma$ 1 (Y783), p-PKC $\theta$  (T538), p-ERK1/2 (T202/Y204), p-MLC2(T18/S19), p-CREB (S133), cJun and p-cJun (S73) expression in microvascular endothelial cells treated with MFAP5, which may lead to up-regulation of LPP and subsequently increased cell motility and permeability.

*In vitro* experiments demonstrated that FAK plays an essential role in multiple signaling pathways that lead to angiogenesis.<sup>134-137</sup> Src-mediated coupling of FAK to integrin  $\alpha_v\beta_5$  has been shown to be essential for VEGF signaling.<sup>138</sup> In addition, recent studies showed that  $Ca^{2+}$  elevations increase the residency of FAK at focal adhesions by means of tyrosine phosphorylation of FAK, which subsequently leads to increased activation of FAK effectors involved in focal adhesion disassembly.<sup>139</sup> Since our data showed that MFAP5 induced microvascular endothelial cell motility activity was suppressed by pre-treated with an anti- $\alpha_v\beta_3$  integrin antibody, and MFAP5 up-regulated p-FAK (Tyr861) expression was suppressed by pretreated cells with calcium chelator, BAPTA/AM (Fig. 92), we hypothesize that MFAP5-mediated response in endothelial cells requires the binding of MFAP5 to  $\alpha_v\beta_3$  integrin, which subsequently leads to the activation of FAK. Activation of FAK will activate PKC $\theta$ , which has

been shown to be able to regulate  $\text{Ca}^{2+}$  influx.<sup>119</sup>  $\text{Ca}^{2+}$  mobilization activates ERK1/2, and subsequently leads to CREB activation, and translocation to the nucleus. Binding of activated CREB to the CRE of c-Jun may transcriptionally up-regulate LPP, which contains multiple AP1 binding sites in the promoter sequence (Fig. 93).

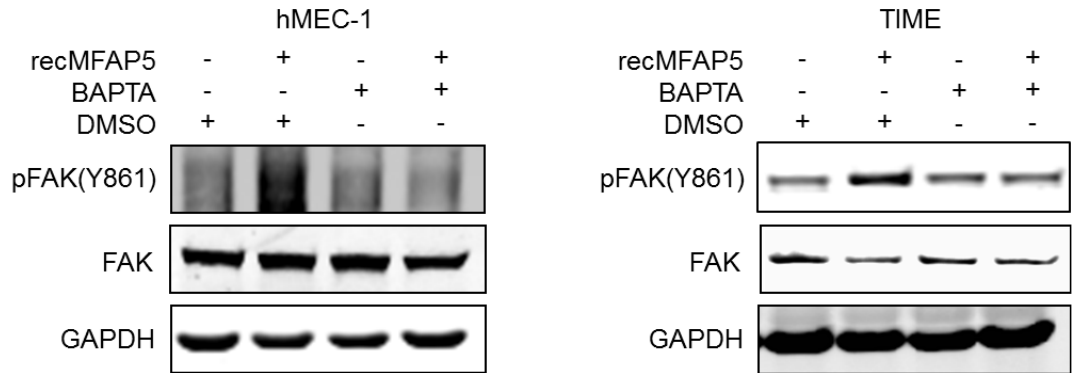


**Fig. 92: Western blots showing the effects calcium chelation on FAK phosphorylation in microvascular endothelial cells.** MFAP5-induced FAK phosphorylation was not observed in BAPTA/AM-loaded hMEC-1 and TIME cells.

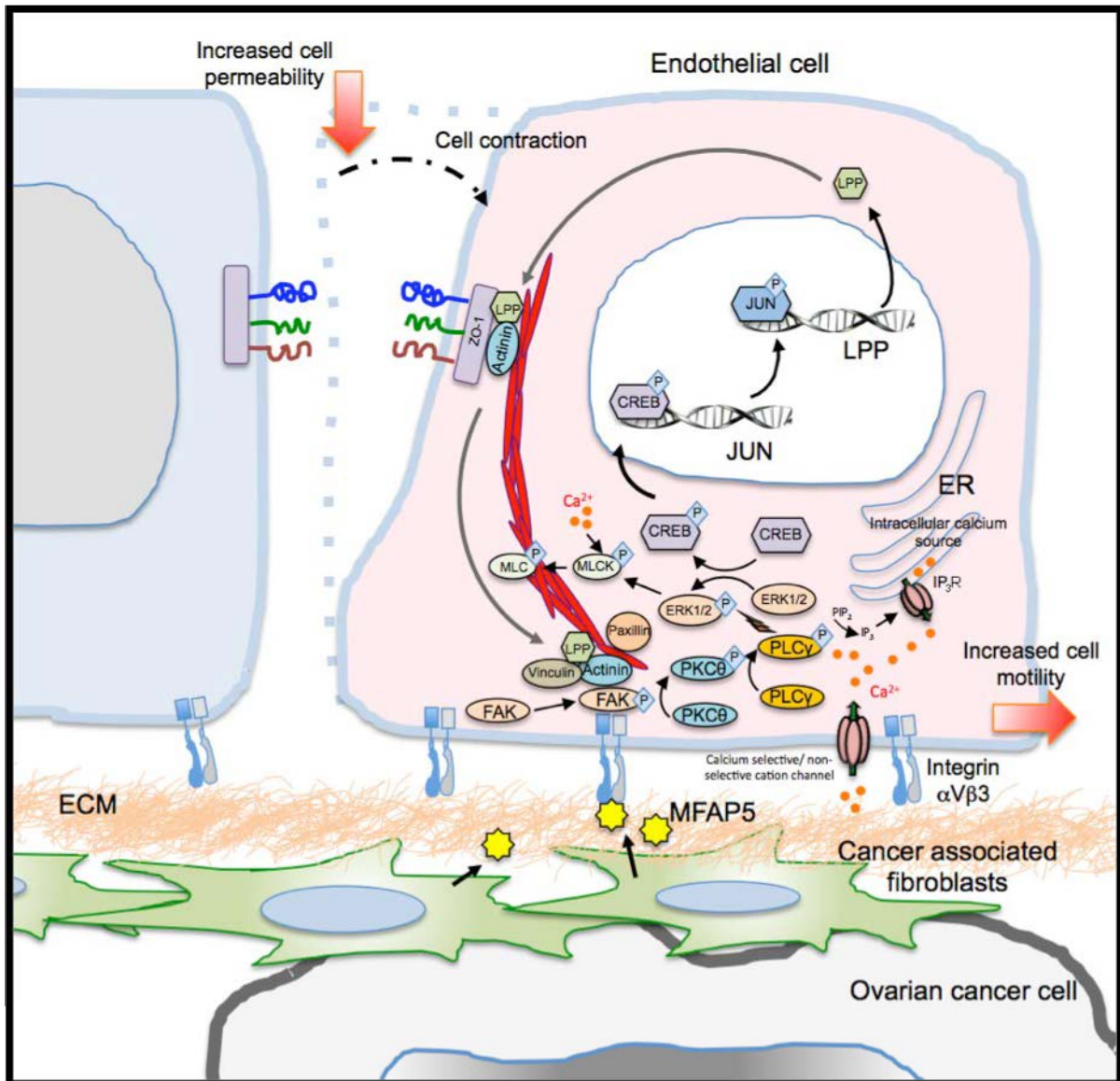


**Fig. 93: Diagram showing the proposed signaling pathways by which MFAP5 regulates LPP expression and LPP increases cell permeability and motility in endothelial cells.**

To evaluate whether MFAP5-induced FAK and PLC $\gamma$ 1 phosphorylation is mediated through its binding to  $\alpha_v\beta_3$  integrin, and the formation of FAK/  $\alpha_v\beta_3$  complex, hMEC-1 and TIME were pretreated with an anti- $\alpha_v\beta_3$  integrin antibody (LM609), anti- $\alpha_5$  antibody or control IgG before treating with recombinant MFAP5. Pre-treated cells with anti-  $\alpha_v\beta_3$  integrin antibody but not anti- $\alpha_5$  antibody or control IgG abrogated the effect of MFAP5 on FAK and PLC $\gamma$ 1 phosphorylation (Figs. 94 and 95).

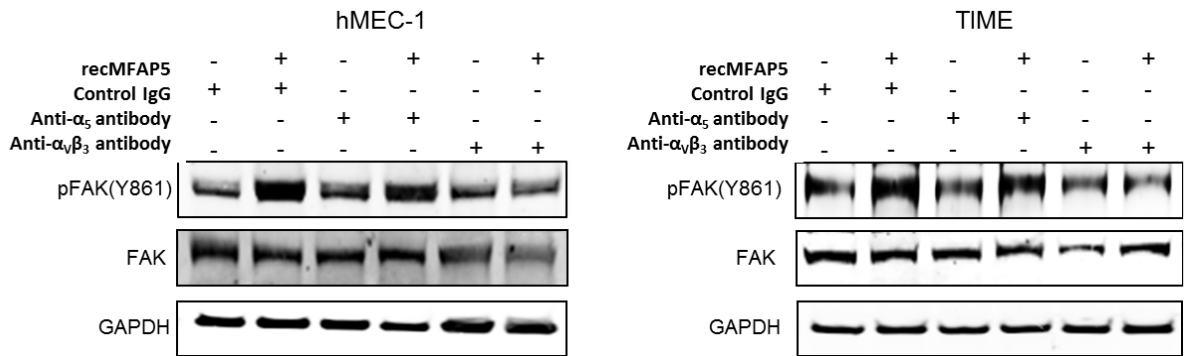


**Fig. 94: Western blots showing blockade of  $\alpha_v\beta_3$  integrin attenuated MFAP5 stimulated FAK phosphorylation in microvascular endothelial cells.** Pretreatment of hMEC-1 and TIME cells with anti-  $\alpha_v\beta_3$  integrin antibody but not anti- $\alpha_5$  antibody or control IgG abrogated the effect of MFAP5 on FAK phosphorylation.

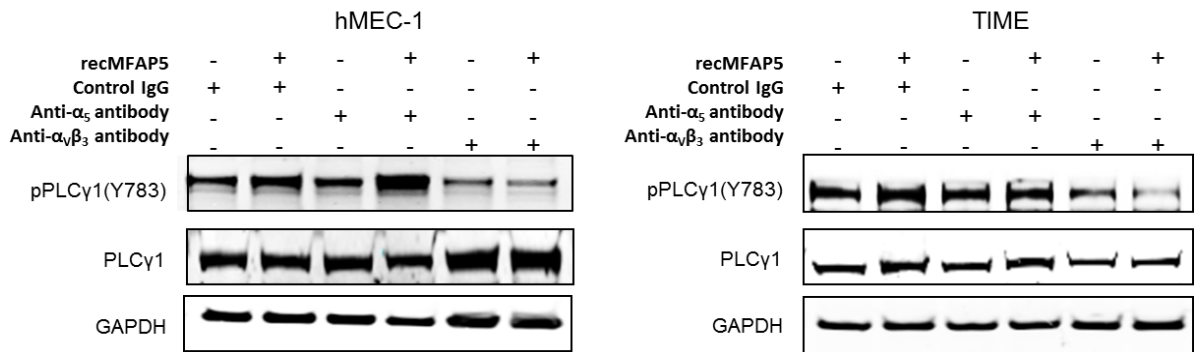


**Fig. 95: Western blots showing blockade of  $\alpha_v\beta_3$  integrin attenuated MFAP5 stimulated PLC- $\gamma$ 1 phosphorylation in microvascular endothelial cells.** Pretreatment of hMEC-1 and TIME cells with anti-  $\alpha_v\beta_3$  integrin antibody but not anti- $\alpha_5$  antibody or control IgG abrogated the effect of MFAP5 on PLC- $\gamma$ 1 phosphorylation.

Next, we evaluated whether PKC $\theta$  stimulated by MFAP5 in microvascular endothelial cells is mediated by FAK phosphorylation. Previous studies showed that p-FAK can activate PKC $\theta$  phosphorylation by promoting (PLC)- $\gamma$ 1 activity.<sup>140</sup> Activated (PLC)- $\gamma$ 1 can increase the hydrolysis of intracellular PIP<sub>2</sub> to form IP<sub>3</sub> and DAG, which can subsequently activate PKC $\theta$ .<sup>141,142</sup> Furthermore, PKC $\theta$  has been shown to be able to mobilize Ca<sup>2+</sup> directly.<sup>119</sup> Since we showed increased p-FAK, and p-PKC $\theta$  expression, and increased Ca<sup>2+</sup> mobilization and oscillation in hMEC-1 cells treated with recMFAP5, we hypothesize that increased Ca<sup>2+</sup>



mobilization and oscillation observed in recMFAP5 treated hMEC-1 cells may be due to an increase in the phosphorylation of PKC $\theta$  by p-FAK. To test this hypothesis, we first evaluated whether PKC $\theta$  activation is mediated by p-FAK in MFAP5 treated microvascular endothelial cells. Western blot analysis on PKC $\theta$  was performed on hMEC-1 and TIME cells treated with MFAP5 in the presence or the absence of FAK inhibitors (PF573228, Sigma-Aldrich Corp. St. Louis, MO). Results showed that increased p-PKC $\theta$  expression in MFAP5 treated microvascular endothelial cells was not observed in the presence of FAK inhibitors (Fig. 96).

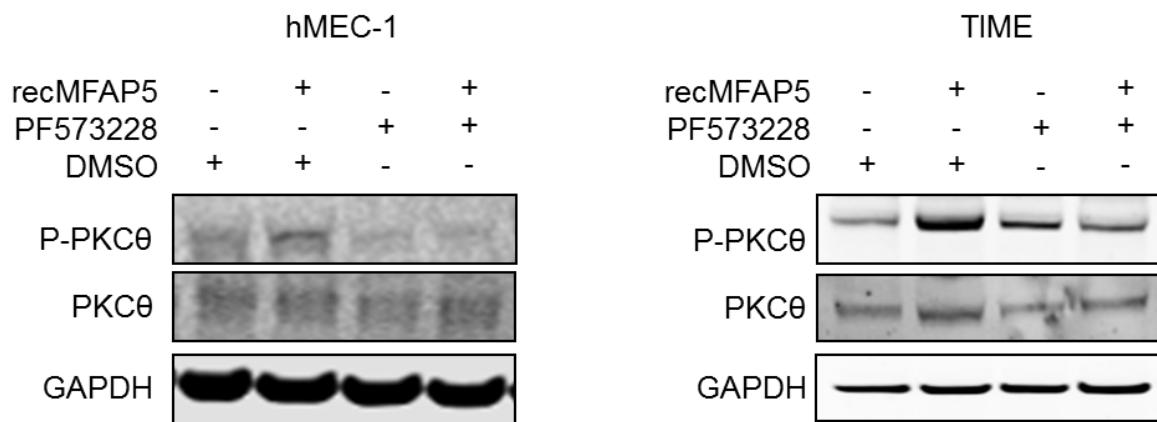


**Fig. 96: Western blots showing FAK inhibitor abrogated MFAP5 stimulated PKC $\theta$  phosphorylation in microvascular endothelial cells.** Increased p-PKC $\theta$  expression occurred only in the absence of a FAK inhibitor in MFAP5-treated endothelial cells but not in DMSO-treated control cells.

Since previous studies showed that PLC- $\gamma$ 1 phosphorylation can not only be stimulated by  $\alpha_v\beta_3$  engagement alone<sup>116</sup> but also by the formation of FAK/  $\alpha_v\beta_3$  complex.<sup>117</sup> FAK inhibitor was therefore employed to investigate whether PLC- $\gamma$ 1 phosphorylation is also FAK dependent. Our result showed that pre-treatment of hMEC-1 and TIME cells with FAK inhibitor followed by treatment of recMFAP5 in the presence of the inhibitor attenuated the phosphorylation of p-PLC- $\gamma$ 1 (Y783) (Fig. 97). This suggested that MFAP5 induced pPLC- $\gamma$ 1 (Y783) phosphorylation was FAK dependent. Besides, MFAP5-induced PKC $\theta$  phosphorylation was attenuated in hMEC-1 and TIME cells treated with PLC inhibitor (U73122; #sc-3574) (Fig.

98). This suggested that PKC $\theta$  activation is regulated by PLC $\gamma$ 1 phosphorylation. However, as described in the MFAP5 stimulated signaling in ovarian cancer cells in Aim 1, PKC $\theta$  inhibitor also abolished p-PLC- $\gamma$ 1 up-regulation indicating that the two pathways are inter-dependent and both affect the Ca<sup>2+</sup> mobilization in MFAP5 treated microvascular endothelial cells (Fig. 99).

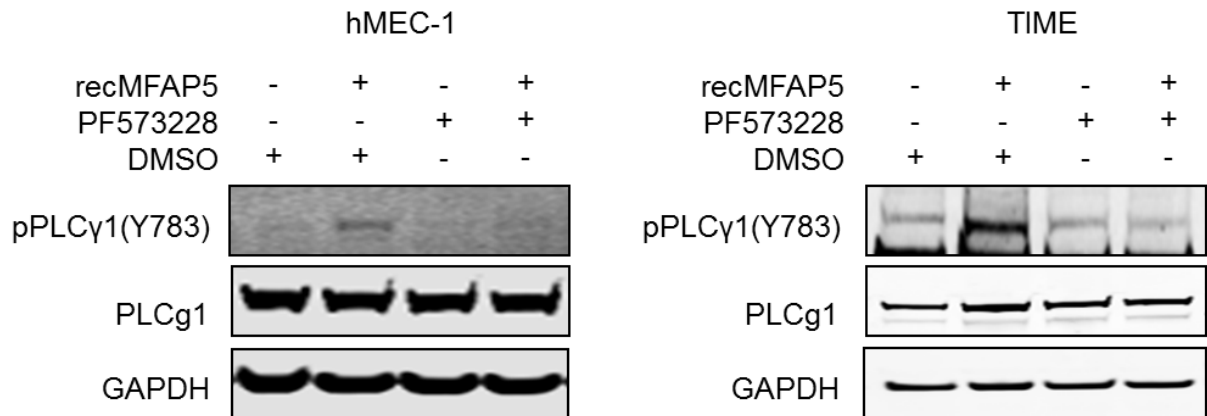


**Fig. 97: Western blots showing FAK inhibitor abrogated MFAP5 stimulated PLC- $\gamma$ 1 phosphorylation in microvascular endothelial cells.** Increased p-PLC- $\gamma$ 1 expression occurred only in the absence of an FAK inhibitor PF573228 in MFAP5-treated endothelial cells but not in DMSO-treated control cells.

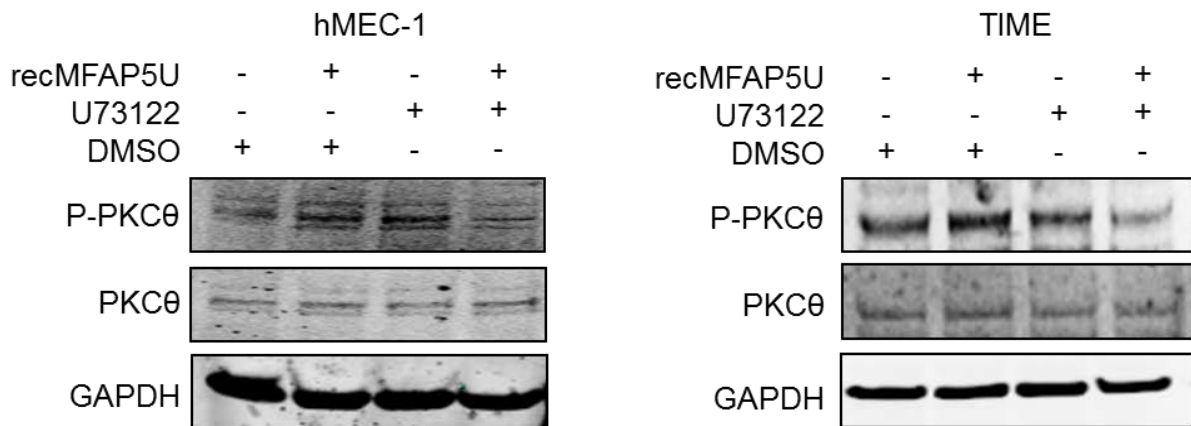


**Fig. 98: Western blots showing PLC inhibitor abrogated MFAP5 stimulated PKC $\theta$  phosphorylation in microvascular endothelial cells.** The PLC inhibitor U71322 abolished the upregulation of p-PKC $\theta$  expression in MFAP5-treated endothelial cells.



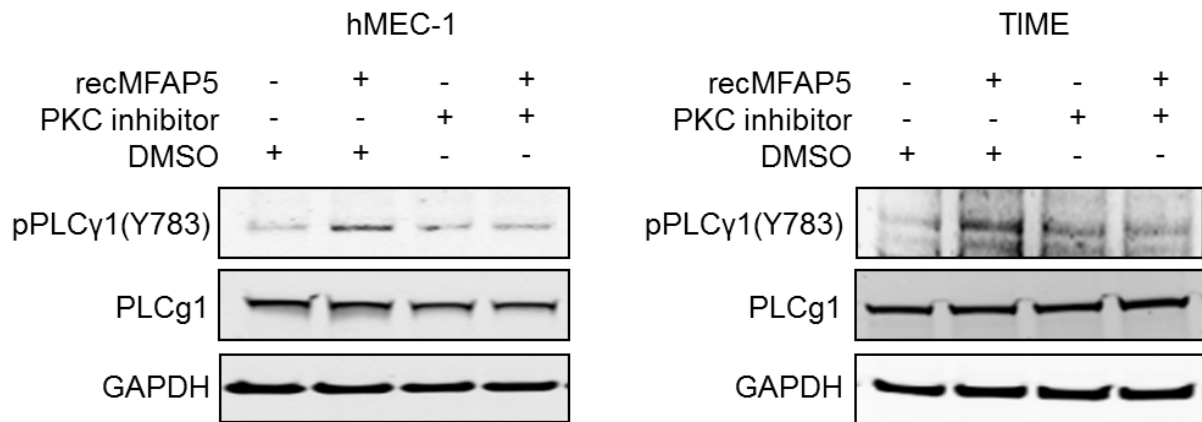


**Fig. 99: Western blots showing PKC inhibitor abrogated MFAP5 stimulated PLC-γ1 phosphorylation in microvascular endothelial cells.** Pretreatment of hMEC-1 and TIME cells with the PKC inhibitor abolished the upregulation of p-PLC-γ1 expression in MFAP5-treated cells.

To investigate whether activation of ERK1/2 and CREB induced by MFAP5 is  $Ca^{2+}$  dependent and is mediated through activation of  $\alpha_v\beta_3$  integrin/FAK/PKC $\theta$ , hMEC-1 and TIME cells were treated with MFAP5 in the presence or the absence of BAPTA/AM and PKC $\theta$  pseudosubstrate inhibitor. The results show that phosphorylation of ERK1/2 and CREB after recMFAP5 treatment was attenuated in BAPTA/AM loaded cells as shown by western blot analyses (Figs. 100 and 101). These data suggest that both MFAP5 induced ERK and CREB activation is calcium dependent. Besides, application of PKC $\theta$  pseudosubstrate inhibitor abrogated phosphorylation of ERK1/2 (Fig. 102). These data suggest that MFAP5 induced ERK1/2 activation is  $\alpha_v\beta_3$  integrin/FAK/PKC $\theta$  dependent.

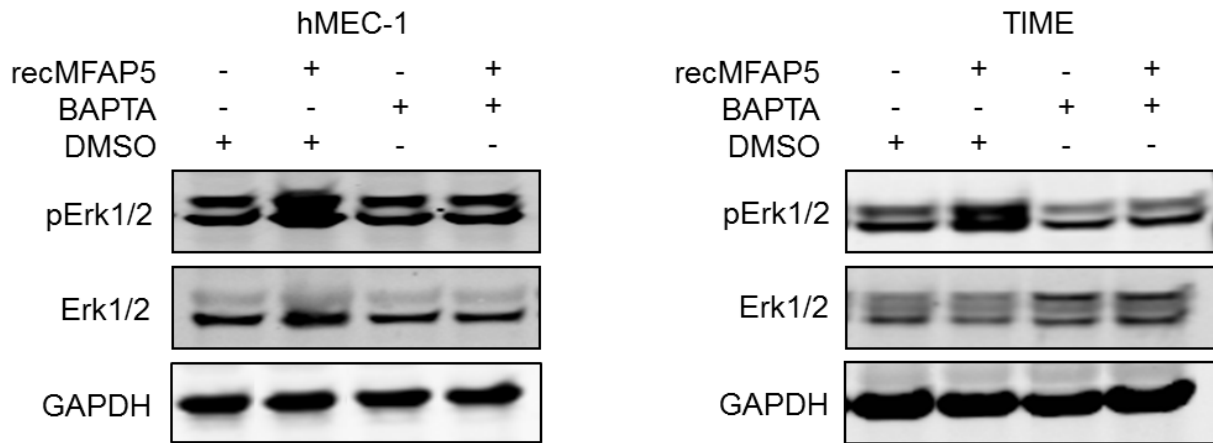


**Fig. 100: Western blots showing the effects of calcium chelation on ERK phosphorylation in microvascular endothelial cells.** MFAP5-induced Erk1/2 phosphorylation was not observed in BAPTA/AM-loaded hMEC-1 and TIME cells.

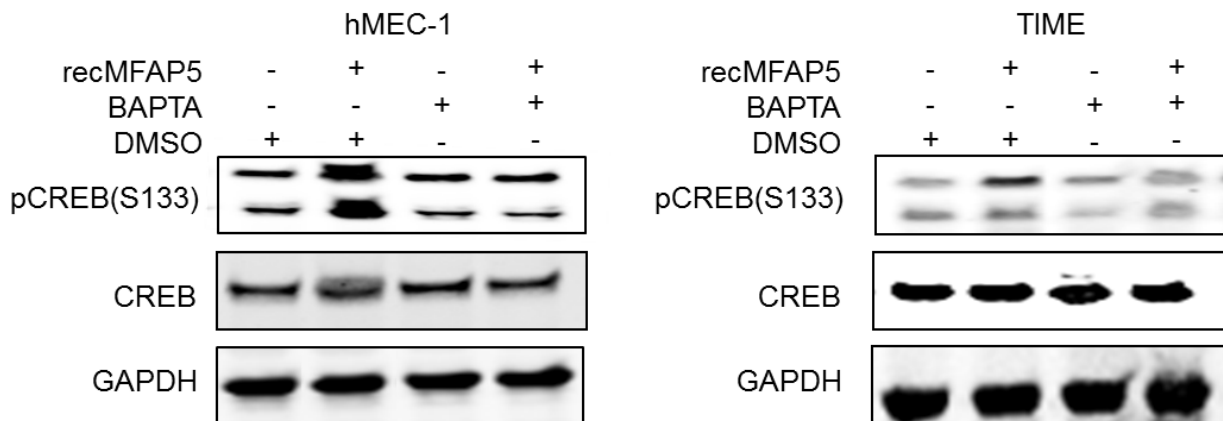


**Fig. 101: Western blots showing the effects of calcium chelation on CREB phosphorylation in microvascular endothelial cells.** MFAP5-induced CREB phosphorylation was not observed in BAPTA/AM-loaded hMEC-1 and TIME cells.

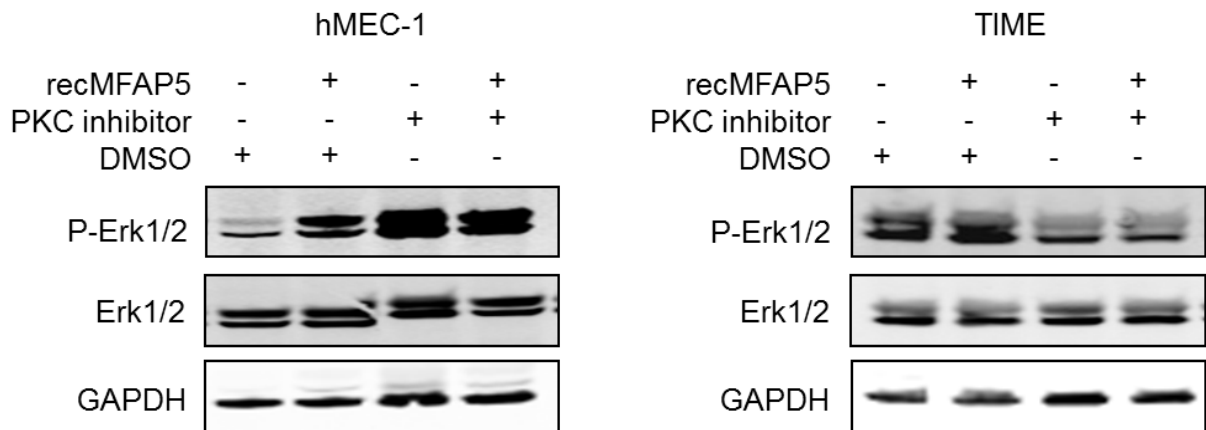


**Fig. 102: Western blots showing PKC inhibitor abrogated MFAP5 stimulated ERK1/2 phosphorylation in microvascular endothelial cells.** Pretreatment of hMEC-1 and TIME cells with the PKC inhibitor abolished the upregulation of p-Erk1/2 expression in MFAP5-treated cells.

Since ERK dependent MLC2 and CREB activation has been reported,<sup>143,144</sup> therefore, we evaluated whether MLC2 and CREB activation is mediated through calcium dependent ERK1/2 phosphorylation. The results showed that MFAP5 stimulated MLC2 and CREB phosphorylation were attenuated by treating hMEC-1 and TIME cells with recMFAP5 in the presence or the absence of ERK1/2 inhibitors (FR180204, Merck, Germany) (Figs. 103 and 104). This demonstrated that MFAP5 induced MLC2 and CREB activation via ERK1/2.

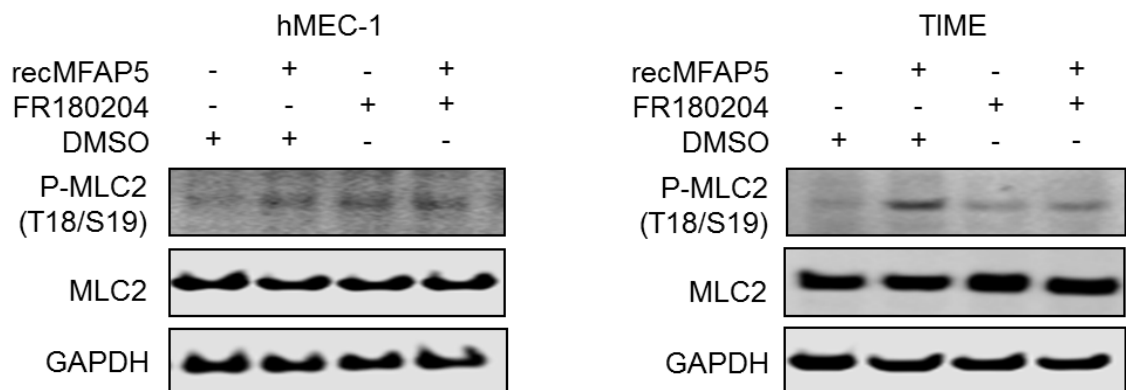


**Fig. 103: Western blots showing ERK inhibitor abrogated MFAP5 stimulated MLC2 phosphorylation in microvascular endothelial cells.** Pretreatment of hMEC-1 and TIME cells with an ERK1/2 inhibitor abolished the upregulation of p-MLC2 expression in MFAP5-treated cells.

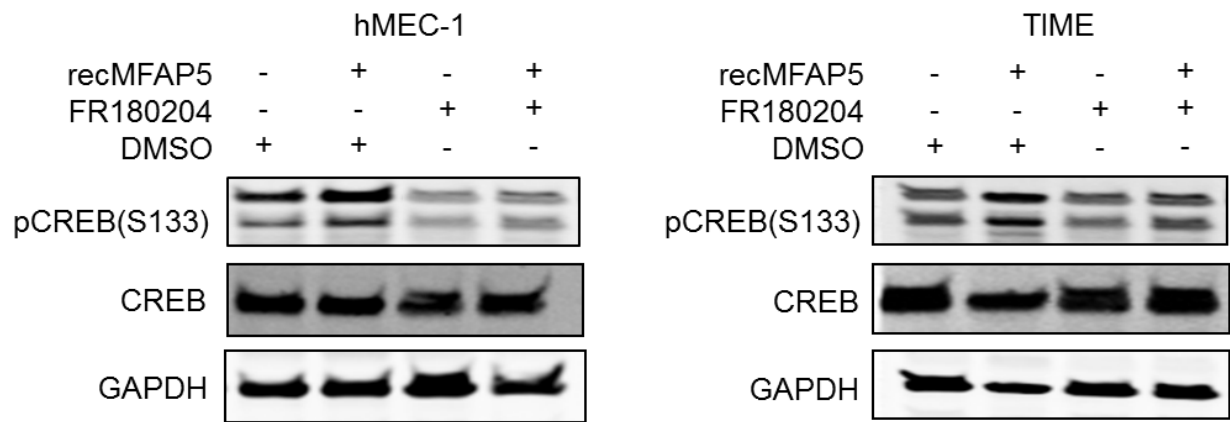


**Fig. 104: Western blots showing ERK inhibitor abrogated MFAP5 stimulated CREB phosphorylation in microvascular endothelial cells.** Pretreatment of hMEC-1 and TIME cells with an ERK1/2 inhibitor abolished the upregulation of p-CREB expression in MFAP5-treated cells.

Finally, our data demonstrated up-regulation of c-Jun, which contains a CRE in its promoter, in MFAP5-treated cells. Also, promoter analysis revealed that the LPP promoter consisted of multiple potential AP-1 binding sites (Fig. 90), suggested that transcriptional up-regulation of LPP expression may be controlled by CREB-mediated c-Jun expression. To test this hypothesis, we evaluated the effects of CBP/CREB interaction inhibitor and c-Jun inhibitor SP600125 on MFAP5-treated cells. Results demonstrated that CBP/CREB interaction inhibitor attenuated the up-regulation of both c-Jun and p-c-Jun while SP600125 abrogated the up-regulation of LPP (Figs. 105 and 106). These data confirmed that the increase of LPP expression induced by MFAP5 is calcium-dependent and mediated via up-regulation of c-Jun by CREB activation.

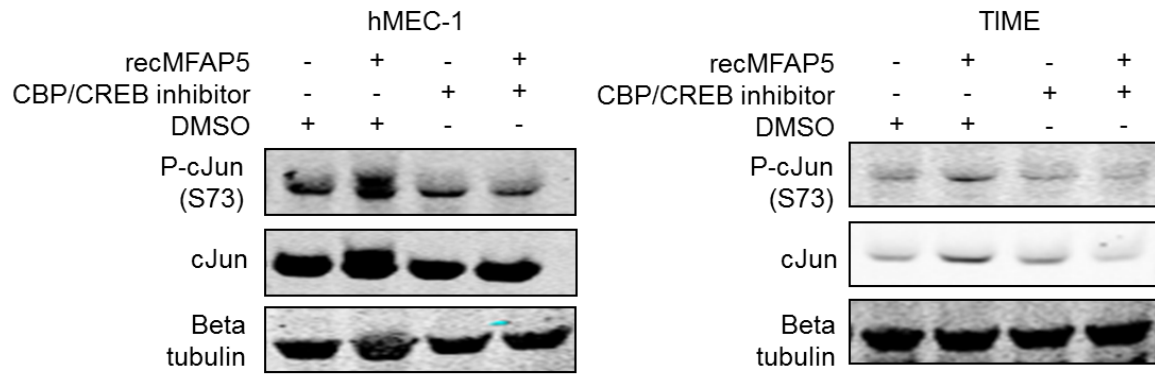


**Fig. 105: Western blots showing CBP/CREB interaction inhibitor abrogated MFAP5 stimulated c-Jun and p-c-Jun expression in microvascular endothelial cells.** Pretreatment with CBP/CREB interaction inhibitor attenuated the upregulation of total c-Jun and p-c-Jun (S73) expression induced by MFAP5 in hMEC-1 and TIME cells.

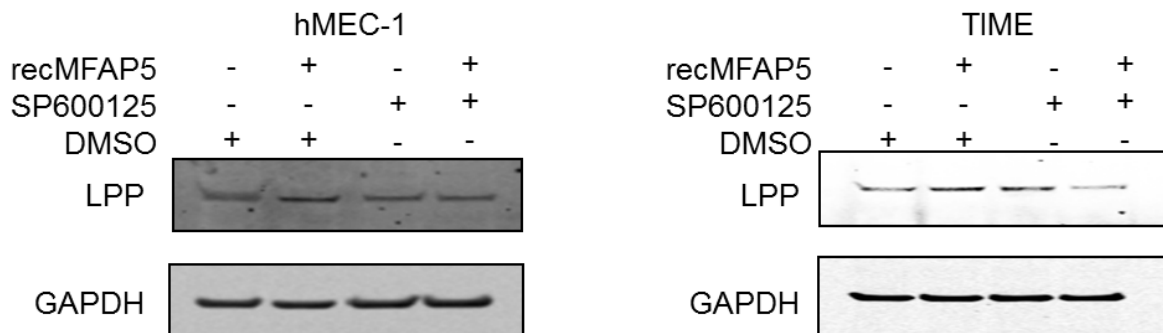


**Fig. 106: Western blots showing the effect of c-Jun inhibitor on MFAP5 induced LPP overexpression in microvascular endothelial cells.** MFAP5-induced LPP upregulation was abrogated in c-Jun inhibitor, SP600125, treated hMEC-1 and TIME cells.

After demonstrating that MFAP5 can up-regulate LPP through the activation of FAK/ERK/CREB signaling network, we determined whether LPP can modulate the effect of MFAP5 on the downstream signaling network activation through a positive feedback loop since LPP has been shown to be recruited to focal adhesions in MDCK epithelial cells, and to interact with  $\alpha$ -actinin to facilitate stress fiber formation.<sup>96,105,145</sup> Western blot analyses on phosphorylation of FAK was determined in MFAP5 treated hMEC-1 and TIME cells transfected with LPP siRNA or the control siRNA. Results showed that LPP siRNA can successfully

abrogate MFAP5 induced FAK phosphorylation (Fig. 107). In addition, our data showed that knockdown of LPP attenuated MFAP5 stimulated increase of focal adhesion (Figs. 87 and 88), these suggest that focal adhesion targeting by LPP may play an essential role in the formation of the focal adhesion complexes and the activation of downstream signaling molecules, which mediate the effect of MFAP5 on endothelial cell motility and permeability.

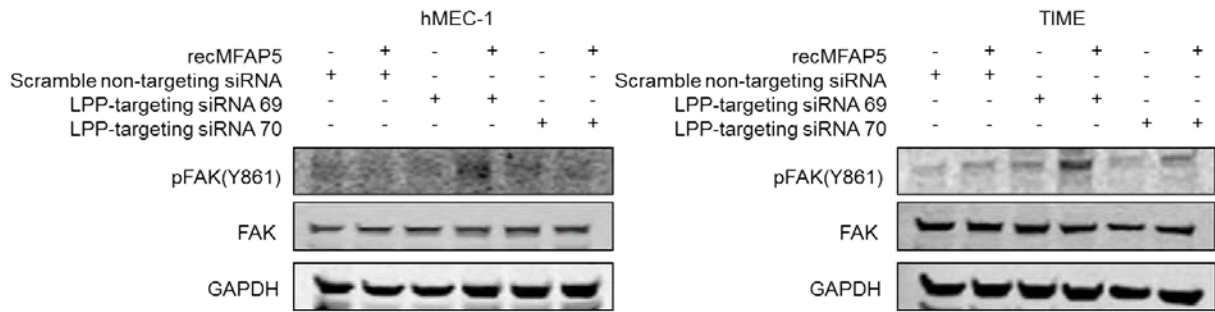


**Fig. 107: Western blots showing the effect of LPP silencing on MFAP5 induced FAK phosphorylation in microvascular endothelial cells.** Knockdown of LPP by LPP-targeting siRNAs abolished MFAP5-induced FAK phosphorylation at Y861 site in hMEC-1 and TIME cells compared to those transfected with scramble non-targeting siRNA.

### **Specific aim III: Development of MFAP5-targeted therapeutic agents for ovarian cancer treatment**

#### **A. Characterization of anti-MFAP5 antibodies by western blot analysis and epitope mapping**

There is ample evidence to indicate that angiogenesis is important to the development, progression and poor prognosis of ovarian cancer,<sup>146</sup> suggesting that agents targeting the tumor vasculatures can be used as a therapeutic regimen in the treatment of ovarian cancer and improve patient survival.

Since our data demonstrated the pro-angiogenic role of MFAP5 *in vitro* and *in vivo*, and showed that targeting stromal MFAP5 by siRNA could suppress ovarian cancer growth and blood vessel permeability in mice, we have generated MFAP5-targeting monoclonal antibodies using purified human recombinant MFAP5 protein as antigen. Monoclonal antibodies from 95 hybridoma clones were showed to bind human recombinant MFAP5 (recMFAP5) by ELISA (data not shown) and western blot analysis using the Bio-rad multiscreen apparatus identified 16 antibody clones with strong binding affinity to human MFAP5 (Fig. 108). 5 clones (50B, 52B, 64A, 75B and 117B) were sent out for epitope mapping and the result showed that all of them recognize the same human MFAP5 protein sequence [DETVLAVLA] (Fig. 109).



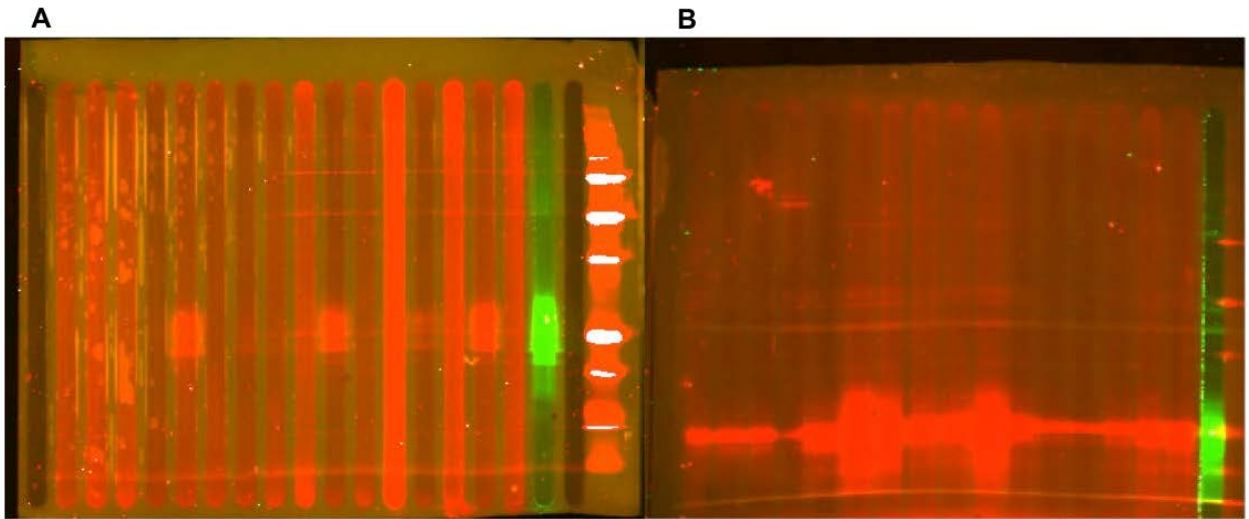
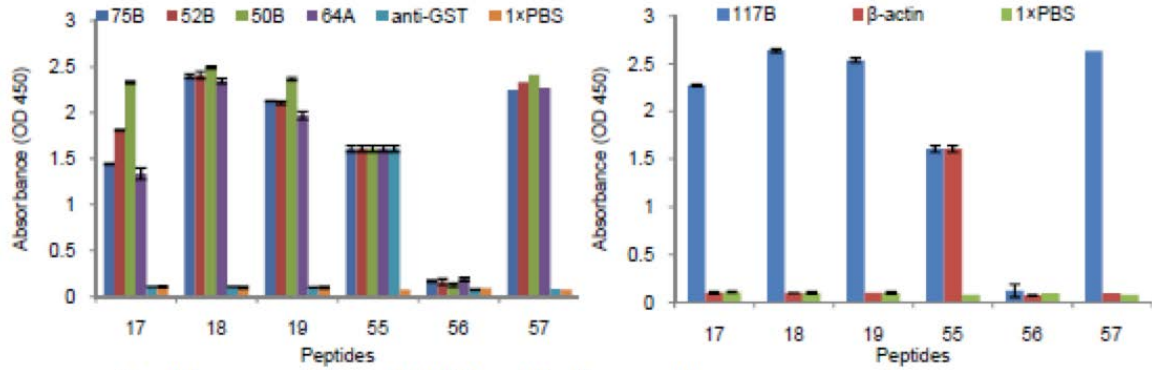


**Fig. 108: Western blot screening to identify specific anti-MFAP5 antibodies.** Western blot analysis using the Bio-rad multiscreen apparatus to screen for (A) positive clones that bind to human recombinant MFAP5 protein and (B) 16 clones that have high binding efficiency to cell lysate from MFAP5 overexpressing fibroblasts, NOF151-LvMFAP5. (Green: positive control of commercially available polyclonal anti-MFAP5 antibody, Sigma # HPA010553)



Graphic presentation of ELISA verification result.

No.	Peptide
17	VNDPATDET <b>VLAVLA</b>
18	PATDET <b>VLAVLA</b> DIA
19	DET <b>VLAVLA</b> DIA PST

**Fig. 109: Epitope mapping for antibodies specific for human MFAP5.** Epitope mapping data showing that clones 50B, 52B, 64A, 75B and 117B recognize the human MFAP5 protein sequence [DET**VLAVLA**].

Next, we used the same screening strategy to screen for anti-mouse MFAP5 clones. One clone, 130A, was showed to bind both recombinant human and mouse MFAP5 proteins (Fig. 110). Epitope mapping result showed that clone 130A recognize the MFAP5 protein sequence [LSRQ**MAGLPP**RRL] (Fig. 111), which is a consensus peptide sequence shared between human and mouse MFAP5 proteins (Fig. 112).

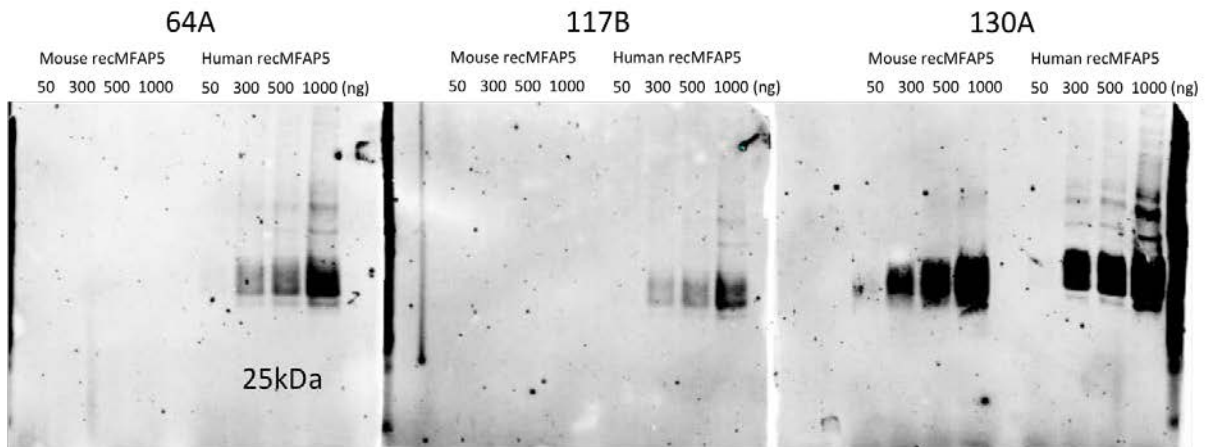
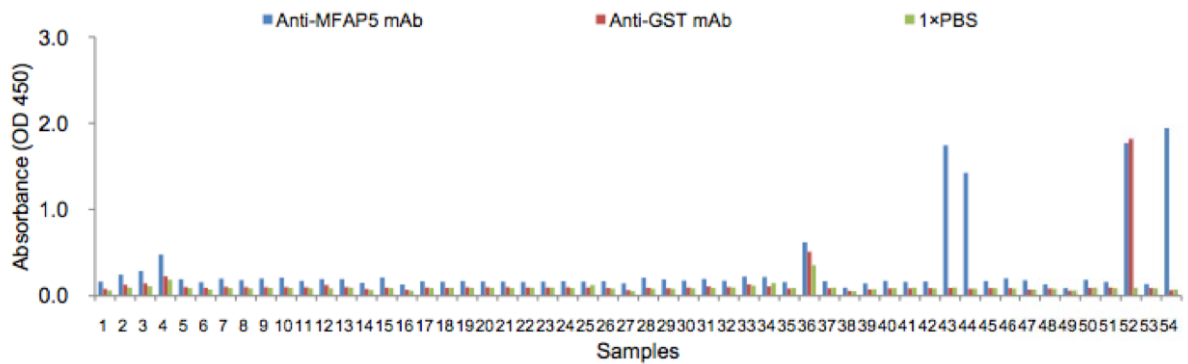


**Fig. 110: Specificity of clone 64A, 117B and 130A to human and/or mouse MFAP5.** Western blot analyses showing the specificity of two clones of mouse monoclonal antibodies (64A and 117B) against human MFAP5 only and one clone of antibody (130A) against both human and mouse MFAP5.



**Graphic presentation of ELISA results**

Epitope of anti-MFAP5 antibody	
No.	Peptide
43	KDEL <b>LSRQMAGLPPRR</b>
44	<b>LSRQMAGLPPRR</b> LRR

**Fig. 111: Epitope mapping for clone 130A anti-MFAP5 antibody.** Epitope mapping data showing that clone 130A recognizes the MFAP5 protein sequence [LSRQMAGLPPRR].



**Fig. 112: Protein sequences of mouse and human MFAP5 showing the epitopes recognized by the three clones (64A, 117B and 130A) of anti-MFAP5 antibodies.** While clones 64A and 117B recognize on human MFAP5, clone 130A is able to recognize both human and mouse MFAP5 proteins.

**B. Functional assays demonstrated inhibitory effect of anti-MFAP5 antibodies on cell motility**

Functional studies on clones 64A and 117B showed that antibody treatment attenuated the stimulatory effect of fibroblast-derived MFAP5 on cell motility in both ovarian cancer cells and endothelial cells (Fig. 113). In addition, clone 130A significantly attenuated the enhanced motility potential in mouse endothelial cells SVEC4-10 (ATCC #CRL-2181) treated with mouse recombinant mfap5 protein (Fig. 114).

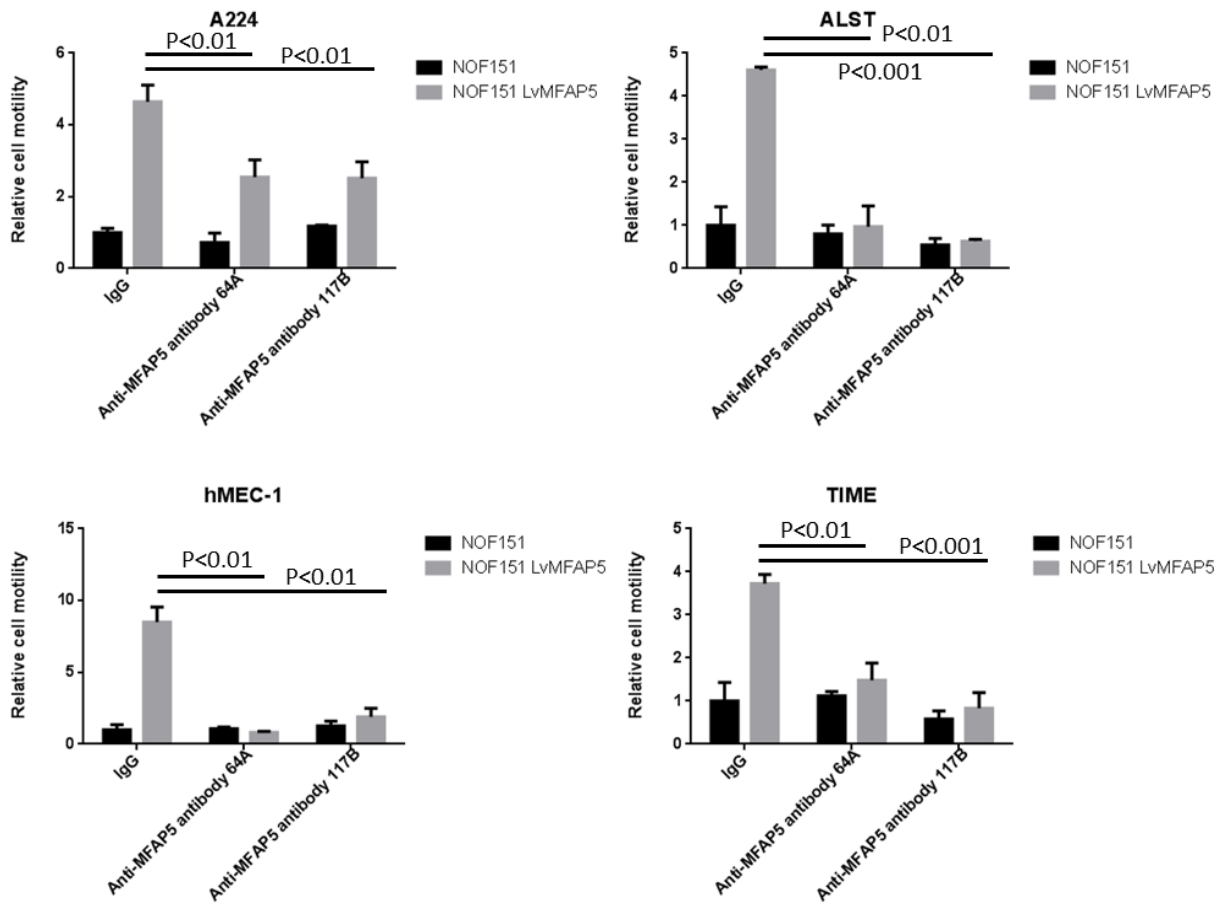


**Fig. 113: *In vitro* functional assay showed inhibitory effects of clones 64A and 117B on MFAP5 enhanced cell motility.** Motility assays were performed on  $\alpha_v\beta_3$  expressing human ovarian cancer cells A224 and ALST and human microvascular endothelial cell lines hMEC-1 and TIME co-cultured with MFAP5-overexpressing fibroblasts or the control fibroblasts in the presence of human IgG or anti-human MFAP5 antibody clones 64A and 117B.

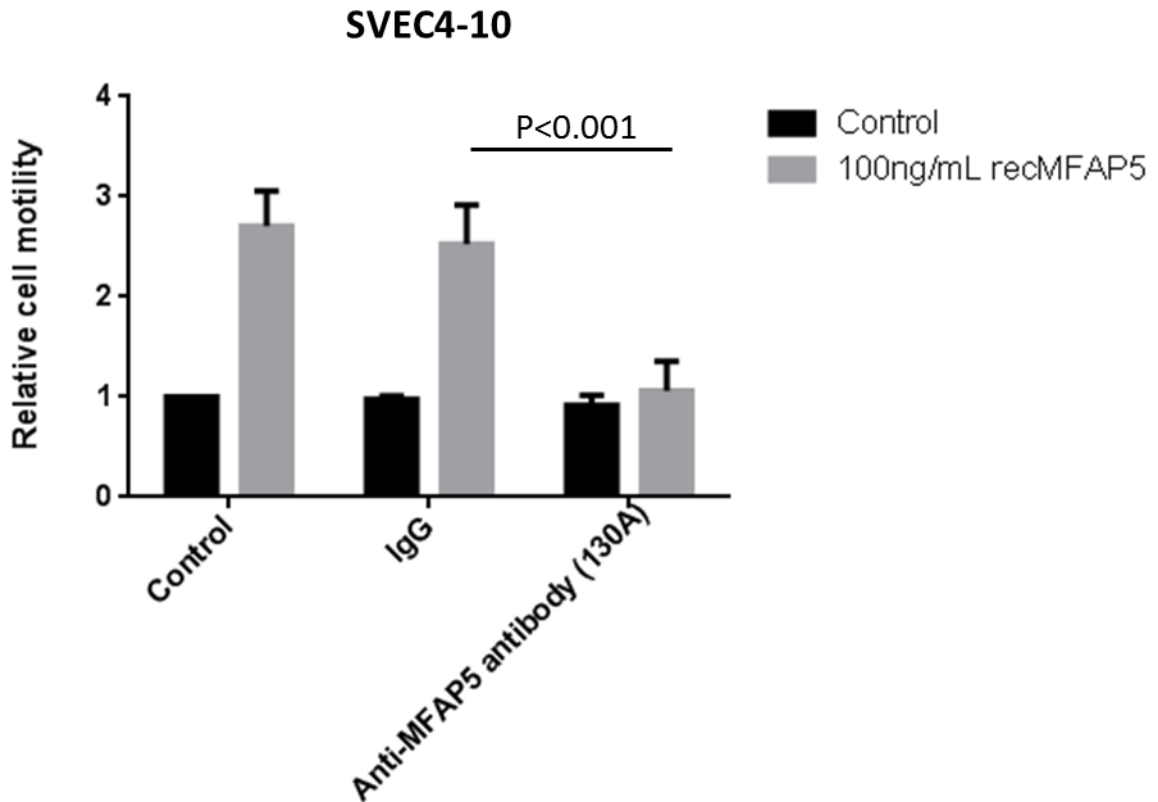


**Fig. 114:** *In vitro* functional assay showed inhibitory effects of clone 130A on mouse mfap5 enhanced mouse endothelial cell motility. Motility assays were performed on mouse endothelial cells SVEC4-10 cultured in media supplemented with MFAP5 or PBS and treated with mouse IgG or anti-mouse MFAP5 antibody clone 130A.

**C. *In vivo* animal study showed tumor suppressing effects of clone 130A anti-mfap5 antibody**

To further evaluate the feasibility in using the anti-MFAP5 antibodies to target stromal MFAP5 *in vivo*, nude mice were injected I.P. with luciferase labeled OVCA432 cells. After one week, the mice were injected twice weekly with anti-MFAP5 antibody clone 130A (15 mg/kg) or the control normal mouse IgG (15 mg/kg) (N=12 per group) and tumor progression was monitored by luciferase based small animal imaging. After six weeks, mice were injected with FITC-labeled dextran before they were sacrificed (Fig. 115A). Results showed that significant lower luciferase activity was detected in mice treated with anti-MFAP5 antibody clone 130A

when compared to the control group treated with control normal mouse IgG (Fig. 115B). Significant lower tumor weight was observed in anti-MFAP5 antibody treated group when compared to control group (Fig. 115C). Also *ex vivo* luminescence data further confirmed the anti-tumor effect of the antibody (Fig. 115D). In addition, FITC-dextran signals in tumor tissues were significantly lower in anti-MFAP5 antibody treated group compared to IgG treated group suggesting that anti-MFAP5 antibody reduced the intratumoral microvessel leakiness (Fig. 116). These data demonstrated that targeting stromal MFAP5 could be a potential therapeutic approach for ovarian cancer.



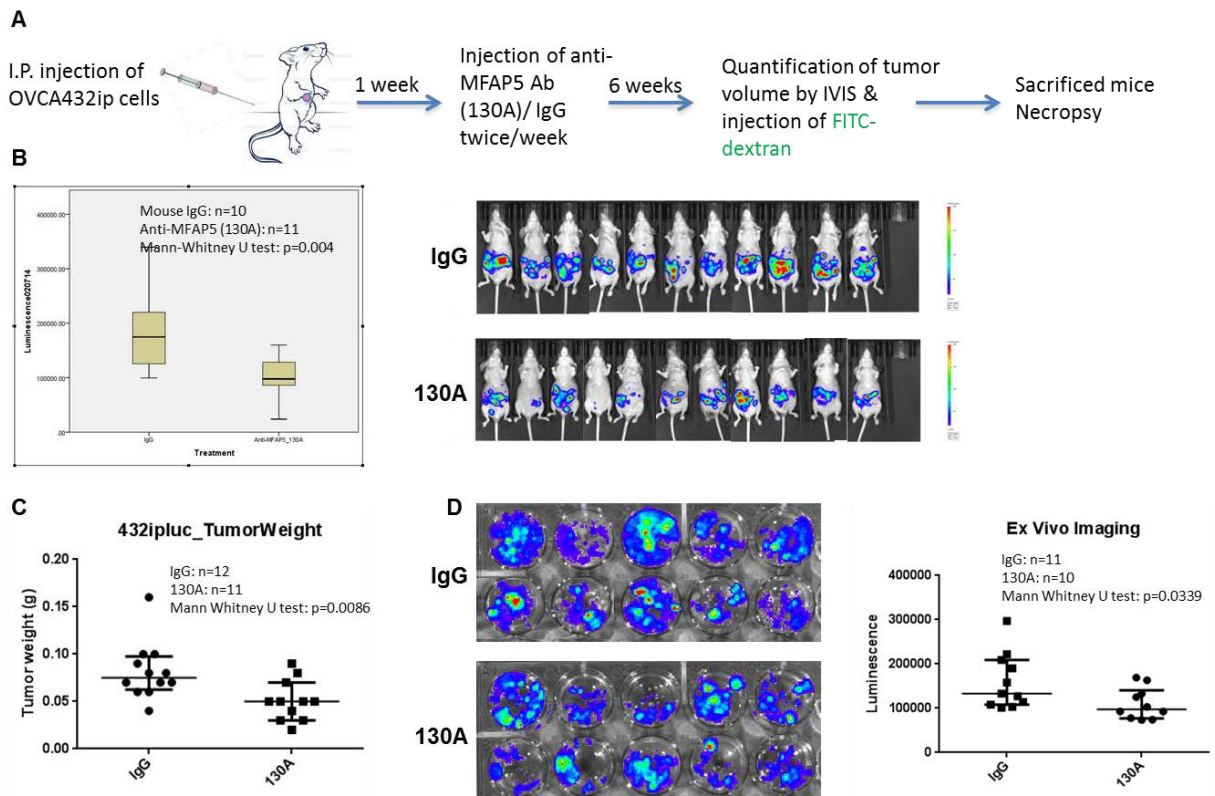


**Fig. 115: Anti-MFAP5 antibody clone 130A suppressed ovarian tumor growth *in vivo*.** (A) A schematic diagram showing the procedures of evaluating the effect of anti-mfap5 antibody treatment *in vivo*. (B) Tumor volume of each treatment group was quantified by the IVIS-200 bioluminescence and fluorescence imaging system (Caliper Life Sciences, Inc., Hopkinton MA). Significant lower luciferase activity was detected in anti-mfap5 antibody treated groups compared to the control group. (p=0.004). The box represents the interquartile range of the records and the line across the box indicates the median. Whiskers indicate the highest and lowest values among the records that are no greater than 1.5 times the interquartile range. (C) After necropsy, tumor weight and *ex vivo* luciferase activity were recorded for each animal. Results showed a significant reduced tumor dry weight after anti-mfap5 antibody treatment (p=0.0086). (D) *Ex vivo* imaging data also demonstrated significantly lower luciferase activity in the tumor tissue in anti-mfap5 antibody treated group compared to IgG treated control (p=0.0339). For scatter plots, upper and lower bars indicate the interquartile range of the records, and the middle line indicates the median.

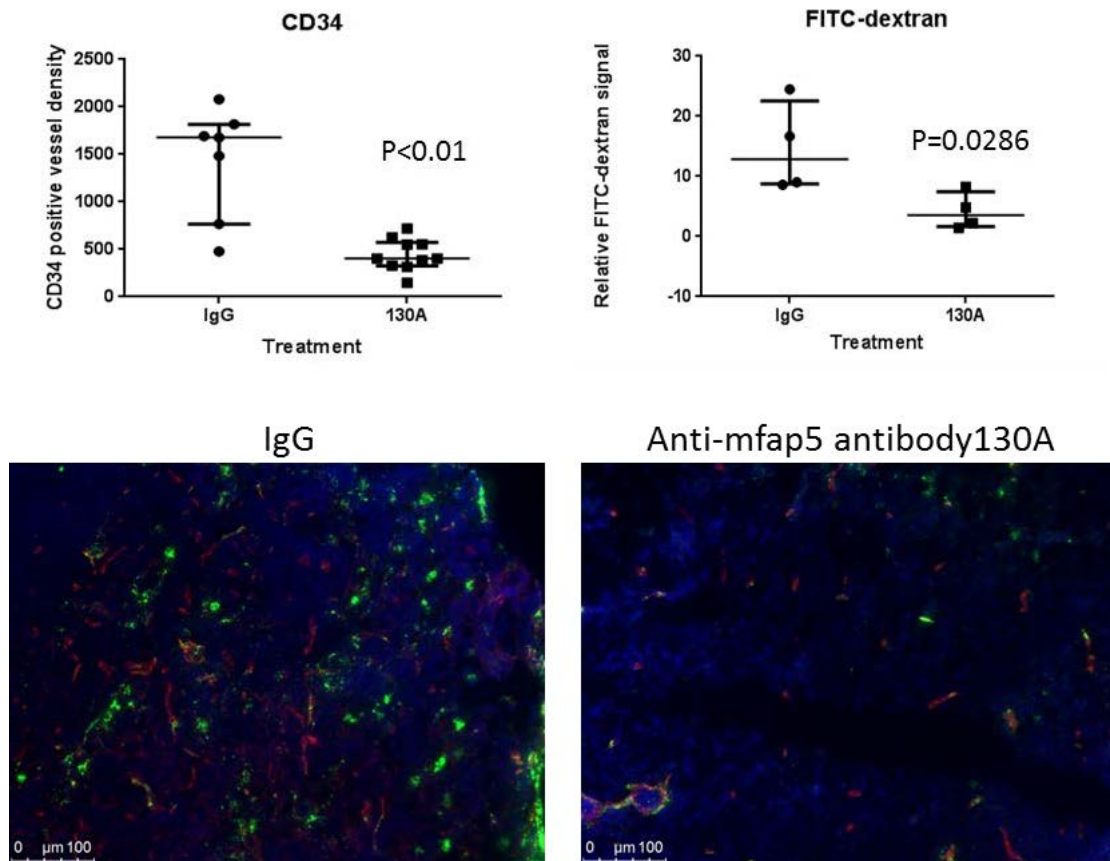


**Fig. 116: Anti-MFAP5 antibody clone 130A reduced tumor angiogenesis and intratumoral microvessel leakiness *in vivo*.** Confocal microscopy demonstrating lower CD34 positive microvessel density (red) and FITC-dextran (green) signals around tumor microvessels in anti-mfap5 antibody treated mice compared to IgG treated mice. For scatter plots, upper and lower bars indicate the interquartile range of the records, and the middle line indicates the median.

#### D. Evaluation of the effect of clone 130A anti-mfap5 antibody on intratumoral microvessel leakiness and drug delivery efficiency

To evaluate whether the reduced intratumoral microvessel leakiness by anti-MFAP5 antibody can affect the bioavailability of systemically administered drugs in ovarian tumors, we treated OVCA432 bearing mice with control IgG or anti-MFAP5 antibody for 4 weeks. 1 mg/kg of Oregon Green 488-conjugated paclitaxel (Life Technologies Corp., Grand Island, NY) was I.V. injected into each of the animals at 1 hour before they were sacrificed. Tumor weight was recorded and 6 μm frozen tissue sections were prepared from tumor tissues harvested.

Fluorescent microscopy and immunolocalization of CD34 showed that significant increased Oregon Green 488-conjugated paclitaxel in the tumor tissue and the density of intratumoral microvessels were decreased in mice treated with 130A anti-MFAP5 antibody when compared to control mice treated with IgG (Fig. 117).

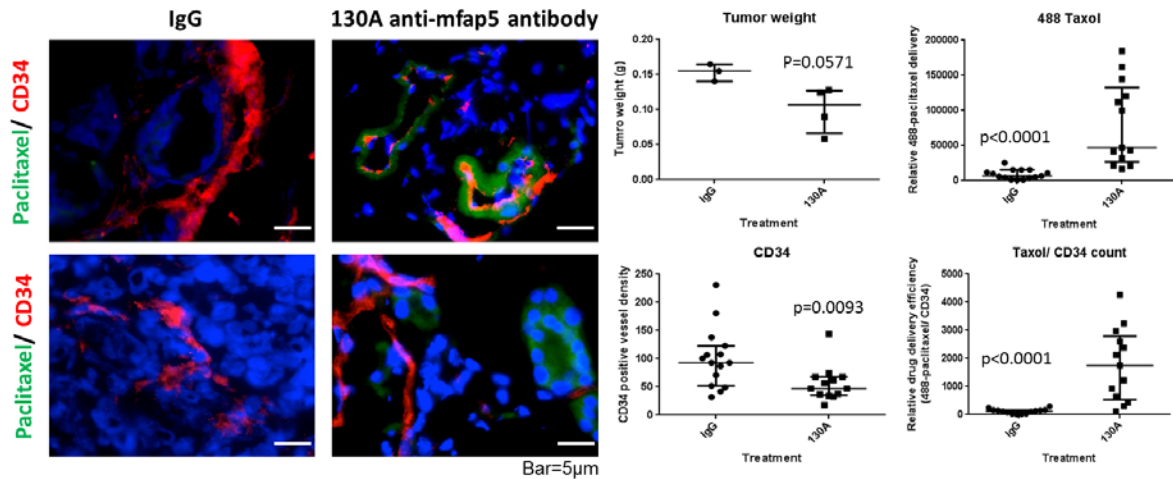


**Fig. 117: Clone 130A anti-mfap5 antibody facilitated systematic administered paclitaxel delivery to ovarian tumors.** Fluorescent microscopy and immunolocalization of CD34 (red) showed significant increase of Oregon Green 488-conjugated paclitaxel (green) was delivered to tumors although intratumoral microvessel density was decreased in mice treated with 130A anti-mfap5 antibody compared to control mice treated with IgG. For scatter plots, upper and lower bars indicate the interquartile range of the records, and the middle line indicates the median.

#### E. Toxicity test showed no observable adverse effects due to administration of anti-MFAP5 antibodies

In addition, toxicity analysis was performed on mice treated with anti-MFAP5 antibodies clone 64A, 117B, 130A or PBS (N=3/group). Complete blood count (CBC) and chemistry panel to measure the levels of (1) albumin, (2) alkaline phosphatase (ALP), (3) alanine aminotransferase (ALT), (4) aspartate aminotransferase (AST), (5) blood urea nitrogen (BUN), (6) creatinine, (7) globulin and (8) total proteins in serum samples collected were performed. The eight parameters were selected to evaluate any liver or kidney damage due to the antibody treatments and no significant toxic effects were observed (Figs. 118 and 119) when compared

to the PBS control. In addition, H&E stained organ and tissue sections were evaluated by a veterinary pathologist and no significant tissue damage was observed (Fig. 120).

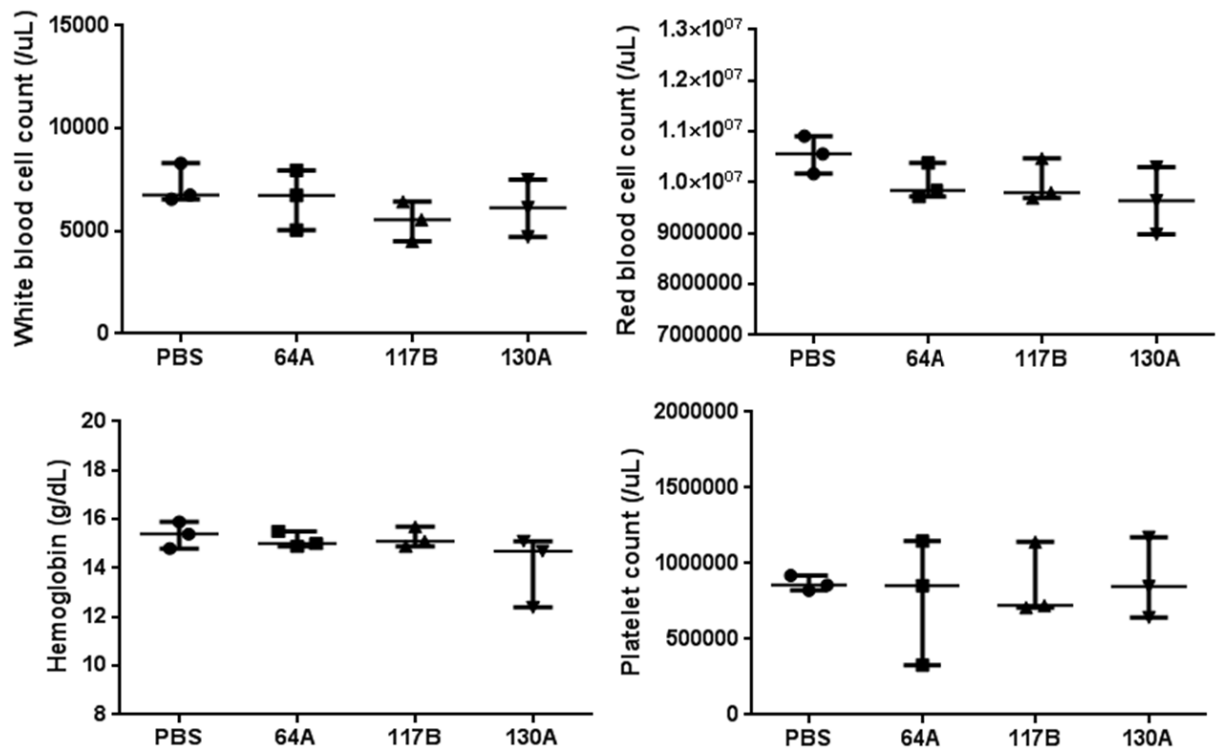


**Fig. 118: Toxicity test on anti-MFAP5 antibodies by complete blood count.** Complete blood count among clone 64A, 117b or 130A anti-MFAP antibody treated groups compared to PBS treated control group revealed no observable adverse effects due to administration of anti-MFAP5 antibodies. For scatter plots, upper and lower bars indicate the interquartile range of the records, and the middle line indicates the median.

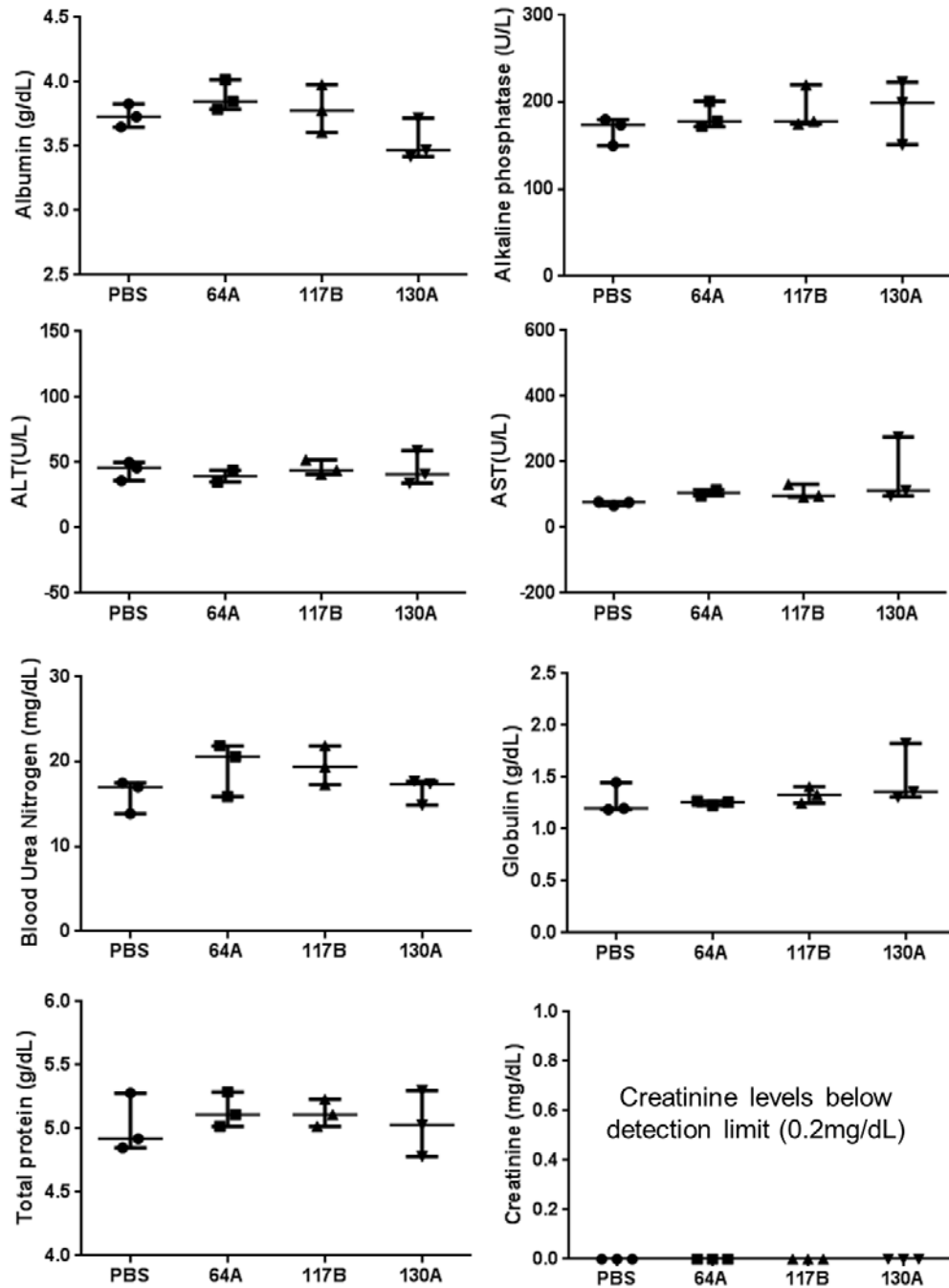


**Fig. 119: Toxicity test on anti-MFAP5 antibodies by chemistry tests.** Chemistry tests on serum collected from clone 64A, 117B or 130A anti-MFAP5 antibody treated group compared to PBS treated control group revealed no significant toxic effect by the antibody treatment to the animal's kidneys and livers. For scatter plots, upper and lower bars indicate the interquartile range of the records, and the middle line indicates the median.



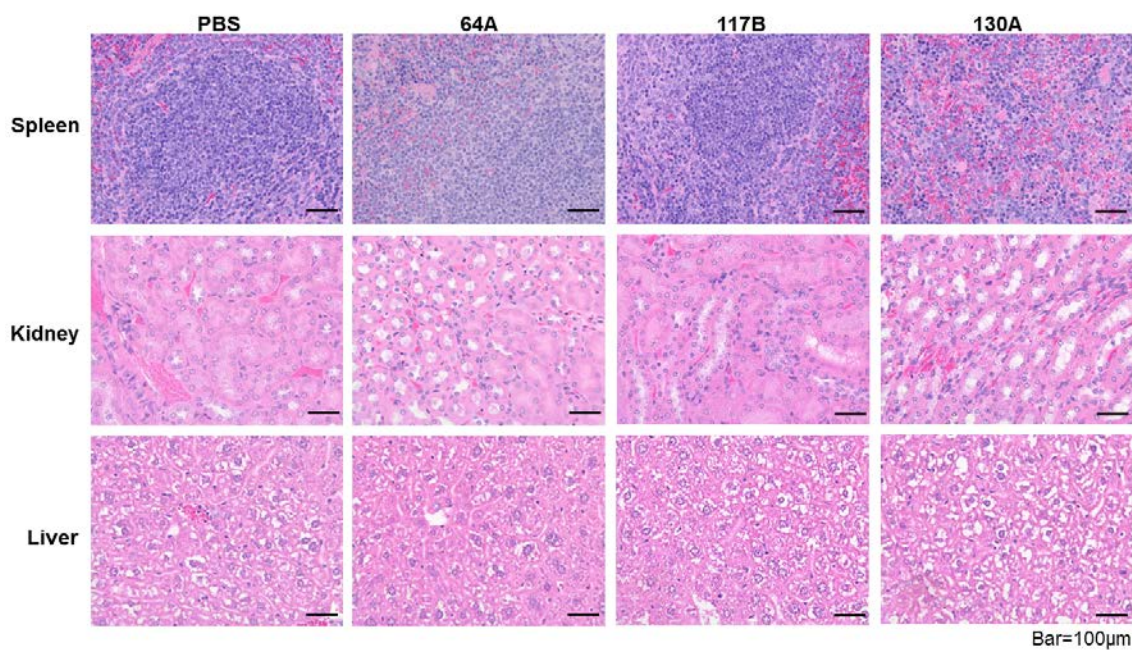


**Fig. 120: Histological examination to evaluate tissue damages due to anti-MFAP5 antibodies treatment.** H&E-stained images from the spleen, kidney and liver tissue samples from mice treated with clone 64A, 117B or 130A anti-MFAP5 antibody compared to PBS treated control group for 2 weeks. No significant toxic effects were observed. Representative images were selected from three individual replicates.

## Discussions



In the tumor microenvironment, the dynamic and reciprocal interactions among cells, the extracellular matrix, and soluble molecules dictate tumor progression.<sup>147</sup> As one of the key cell types that modulate cancer progression in the tumor microenvironment, CAFs have higher proliferation rates than normal fibroblasts and often have enhanced production of collagen, hyaluronate and epithelial growth factors.<sup>148,149</sup> Researchers have demonstrated that CAFs that secrete chemokines at elevated levels promote the initiation and development of ovarian cancer.<sup>50</sup> Furthermore, the complex stromal microenvironment has made therapeutic elimination of cancer impossible for decades.<sup>2</sup>

In the present study, we identified a stromal gene signature for HGSOC using microdissected tumor samples and found that CAF-derived MFAP5 is a prognostic marker of poor ovarian cancer patient survival. MFAP5 is involved in elastic microfibril assembly and modulates endothelial cell behavior.<sup>72,150</sup> Focusing on the epithelial component of HGSOC, our group previously identified MFAP5 as a survival-associated gene in HGSOC. We observed MFAP5 amplification and overexpression in a small percentage of advanced HGSOC cases.<sup>75</sup> In addition, we found that ovarian cancer-derived MFAP5 promoted tumor cell survival and stimulated endothelial cell motility and survival via the  $\alpha_v\beta_3$  integrin receptor. However, to our surprise, transcriptome profiling of the microdissected stromal component of HGSOCs revealed that CAFs had much higher expression of MFAP5 mRNA than did the normal ovarian stroma and epithelial components of ovarian tissue. In addition, immunolocalization of MFAP5 using a newly available polyclonal antibody confirmed that ovarian cancer stroma indeed has markedly higher levels of MFAP5 expression than did the epithelial component, which we did not observe in our previous study. The discrepancy is likely due to the fact that stromal MFAP5 may be cross-linked with other proteins in the stroma more tightly during the formalin fixation process and requires higher antigen retrieval temperatures to re-expose the epitope recognized by the antibodies that have higher affinity to MFAP5. To strengthen the significance of CAFs as source of MFAP5 in the tumor microenvironment, western blot analyses on samples from

immortalized CAFs, primary CAFs, as well as HGSOC cell lines were also performed. While some HGSOC cell lines express a detectable amount of MFAP5, our data confirmed that CAFs are the major sources of MFAP5 in the ovarian tumor microenvironment. In addition, in cases which tumor cells have low levels of MFAP5 expression but high levels of stromal MFAP5 expression, stromal MFAP5 secreted from CAFs may exert a paracrine effect on ovarian cancer cells and contribute to ovarian tumor progression. Our correlation studies showed that epithelial and stromal MFAP5 expressions in tumor tissue were significantly associated with each other. Therefore, it is not a surprise to find out that high levels of stromal MFAP5 expression, similar to the epithelial MFAP5 expression as reported in the previous study, were also significantly associated with poor patient survival. The significant association between stromal and epithelial MFAP5 expression suggests that MFAP5 is regulated by certain tumor microenvironmental cues in the same manner. However, the molecular mechanism by which stromal MFAP5 is expressed at high levels remains to be elucidated.

Our *in vitro* data demonstrated a significant increase in cell motility and invasion potential but not cell proliferation after treatment with recombinant MFAP5 protein in both ovarian cancer cells and microvascular endothelial cells. To evaluate the role of CAF-derived MFAP5 on ovarian cancer cell migration and invasion potentials *in vivo*, we developed a new model that allows the interaction between MFAP5-secreting CAFs and cancer cells in the intraperitoneal microenvironment. In this model, a Matrigel plug embedded with MFAP5-secreting CAFs recapitulates a substratum through which ovarian cancer cells invade MFAP5-expressing CAFs in the tumor. The results of our study using this model demonstrated that Matrigel plugs with MFAP5 represent a better soil for cancer cells to invade. Similarly, an *in vivo* angiogenesis assay was performed and enhanced formation of endothelial cell network was observed in recombinant MFAP5 containing matrigel plugs implanted subcutaneously into mice. Effects of MFAP5 on cancer metastasis was further evaluated by injecting MFAP5-specific siRNA-encapsulated nanoparticles into an orthotopic model in which ovarian cancer

cells were directly injected into the ovary. The significantly decreased in the number of metastatic nodules, the organs involved and intratumoral microvessel density in MFAP5 siRNA-treated mice compared with the control, suggesting the therapeutic potential of targeting stromal MFAP5 as a new treatment modality, which may inhibit disease progression and improve survival.

Since the N-terminal of MFAP5 contains an RGD motif which binds to  $\alpha_v\beta_3$  integrin receptor and integrin-mediated FAK signaling promotes cell motility has been well documented,<sup>151-153</sup> we therefore tested whether MFAP5 promoted ovarian cancer cell and endothelial cell motility via FAK phosphorylation. Interestingly, instead of the best-characterized FAK phosphorylation event at Tyr<sup>397</sup>,<sup>154</sup> we observed significant increase of FAK phosphorylation at Tyr<sup>861</sup>. Phosphorylation of FAK at Tyr<sup>861</sup> has been reported to regulate migration and metastatic potential of prostate and breast cancer cells.<sup>155,156</sup> It is also crucial for RAS transformation of fibroblasts as well as migration and survival of vascular endothelial cells.<sup>134,157</sup> Although it is commonly believed that phosphorylation of FAK at Tyr<sup>397</sup>, which creates a motif that is recognized by various SH2-domain containing proteins such as Src, is a prerequisite for FAK phosphorylation at additional tyrosine sites, recent evidence suggested that FAK Tyr<sup>861</sup> phosphorylation can be Src and Tyr<sup>397</sup> phosphorylation independent.<sup>157-160</sup> In a study on colon cancer cell line KM12C, phosphorylation of FAK at Tyr<sup>407</sup>, Tyr<sup>566</sup>, Tyr<sup>567</sup> and Tyr<sup>861</sup>, which previously attributed to Src kinase activity, was shown to be mediated by a functional Src Homology 2 (SH2) domain instead of by the Src kinase.<sup>159</sup> In addition, recent studies on RAS-transformed cells indicate that phosphorylation of FAK at Tyr<sup>861</sup> promotes its association with CRK-associated substrate (CAS, also known as p130cas) and recruitment of a CRK-DOCK 180-ELMO complex (DOCK 180: Deducator of cytokinesis of 180kDa; ELMO: Engulfment and cell motility protein) that activates RAC1, subsequently activating JUN N-terminal kinase (JNK) that promotes MMP expression and cell invasion.<sup>157</sup> We therefore hypothesize that the binding of MFAP5 to  $\alpha_v\beta_3$  integrin might modulate downstream signaling

for cell migration and invasion via regulation of the interactions between FAK and other SH2-domain-containing proteins. Indeed, a detailed bioinformatics examination of SH2 domains reveals 120 SH2 domains in 110 proteins encoded by the human genome, suggesting that other potential SH2 domain-containing proteins instead of Src may be involved in the MFAP5-mediated FAK Tyr<sup>861</sup> phosphorylation.<sup>161</sup> Further investigation on which particular SH2 domain containing-protein is involved in the MFAP5-integrin signaling transduction may identify a new mechanism of how FAK phosphorylation promotes cell migration and invasion.

On the other hand, our findings demonstrated that Ca<sup>2+</sup> mobilization is essential for MFAP5's effects on ovarian cancer and endothelial cell motility and invasion potential. Ca<sup>2+</sup> plays a multifunctional role in regulating cell migration, including cytoskeleton redistribution and focal adhesion relocation.<sup>90,162-164</sup> Five major classes of membrane Ca<sup>2+</sup>-permeable channels are known to be differentially expressed in various cell types although there are other channels recently proposed.<sup>82,165</sup> First, voltage-gated calcium channels which are activated by depolarizing membrane potentials and expressed mostly in excitable cells. Second, the ligand-gated channels mainly involved in fast chemical synaptic transmission in the nervous system. Third, transient receptor potential channels that mediate Ca<sup>2+</sup> entry through a large variety of gating mechanisms, including stretching of plasma membrane. Fourth, store-operated calcium (SOC) channels that required calcium release-activated calcium channel protein 1 (ORAI1) and stromal interaction molecule 1 (STIM1) to function. SOC channels are the major Ca<sup>2+</sup> entry pathways in non-excitable cells and are widely distributed in various cell types. Finally, arachidonate-regulated Ca<sup>2+</sup> (ARC) entry channels which are activated in response to receptor-mediated derivation of arachidonic acid.

The present study demonstrated that treatment with an L-type voltage-gated Ca<sup>2+</sup> channel blocker attenuated MFAP5-induced calcium influx but did not abolish this effect, whereas treatment with an L-type voltage-gated Ca<sup>2+</sup> channel opener successfully stimulated calcium entry in ALST cells, suggesting that MFAP5 triggers exogenous Ca<sup>2+</sup> entry into cells

via the L-type voltage-gated channel, although other channels may be involved. Treatment with an IP<sub>3</sub> receptor inhibitor but not a ryanodine receptor blocker attenuated MFAP5-induced calcium mobilization, suggesting that MFAP5 induces calcium release via the IP<sub>3</sub> receptor instead of the ryanodine receptor. This was supported by our finding that MFAP5 activates PLC- $\gamma$ 1 phosphorylation, which may lead to hydrolysis of intracellular phosphatidylinositol-4, 5-bisphosphate to IP<sub>3</sub> and DAG. IP<sub>3</sub> binds to its receptor, causing Ca<sup>2+</sup> release from the endoplasmic reticulum.<sup>77,82</sup>

Calcium is a prominent regulator of cell migration, exerting multiple effects on the contractility of the actin cytoskeleton.<sup>115,166</sup> Our findings of abrogation of MFAP5-induced actin rearrangement, stress fiber condensation, and traction force induction by BAPTA/AM, suggested that calcium-dependent actin reorganization, together with increased traction force modulate MFAP5's motility and invasion promoting effects. Of note, for a typical human cell, the cytoplasmic free Ca<sup>2+</sup> concentration ([Ca<sup>2+</sup>]<sub>c</sub>) is maintained at about 100nM, a very low level relative to the extracellular fluid ([Ca<sup>+</sup>]<sub>Ec</sub>≈1.2mM).<sup>167</sup> Upon stimuli activation, [Ca<sup>2+</sup>]<sub>c</sub> will rise to 500-1000nM due to the entry of external Ca<sup>2+</sup> or the release of Ca<sup>2+</sup> from internal stores.<sup>77</sup> On the other hand, the off mechanisms composed of pumps and exchangers that will remove Ca<sup>2+</sup> from the cytoplasm and restore the resting state. In the case of calcium accumulation and mitochondrial Ca<sup>2+</sup> uptake, apoptosis may take place.<sup>167-169</sup> However, treatment of ovarian cancer cells and microvascular endothelial cells with recombinant MFAP5, which triggered transient and partial discharge of Ca<sup>2+</sup> from the ER store at nanomolar level, should not induce a stress condition that initiates apoptosis.

Regarding MFAP5 induced ovarian cancer cell motility and invasion potential, we have identified TNNC1 as the effector molecule of such cancer cell phenotypes. TNNC1 contains a calcium-binding subunit and facilitates the interaction between actin and myosin in muscle cells and the formation of stress fibers.<sup>170</sup> Indeed, troponin is expressed not only in striated muscle cells but also fibroblasts.<sup>93</sup> In nonmuscle cells, TNNC1 may not serve as a structural protein but

rather as a regulatory protein for cellular locomotion, cytoplasmic streaming, and cytokinesis.<sup>170</sup> In the present study, we have demonstrated TNNC1 upregulation in MFAP5 treated epithelial ovarian cancer cells and that siRNA silencing of TNNC1 abolishes MFAP5's stimulatory effect on cancer cell motility. This is the first study to demonstrate that increased TNNC1 expression modulates epithelial cancer cell motility and invasion potential via cytoskeleton reorganization. In addition, immunolocalization of TNNC1 on HGSOC samples demonstrated the positive correlation between cancer cell TNNC1 expression and stromal MFAP5 expression and the association between increased TNNC1 expression and poor survival. These data confirmed that TNNC1 is the effector protein for stromal MFAP5, which can promote cell motility and invasion potential via tumor-stromal crosstalk and subsequently affect clinical outcome. Of note, we observed that TNNC1 silencing did not affect ovarian cancer cell proliferation, suggesting that the effect of MFAP5 on tumor growth we observed *in vivo* is indirect, most likely via its effect on other cell types in the microenvironment. This can be explained by the data obtained from aim 2 of this study, which we demonstrated a pro-angiogenic role of MFAP5 that enhanced intratumoral microvessel density and subsequently lead to increased tumor growth *in vivo*.

Our mechanistic studies demonstrated that both stimulatory effects of MFAP5 on ovarian cancer cells and microvascular endothelial cells share similar calcium dependent signaling pathways via upregulation of p-FAK, p-PLC $\gamma$ 1, p-PKC $\theta$ , p-ERK1/2, p-CREB, c-Jun and p-c-Jun. Yet, TNNC1 expression was not detected in both control and MFAP5 treated hMEC-1 and TIME cells by qRT-PCR, suggesting that the stimulatory effect of MFAP5 does not share the same effector molecule in ovarian cancer cells and microvascular endothelial cells. Further microarray analysis on endothelial cells invaded into Matrigel plug identified upregulation of Lipoma-Preferred Partner (LPP), an actin cytoskeleton protein that is associated with calcium signaling, in microvessels infiltrating the Matrigel reconstituted with MFAP5 compared to those with PBS and in hMEC-1 and TIME cells treated with exogenous

MFAP5. Immunofluorescent microscopy indicated MFAP5 induced increased LPP expression particularly in the focal adhesions at the cell periphery, which strongly support its role in cell motility. Furthermore, transfecting LPP siRNAs into MFAP5 treated endothelial cell lines hMEC-1 and TIME abrogated the effect of MFAP5 on cell motility, suggesting that LPP is a key downstream effector molecule for MFAP5 in controlling endothelial cell motility. Further analyses on MFAP5 treated endothelial cells showed that MFAP5 mediated the formation of focal adhesion complexes through regulation of LPP.

Another novelty of this project is that anti-MFAP5 monoclonal antibodies were developed and tested as a therapeutic agent for ovarian cancer treatment. By western blot analyses, we identified two clones of mouse monoclonal antibodies (64A and 117B) against human MFAP5 only and one clone of antibody (130A) against both human and mouse MFAP5. While all three antibody clones demonstrated inhibitory effects on cancer cell and endothelial cells motility *in vitro*, clone 130A was chosen for further *in vivo* evaluation using orthotopic mouse model due to its ability to recognize and target MFAP5 protein derived from mouse stromal fibroblasts. Our *in vivo* data demonstrated suppressed ovarian tumor progression and tumor angiogenesis by targeting stromal mfap5 using clone 130A with no observable toxicity, suggesting that targeting stromal MFAP5 may improve therapeutic benefit from anti-angiogenic strategies in ovarian cancer patients. This is exciting as MFAP5 is only detected at medium level in 1/81 normal tissue samples compared to the extensively studied VEGF, which has high or medium expression level in 75/80 analyzed normal tissue samples (The Human Protein Atlas). Therefore, reduce drug-associated side effects could be expected.

As described in the introduction, tumor vasculatures were found to be both functionally and structurally abnormal with decreased perfusion and increased leakiness.<sup>64</sup> Vessel normalization is therefore being proposed by a number of research groups as a mean to restore vessel functions and integrity, which could subsequently facilitates delivery of cancer therapeutic agents.<sup>60,171</sup> Vessel normalization could be achieved by using anti-angiogenic



agents that inhibit uncontrolled angiogenesis and favor the formation of structurally normal vessels. Since our experimental results suggested that MFAP5 induced motility and traction force generation of endothelial cells, we further analyzed the effects of MFAP5 treatment on the integrity of endothelial cell monolayer cultures. Endothelial cell monolayers treated with MFAP5 protein demonstrated increased leakiness and therefore suggested that targeting MFAP5 in the tumor microenvironment could potentially facilitate vessel normalization. We therefore evaluated the effect of targeting stromal MFAP5 by monoclonal antibodies on tumor vessel leakiness and chemotherapeutic agent delivery. Experimental results demonstrated that tumor tissues harvested from MFAP5-targeting antibody clone 130A treated mice had reduced vessel leakiness and increased bioavailability of paclitaxel, suggested that targeting stromal MFAP5 by monoclonal antibodies could facilitate tumor inhibition via vessel normalization.

Since increased paclitaxel bioavailability in tumor tissues was observed in MFAP5-targeted animals, therefore we would like to propose to study whether targeting stromal MFAP5 by the monoclonal antibodies could potentiate the effect of therapeutic efficacy of chemotherapy for ovarian cancer treatment in the future. Combination of MFAP5-targeting therapy and chemotherapy could be beneficial with two possible mechanisms: 1) By normalizing the vascular permeability: Anti-MFAP5 antibodies could allow better tumor perfusion, and thus chemo drugs will be delivered to the tumors more efficiently.<sup>172</sup> 2) The dividing, genetically stable endothelial cells of newly forming tumor vessels are believed to be sensitive to chemo drugs and the anti-angiogenic anti-MFAP5 antibodies may enhance this sensitivity.<sup>171,173,174</sup> It is believed that targeting the whole tumor organ and not just its epithelial component would benefit patients and increase survival.<sup>45,175</sup> Indeed, our data showing increased paclitaxel delivery (Fig. 118) after treating ovarian tumors with anti-MFAP5 monoclonal antibody clone 130A in line with proposed mechanism 1 provided a strong background for us to explore the synergistic effect of combining paclitaxel with anti-MFAP5 monoclonal antibody for ovarian cancer treatment.

Drug combinations is widely used in cancer therapies and there is an increasing awareness that the use of synergistic drug combinations in treating cancer allows lower doses of each constituent drug and consequently reduces toxicity and minimize or delay the induction of drug resistance.<sup>176,177</sup> However, when two or more therapeutic agents are given in combination, it is possible that instead of a superadditive (synergistic) effect, subadditivity or simply additivity may be observed. To address this, the Chou-Talalay combination index theorem offers quantitative definition for additive effect (combination index = 1), synergism (combination index < 1) and antagonism (combination index > 1) in drug combinations.<sup>178</sup> In addition, based on the concept of dose equivalence, the isobolographic analysis provides the mathematical basis for assessing synergy and an optimization strategy for determining the dose combination.<sup>177,179</sup> A straight line connecting the dose pairs on the x- and y-axes when there is no interaction between the drugs is called an isobole. The isobole allows the assessment of superadditive and subadditive interactions when actual combination doses are tested. If a dose pair that plots as a point below the isobole, this means that the effect was attained with doses less than those on the line, a situation that denotes superadditivity or synergism. In contrast, if a dose pair plots as a point above the isobole line, this indicates a greater combination doses are required to generate the specified effect and therefore depicting a subadditive (antagonism) situation. For dose pairs that experimentally lie on the isobole, the term additive applied showing a situation that there is no interaction between the two drugs. However, the prerequisite for all drug combination studies is the dose-effect curves for each single drug. For our *in vivo* studies using monoclonal antibodies to target stromal MFAP5, a single dosage design was used. While it served well in demonstrating the therapeutic potential of targeting MFAP5 in ovarian cancer, in order to explore the synergistic effect of combining paclitaxel with anti-MFAP5 monoclonal antibody for ovarian cancer treatment, dose-effect curves for both anti-MFAP5 monoclonal antibody and paclitaxel using a range of different treatment dosages will need to be generated. In addition, further evaluating the therapeutic efficacy of MFAP5-targeting monoclonal antibodies with a range of dosages using animal

models will allow us to determine the optimal antibody dosage and vessel normalization window for the MFAP5-targeting anti-angiogenic therapy for ovarian cancer. It is believed that optimizing drug dosage and finding the suitable vessel normalization window is crucial because sustained or aggressive antiangiogenic regimens may prune away tumor vessels, resulting in a vasculature that is both resistant to further treatment and inadequate for the delivery of drugs and oxygen.<sup>35,60,65</sup> Under hypoxic conditions, radiation therapy and a subset of chemotherapy drugs that require oxygen to kill tumor cells are ineffective. In addition, immune cells, which might help fight cancer cells, are hampered by high acidity and low oxygen.<sup>35,64</sup>

Moreover, the dosing schedule may play an important role in both vessel normalization and the effects of drug combination. In the present study, tumor shrinkage and reduced intratumoral microvessel density were observed by treating tumor bearing mice with anti-MFAP5 antibody twice weekly for 6 weeks. However, it would be favorable if similar therapeutic effects could be observed using a less frequent drug administration schedule as antibodies are generally considered as stable drugs and patients may save their trips to the hospital for injections. For drug combination, we might pre-treat tumor bearing mice with anti-MFAP5 monoclonal antibody for one to two weeks before the combination drug treatment with paclitaxel. The rationale behind is to normalize the pathologic tumor vasculature, i.e. reduces intratumoral vessel leakiness, decreases interstitial fluid pressure and increases intratumoral blood flow, for optimal uptake of paclitaxel when it is injected into the mice. On the other hand, the duration of the combination treatment may also be optimized. The concept of metronomic chemotherapy suggested that administering comparatively low doses of chemotherapy drugs on a frequent or continuous schedule, with no drug-free breaks might enhance the anti-angiogenic efficacy of conventional cytotoxic chemotherapeutics and facilitate tumor response toward combination therapy of anti-angiogenic drugs and chemotherapy. It stands as a different philosophy from the maximum tolerated dose (MTD) method typically used but it might serve to reduce acute toxicity and the development of drug resistance.<sup>180</sup> After the optimal dosage and

dosing schedule of MFAP5-targeting monoclonal antibodies have been identified, to move forward, preclinical toxicity test will be performed on rhesus monkey because MFAP5 protein in rhesus monkey and human shared a 98.24% homology. Rhesus monkeys will be dosed at two dose levels with optimized dosing schedule. In life testing such as hematology, clinical chemistry, urinalysis, coagulation, bone marrow evaluation will be performed. In addition, anatomic pathology after necropsy will be performed to determine any adverse effects made to the major organs due to the antibody treatment. If satisfactory result could be obtained from the preclinical toxicity test, human clinical trial would be the next step to evaluate the therapeutic potential of using anti-MFAP5 monoclonal antibody to target stromal MFAP5 for ovarian cancer treatment. Humanized anti-MFAP5 monoclonal antibodies may be developed to decrease the murine components and reduce the risk of developing human anti-mouse antibody (HAMA), which may cause a mild allergic reaction such as a rash to a more extreme and life-threatening situation like renal failure.<sup>181,182</sup> These humanized or chimarized monoclonal antibodies have a longer half-life in the patients' blood stream, and enables better interactions with human effector cells in the patients' bodies.<sup>181</sup>

To increase the potency of the monoclonal antibody, the humanized anti-MFAP5 antibody could be modified as immunoconjugate therapy by conjugating with drugs, toxins and radioisotopes to carry enhanced killing capacity directly to the tumors.<sup>181,183</sup> Further, we could determine the sequence of the light and heavy chains (LV and HV) of the variable region of the anti-MFAP5 antibody developed, and use the single chain variable fragment (scFv) technology to develop scFv multimers as described,<sup>184</sup> which will potentially increase the affinity of the antibody to MFAP5.

In conclusion, we found that CAF-derived MFAP5 modulated motility and invasion potential in ovarian cancer cells and microvascular endothelial cells and promoted tumor angiogenesis via the calcium signaling pathway (Fig. 121). Targeting stromal MFAP5 with anti-MFAP5 monoclonal antibody markedly decreased tumor growth and metastasis *in vivo*,

suggesting that it is a new treatment modality for ovarian cancer. The possible modifications of the anti-MFAP5 monoclonal antibody predict a more specific and less toxic therapy for ovarian cancer treatment in the future. More importantly, this study demonstrated the possibility of targeting/ reprogramming CAF-derived tumor-promoting factors to inhibit tumor progression, thereby presenting an alternative approach to the treatment of cancer.<sup>185</sup> We believe that targeting CAFs in the tumor microenvironment may synergize with other cancer cells-targeting treatment regimens to increase treatment efficacy.

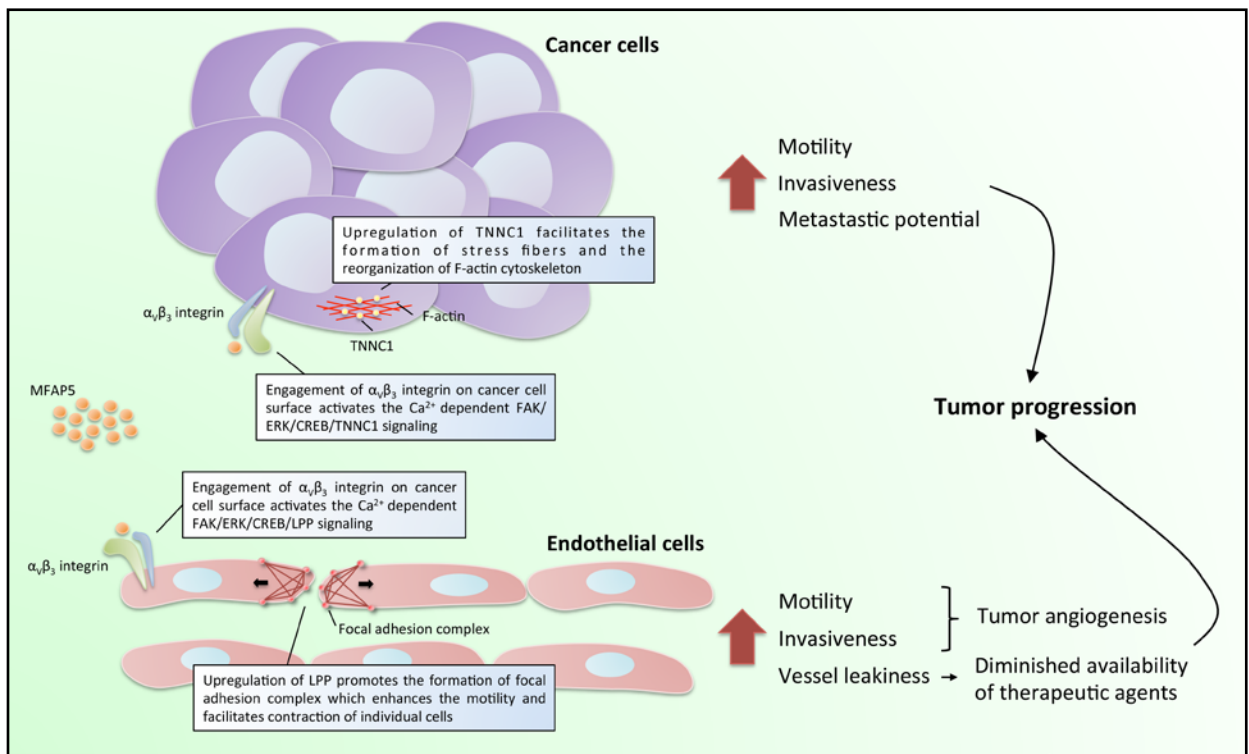


**Fig. 121: The overall mechanism by which stromal MFAP5 stimulates ovarian cancer progression, metastasis and tumor angiogenesis.** Stromal MFAP5, which is significantly upregulated in ovarian CAFs, activates the calcium-dependent signaling pathways in cancer and endothelial cells via the engagement of the  $\alpha_v\beta_3$  integrin receptor. This figure summarized the roles of MFAP5 in tumor progression through enhancing cancer cell metastasis and promoting tumor angiogenesis.

## Bibliography

1. Siegel, R.L., Miller, K.D. & Jemal, A. Cancer statistics, 2015. *CA: a cancer journal for clinicians* **65**, 5-29 (2015).
2. Tlsty, T.D. & Coussens, L.M. Tumor stroma and regulation of cancer development. *Annual review of pathology* **1**, 119-150 (2006).
3. Berchuck, A., Iversen, E.S., Lancaster, J.M., Pittman, J., Luo, J., Lee, P., Murphy, S., Dressman, H.K., Febbo, P.G., West, M., Nevins, J.R. & Marks, J.R. Patterns of gene expression that characterize long-term survival in advanced stage serous ovarian cancers. *Clinical cancer research : an official journal of the American Association for Cancer Research* **11**, 3686-3696 (2005).
4. Lancaster, J.M., Dressman, H.K., Whitaker, R.S., Havrilesky, L., Gray, J., Marks, J.R., Nevins, J.R. & Berchuck, A. Gene expression patterns that characterize advanced stage serous ovarian cancers. *J Soc Gynecol Investig* **11**, 51-59 (2004).
5. Cancer Genome Atlas Research, N. Integrated genomic analyses of ovarian carcinoma. *Nature* **474**, 609-615 (2011).
6. Blood, C.H. & Zetter, B.R. Tumor interactions with the vasculature: angiogenesis and tumor metastasis. *Biochimica et biophysica acta* **1032**, 89-118 (1990).
7. D'Amore, P.A. Capillary growth: a two-cell system. *Seminars in cancer biology* **3**, 49-56 (1992).
8. Folkman, J. The role of angiogenesis in tumor growth. *Seminars in cancer biology* **3**, 65-71 (1992).
9. Folkman, J. & Ingber, D. Inhibition of angiogenesis. *Seminars in cancer biology* **3**, 89-96 (1992).
10. Canoglu, A., Gogus, C., Beduk, Y., Orhan, D., Tulunay, O. & Baltaci, S. Microvessel density as a prognostic marker in bladder carcinoma: correlation with tumor grade, stage and prognosis. *International urology and nephrology* **36**, 401-405 (2004).
11. Chavez-Macgregor, M., Aviles-Salas, A., Green, D., Fuentes-Albuero, A., Gomez-Ruiz, C. & Aguayo, A. Angiogenesis in the bone marrow of patients with breast cancer.



- Clinical cancer research : an official journal of the American Association for Cancer Research* **11**, 5396-5400 (2005).
12. Korkolopoulou, P., Thymara, I., Kavantzias, N., Vassilakopoulos, T.P., Angelopoulou, M.K., Kokoris, S.I., Dimitriadou, E.M., Siakantaris, M.P., Anargyrou, K., Panayiotidis, P., Tsenga, A., Androulaki, A., Doussis-Anagnostopoulou, I.A., Patsouris, E. & Pangalis, G.A. Angiogenesis in Hodgkin's lymphoma: a morphometric approach in 286 patients with prognostic implications. *Leukemia* **19**, 894-900 (2005).
  13. Ribas, C., Colleoni, G.W., Silva, M.R., Carreagoza, M.J. & Bordin, J.O. Prognostic significance of vascular endothelial growth factor immunoexpression in the context of adverse standard prognostic factors in multiple myeloma. *European journal of haematology* **73**, 311-317 (2004).
  14. Carmeliet, P. & Jain, R.K. Molecular mechanisms and clinical applications of angiogenesis. *Nature* **473**, 298-307 (2011).
  15. Fan, F., Schimming, A., Jaeger, D. & Podar, K. Targeting the tumor microenvironment: focus on angiogenesis. *Journal of oncology* **2012**, 281261 (2012).
  16. Kut, C., Mac Gabhann, F. & Popel, A.S. Where is VEGF in the body? A meta-analysis of VEGF distribution in cancer. *British journal of cancer* **97**, 978-985 (2007).
  17. Jayson, G.C., Kohn, E.C., Kitchener, H.C. & Ledermann, J.A. Ovarian cancer. *Lancet* (2014).
  18. Smith, L.H., Morris, C.R., Yasmeen, S., Parikh-Patel, A., Cress, R.D. & Romano, P.S. Ovarian cancer: can we make the clinical diagnosis earlier? *Cancer* **104**, 1398-1407 (2005).
  19. Goff, B.A., Mandel, L., Muntz, H.G. & Melancon, C.H. Ovarian carcinoma diagnosis. *Cancer* **89**, 2068-2075 (2000).
  20. Goff, B.A., Mandel, L.S., Melancon, C.H. & Muntz, H.G. Frequency of symptoms of ovarian cancer in women presenting to primary care clinics. *Jama* **291**, 2705-2712 (2004).

21. Prat, J. & Oncology, F.C.o.G. Staging classification for cancer of the ovary, fallopian tube, and peritoneum. *International journal of gynaecology and obstetrics: the official organ of the International Federation of Gynaecology and Obstetrics* **124**, 1-5 (2014).
22. Siegel, R., Ma, J., Zou, Z. & Jemal, A. Cancer statistics, 2014. *CA: a cancer journal for clinicians* **64**, 9-29 (2014).
23. Vaughan, S., Coward, J.I., Bast, R.C., Jr., Berchuck, A., Berek, J.S., Brenton, J.D., Coukos, G., Crum, C.C., Drapkin, R., Etemadmoghadam, D., Friedlander, M., Gabra, H., Kaye, S.B., Lord, C.J., Lengyel, E., Levine, D.A., McNeish, I.A., Menon, U., Mills, G.B., Nephew, K.P., Oza, A.M., Sood, A.K., Stronach, E.A., Walczak, H., Bowtell, D.D. & Balkwill, F.R. Rethinking ovarian cancer: recommendations for improving outcomes. *Nature reviews. Cancer* **11**, 719-725 (2011).
24. Ahmed, A.A., Etemadmoghadam, D., Temple, J., Lynch, A.G., Riad, M., Sharma, R., Stewart, C., Fereday, S., Caldas, C., Defazio, A., Bowtell, D. & Brenton, J.D. Driver mutations in TP53 are ubiquitous in high grade serous carcinoma of the ovary. *The Journal of pathology* **221**, 49-56 (2010).
25. Kobel, M., Reuss, A., Bois, A., Kommoss, S., Kommoss, F., Gao, D., Kalloger, S.E., Huntsman, D.G. & Gilks, C.B. The biological and clinical value of p53 expression in pelvic high-grade serous carcinomas. *The Journal of pathology* **222**, 191-198 (2010).
26. Wiegand, K.C., Shah, S.P., Al-Agha, O.M., Zhao, Y., Tse, K., Zeng, T., Senz, J., McConechy, M.K., Anglesio, M.S., Kalloger, S.E., Yang, W., Heravi-Moussavi, A., Giuliany, R., Chow, C., Fee, J., Zayed, A., Prentice, L., Melnyk, N., Turashvili, G., Delaney, A.D., Madore, J., Yip, S., McPherson, A.W., Ha, G., Bell, L., Fereday, S., Tam, A., Galletta, L., Tonin, P.N., Provencher, D., Miller, D., Jones, S.J., Moore, R.A., Morin, G.B., Oloumi, A., Boyd, N., Aparicio, S.A., Shih, M., Mes-Masson, A.M., Bowtell, D.D., Hirst, M., Gilks, B., Marra, M.A. & Huntsman, D.G. ARID1A mutations in endometriosis-associated ovarian carcinomas. *The New England journal of medicine* **363**, 1532-1543 (2010).

27. King, M.C., Marks, J.H., Mandell, J.B. & New York Breast Cancer Study, G. Breast and ovarian cancer risks due to inherited mutations in BRCA1 and BRCA2. *Science* **302**, 643-646 (2003).
28. Trimbos, J.B., Parmar, M., Vergote, I., Guthrie, D., Bolis, G., Colombo, N., Vermorken, J.B., Torri, V., Mangioni, C., Pecorelli, S., Lissoni, A., Swart, A.M., International Collaborative Ovarian, N., European Organisation for, R. & Treatment of Cancer Collaborators-Adjuvant ChemoTherapy un Ovarian, N. International Collaborative Ovarian Neoplasm trial 1 and Adjuvant ChemoTherapy In Ovarian Neoplasm trial: two parallel randomized phase III trials of adjuvant chemotherapy in patients with early-stage ovarian carcinoma. *Journal of the National Cancer Institute* **95**, 105-112 (2003).
29. Trimbos, J.B., Vergote, I., Bolis, G., Vermorken, J.B., Mangioni, C., Madronal, C., Franchi, M., Tateo, S., Zanetta, G., Scarfone, G., Giurgea, L., Timmers, P., Coens, C., Pecorelli, S., Research, E.-A.c.E.O.f. & Treatment of Cancer-Adjuvant ChemoTherapy in Ovarian, N. Impact of adjuvant chemotherapy and surgical staging in early-stage ovarian carcinoma: European Organisation for Research and Treatment of Cancer-Adjuvant ChemoTherapy in Ovarian Neoplasm trial. *Journal of the National Cancer Institute* **95**, 113-125 (2003).
30. Ozols, R.F., Bundy, B.N., Greer, B.E., Fowler, J.M., Clarke-Pearson, D., Burger, R.A., Mannel, R.S., DeGeest, K., Hartenbach, E.M., Baergen, R. & Gynecologic Oncology, G. Phase III trial of carboplatin and paclitaxel compared with cisplatin and paclitaxel in patients with optimally resected stage III ovarian cancer: a Gynecologic Oncology Group study. *Journal of clinical oncology : official journal of the American Society of Clinical Oncology* **21**, 3194-3200 (2003).
31. Vasey, P.A., Jayson, G.C., Gordon, A., Gabra, H., Coleman, R., Atkinson, R., Parkin, D., Paul, J., Hay, A., Kaye, S.B. & Scottish Gynaecological Cancer Trials, G. Phase III randomized trial of docetaxel-carboplatin versus paclitaxel-carboplatin as first-line

- chemotherapy for ovarian carcinoma. *Journal of the National Cancer Institute* **96**, 1682-1691 (2004).
32. Bookman, M.A., Brady, M.F., McGuire, W.P., Harper, P.G., Alberts, D.S., Friedlander, M., Colombo, N., Fowler, J.M., Argenta, P.A., De Geest, K., Mutch, D.G., Burger, R.A., Swart, A.M., Trimble, E.L., Accario-Winslow, C. & Roth, L.M. Evaluation of new platinum-based treatment regimens in advanced-stage ovarian cancer: a Phase III Trial of the Gynecologic Cancer Intergroup. *Journal of clinical oncology : official journal of the American Society of Clinical Oncology* **27**, 1419-1425 (2009).
33. Fong, P.C., Boss, D.S., Yap, T.A., Tutt, A., Wu, P., Mergui-Roelvink, M., Mortimer, P., Swaisland, H., Lau, A., O'Connor, M.J., Ashworth, A., Carmichael, J., Kaye, S.B., Schellens, J.H. & de Bono, J.S. Inhibition of poly(ADP-ribose) polymerase in tumors from BRCA mutation carriers. *The New England journal of medicine* **361**, 123-134 (2009).
34. Kaye, S.B., Lubinski, J., Matulonis, U., Ang, J.E., Gourley, C., Karlan, B.Y., Amnon, A., Bell-McGuinn, K.M., Chen, L.M., Friedlander, M., Safra, T., Vergote, I., Wickens, M., Lowe, E.S., Carmichael, J. & Kaufman, B. Phase II, open-label, randomized, multicenter study comparing the efficacy and safety of olaparib, a poly (ADP-ribose) polymerase inhibitor, and pegylated liposomal doxorubicin in patients with BRCA1 or BRCA2 mutations and recurrent ovarian cancer. *Journal of clinical oncology : official journal of the American Society of Clinical Oncology* **30**, 372-379 (2012).
35. Goel, S., Wong, A.H. & Jain, R.K. Vascular normalization as a therapeutic strategy for malignant and nonmalignant disease. *Cold Spring Harbor perspectives in medicine* **2**, a006486 (2012).
36. Burger, R.A., Brady, M.F., Bookman, M.A., Fleming, G.F., Monk, B.J., Huang, H., Mannel, R.S., Homesley, H.D., Fowler, J., Greer, B.E., Boente, M., Birrer, M.J., Liang, S.X. & Gynecologic Oncology, G. Incorporation of bevacizumab in the primary

- treatment of ovarian cancer. *The New England journal of medicine* **365**, 2473-2483 (2011).
37. Perren, T.J., Swart, A.M., Pfisterer, J., Ledermann, J.A., Pujade-Lauraine, E., Kristensen, G., Carey, M.S., Beale, P., Cervantes, A., Kurzeder, C., du Bois, A., Sehouli, J., Kimmig, R., Stahle, A., Collinson, F., Essapen, S., Gourley, C., Lortholary, A., Selle, F., Mirza, M.R., Leminen, A., Plante, M., Stark, D., Qian, W., Parmar, M.K., Oza, A.M. & Investigators, I. A phase 3 trial of bevacizumab in ovarian cancer. *The New England journal of medicine* **365**, 2484-2496 (2011).
  38. Swartz, M.A., Iida, N., Roberts, E.W., Sangaletti, S., Wong, M.H., Yull, F.E., Coussens, L.M. & DeClerck, Y.A. Tumor microenvironment complexity: emerging roles in cancer therapy. *Cancer research* **72**, 2473-2480 (2012).
  39. Hanahan, D. & Weinberg, R.A. Hallmarks of cancer: the next generation. *Cell* **144**, 646-674 (2011).
  40. Koehne, C.H. & Dubois, R.N. COX-2 inhibition and colorectal cancer. *Seminars in oncology* **31**, 12-21 (2004).
  41. Patel, L.R., Camacho, D.F., Shiozawa, Y., Pienta, K.J. & Taichman, R.S. Mechanisms of cancer cell metastasis to the bone: a multistep process. *Future oncology* **7**, 1285-1297 (2011).
  42. Dvorak, H.F., Weaver, V.M., Tlsty, T.D. & Bergers, G. Tumor microenvironment and progression. *Journal of surgical oncology* **103**, 468-474 (2011).
  43. DuFort, C.C., Paszek, M.J. & Weaver, V.M. Balancing forces: architectural control of mechanotransduction. *Nature reviews. Molecular cell biology* **12**, 308-319 (2011).
  44. Orimo, A. & Weinberg, R.A. Stromal fibroblasts in cancer: a novel tumor-promoting cell type. *Cell cycle* **5**, 1597-1601 (2006).
  45. Labiche, A., Heutte, N., Herlin, P., Chasle, J., Gauduchon, P. & Elie, N. Stromal compartment as a survival prognostic factor in advanced ovarian carcinoma.

- International journal of gynecological cancer : official journal of the International Gynecological Cancer Society* **20**, 28-33 (2010).
46. Madar, S., Goldstein, I. & Rotter, V. 'Cancer associated fibroblasts'--more than meets the eye. *Trends in molecular medicine* **19**, 447-453 (2013).
  47. Mueller, M.M. & Fusenig, N.E. Friends or foes - bipolar effects of the tumour stroma in cancer. *Nature reviews. Cancer* **4**, 839-849 (2004).
  48. Serini, G. & Gabbiani, G. Mechanisms of myofibroblast activity and phenotypic modulation. *Experimental cell research* **250**, 273-283 (1999).
  49. Huang, M., Li, Y., Zhang, H. & Nan, F. Breast cancer stromal fibroblasts promote the generation of CD44+CD24- cells through SDF-1/CXCR4 interaction. *Journal of experimental & clinical cancer research : CR* **29**, 80 (2010).
  50. Schauer, I.G., Sood, A.K., Mok, S. & Liu, J. Cancer-associated fibroblasts and their putative role in potentiating the initiation and development of epithelial ovarian cancer. *Neoplasia* **13**, 393-405 (2011).
  51. Liu, Y., Hu, T., Shen, J., Li, S.F., Lin, J.W., Zheng, X.H., Gao, Q.H. & Zhou, H.M. Separation, cultivation and biological characteristics of oral carcinoma-associated fibroblasts. *Oral diseases* **12**, 375-380 (2006).
  52. Sugimoto, H., Mundel, T.M., Kieran, M.W. & Kalluri, R. Identification of fibroblast heterogeneity in the tumor microenvironment. *Cancer biology & therapy* **5**, 1640-1646 (2006).
  53. Zhang, Y., Tang, H., Cai, J., Zhang, T., Guo, J., Feng, D. & Wang, Z. Ovarian cancer-associated fibroblasts contribute to epithelial ovarian carcinoma metastasis by promoting angiogenesis, lymphangiogenesis and tumor cell invasion. *Cancer letters* **303**, 47-55 (2011).
  54. Mueller, L., Goumas, F.A., Affeldt, M., Sandtner, S., Gehling, U.M., Brillhoff, S., Walter, J., Karnatz, N., Lamszus, K., Rogiers, X. & Broering, D.C. Stromal fibroblasts in colorectal liver metastases originate from resident fibroblasts and generate an

- inflammatory microenvironment. *The American journal of pathology* **171**, 1608-1618 (2007).
55. Rege, T.A. & Hagood, J.S. Thy-1 as a regulator of cell-cell and cell-matrix interactions in axon regeneration, apoptosis, adhesion, migration, cancer, and fibrosis. *FASEB journal : official publication of the Federation of American Societies for Experimental Biology* **20**, 1045-1054 (2006).
  56. Koumas, L., Smith, T.J., Feldon, S., Blumberg, N. & Phipps, R.P. Thy-1 expression in human fibroblast subsets defines myofibroblastic or lipofibroblastic phenotypes. *The American journal of pathology* **163**, 1291-1300 (2003).
  57. Fukino, K., Shen, L., Matsumoto, S., Morrison, C.D., Mutter, G.L. & Eng, C. Combined total genome loss of heterozygosity scan of breast cancer stroma and epithelium reveals multiplicity of stromal targets. *Cancer research* **64**, 7231-7236 (2004).
  58. Micke, P. & Ostman, A. Tumour-stroma interaction: cancer-associated fibroblasts as novel targets in anti-cancer therapy? *Lung cancer* **45 Suppl 2**, S163-175 (2004).
  59. Joyce, J.A. Therapeutic targeting of the tumor microenvironment. *Cancer cell* **7**, 513-520 (2005).
  60. Jain, R.K. Normalization of tumor vasculature: an emerging concept in antiangiogenic therapy. *Science* **307**, 58-62 (2005).
  61. Papetti, M. & Herman, I.M. Mechanisms of normal and tumor-derived angiogenesis. *American journal of physiology. Cell physiology* **282**, C947-970 (2002).
  62. Hanahan, D. & Folkman, J. Patterns and emerging mechanisms of the angiogenic switch during tumorigenesis. *Cell* **86**, 353-364 (1996).
  63. Bergers, G. & Benjamin, L.E. Tumorigenesis and the angiogenic switch. *Nature reviews. Cancer* **3**, 401-410 (2003).
  64. Jain, R.K. Taming vessels to treat cancer. *Scientific American* **298**, 56-63 (2008).



65. Goel, S., Duda, D.G., Xu, L., Munn, L.L., Boucher, Y., Fukumura, D. & Jain, R.K. Normalization of the vasculature for treatment of cancer and other diseases. *Physiological reviews* **91**, 1071-1121 (2011).
66. Teicher, B.A. A systems approach to cancer therapy. (Antioncogenics + standard cytotoxics-->mechanism(s) of interaction). *Cancer metastasis reviews* **15**, 247-272 (1996).
67. Hamzah, J., Jugold, M., Kiessling, F., Rigby, P., Manzur, M., Marti, H.H., Rabie, T., Kaden, S., Grone, H.J., Hammerling, G.J., Arnold, B. & Ganss, R. Vascular normalization in Rgs5-deficient tumours promotes immune destruction. *Nature* **453**, 410-414 (2008).
68. Jain, R.K. Normalizing tumor vasculature with anti-angiogenic therapy: a new paradigm for combination therapy. *Nature medicine* **7**, 987-989 (2001).
69. Hurwitz, H., Fehrenbacher, L., Novotny, W., Cartwright, T., Hainsworth, J., Heim, W., Berlin, J., Baron, A., Griffing, S., Holmgren, E., Ferrara, N., Fyfe, G., Rogers, B., Ross, R. & Kabbinavar, F. Bevacizumab plus irinotecan, fluorouracil, and leucovorin for metastatic colorectal cancer. *The New England journal of medicine* **350**, 2335-2342 (2004).
70. Saltz, L.B., Clarke, S., Diaz-Rubio, E., Scheithauer, W., Figer, A., Wong, R., Koski, S., Lichinitser, M., Yang, T.S., Rivera, F., Couture, F., Sirzen, F. & Cassidy, J. Bevacizumab in combination with oxaliplatin-based chemotherapy as first-line therapy in metastatic colorectal cancer: a randomized phase III study. *Journal of clinical oncology : official journal of the American Society of Clinical Oncology* **26**, 2013-2019 (2008).
71. Tebbutt, N.C., Wilson, K., GebSKI, V.J., Cummins, M.M., Zannino, D., van Hazel, G.A., Robinson, B., Broad, A., Ganju, V., Ackland, S.P., Forgeson, G., Cunningham, D., Saunders, M.P., Stockler, M.R., Chua, Y., Zalberg, J.R., Simes, R.J. & Price, T.J. Capecitabine, bevacizumab, and mitomycin in first-line treatment of metastatic

- colorectal cancer: results of the Australasian Gastrointestinal Trials Group Randomized Phase III MAX Study. *Journal of clinical oncology : official journal of the American Society of Clinical Oncology* **28**, 3191-3198 (2010).
72. Gibson, M.A., Finnis, M.L., Kumaratilake, J.S. & Cleary, E.G. Microfibril-associated glycoprotein-2 (MAGP-2) is specifically associated with fibrillin-containing microfibrils but exhibits more restricted patterns of tissue localization and developmental expression than its structural relative MAGP-1. *The journal of histochemistry and cytochemistry : official journal of the Histochemistry Society* **46**, 871-886 (1998).
73. Hanssen, E., Hew, F.H., Moore, E. & Gibson, M.A. MAGP-2 has multiple binding regions on fibrillins and has covalent periodic association with fibrillin-containing microfibrils. *The Journal of biological chemistry* **279**, 29185-29194 (2004).
74. Gibson, M.A., Leavesley, D.I. & Ashman, L.K. Microfibril-associated glycoprotein-2 specifically interacts with a range of bovine and human cell types via alphaVbeta3 integrin. *The Journal of biological chemistry* **274**, 13060-13065 (1999).
75. Mok, S.C., Bonome, T., Vathipadiekal, V., Bell, A., Johnson, M.E., Wong, K.K., Park, D.C., Hao, K., Yip, D.K., Donniger, H., Ozbun, L., Samimi, G., Brady, J., Randonovich, M., Pise-Masison, C.A., Barrett, J.C., Wong, W.H., Welch, W.R., Berkowitz, R.S. & Birrer, M.J. A gene signature predictive for outcome in advanced ovarian cancer identifies a survival factor: microfibril-associated glycoprotein 2. *Cancer Cell* **16**, 521-532 (2009).
76. Clapham, D.E. Calcium signaling. *Cell* **131**, 1047-1058 (2007).
77. Berridge, M.J., Lipp, P. & Bootman, M.D. The versatility and universality of calcium signalling. *Nature reviews. Molecular cell biology* **1**, 11-21 (2000).
78. Kiselyov, K., Xu, X., Mozhayeva, G., Kuo, T., Pessah, I., Mignery, G., Zhu, X., Birnbaumer, L. & Muallem, S. Functional interaction between InsP3 receptors and store-operated Htrp3 channels. *Nature* **396**, 478-482 (1998).

79. Boulay, G., Brown, D.M., Qin, N., Jiang, M., Dietrich, A., Zhu, M.X., Chen, Z., Birnbaumer, M., Mikoshiba, K. & Birnbaumer, L. Modulation of Ca(2+) entry by polypeptides of the inositol 1,4, 5-trisphosphate receptor (IP3R) that bind transient receptor potential (TRP): evidence for roles of TRP and IP3R in store depletion-activated Ca(2+) entry. *Proceedings of the National Academy of Sciences of the United States of America* **96**, 14955-14960 (1999).
80. Berridge, M.J. Capacitative calcium entry. *The Biochemical journal* **312 ( Pt 1)**, 1-11 (1995).
81. Taylor, C.W. & Thorn, P. Calcium signalling: IP3 rises again...and again. *Current biology : CB* **11**, R352-355 (2001).
82. Prevarskaya, N., Skryma, R. & Shuba, Y. Calcium in tumour metastasis: new roles for known actors. *Nat Rev Cancer* **11**, 609-618 (2011).
83. Pozzan, T., Rizzuto, R., Volpe, P. & Meldolesi, J. Molecular and cellular physiology of intracellular calcium stores. *Physiological reviews* **74**, 595-636 (1994).
84. Blaustein, M.P. & Lederer, W.J. Sodium/calcium exchange: its physiological implications. *Physiological reviews* **79**, 763-854 (1999).
85. Budd, S.L. & Nicholls, D.G. A reevaluation of the role of mitochondria in neuronal Ca<sup>2+</sup> homeostasis. *Journal of neurochemistry* **66**, 403-411 (1996).
86. Jouaville, L.S., Ichas, F., Holmuhamedov, E.L., Camacho, P. & Lechleiter, J.D. Synchronization of calcium waves by mitochondrial substrates in *Xenopus laevis* oocytes. *Nature* **377**, 438-441 (1995).
87. Collins, T.J., Lipp, P., Berridge, M.J., Li, W. & Bootman, M.D. Inositol 1,4,5-trisphosphate-induced Ca<sup>2+</sup> release is inhibited by mitochondrial depolarization. *The Biochemical journal* **347**, 593-600 (2000).
88. Duchen, M.R. Contributions of mitochondria to animal physiology: from homeostatic sensor to calcium signalling and cell death. *The Journal of physiology* **516 ( Pt 1)**, 1-17 (1999).

89. Shimizu, S., Narita, M. & Tsujimoto, Y. Bcl-2 family proteins regulate the release of apoptogenic cytochrome c by the mitochondrial channel VDAC. *Nature* **399**, 483-487 (1999).
90. Brundage, R.A., Fogarty, K.E., Tuft, R.A. & Fay, F.S. Calcium gradients underlying polarization and chemotaxis of eosinophils. *Science* **254**, 703-706 (1991).
91. Hahn, K., DeBiasio, R. & Taylor, D.L. Patterns of elevated free calcium and calmodulin activation in living cells. *Nature* **359**, 736-738 (1992).
92. Robertson, I.M., Sun, Y.B., Li, M.X. & Sykes, B.D. A structural and functional perspective into the mechanism of Ca<sup>2+</sup>-sensitizers that target the cardiac troponin complex. *Journal of molecular and cellular cardiology* **49**, 1031-1041 (2010).
93. Gahlmann, R., Wade, R., Gunning, P. & Kedes, L. Differential expression of slow and fast skeletal muscle troponin C. Slow skeletal muscle troponin C is expressed in human fibroblasts. *J Mol Biol* **201**, 379-391 (1988).
94. Mudd, J.O. & Kass, D.A. Tackling heart failure in the twenty-first century. *Nature* **451**, 919-928 (2008).
95. Berezowsky, C. & Bag, J. Slow troponin C is present in both muscle and nonmuscle cells. *Biochemistry and cell biology = Biochimie et biologie cellulaire* **70**, 691-697 (1992).
96. Petit, M.M., Fradelizi, J., Golsteyn, R.M., Ayoubi, T.A., Menichi, B., Louvard, D., Van de Ven, W.J. & Friederich, E. LPP, an actin cytoskeleton protein related to zyxin, harbors a nuclear export signal and transcriptional activation capacity. *Molecular biology of the cell* **11**, 117-129 (2000).
97. Petit, M.M., Mols, R., Schoenmakers, E.F., Mandahl, N. & Van de Ven, W.J. LPP, the preferred fusion partner gene of HMGIC in lipomas, is a novel member of the LIM protein gene family. *Genomics* **36**, 118-129 (1996).

98. Price, G.J., Jones, P., Davison, M.D., Patel, B., Bendori, R., Geiger, B. & Critchley, D.R. Primary sequence and domain structure of chicken vinculin. *The Biochemical journal* **259**, 453-461 (1989).
99. Theriot, J.A. & Mitchison, T.J. The three faces of profilin. *Cell* **75**, 835-838 (1993).
100. Reinhard, M., Halbrugge, M., Scheer, U., Wiegand, C., Jockusch, B.M. & Walter, U. The 46/50 kDa phosphoprotein VASP purified from human platelets is a novel protein associated with actin filaments and focal contacts. *The EMBO journal* **11**, 2063-2070 (1992).
101. Reinhard, M., Giehl, K., Abel, K., Haffner, C., Jarchau, T., Hoppe, V., Jockusch, B.M. & Walter, U. The proline-rich focal adhesion and microfilament protein VASP is a ligand for profilins. *The EMBO journal* **14**, 1583-1589 (1995).
102. Wang, Y. & Gilmore, T.D. Zyxin and paxillin proteins: focal adhesion plaque LIM domain proteins go nuclear. *Biochimica et biophysica acta* **1593**, 115-120 (2003).
103. Beckerle, M.C. Zyxin: zinc fingers at sites of cell adhesion. *BioEssays : news and reviews in molecular, cellular and developmental biology* **19**, 949-957 (1997).
104. Dawid, I.B., Breen, J.J. & Toyama, R. LIM domains: multiple roles as adapters and functional modifiers in protein interactions. *Trends in genetics : TIG* **14**, 156-162 (1998).
105. Hansen, M.D. & Beckerle, M.C. alpha-Actinin links LPP, but not zyxin, to cadherin-based junctions. *Biochemical and biophysical research communications* **371**, 144-148 (2008).
106. Passaniti, A., Taylor, R.M., Pili, R., Guo, Y., Long, P.V., Haney, J.A., Pauly, R.R., Grant, D.S. & Martin, G.R. A simple, quantitative method for assessing angiogenesis and antiangiogenic agents using reconstituted basement membrane, heparin, and fibroblast growth factor. *Laboratory investigation; a journal of technical methods and pathology* **67**, 519-528 (1992).

107. Ben-Ami, R., Lewis, R.E., Leventakos, K. & Kontoyiannis, D.P. Aspergillus fumigatus inhibits angiogenesis through the production of gliotoxin and other secondary metabolites. *Blood* **114**, 5393-5399 (2009).
108. Dembo, M. & Wang, Y.L. Stresses at the cell-to-substrate interface during locomotion of fibroblasts. *Biophysical journal* **76**, 2307-2316 (1999).
109. Lo, C.M., Glogauer, M., Rossi, M. & Ferrier, J. Cell-substrate separation: effect of applied force and temperature. *European biophysics journal : EBJ* **27**, 9-17 (1998).
110. Lo, C.M., Buxton, D.B., Chua, G.C., Dembo, M., Adelstein, R.S. & Wang, Y.L. Nonmuscle myosin IIb is involved in the guidance of fibroblast migration. *Molecular biology of the cell* **15**, 982-989 (2004).
111. Yeung, T.L., Leung, C.S., Wong, K.K., Samimi, G., Thompson, M.S., Liu, J., Zaid, T.M., Ghosh, S., Birrer, M.J. & Mok, S.C. TGF-beta modulates ovarian cancer invasion by upregulating CAF-derived versican in the tumor microenvironment. *Cancer research* **73**, 5016-5028 (2013).
112. Lu, C., Han, H.D., Mangala, L.S., Ali-Fehmi, R., Newton, C.S., Ozbun, L., Armaiz-Pena, G.N., Hu, W., Stone, R.L., Munkarah, A., Ravoori, M.K., Shahzad, M.M., Lee, J.W., Mora, E., Langley, R.R., Carroll, A.R., Matsuo, K., Spannuth, W.A., Schmandt, R., Jennings, N.B., Goodman, B.W., Jaffe, R.B., Nick, A.M., Kim, H.S., Guven, E.O., Chen, Y.H., Li, L.Y., Hsu, M.C., Coleman, R.L., Calin, G.A., Denkbass, E.B., Lim, J.Y., Lee, J.S., Kundra, V., Birrer, M.J., Hung, M.C., Lopez-Berestein, G. & Sood, A.K. Regulation of tumor angiogenesis by EZH2. *Cancer cell* **18**, 185-197 (2010).
113. Masiero, M., Simoes, F.C., Han, H.D., Snell, C., Peterkin, T., Bridges, E., Mangala, L.S., Wu, S.Y., Pradeep, S., Li, D., Han, C., Dalton, H., Lopez-Berestein, G., Tuynman, J.B., Mortensen, N., Li, J.L., Patient, R., Sood, A.K., Banham, A.H., Harris, A.L. & Buffa, F.M. A core human primary tumor angiogenesis signature identifies the endothelial orphan receptor ELTD1 as a key regulator of angiogenesis. *Cancer cell* **24**, 229-241 (2013).

(2013).

114. Doyle, A., Marganski, W. & Lee, J. Calcium transients induce spatially coordinated increases in traction force during the movement of fish keratocytes. *Journal of cell science* **117**, 2203-2214 (2004).
115. Wei, C., Wang, X., Chen, M., Ouyang, K., Zheng, M. & Cheng, H. Flickering calcium microdomains signal turning of migrating cells. *Canadian journal of physiology and pharmacology* **88**, 105-110 (2010).
116. Nakamura, I., Lipfert, L., Rodan, G.A. & Le, T.D. Convergence of alpha(v)beta(3) integrin- and macrophage colony stimulating factor-mediated signals on phospholipase Cgamma in perfusion osteoclasts. *The Journal of cell biology* **152**, 361-373 (2001).
117. Masson-Gadais, B., Houle, F., Laferriere, J. & Huot, J. Integrin alphavbeta3, requirement for VEGFR2-mediated activation of SAPK2/p38 and for Hsp90-dependent phosphorylation of focal adhesion kinase in endothelial cells activated by VEGF. *Cell stress & chaperones* **8**, 37-52 (2003).
118. Altman, A. & Villalba, M. Protein kinase C-theta (PKCtheta): it's all about location, location, location. *Immunological reviews* **192**, 53-63 (2003).
119. Manicassamy, S., Sadim, M., Ye, R.D. & Sun, Z. Differential roles of PKC-theta in the regulation of intracellular calcium concentration in primary T cells. *J Mol Biol* **355**, 347-359 (2006).
120. Pfeifhofer, C., Kofler, K., Gruber, T., Tabrizi, N.G., Lutz, C., Maly, K., Leitges, M. & Baier, G. Protein kinase C theta affects Ca<sup>2+</sup> mobilization and NFAT cell activation in primary mouse T cells. *The Journal of experimental medicine* **197**, 1525-1535 (2003).
121. Park, E.M. & Cho, S. Enhanced ERK dependent CREB activation reduces apoptosis in staurosporine-treated human neuroblastoma SK-N-BE(2)C cells. *Neuroscience letters* **402**, 190-194 (2006).
122. Stylianopoulos, T. & Jain, R.K. Combining two strategies to improve perfusion and drug delivery in solid tumors. *Proc Natl Acad Sci U S A* **110**, 18632-18637 (2013).



123. Ingber, D.E. & Folkman, J. Mechanochemical switching between growth and differentiation during fibroblast growth factor-stimulated angiogenesis in vitro: role of extracellular matrix. *The Journal of cell biology* **109**, 317-330 (1989).
124. Matsumoto, T., Yung, Y.C., Fischbach, C., Kong, H.J., Nakaoka, R. & Mooney, D.J. Mechanical strain regulates endothelial cell patterning in vitro. *Tissue Eng* **13**, 207-217 (2007).
125. Ghosh, K., Thodeti, C.K., Dudley, A.C., Mammoto, A., Klagsbrun, M. & Ingber, D.E. Tumor-derived endothelial cells exhibit aberrant Rho-mediated mechanosensing and abnormal angiogenesis in vitro. *Proceedings of the National Academy of Sciences of the United States of America* **105**, 11305-11310 (2008).
126. Amado-Azevedo, J., Valent, E.T. & Van Nieuw Amerongen, G.P. Regulation of the endothelial barrier function: a filum granum of cellular forces, Rho-GTASE SIGNALING AND MICROENVIRONMENT. *Cell and tissue research* (2014).
127. Califano, J.P. & Reinhart-King, C.A. Exogenous and endogenous force regulation of endothelial cell behavior. *Journal of biomechanics* **43**, 79-86 (2010).
128. Krishnan, R., Klumpers, D.D., Park, C.Y., Rajendran, K., Trepap, X., van Bezu, J., van Hinsbergh, V.W., Carman, C.V., Brain, J.D., Fredberg, J.J., Butler, J.P. & van Nieuw Amerongen, G.P. Substrate stiffening promotes endothelial monolayer disruption through enhanced physical forces. *American journal of physiology. Cell physiology* **300**, C146-154 (2011).
129. Munevar, S., Wang, Y. & Dembo, M. Traction force microscopy of migrating normal and H-ras transformed 3T3 fibroblasts. *Biophysical journal* **80**, 1744-1757 (2001).
130. Kerr, J.S., Mousa, S.A. & Slee, A.M. Alpha(v)beta(3) integrin in angiogenesis and restenosis. *Drug news & perspectives* **14**, 143-150 (2001).
131. Eddy, R.J., Pierini, L.M., Matsumura, F. & Maxfield, F.R. Ca<sup>2+</sup>-dependent myosin II activation is required for uropod retraction during neutrophil migration. *Journal of cell science* **113 ( Pt 7)**, 1287-1298 (2000).

132. Lawson, M.A. & Maxfield, F.R. Ca(2+)- and calcineurin-dependent recycling of an integrin to the front of migrating neutrophils. *Nature* **377**, 75-79 (1995).
133. Coppelino, M.G., Woodside, M.J., Demaurex, N., Grinstein, S., St-Arnaud, R. & Dedhar, S. Calreticulin is essential for integrin-mediated calcium signalling and cell adhesion. *Nature* **386**, 843-847 (1997).
134. Abu-Ghazaleh, R., Kabir, J., Jia, H., Lobo, M. & Zachary, I. Src mediates stimulation by vascular endothelial growth factor of the phosphorylation of focal adhesion kinase at tyrosine 861, and migration and anti-apoptosis in endothelial cells. *The Biochemical journal* **360**, 255-264 (2001).
135. Kim, I., Moon, S.O., Park, S.K., Chae, S.W. & Koh, G.Y. Angiotensin-1 reduces VEGF-stimulated leukocyte adhesion to endothelial cells by reducing ICAM-1, VCAM-1, and E-selectin expression. *Circulation research* **89**, 477-479 (2001).
136. Qi, J.H. & Claesson-Welsh, L. VEGF-induced activation of phosphoinositide 3-kinase is dependent on focal adhesion kinase. *Experimental cell research* **263**, 173-182 (2001).
137. Braren, R., Hu, H., Kim, Y.H., Beggs, H.E., Reichardt, L.F. & Wang, R. Endothelial FAK is essential for vascular network stability, cell survival, and lamellipodial formation. *The Journal of cell biology* **172**, 151-162 (2006).
138. Eliceiri, B.P., Puente, X.S., Hood, J.D., Stupack, D.G., Schlaepfer, D.D., Huang, X.Z., Sheppard, D. & Cheresch, D.A. Src-mediated coupling of focal adhesion kinase to integrin alpha(v)beta5 in vascular endothelial growth factor signaling. *The Journal of cell biology* **157**, 149-160 (2002).
139. Giannone, G., Ronde, P., Gaire, M., Beaudouin, J., Haiech, J., Ellenberg, J. & Takeda, K. Calcium rises locally trigger focal adhesion disassembly and enhance residency of focal adhesion kinase at focal adhesions. *The Journal of biological chemistry* **279**, 28715-28723 (2004).
140. Zhang, X., Chattopadhyay, A., Ji, Q.S., Owen, J.D., Ruest, P.J., Carpenter, G. & Hanks, S.K. Focal adhesion kinase promotes phospholipase C-gamma1 activity. *Proceedings*

- of the National Academy of Sciences of the United States of America **96**, 9021-9026 (1999).
141. Segal, R.A. Selectivity in neurotrophin signaling: theme and variations. *Annu Rev Neurosci* **26**, 299-330 (2003).
  142. Melowic, H.R., Stahelin, R.V., Blatner, N.R., Tian, W., Hayashi, K., Altman, A. & Cho, W. Mechanism of diacylglycerol-induced membrane targeting and activation of protein kinase C $\theta$ . *The Journal of biological chemistry* **282**, 21467-21476 (2007).
  143. Curtis, J. & Finkbeiner, S. Sending signals from the synapse to the nucleus: possible roles for CaMK, Ras/ERK, and SAPK pathways in the regulation of synaptic plasticity and neuronal growth. *Journal of neuroscience research* **58**, 88-95 (1999).
  144. Mavria, G., Vercoulen, Y., Yeo, M., Paterson, H., Karasarides, M., Marais, R., Bird, D. & Marshall, C.J. ERK-MAPK signaling opposes Rho-kinase to promote endothelial cell survival and sprouting during angiogenesis. *Cancer cell* **9**, 33-44 (2006).
  145. Van Itallie, C.M., Tietgens, A.J., Aponte, A., Fredriksson, K., Fanning, A.S., Gucek, M. & Anderson, J.M. Biotin ligase tagging identifies proteins proximal to E-cadherin, including lipoma preferred partner, a regulator of epithelial cell-cell and cell-substrate adhesion. *Journal of cell science* **127**, 885-895 (2014).
  146. Byrne, A.T., Ross, L., Holash, J., Nakanishi, M., Hu, L., Hofmann, J.I., Yancopoulos, G.D. & Jaffe, R.B. Vascular endothelial growth factor-trap decreases tumor burden, inhibits ascites, and causes dramatic vascular remodeling in an ovarian cancer model. *Clinical cancer research : an official journal of the American Association for Cancer Research* **9**, 5721-5728 (2003).
  147. Lawler, J. Introduction to the tumour microenvironment review series. *Journal of cellular and molecular medicine* **13**, 1403-1404 (2009).
  148. Bauer, E.A., Uitto, J., Walters, R.C. & Eisen, A.Z. Enhanced collagenase production by fibroblasts derived from human basal cell carcinomas. *Cancer research* **39**, 4594-4599 (1979).

149. Knudson, W., Biswas, C. & Toole, B.P. Interactions between human tumor cells and fibroblasts stimulate hyaluronate synthesis. *Proceedings of the National Academy of Sciences of the United States of America* **81**, 6767-6771 (1984).
150. Spivey, K.A. & Banyard, J. A prognostic gene signature in advanced ovarian cancer reveals a microfibril-associated protein (MAGP2) as a promoter of tumor cell survival and angiogenesis. *Cell adhesion & migration* **4**, 169-171 (2010).
151. Sieg, D.J., Hauck, C.R., Ilic, D., Klingbeil, C.K., Schaefer, E., Damsky, C.H. & Schlaepfer, D.D. FAK integrates growth-factor and integrin signals to promote cell migration. *Nature cell biology* **2**, 249-256 (2000).
152. McLean, G.W., Carragher, N.O., Avizienyte, E., Evans, J., Brunton, V.G. & Frame, M.C. The role of focal-adhesion kinase in cancer - a new therapeutic opportunity. *Nature reviews. Cancer* **5**, 505-515 (2005).
153. Mitra, S.K., Hanson, D.A. & Schlaepfer, D.D. Focal adhesion kinase: in command and control of cell motility. *Nature reviews. Molecular cell biology* **6**, 56-68 (2005).
154. Toutant, M., Costa, A., Studler, J.M., Kadare, G., Carnaud, M. & Girault, J.A. Alternative splicing controls the mechanisms of FAK autophosphorylation. *Molecular and cellular biology* **22**, 7731-7743 (2002).
155. Slack, J.K., Adams, R.B., Rovin, J.D., Bissonette, E.A., Stoker, C.E. & Parsons, J.T. Alterations in the focal adhesion kinase/Src signal transduction pathway correlate with increased migratory capacity of prostate carcinoma cells. *Oncogene* **20**, 1152-1163 (2001).
156. Vadlamudi, R.K., Sahin, A.A., Adam, L., Wang, R.A. & Kumar, R. Heregulin and HER2 signaling selectively activates c-Src phosphorylation at tyrosine 215. *FEBS letters* **543**, 76-80 (2003).
157. Lim, Y., Han, I., Jeon, J., Park, H., Bahk, Y.Y. & Oh, E.S. Phosphorylation of focal adhesion kinase at tyrosine 861 is crucial for Ras transformation of fibroblasts. *The Journal of biological chemistry* **279**, 29060-29065 (2004).

158. Lunn, J.A., Jacamo, R. & Rozengurt, E. Preferential phosphorylation of focal adhesion kinase tyrosine 861 is critical for mediating an anti-apoptotic response to hyperosmotic stress. *The Journal of biological chemistry* **282**, 10370-10379 (2007).
159. Brunton, V.G., Avizienyte, E., Fincham, V.J., Serrels, B., Metcalf, C.A., 3rd, Sawyer, T.K. & Frame, M.C. Identification of Src-specific phosphorylation site on focal adhesion kinase: dissection of the role of Src SH2 and catalytic functions and their consequences for tumor cell behavior. *Cancer research* **65**, 1335-1342 (2005).
160. Zheng, Y., Gierut, J., Wang, Z., Miao, J., Asara, J.M. & Tyner, A.L. Protein tyrosine kinase 6 protects cells from anoikis by directly phosphorylating focal adhesion kinase and activating AKT. *Oncogene* **32**, 4304-4312 (2013).
161. Liu, B.A., Jablonowski, K., Raina, M., Arce, M., Pawson, T. & Nash, P.D. The human and mouse complement of SH2 domain proteins-establishing the boundaries of phosphotyrosine signaling. *Molecular cell* **22**, 851-868 (2006).
162. Pettit, E.J. & Fay, F.S. Cytosolic free calcium and the cytoskeleton in the control of leukocyte chemotaxis. *Physiological reviews* **78**, 949-967 (1998).
163. Ridley, A.J., Schwartz, M.A., Burridge, K., Firtel, R.A., Ginsberg, M.H., Borisy, G., Parsons, J.T. & Horwitz, A.R. Cell migration: integrating signals from front to back. *Science* **302**, 1704-1709 (2003).
164. Van Haastert, P.J. & Devreotes, P.N. Chemotaxis: signalling the way forward. *Nature reviews. Molecular cell biology* **5**, 626-634 (2004).
165. Feng, M., Grice, D.M., Faddy, H.M., Nguyen, N., Leitch, S., Wang, Y., Muend, S., Kenny, P.A., Sukumar, S., Roberts-Thomson, S.J., Monteith, G.R. & Rao, R. Store-independent activation of Orai1 by SPCA2 in mammary tumors. *Cell* **143**, 84-98 (2010).
166. Furukawa, R., Maselli, A., Thomson, S.A., Lim, R.W., Stokes, J.V. & Fechheimer, M. Calcium regulation of actin crosslinking is important for function of the actin cytoskeleton in Dictyostelium. *Journal of cell science* **116**, 187-196 (2003).

167. Hajnoczky, G., Davies, E. & Madesh, M. Calcium signaling and apoptosis. *Biochemical and biophysical research communications* **304**, 445-454 (2003).
168. Rizzuto, R., Pinton, P., Ferrari, D., Chami, M., Szabadkai, G., Magalhaes, P.J., Di Virgilio, F. & Pozzan, T. Calcium and apoptosis: facts and hypotheses. *Oncogene* **22**, 8619-8627 (2003).
169. Pinton, P., Giorgi, C., Siviero, R., Zecchini, E. & Rizzuto, R. Calcium and apoptosis: ER-mitochondria Ca<sup>2+</sup> transfer in the control of apoptosis. *Oncogene* **27**, 6407-6418 (2008).
170. Tash, J.S. & Means, A.R. Regulation of protein phosphorylation and motility of sperm by cyclic adenosine monophosphate and calcium. *Biology of reproduction* **26**, 745-763 (1982).
171. Ma, J. & Waxman, D.J. Combination of antiangiogenesis with chemotherapy for more effective cancer treatment. *Molecular cancer therapeutics* **7**, 3670-3684 (2008).
172. Yagi, Y., Fushida, S., Harada, S., Tsukada, T., Kinoshita, J., Oyama, K., Fujita, H., Ninomiya, I., Fujimura, T., Kayahara, M., Kinuya, S., Yashiro, M., Hirakawa, K. & Ohta, T. Biodistribution of humanized anti-VEGF monoclonal antibody/bevacizumab on peritoneal metastatic models with subcutaneous xenograft of gastric cancer in mice. *Cancer chemotherapy and pharmacology* **66**, 745-753 (2010).
173. Belotti, D., Vergani, V., Drudis, T., Borsotti, P., Pitelli, M.R., Viale, G., Giavazzi, R. & Taraboletti, G. The microtubule-affecting drug paclitaxel has antiangiogenic activity. *Clinical cancer research : an official journal of the American Association for Cancer Research* **2**, 1843-1849 (1996).
174. Browder, T., Butterfield, C.E., Kraling, B.M., Shi, B., Marshall, B., O'Reilly, M.S. & Folkman, J. Antiangiogenic scheduling of chemotherapy improves efficacy against experimental drug-resistant cancer. *Cancer research* **60**, 1878-1886 (2000).

175. Anttila, M.A., Tammi, R.H., Tammi, M.I., Syrjanen, K.J., Saarikoski, S.V. & Kosma, V.M. High levels of stromal hyaluronan predict poor disease outcome in epithelial ovarian cancer. *Cancer research* **60**, 150-155 (2000).
176. Chou, T.C. Drug combination studies and their synergy quantification using the Chou-Talalay method. *Cancer research* **70**, 440-446 (2010).
177. Tallarida, R.J. Quantitative methods for assessing drug synergism. *Genes & cancer* **2**, 1003-1008 (2011).
178. Chou, T.C. & Talalay, P. Quantitative analysis of dose-effect relationships: the combined effects of multiple drugs or enzyme inhibitors. *Advances in enzyme regulation* **22**, 27-55 (1984).
179. Loewe, S. The problem of synergism and antagonism of combined drugs. *Arzneimittel-Forschung* **3**, 285-290 (1953).
180. Kerbel, R.S. & Kamen, B.A. The anti-angiogenic basis of metronomic chemotherapy. *Nature reviews. Cancer* **4**, 423-436 (2004).
181. Oldham, R.K. & Dillman, R.O. Monoclonal antibodies in cancer therapy: 25 years of progress. *Journal of clinical oncology : official journal of the American Society of Clinical Oncology* **26**, 1774-1777 (2008).
182. Dillman, R.O., Beauregard, J.C., Halpern, S.E. & Clutter, M. Toxicities and side effects associated with intravenous infusions of murine monoclonal antibodies. *Journal of biological response modifiers* **5**, 73-84 (1986).
183. van Dongen, G.A., Visser, G.W., Lub-de Hooge, M.N., de Vries, E.G. & Perk, L.R. Immuno-PET: a navigator in monoclonal antibody development and applications. *The oncologist* **12**, 1379-1389 (2007).
184. Asano, R., Hagiwara, Y., Koyama, N., Masakari, Y., Orimo, R., Arai, K., Ogata, H., Furumoto, S., Umetsu, M. & Kumagai, I. Multimerization of anti-(epidermal growth factor receptor) IgG fragments induces an antitumor effect: the case for humanized 528 scFv multimers. *The FEBS journal* **280**, 4816-4826 (2013).



185. Yeung, T.L., Leung, C.S. & Mok, S.C. CAF reprogramming inhibits ovarian cancer progression. *Cell cycle* **13**, 3783-3784 (2014).

## Vita

Cecilia S. Leung was born in Hong Kong on September 29, 1984. She is the second daughter of Yin-Ling Wong and William M. Leung. She enrolled at the Hong Kong Polytechnic University in 2003 with a major in Biotechnology and graduated with a B.Sc. (Hons) degree in 2006. After that, she matriculated into The Chinese University of Hong Kong and completed her postgraduate study in 2008 with an M.Phil. degree in Biochemistry. In November 2010, she joined the Department of Gynecologic Oncology and Reproductive Medicine at the University of Texas MD Anderson Cancer Center as a research technician. Later in August 2012, she enrolled at the University of Texas Health Science Center Graduate School of Biomedical Science at Houston and started her Ph.D. study. She joined Dr. Samuel C. Mok's research laboratory and had research focused on the ovarian tumor microenvironment. She also joined the Cancer Biology Program at M.D. Anderson Cancer Center after completing her research tutorials.

Permanent address:

4002 Medici Ct.,

Missouri City, TX 77459